

# **STRUCTURAL BEHAVIOR OF MODIFIED GEOPOLYMER CONCRETE**

*Thesis submitted in partial fulfilment of the requirement for  
the degree of*  
**Doctor of Philosophy (Engineering)**

**By**

**Dibyendu Adak**

Department of Civil Engineering  
Faculty of Engineering & Technology,  
Jadavpur University,  
Kolkata – 700032, India

**2017**

যাদবপুর বিশ্ববিদ্যালয়  
কলকাতা-৭০০০৩২, ভারত



JADAVPUR UNIVERSITY  
KOLKATA-700 032, INDIA

---

## Certificate from the Supervisor

This is to certify that the thesis entitled “**STRUCTURAL BEHAVIOR OF MODIFIED GEOPOLYMER CONCRETE**” submitted by Sri **Dibyendu Adak** who got his name registered on 24/04/2013 for the award of Ph.D. (Engineering) degree of Jadavpur University, is absolutely based upon his own work under the supervision of Prof. Saroj Mandal and that neither this thesis nor any part of it has been submitted for either any degree/diploma or any other academic award anywhere before.

.....

**Signature of the Supervisor**

**Date:**

**JADAVPUR UNIVERSITY**  
**KOLKATA – 700032, INDIA**

1. Title of the thesis:

Index No. 165/13/E

**Structural Behavior of Modified Geopolymer Concrete.**

2. Name, Designation & Institution of the Supervisor:

**Prof. (Dr.) Saroj Mandal**


Professor,


Department of Civil Engineering,


Jadavpur University,


Kolkata – 700032, India.

3. List of Publication (Related to thesis):

 **Dibyendu Adak**, Manas Sarkar, Saroj Mandal; Effect of Nano silica on Strength and durability of Fly Ash based Geopolymer mortar. Construction and Building Materials, 70 (2014), 453–459.

 **Dibyendu Adak**, Manas Sarkar, Moumita Maiti, Abiral Tamang, Saroj Mandal and Brajadulal Chattopadhyay; Antimicrobial efficiency of Silver aided silica nano composite modified fly ash based geopolymer concrete for eco-friendly construction technology. RSC Adv., 5(2015), 64037 - 64045.

 **Dibyendu Adak**, Saroj Mandal; Study on Two Different Processes for the Development of Fly Ash Based Geopolymer Mortar Curing at Ambient Temperature. Indian Concrete Journal, 89(2015), 31-40.

 **Dibyendu Adak**, Manas Sarkar, Saroj Mandal; Structural performance of nano-silica modified fly ash based geopolymer concrete. Construction and Building Materials, 135 (2017), 430 – 439.

✚ Manas Sarkar, **Dibyendu Adak**, Abiral Tamang, Brajadulal Chattopadhyay and Saroj Mandal; Genetically-enriched microbe-facilitated self-healing concrete - A sustainable material for a new generation of construction technology. Rsc. Adv., RSC Adv., 5(2015), 105363.

✚ Dibyendu Adak, Saroj Mandal; Strength and durability performance of process modified fly ash based geopolymer concrete. Resource, Conservation and Recycling (Elsevier), Under Review.

#### 4. Conference Proceedings:

❖ **Dibyendu Adak**, Saroj Mandal, “Durability study of fly ash based geopolymer concrete and conventional concrete”, YRGS International Conference 2013, October 15-16, 2013, Jaipur, India, Current challenges in Structural engineering.

❖ **Dibyendu Adak**, Saroj Mandal, “Geopolymer concrete: an economic material that needs to be improved”, Asia-Pacific Conclave, International Conference 2013, Kolkata, Coal Ash Institute of India.

❖ Saroj Mandal, **Dibyendu Adak**, “Anti-microbial efficiency of nano silver-silica modified geopolymer mortar”, CONSEC 2016, Politecnico di Milano, 12-14 September 2016, Lecco, Lake Como, Italy.

#### 5. List of Patents:

**NIL**

## DECLARATION

I do hereby declare that the work embodied in this thesis entitled **“STRUCTURAL BEHAVIOR OF MODIFIED GEOPOLYMER CONCRETE”** which is being submitted for the degree of Doctor of Philosophy (Engineering) has been carried out by me in the Concrete and Structural laboratory, Department of Civil Engineering, Jadavpur University, Kolkata, India. Neither this thesis nor any part thereof has been presented/submitted anywhere for either any degree/diploma or any other academic award before.

Date:

Kolkata, India

.....

(Dibyendu Adak)

## ACKNOWLEDGEMENT

The title *Doctor of Philosophy* is one of the hardest earned of all those we struggle for and it carries with it a sense of satisfaction and achievement. It is a really great opportunity to express my sincere gratitude to the people who have helped me in a correct way to achieve this goal.

Exploration of this thesis titled “**STRUCTURAL BEHAVIOR OF MODIFIED GEOPOLYMER CONCRETE**” has been commenced from under the supervision of **Prof. Dr. Saroj Mandal**, Civil Engineering Dept. Jadavpur University, Kolkata, India.

Firstly, I would like to utter my profound gratitude to my valued, proficient guide, Prof. Dr. S. Mandal, without whose active assistance, ample support and apt guidance, it wouldn't have been possible for me to achieve this work. I feel contented to have him for his constructive and priceless suggestions, active teamwork and unvarying back-up all the way through the exploration.

For financial support during the execution of the works I am grateful to University Grant Commission (UGC), The Govt. of India for providing me fellowship during this exertion.

I am sincerely grateful to Dr. Manas Sarkar, Dr. Moumita Maiti and Mr. A. Tamang, (Assistant Professor, Dept. of Physics) who have helped me a lot in my technical work.

I would like to thank all my family members, especially my parents who always inspired me in all my success and failures. Without their immense support it could not have been possible for me to complete my Ph.D. work.

Above all, I thank **Almighty** for everything he has offered & blessed me into my life.

August 2017, KOLKATA

**Dibyendu Adak**

Learning Is A Treasure That Will Follow Its Owner  
Everywhere.

***Dedicated to  
my beloved parents***



# SYNOPSIS

---

The sustainability of the cement and concrete industries is imperative to the wellbeing of our planet and human development. The production of Portland cement, an essential constituent of concrete, releases about one tone of carbon dioxide (CO<sub>2</sub>) into the atmosphere per tone of cement. On the other hand, coal based thermal power stations produce a huge amount of fly ash, of which about 35% used in construction of landfills, embankments, production blended cement etc. and remaining as an industrial hazards. Alkali activated geopolymer mortar/concrete are being introduced to reduce the rapid utilization of Portland cement mortar/concrete throughout the world. In the last few decades, the application of geopolymer concrete using mainly fly ash has become an important area of research.

Geopolymer is an inorganic alumino-silicate polymer synthesized from alkaline activation of various alumino-silicate materials of geological origin or by product materials like fly ash, metakaolin, blast furnace slag etc. Geo-polymeric reaction generally depends on the activation with alkali solutions and heat activation at different temperature to obtain better strength and durability compared to normal concrete. A lot of research work already have been reported on the development of strength and durability of geopolymer mortar/concrete at different molar concentrations cured at different temperature and period. It was recognized in the previous studies that at higher concentration of sodium hydroxide (NaOH) solution and higher ratio of sodium silicate (Na<sub>2</sub>SiO<sub>3</sub>) to sodium hydroxide ratio (by mass) the fly ash based geopolymer concrete results in higher compressive strength. However, heat activation was the much needed property for geopolymer mortar/concrete to develop early strength. With the increase in curing temperature (for heat activation) in the range of 30°C to 90°C, the compressive strength of fly ash-based geopolymer mortar/concrete also increases. Geopolymer concrete without heat activation showed poor strength and durability due to slow polymerization process. Thus, the use of geopolymer mortar/concrete is presently limited to the pre-cast member due to requirement of heat activation after casting.

This thesis reports the details of development of low calcium fly ash-based geopolymer mortar/concrete cured at ambient temperature. There are limited literatures

available on geopolymer mortar/concrete cured at ambient temperature. This study narrates two new different techniques to develop low calcium fly ash based geopolymer mortar/concrete without heat activation - (1) **the addition of nano silica in geopolymer mortar/concrete mix** and (2) **the geopolymeric process modification**. Also due to the lack of knowledge on structural behaviors of fly ash based geopolymer concrete with/without heat activation, the structural behaviors of the above two geopolymer concrete has been also incorporated. Low calcium fly ash was chosen as the basic material to be activated by geopolymerization process in presence of alkali activator solution of sodium hydroxide and sodium silicate throughout the study. Nano silica has been in partial replacement of fly ash.

Addition of colloidal nano silica in geopolymer mortar cured at ambient temperature shows an appreciable improvement in mechanical strength (compressive, split tensile and flexural strength) and durability (Rapid Chloride Ion Penetration Test, water absorption and sulphate test). Geopolymer mortar (cured at ambient temperature) with the addition of different percentages colloidal nano silica (w/w) of fly ash with the activator fluid ( $\text{NaOH} + \text{Na}_2\text{SiO}_3 + \text{H}_2\text{O}$ ) at different molar concentrations (8M, 10M, 12M) were investigated and compared with heat activated conventional geopolymer mortar (without nano silica) and control cement mortar. The experimental results of this study clearly elucidates that with the addition of nano silica of 6% of fly ash at 12 molar NaOH solution, geopolymer mortar cured at ambient temperature shows better mechanical strength and durability performance than conventional heat cured geopolymer mortar and control cement mortar.

Based on the preminent results of nano silica modified geopolymer mortar and to establish structural behavior of geopolymer concrete with nano silica, a series of tests of the compressive strength, split tensile strength, modulus of elasticity and bond strength were investigated and also compared with conventional heat cured geopolymer concrete without nano silica and OPC based control cement concrete. Flexural behavior of reinforced nano silica modified geopolymer concrete beam at different percentages of tension, compression and shear reinforcement were investigated. This experimental study reveals that the compressive strength, bond strength, split tensile strength of nano silica modified geopolymer concrete is higher than heat activated geopolymer concrete

without nano silica and OPC concrete. Field Emission Scanning Microscope (FESM) images show that the geopolymer matrix with 6% nano silica seemed to consist of more amount of crystalline compound transformed from amorphous compound than that of geopolymer mortar without nano silica. Also the X-ray Diffraction (XRD) analysis shows the wide diffraction hump identified around  $25 - 30^\circ$  2theta that confirms the presence of crystalline phases in nano silica modified geopolymer matrix.

Beside the mechanical strength and durability the mechanistic anti-bacterial activity of the silver-silica nano composite modified geopolymer mortar were investigated and compared to nano silica modified geopolymer mortar and control cement mortar. The result shows that silver-silica nano composite modified geopolymer mortar cured at room temperature shows almost similar strength and durability with respect to nano silica modified geopolymer mortar but better anti-bacterial property.

The work also includes to develop a modified geopolymer process (Process – I) in which heat activation of fly ash and activator fluid mixture had been made before casting. The duration of such heat activation is substantially reduced to 45 minutes compared to 48 hours and more. The mechanical strength and durability behavior of this modified geopolymer mortar (Process – I) had been compared to that of conventional heat activated geopolymer mortar (Process – II) in which the heat activation has been made after casting for 48 hours. Geopolymer mortar made by Process – I shows better strength and durability than Processes – II geopolymer mortar at different fluid to fly ash ratio. In Process – I geopolymer mortar, fly ash has been more uniformly polymerized within the whole matrix than Process – II geopolymer mortar as per FESEM analysis. Energy Dispersive X-Ray (EDS) and XRD analysis also confirm the presence more crystalline compound in Process – I geopolymer mortar than Process – II geopolymer mortar. Finally, an economical benefit for the Process-I in terms of energy savings and practical applicability had been presented.

Based on the performance of process modified geopolymer mortar, the study has been further extended on geopolymer concrete. The structural behavior (compressive, split tensile, flexural strength, bond strength and modulus of elasticity) of such process modified geopolymer concrete (Process – I) has been studied and compared with conventional heat cured geopolymer concrete (Process – II). The process modified

geopolymer concrete (Process – I) shows better structural performance than that of conventional geopolymer concrete (Process – II) due to early age polymerization of fly ash and activator fluid.

Finally two novel techniques to develop the geopolymer concrete without heat activation have been identified. Besides the elimination of heat activation, nano silica modified geopolymer and process modified (Process – I) mortar/concrete show improved mechanical strength and durability. Silver-silica modified geopolymer mortar demonstrates better anti-bacterial property than conventional cement mortar and silica modified geopolymer mortar. Therefore, this innovative technology can be implemented in practical construction in terms of strength, durability, energy savings and substantial reduction of greenhouse gas emissions for sustainable development.

# CONTENTS

<u>Sl. No:</u>		<u>Pg. No:</u>
❖	<b>CHAPTER – I: INTRODUCTION</b>	<b>1-11</b>
1.0	General view	1-3
1.1	Background	4
1.2	Goals	4-5
1.3	Research objectives	5-6
)	References	07-11
❖	<b>CHAPTER – II: REVIEW OF LITERATURE</b>	<b>12-71</b>
2.0	General view	12
2.1	History of geopolimer	12
2.1.1	Source material	12-14
2.1.2	Activator solutions	15-17
2.1.3	Curing conditions	17-19
2.2	Current Trend of Research on Fly Ash Based Geopolymer concrete	19
2.2.1	Properties of fresh and hardened geopolimer concrete	19-39
2.2.1.1	Compressive strength	22-26
2.2.1.2	Modulus of elasticity	27-29
2.2.1.3	Tensile strength	29-32
2.2.1.4	Flexural strength	33
2.2.1.5	Bond strength	34-38
2.2.1.6	Flexural strength of reinforced GPC beam	38-40
2.2.2	Microstructural analysis of geopolimer mortar/concrete	41
2.2.2.1	X-ray Diffraction analysis	41-44
2.2.2.2	SEM with EDS analysis	44-49
2.2.2.3	Fourier Transform Infra-Red Spectroscopy	49-51

2.3	Application of geopolymer mortar/concrete	52
2.4	Modified geopolymer without heat activation	53-58
2.5	Antibacterial activity of conventional concrete and geopolymer concrete	58-61
)	Aim of the study	61-62
)	References	63-71
❖	<b>CHAPTER – III: INSTRUMENTS &amp; APPARETUS</b>	<b>72-83</b>
3.0	General	72
3.1	Bond strength	72-73
3.2	Flexural strength of reinforced concrete beam	73-74
3.3	Chloride ion permeability test	74-75
3.4	Field Emission Scanning Electron Microscope (FESEM)	75-77
3.5	HI-Resolution Transmission Electron Microscope (HRTEM)	77-78
3.6	X-RAY Diffraction (XRD)	79-80
3.7	Fourier Transform Infra-red Spectroscopy (FTIR)	80-82
3.8	Fluorescence Microscopy	82-83
❖	<b>CHAPTER – IV: MATERIALS &amp; METHODS</b>	<b>84-107</b>
4.0	Experimental details	84
4.1	Materials and chemicals	84-85
4.2	Geopolymer mortar with nano silica and control mortar	86-89
4.2.1	Compressive strength of mortar	86
4.2.2	Split tensile strength of mortar	88
4.2.3	Flexural strength of mortar	88
4.2.4	RCPT of mortar	88
4.2.5	Water absorption test of mortar	88
4.2.6	Microstructural analysis of mortar	89
4.2.6.1	X-ray diffraction analysis	89
4.2.6.2	FESEM analysis	89
4.3	Geopolymer concrete with nano silica	90-94
4.3.1	Compressive strength of concrete	91

4.3.2	Split tensile strength and modulus of elasticity	91
4.3.3	Bond strength	91
4.3.4	Flexural strength of reinforced concrete beam	91-92
4.3.5	Microstructural analysis of concrete	94
4.3.5.1	XRD analysis	94
4.3.5.2	FESEM with EDS analysis	94
4.3.5.3	FTIR analysis	94
4.4	Silver-silica modified geopolymer mortar	95-99
4.4.1	Preparation of silver silica nano composite	95
4.4.2	Confirmative test on silver silica nano composite	95
4.4.3	Preparation of mortar samples	96
4.4.4	Mechanical strength and durability study	97
4.4.5	Antibacterial study	97-99
4.4.5.1	Bacterial kinetics study	97
4.4.5.2	Minimum Inhibitory Concentration (MIC) and Minimum Bactericidal Concentration (MBC) test of Mortar samples	98
4.4.5.3	Fluorescence Microscopic analysis	98
4.4.5.4	Morphological investigation of bacterial strain	98-99
4.5	Process development for geopolymer mortar	100-103
4.5.1	Mechanical strength	100-101
4.5.2	Durability test	101
4.5.3	Microstructural study	101
4.5.3.1	FESEM with EDS analysis	101
4.5.3.2	X-ray Diffractive (XRD) analysis	101
4.6	Process development for geopolymer concrete	104-106
4.6.1	Mechanical strength of process developed geopolymer concrete	104
4.6.1.1	X-ray Diffraction analysis	105
4.6.1.2	SEM with EDS analysis	106
)	References	107-108
❖	<b>CHAPTER – V: RESULT AND DISCUSSION</b>	<b>109-159</b>

<b>5.0</b>	<b>General</b>	<b>109</b>
<b>5.1</b>	<b>Nano silica modified geopolymer mortar</b>	<b>110-117</b>
<b>5.2</b>	<b>Nano silica modified geopolymer concrete</b>	<b>118-130</b>
<b>5.3</b>	<b>Antibacterial activity of silver-silica modified geopolymer mortar</b>	<b>131-140</b>
<b>5.4</b>	<b>Process development for geopolymer mortar</b>	<b>141-153</b>
<b>5.5</b>	<b>Process development for geopolymer concrete</b>	<b>154-159</b>
)	<b>References</b>	<b>160-162</b>
❖	<b>CHAPTER – VI: CONCLUSION</b>	<b>163-166</b>
❖	<b>FUTURE SCOPE</b>	



# LIST OF FIGURES

<u>Literature Review</u>	<u>Pg. No</u>
<b>Figure 2.1:</b> Compressive strength of geopolymer concrete after 28day at different temperature (2002).	18
<b>Figure 2.2:</b> Variation of compressive strength with curing time (2008).	19
<b>Figure 2.3:</b> Workability of lignite bottom ash geopolymer concrete at different sodium silicate to 10M sodium hydroxide ratio (2009).	20
<b>Figure 2.4:</b> Slump of different geopolymer concrete with different slag content (2014).	21
<b>Figure 2.5:</b> Effect of curing temperature on setting time of geopolymer concrete (2008).	21
<b>Figure 2.6:</b> Mixing time vs. slump value of geopolymer concrete (2005).	22
<b>Figure 2.7:</b> Compressive strength of fly ash and bottom ash based geopolymer at different molar concentration (2009).	23
<b>Figure 2.8:</b> Compressive strength of based geopolymer at different molar concentration (2008).	23
<b>Figure 2.9:</b> Compressive strength of geopolymer concrete at different molar concentration (2007).	24
<b>Figure 2.10:</b> Compressive strength of geopolymer concrete at different $\text{Na}_2\text{SiO}_3/\text{NaOH}$ ratio (2014).	25
<b>Figure 2.11:</b> Compressive strength of bottom ash geopolymer mortar (2009).	25
<b>Figure 2.12:</b> Compressive strength of geopolymer at different curing temperature and curing time (2012).	26
<b>Figure 2.13:</b> Modulus of elasticity of geopolymer concrete (2007).	27
<b>Figure 2.14:</b> Modulus of elasticity as a function of NaOH Concentration (2013).	28
<b>Figure 2.15:</b> Modulus of elasticity as a function of $\text{Na}_2\text{SiO}_3/\text{NaOH}$ ratio (2013).	29
<b>Figure 2.16:</b> Split tensile strength vs. compressive strength of GPC (2011).	30
<b>Figure 2.17:</b> Relation between compressive strength and split tensile strength of concrete (2013).	31
<b>Figure 2.18:</b> Variation of direct tensile strength with compressive strength of geopolymer (2014).	32

<b>Figure 2.19:</b> Variation of tensile strength with alkali activator and fly ash ratio (2014).	<b>32</b>
<b>Figure 2.20:</b> Variation of modulus of rupture with alkaline activator / fly ash ratio for different curing temperature (2014).	<b>33</b>
<b>Figure 2.21:</b> Bond strengths of beam-end and direct type specimens (2007).	<b>35</b>
<b>Figure 2.22:</b> Variation of bond strength with concrete compressive strength for 20 mm bar and 45 mm cover (2011).	<b>35</b>
<b>Figure 2.23:</b> Bonding strength of fly ash–MIRHA based geopolymer concrete in ambient curing (2012).	<b>36</b>
<b>Figure 2.24:</b> Bonding strength of fly ash–MIRHA based geopolymer concrete in external exposure curing (2012).	<b>37</b>
<b>Figure 2.25:</b> Bonding strength of fly ash–MIRHA based geopolymer concrete in oven curing (2012).	<b>37</b>
<b>Figure 2.26:</b> The bond stress–slip curves of geopolymer and OPC concretes after 28 days curing (2015).	<b>38</b>
<b>Figure 2.27:</b> Effect of percentages of tensile reinforcement on the flexural capacity of beam (2006).	<b>39</b>
<b>Figure 2.28:</b> Effect of Concrete Compressive Strength on Cracking Moment (2006).	<b>40</b>
<b>Figure 2.29:</b> XRD analysis fly ash based geopolymer concrete (2005).	<b>42</b>
<b>Figure 2.30:</b> XRD analysis of fly ash and geopolymer matrix (2013).	<b>43</b>
<b>Figure 2.31:</b> XRD patterns of geopolymer pastes with microwave radiation and additional 65°C heat curing (2013).	<b>44</b>
<b>Figure 2.32:</b> Unreacted fly ash and reaction product after polymerization (2013).	<b>45</b>
<b>Figure 2.33:</b> EDX analysis of the geopolymer matrix (2013).	<b>45</b>
<b>Figure 2.34:</b> Microstructure of geopolymer pastes with microwave radiation and additional 65°C heat curing of 3h, 6h, 12h, and Control (2013).	<b>46</b>
<b>Figure 2.35:</b> SEM-EDX analysis of fly ash based geopolymer (2009).	<b>47</b>
<b>Figure 2.36:</b> SEM-EDX analysis of bottom ash based geopolymer (2009).	<b>47</b>
<b>Figure 2.37:</b> SEM micrographs of the hardened alkali activated fly ash samples (2012).	<b>48</b>
<b>Figure 2.38:</b> SEM and EDX analysis of alkali activated fly ash sample (2009).	<b>49</b>
<b>Figure 2.39:</b> FTIR spectra of fly ash based geopolymer (2000).	<b>50</b>

<b>Figure 2.40:</b> FTIR study of fly ash with (a) sodium hydroxide (b) sodium silicate activator (2005).	<b>51</b>
<b>Figure 2.41:</b> FTIR spectra for the original FA and AAFA systems (2012).	<b>51</b>
<b>Figure 2.42:</b> Compressive strength of bottom ash, fly ash and mix of fly ash and bottom ash geopolymer concrete (2015).	<b>54</b>
<b>Figure 2.43:</b> FESM image of (a) 100% BA, (b) 50 % BA + 50% FA, (c) 25% BA + 75% FA, (d) 100% FA geopolymer concrete.	<b>54</b>
<b>Figure 2.44:</b> Relation between compressive strength and paste to aggregate ratio of IPCs (2010).	<b>56</b>
<b>Figure 2.45:</b> Compressive strength of the geopolymer concrete at different percentage of GBFS (2012).	<b>57</b>
<b>Figure 2.46:</b> Bacterial attack on concrete.	<b>59</b>
<b>Figure 2.47:</b> Optical photograph of samples of snow dust with oyster mushroom hyphae and copper chloride solution at various concentration.	<b>61</b>

### Instrument & Apparatus

### Pg. No

<b>Figure 3.1:</b> Bond strength testing arrangement.	<b>73</b>
<b>Figure 3.2:</b> Flexural strength test setup for reinforced concrete beam.	<b>74</b>
<b>Figure 3.3:</b> RCPT arrangement.	<b>75</b>
<b>Figure 3.4A:</b> Graphical presentation of FESEM setup.	<b>76</b>
<b>Figure 3.4B:</b> FESEM laboratory test arrangement.	<b>77</b>
<b>Figure 3.5:</b> HRTEM test setup.	<b>78</b>
<b>Figure 3.6A:</b> Graphical presentation of XRD test.	<b>79</b>
<b>Figure 3.6B:</b> XRD test arrangement.	<b>80</b>
<b>Figure 3.7:</b> Graphical presentation of FTIR working principal.	<b>81</b>
<b>Figure 3.8A:</b> Graphical presentation Fluorescence Microscopy.	<b>82</b>
<b>Figure 3.8B:</b> Fluorescence Microscopy laboratory setup.	<b>83</b>

### Material & Method

### Pg. No

<b>Figure 4.1:</b> Typical beam details and loading arrangement.	<b>92</b>
<b>Figure 4.2:</b> Flexural strength test setup for reinforced concrete beam.	<b>92</b>
<b>Figure 4.3:</b> Details of Process – I and Process – II geopolymer mortar.	<b>102</b>

<b>Figure 4.4:</b>	Graphical presentation of synthesis of process modified geopolymer concrete (GPC – I)	<b>104</b>
<b>Figure 4.4:</b>	Graphical presentation of synthesis of conventional heat cured geopolymer concrete (GPC – II)	<b>105</b>

*Result and Discussion*

*Pg. No*

<b>Figure 5.1:</b>	Compressive strength of 8(M) geopolymer mortar and cement mortar samples.	<b>110</b>
<b>Figure 5.2:</b>	Compressive strength of 10(M) geopolymer and cement mortar samples.	<b>110</b>
<b>Figure 5.3:</b>	Compressive strength of 12(M) geopolymer and cement mortar samples.	<b>111</b>
<b>Figure 5.4:</b>	Compressive strength of geopolymer mortar & cement mortar at 28 days.	<b>112</b>
<b>Figure 5.5:</b>	Initial and final setting time of geopolymer mortar (with / without nano silica).	<b>113</b>
<b>Figure 5.6:</b>	Flexural strength of fly ash based geopolymer mortar and cement mortar samples.	<b>114</b>
<b>Figure 5.7:</b>	Tensile strength of fly ash based geopolymer mortar and cement mortar samples.	<b>114</b>
<b>Figure 5.8:</b>	Charge passed through geopolymer mortar samples (with/without nano silica) at different molar concentration and cement mortar samples.	<b>115</b>
<b>Figure 5.9:</b>	Water absorption test on geopolymer mortar (with / without nano silica) of different molar concentration and cement mortar samples.	<b>116</b>
<b>Figure 5.10:</b>	XRD Analysis of fly ash based geopolymer mortar sample (12GM0H and 12GM6) and cement mortar (CM) samples.	<b>117</b>
<b>Figure 5.11:</b>	FESEM image of (A) 12GM0H geopolymer mortar sample (B) 12M6 geopolymer mortar sample (C) CM sample.	<b>118</b>
<b>Figure 5.12:</b>	Compressive strength of 12GC6, 12GC0H geopolymer concrete and control cement concrete (CC) at 3, 7 and 28 days.	<b>119</b>
<b>Figure 5.13:</b>	Stress-strain curve of 12GC6, 12GC0H geopolymer concrete and CC concrete.	<b>121</b>

<b>Figure 5.14:</b> Bond strength vs. slip curve of geopolymer concrete (12GC6 & 12GC0H) and control cement concrete (CC) with deformed and mild steel bar.	<b>122</b>
<b>Figure 5.15:</b> Load vs. deflection curve capacity of 12GC6, 12GC0H and CC concrete beams with different percentages of tensile reinforcement.	<b>123</b>
<b>Figure 5.16:</b> Load vs. deflection curve of 12GC6, 12GC0H and CC concrete beams with different percentages of compressive reinforcement.	<b>124</b>
<b>Figure 5.17:</b> Load vs. deflection curve of 12GC6, 12GC0H and CC concrete beams with different amount of shear reinforcement.	<b>124</b>
<b>Figure 5.18:</b> Crack patterns of 12GC6, 12GC0H and CC concrete beams.	<b>126</b>
<b>Figure 5.19:</b> XRD analysis of 12GC6 & 12GC0H and CC concrete.	<b>127</b>
<b>Figure 5.20:</b> FTIR analysis of geopolymer concrete (12GC6 & 12GC0H).	<b>128</b>
<b>Figure 5.21:</b> SEM micrographs and EDX analysis of 12GC6, 12GC0H geopolymer concrete and control cement concrete (CC).	<b>129</b>
<b>Figure 5.22:</b> TEM image of (A) Silica NPs & (B) Silver-silica NPs with inset representing elemental analysis by EDS. Zeta size (C-I & D-I) and Zeta potential (C-II & D-II) distribution graph of silica NPs & silver-silica NPs respectively.	<b>132</b>
<b>Figure 5.23A:</b> XRD spectra of (I) SiO <sub>2</sub> NPs & (II) Ag-SiO <sub>2</sub> NPs.	<b>134</b>
<b>Figure 5.23B:</b> XRD spectra of (I) GM <sub>Si</sub> and (II) GM <sub>Ag-Si</sub> .	<b>134</b>
<b>Figure 5.24:</b> Compressive strength of GM <sub>Ag-Si</sub> , GM <sub>Si</sub> geopolymer mortar and control cement mortar at different ages.	<b>134</b>
<b>Figure 5.25:</b> Flexural and tensile strength of GM <sub>Ag-Si</sub> , GM <sub>Si</sub> geopolymer and CM.	<b>135</b>
<b>Figure 5.26:</b> RCPT of different mortar samples (CM, GM <sub>Si</sub> and GM <sub>Ag-Si</sub> ).	<b>135</b>
<b>Figure 5.27:</b> Photographs of colonies of (A) <i>E. coli</i> & (B) <i>S. aureus</i> incubated on agar plates obtained from cultivated suspensions with (CM, GM <sub>Si</sub> & GM <sub>Ag-Si</sub> ) and mortality curve of (C) Gram -ve bacteria (D) Gram +ve bacteria in presence of CM, GM <sub>Si</sub> & GM <sub>Ag-Si</sub> .	<b>137</b>
<b>Figure 5.28:</b> Fluorescence microscopic images of (A) CM treated <i>E. coli</i> , (B) GM <sub>Si</sub> treated <i>E. coli</i> , (C) GM <sub>Ag-Si</sub> treated <i>E. coli</i> , (D) CM treated <i>S. aureus</i> , (E) GM <sub>Si</sub> treated <i>S. aureus</i> , (F) GM <sub>Ag-Si</sub> treated <i>S. aureus</i> bacterial cells.	<b>138</b>

<b>Figure 5.29:</b> FESEM images of (A) CM treated <i>E. coli</i> (B) GM <sub>Si</sub> treated <i>E. coli</i> (C) GM <sub>Ag-Si</sub> treated <i>E. coli</i> (D) CM treated <i>S. aureus</i> (E) GM <sub>Si</sub> treated <i>S. aureus</i> (F) GM <sub>Ag-Si</sub> treated <i>S. aureus</i> .	<b>139</b>
<b>Figure 5.30:</b> Compressive strength of geopolymer mortar at fluid/ fly ash ratio 0.35 in Process – I and Process – II.	<b>142</b>
<b>Figure 5.31:</b> Compressive strength of geopolymer mortar at fluid/ fly ash ratio 0.40 in Process – I and Process – II.	<b>143</b>
<b>Figure 5.32:</b> Compressive strength of geopolymer mortar at fluid/ fly ash ratio 0.45 in Process – I and Process – II.	<b>143</b>
<b>Figure 5.33:</b> Flexural strength of geopolymer mortar at fluid/ fly ash ratio 0.35 in Process – I and Process – II.	<b>144</b>
<b>Figure 5.34:</b> Flexural strength of geopolymer mortar at fluid/ fly ash ratio 0.40 in Process – I and Process – II.	<b>145</b>
<b>Figure 5.35:</b> Flexural strength of geopolymer mortar at fluid/ fly ash ratio 0.35 in Process – I and Process – II.	<b>145</b>
<b>Figure 5.36:</b> Tensile strength of geopolymer mortar at fluid/ fly ash ratio 0.35 in Process – I and Process – II.	<b>146</b>
<b>Figure 5.37:</b> Tensile strength of geopolymer mortar at fluid/ fly ash ratio 0.40 in Process – I and Process – II.	<b>146</b>
<b>Figure 5.38:</b> Tensile strength of geopolymer mortar at fluid/ fly ash ratio 0.45 in Process – I and Process – II.	<b>147</b>
<b>Figure 5.39:</b> Charge passed through geopolymer mortar at fluid/ fly ash ratio 0.35 in Process I and Process II.	<b>148</b>
<b>Figure 5.40:</b> Charge passed through geopolymer mortar at fluid/ fly ash ratio 0.40 in Process I and Process II.	<b>148</b>
<b>Figure 5.41:</b> Charge passed through geopolymer mortar at fluid/ fly ash ratio 0.45 in Process I and Process II.	<b>149</b>
<b>Figure 5.42:</b> XRD analysis of Process – I and Process – II geopolymer mortar at fluid/fly ash ratio 0.35.	<b>151</b>
<b>Figure 5.43:</b> FESEM image of Process – I and Process –II geopolymer mortar of fluid to fly ash ratio 0.35.	<b>152</b>
<b>Figure 5.44:</b> EDS analysis of (A) Process – I and (B) Processes – II geopolymer mortar of fluid to fly ash ratio 0.35.	<b>152</b>
<b>Figure 5.45:</b> Compressive strength of GPC – I and GPC – II geopolymer concrete at 3, 7 and 28days.	<b>154</b>
<b>Figure 5.46:</b> Flexural and tensile strength of GPC – I and GPC – II	

geopolymer concrete at 28 days of curing.	155
<b>Figure 5.47:</b> Bond stress vs. slip curve of GPC – I and GPC – II geopolymer concrete with deformed and mild rebar.	156
<b>Figure 5.48:</b> XRD analysis of GPC – I and GPC – II concrete.	158
<b>Figure 5.51:</b> FESEM images EDS analysis of GPC – I and GPC – II concrete.	159

# LIST OF TABLES

<b>Table 2.1:</b>	Application of geopolymer mortar/concrete.	<b>52</b>
<b>Table 4.1:</b>	Chemical analysis report of fly ash.	<b>84</b>
<b>Table 4.2:</b>	Particle size analysis report of fly ash.	<b>84</b>
<b>Table 4.3:</b>	Properties of colloidal nano silica.	<b>85</b>
<b>Table 4.4:</b>	Mix proportion varying molar concentration, percentage of nano silica and curing condition.	<b>87</b>
<b>Table 4.5:</b>	Details of nano-silica modified geopolymer (12GC6), conventional heat cured geopolymer (12GC0H) concrete and control cement concrete (CC) mix.	<b>90</b>
<b>Table 4.6:</b>	Reinforcement details of nano-silica modified geopolymer (A1 to A7), conventional geopolymer (B1 to B7) concrete and control concrete (C1 to C7) beam.	<b>93</b>
<b>Table 4.7:</b>	Nano silica modified geopolymer (GMSi), silver silica modified geopolymer mortar (GMAg-Si) and control mortar (CM), mix proportions.	<b>96</b>
<b>Table 4.8:</b>	Mix proportion for different process (Process – I and Processes – II).	<b>103</b>
<b>Table 4.9:</b>	Details of GPC – I and GPC – II conventional heat cured geopolymer concrete mix.	<b>105</b>
<b>Table 5.1:</b>	Fresh concrete and harden concrete properties of different mixes.	<b>120</b>
<b>Table 5.2:</b>	Details of bond stress test result of 12GC6, 12GC0H and CC reinforced concrete.	<b>122</b>
<b>Table 5.3:</b>	Theoretical (M <sub>th</sub> ) and experimentally (M <sub>exp</sub> ) calculated bending moment of 12GC6, 12GC0H and CC reinforced concrete beam	<b>125</b>
<b>Table 5.4:</b>	Minimum Inhibitory Concentration (MIC) ASSAY (mg/mL).	<b>137</b>
<b>Table 5.5:</b>	Minimum Bactericidal Concentration (MBC) ASSAY (mg/mL).	<b>137</b>
<b>Table 5.6:</b>	Water absorption test results of geopolymer mortar samples in Process I & II (fluid/ fly ash = 0.35).	<b>150</b>
<b>Table 5.7:</b>	Sulphate test results of geopolymer mortar samples in process I & II (fluid/ fly ash = 0.35).	<b>150</b>

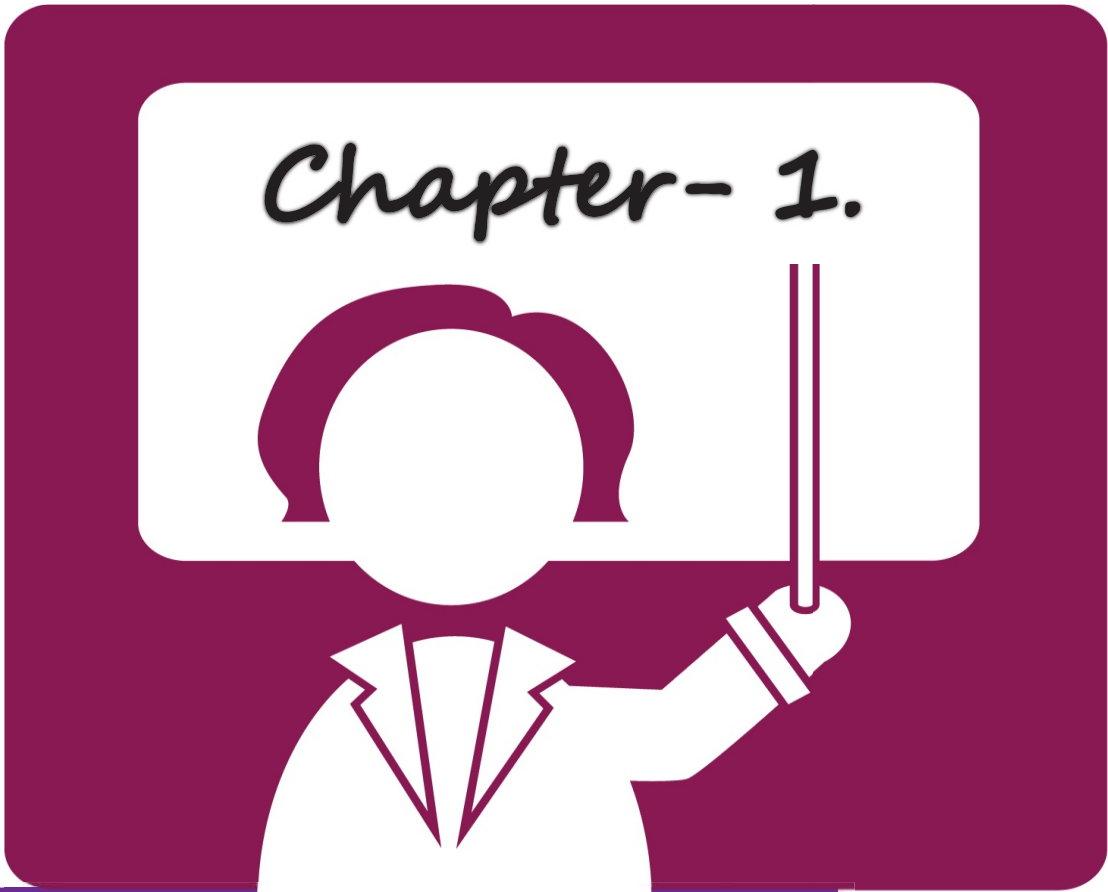


# ABBREVIATIONS

- MPa - Mega Pascal
- kN - Kilo Newton
- GPa - Giga Pascal
- CM - Control Cement Mortar
- GPC - Geopolymer Concrete
- GCOH - Geopolymer Concrete Heat Cured
- GM<sub>Si</sub> - Geopolymer Mortar with Nano Silica
- GM<sub>Ag-Si</sub> - Geopolymer Mortar with Silver-silica NPs
- FESEM - Field Emission Scanning Electron Microscope
- BSE - Backscattered Electron
- TEM - Transmission Electron Microscope
- μL - Micro-litre
- μg - Micro-gram
- RCPT - Rapid Chloride Penetration Test
- XRD - X-Ray Diffraction
- EDS - Energy Dispersive Spectroscopy
- EDTA - Ethylene Diamine Tetra-Acetate
- S.D. - Standard Deviation
- MIC - Minimum Inhibitory Concentration
- MBC - Minimum Bactericidal Concentration



**I  
N  
T  
R  
O  
D  
U  
C  
T  
I  
O  
N**





## **1.0. General view**

According to the World Business Council for Sustainable Development, “Concrete is the most widely used material on earth apart from water, with nearly three tons used annually for each man, woman, and child.” In general, concrete industry contributes at least 5 - 8% of the global carbon dioxide emissions [1]. The decomposition of lime stone emits a substantial amount of CO<sub>2</sub> in the atmosphere and reduce the lime stone resources during the manufacturing of cement. During the last few decades, there has been a rapid increase in production of coal ash, which is annually estimated to be around 780 million in the world due to increased amount of energy being generated by coal-fired power plants [2 – 4]. The utilization of fly ash is about 35% in landfills, embankments, production of blended cement etc. and remaining as an industrial waste. Being a waste from thermal power plants, ‘Internal Energy Content’ or ‘Embodied Energy’ and CO<sub>2</sub> emission of fly ash can be considered as nil.

Therefore, there is a need to develop an alternative material, which will not only reduce the demand for Portland cement, but also decrease the CO<sub>2</sub> emission and increase the utilization of fly ash. From these criteria, the proposed alternative material must possess mechanical and structural properties comparable to the Portland cement, but it should emit CO<sub>2</sub> at a much lower rate. A possible solution to this problem might be the use of fly ash based geopolymer mortar/concrete.

Geopolymers are a novel class of materials that are formed by the polymerization of silicon, aluminium and oxygen species from an amorphous three dimensional structures [5-8]. There are two main constituents of geopolymers, namely the source material and alkaline activator liquid. The source materials for geopolymer based on alumina-silicate should be rich in silica and aluminium. The source materials could be obtained from natural minerals such as kaolinite, clays, etc. and the by-product materials such as silica fume, slag, red mud and fly ash. The combination of sodium hydroxide or potassium hydroxide and sodium silicate or potassium silicate used as an activator liquid for geopolymerisation. Davidovits claims that the Egyptian Pyramids were built by casting geopolymer on site [9]. He also reported that this geopolymer material has excellent mechanical properties, does not dissolve in acidic solutions, and does not generate any deleterious alkali-aggregate reaction even in the presence of high alkalinity [10].

Kaolinite materials have been used as an alumino-silicate oxide source to synthesize geopolymer products [11, 12]. Alkali activation of metakaoline based geopolymer concrete

showed the enhanced mechanical strength and durability with an increase of NaOH concentration [13]. Development of alkali-activated kaolin-based concrete seems to present a greener alternative to OPC.

The most common industrial by-products used as binder materials are fly ash (FA) and ground granulated blast furnace slag (GGBS). GGBS had been widely used as a cement replacement material due to its latent hydraulic properties. GGBS shows an important role in the development of the compressive strength of alkali activated geopolymer concrete. GGBS (slag) based geopolymer concrete in the presence of high concentration of alkaline solution results higher compressive strength when heat cured at 60°C from 6 to 24 hours [14-16].

Fly ash is another industrial by-product, which is most common sources for geopolymer mortar/concrete because it is available throughout the world. Low calcium fly ash (ASTM Class-F) based geopolymer mortar/concrete have been used as the binder, instead of Portland or any other hydraulic cement paste, to produce concrete [17]. The fly ash-based geopolymer matrix binds the loose coarse aggregates, fine aggregates and other un-reacted materials together to form the geopolymer concrete. The strength and durability of geopolymer mortar/concrete depends on several factors, such as the molar concentration of alkali activator, mix proportion, curing time and curing temperature. It has been noted that a higher molarity of NaOH used as an alkali activator appeared to provide higher compressive strength at early age [18, 19]. The sodium hydroxide leaches the silicon and aluminium in the amorphous phase of fly ash and the sodium silicate acts as a binder. Also, the mechanical strength of geopolymer mortar/concrete depends on the ratio of sodium hydroxide and sodium silicate [20-23]. In general, heat activation is needed for the development of geopolymer mortar/concrete in the presence of alkali activator. Several researchers have been reported that the mechanical strength and durability of geopolymer concrete depends on heat curing period and temperature [24-27]. The Compressive strength of such geopolymer mortar is more at 60°C comparable to 80°C for a given molar concentration [22-27]. It has been reported in previous studies that the indirect tensile strength of fly ash-based geopolymer concrete (heat cured) is greater than the values recommends by the draft Australian Standard AS3600 (2005) and Neville (2000) for Portland cement concrete [28]. The flexural behaviour of geopolymer mortar/concrete have been investigated and compared with control cement mortar/concrete. It was reported that the flexural strength of heat cured geopolymer mortar/concrete is about 1 – 1.4 times higher than that of OPC cement concrete [29]. The high tensile and flexural strength of the geopolymer concretes help to decrease the rate and

extent of cracking in response to corrosion of steel reinforcements [30]. It has been observed that the modulus of elasticity of geopolymer concrete increased, as the compressive strength increased [31]. However, the modulus of elasticity of heat activated geopolymer concrete is lower than OPC concrete at equivalent compressive strength [32 – 34]. The modulus of elasticity of heat cured geopolymer concrete is affected by the nature of interfacial transition between the aggregates and the paste. Bond strength of concrete with reinforcement bar is another important property of hardened concrete. It has been found in previous research article that bond strength of fly ash based geopolymer concrete depends on the curing conditions. Bond strength of heat activated geopolymer concrete using plain rebar and deformed bar is higher than OPC concrete for equivalent compressive strength [35, 36]. It has been described that the main reason for higher bond strength of geopolymer concrete (heat cured) is attributed to the higher split tensile strength of geopolymer concrete than OPC concrete [37]. However, geopolymer product does not have stoichiometric composition and comprise mixtures of amorphous to semi-crystalline structure and crystalline Al-Si particles [38]. In spite of the complexities in their molecular structures, they can be used extensively in real world applications. The previous literature review has reported microstructural analysis of heat cured geopolymer mortar/concrete using Scanning Electron Microscopy (SEM) and Energy Dispersive X-ray (EDS), X-ray diffraction (XRD), Fourier Transform Infrared Spectroscopy (FTIR), to understand the underlying mechanisms of reactions and morphology of this complex system [27, 39-43]. All the studies referred above mainly based on heat activated geopolymer concrete.

However, geopolymer mortar / concrete provides poor strength at ambient temperature (about  $27 \pm 2^\circ\text{C}$ ) curing due to slow polymerization process. Thus the scope of geopolymer concrete is supposed to be limited to the precast member due to the requirement of heat activation after casting. Therefore, the motivation behind the present study is (a) the development of geopolymer mortar/concrete without heat activation after casting and (b) assessment of structural behaviour of such modified geopolymer mortar/concrete and their microstructural studies.

## **1.1. Background**

There are limited literatures available on geopolymer to eliminate the shortcomings of ambient temperature curing [44-46]. It has been reported that mechanically activated fly ash based geopolymer paste cured at ambient temperature showed about 80% more compressive strength compared to raw fly ash based geopolymer paste [44]. Geopolymer concrete with 70% fly ash and 30 % GBFS (ground blast furnace slag) cured at ambient temperature decreased the setting time but increased the compressive strength [45]. Ambient temperature cured geopolymer mortar / paste of Na<sub>2</sub>O to SiO<sub>2</sub> molar ratio 0.40 showed better compressive strength [47]. It has been reported that the compressive strength and microstructure of the ground fly ash based geopolymer pastes cured at ambient temperatures depends on NaOH concentration [48]. It has been established that the application of nano particle in geopolymer concrete is an important area of research. The incorporation of 2% nano silica by mass of cementitious materials increased compressive strengths of high-volume fly ash concrete cured at ambient temperature has been reported in previous studies [49]. Geopolymer concrete containing 97 wt. % rice husk ash + fly ash and 3 wt. % nano alumina + nano silica showed better compressive strength at lower (8M) molar concentration of NaOH solution cured at 90°C [50]. Mechanical strength of high calcium fly ash based geopolymer paste had been increased with the addition of nano-SiO<sub>2</sub> and nano-Al<sub>2</sub>O<sub>3</sub> due to formation of Calcium Silicate Hydrate (CSH or CASH) and Sodium Alumino-Silicate Hydrate (NASH) gels in the matrix [51]. However there is almost no systematic study on structural behaviour of low calcium fly ash based geopolymer concrete cured at ambient temperature and their micro-structural study. Based on the above background the following section discusses the goals of the present study.

## **1.2. Goals**

The present research is aimed at making a significant contribution towards the development of structural behaviours of alkali-activated fly ash based geopolymer mortar/concrete cured at ambient temperature and also to promote its use for practical purposes. The use of geopolymer mortar/concrete for practical purposes will certainly reduce CO<sub>2</sub> emission. Heat activation is an essential requirement to accelerate the polymerization process for the development of physical and mechanical properties of geopolymer concrete.



Thus, the scope of geopolymer concrete is limited to the precast member due to requirement of heat activation after casting. The present study focuses on developing a modified geopolymer concrete cured at ambient temperature and their structural performances. Also, the micro-structural properties of these modified geopolymer concrete (without heat activation) are another aim of this study.

### **1.3. Research Objectives:**

The objectives of the research are:

- To develop nano silica modified geopolymer mortar cured at ambient temperature at different molar concentrations of activator fluid.
- Mechanical strength and durability study of nano silica modified geopolymer mortar (cured at ambient temperature) and compare with heat cured geopolymer mortar and control cement mortar.
- Microstructural study of nano silica modified geopolymer mortar by Field Emission Scanning Electron Microscopy with Energy Dispersive X-Ray and X-Ray Diffraction analysis.
- Study on structural behaviours (compressive, split tensile, bond strength, modulus of elasticity and flexural behaviour) of nano silica modified geopolymer concrete and to compare with heat cured geopolymer concrete and OPC concrete.
- Assessment of antibacterial property of nano silver-silica modified geopolymer mortar, nano silica modified geopolymer cured at ambient temperature and control cement mortar.
- Development of a process modified geopolymer mortar at different fluid to fly ash ratio, cured at ambient temperature after casting.
- Mechanical strength and durability study of process modified geopolymer mortar and compare with conventional heat cured geopolymer and control cement mortar.
- Study on structural behaviours such as compressive strength, flexural strength, split tensile strength and bond strength of process modified geopolymer concrete and to compare with conventional heat cured geopolymer concrete.
- X-Ray Diffraction (XRD) and Fourier Transform Infrared Spectroscopy (FTIR) for qualitative identification of the chemical composition of the process modified geopolymer mortar / concrete.

- Field Emission Scanning Electron Microscopy (FESEM) and Energy Dispersive X-Ray Spectroscopy (EDS) for observing the morphology of process modified geopolymer mortar / concrete.

The next chapter presents a detailed literature review on geopolymer mortar/concrete.

## REFERENCES:

---

- [1] Abd SM, Zain MFM, Abdul Hamid R. Modelling the Prediction of Compressive Strength for Cement and Foam Concrete, Proc. of International Conference on Construction and Building Technology, Kuala Lumpur, 2008, 343 – 354.
- [2] Clarke L. B. Utilization Options for Coal Use Residues: An International Overview. Proceedings of the Tenth International Ash Use Symposium, ACAA, Orlando, Florida, January 1993, 2, 66-1 to 66-14.
- [3] Manz O. E. Worldwide Production of Coal Ash and Utilization in Concrete and Other Products. Proceedings of the Tenth International Ash Use Symposium, ACAA, Orlando, Florida, January 1993; 2, 64-1 to 64-12.
- [4] Heidrich C, Joachim F. H., Anne W. Coal Combustion Products: a Global Perspective. 2013 world of coal ash (WOCA) conference, Lexington, Kentucky, April 2013.
- [5] Krivenko, P.V. Proceedings of the First International Conference on Alkaline Cements and Concretes, Kiev, Ukraine, 1994, 11-129.
- [6] Davidovits J. Properties of Geopolymer Cement. Proceedings of First International Conference of Alkaline Cements and Concretes, State Technical University, Kiev, Ukraine, 1994, 131–149.
- [7] Fernández-Jiménez, A., A. Palomo, and M. Criado. "Alkali activated fly ash binders. A comparative study between sodium and potassium activators." *Materiales de Construcción* 56.281 (2006): 51-65.
- [8] Xu, Hua, and J. S. J. Van Deventer. "The geopolymerisation of alumino-silicate minerals." *International Journal of Mineral Processing* 59.3 (2000): 247-266.
- [9] Davidovits, Joseph. "Ancient and modern concretes: What is the real difference?." *Concrete International* 9.12 (1987): 23-28.
- [10] Davidovits, J. "Chemistry of Geopolymeric Systems, Terminology In: Proceedings of 99 International Conference." eds. Joseph Davidovits, R. Davidovits & C. James, France (1999).

- [11] Xu, Hua, and Jannie SJ Van Deventer. "Microstructural characterisation of geopolymers synthesised from kaolinite/stilbite mixtures using XRD, MAS-NMR, SEM/EDX, TEM/EDX, and HREM." *Cement and Concrete Research* 32.11 (2002): 1705-1716.
- [12] Komnitsas, Kostas, and Dimitra Zaharaki. "Geopolymerisation: A review and prospects for the minerals industry." *Minerals Engineering* 20.14 (2007): 1261-1277.
- [13] Wang, Hongling, Haihong Li, and Fengyuan Yan. "Synthesis and mechanical properties of metakaolinite-based geopolymer." *Colloids and Surfaces A: Physicochemical and Engineering Aspects* 268.1 (2005): 1-6.
- [14] Ganapati Naidu, Prasad A.S.S.N, Adishesu S. and Satyanarayana P.V.V "A study on strength properties of Geopolymer concrete with the addition of G.G.B.S" *International Journal of Engineering Research and Development*, (2011), 2, 19-28.
- [15] Yusuf, Moruf Olalekan, et al. "Evolution of alkaline activated ground blast furnace slag-ultrafine palm oil fuel ash based concrete." *Materials & Design* 55 (2014): 387-393.
- [16] Ranjbar, Navid, et al. "Compressive strength and microstructural analysis of fly ash/palm oil fuel ash based geopolymer mortar." *Materials & Design* 59 (2014): 532-539.
- [17] ASTM C618-12a: Standard Specification for Coal Fly Ash and Raw or Calcined Natural Pozzolan for Use in Concrete; ASTM International, West Conshohocken, PA, 2012.
- [18] Ryu, Gum Sung, et al. "The mechanical properties of fly ash-based geopolymer concrete with alkaline activators." *Construction and Building Materials* 47 (2013): 409-418.
- [19] Sukmak, Patimapon, et al. "Factors influencing strength development in clay-fly ash geopolymer." *Construction and Building Materials* 47 (2013): 1125-1136.
- [20] Pal Santanu, Mandal Saroj. "Different Thermal activation effect on fly ash Based Geo-polymer Concrete". *Indian Concrete Institute Journal* 12 (2011): 23-25.

- [21] Görhan, Gökhan, and Gökhan Kürklü. "The influence of the NaOH solution on the properties of the fly ash-based geopolymer mortar cured at different temperatures." *Composites part b: engineering* 58 (2014): 371-377.
- [22] Kong, Daniel LY, and Jay G. Sanjayan. "Effect of elevated temperatures on geopolymer paste, mortar and concrete." *Cement and concrete research* 40.2 (2010): 334-339.
- [23] Chindaprasirt, Prinya, Ubolluk Rattanasak, and Sompop Taebuanhuad. "Role of microwave radiation in curing the fly ash geopolymer." *Adv Powder Technol* 24 (2013): 703-707.
- [24] He, Peigang, et al. "Thermal evolution and crystallization kinetics of potassium-based geopolymer." *Ceramics International* 37.1 (2011): 59-63.
- [25] Hussin, M. W., et al. "Performance of blended ash geopolymer concrete at elevated temperatures." *Materials and Structures* 48.3 (2015): 709-720.
- [26] Vijai, K., R. Kumutha, and B. G. Vishnuram. "Effect of types of curing on strength of geopolymer concrete." *International Journal of the Physical Sciences* 5.9 (2010): 1419-1423.
- [27] Barbosa, Valeria FF, Kenneth JD Mackenzie, and Clelio Thaumaturgo. "Synthesis and characterisation of materials based on inorganic polymers of alumina and silica: sodium polysialate polymers." *International Journal of Inorganic Materials* 2.4 (2000): 309-317.
- [28] Rangan B. V. Engineering properties of geopolymer concrete. In: Provis JL, van Deventer J. S. J, editors. *Geopolymers, structure, processing, properties and industrial applications*. Oxford: Woodhead Publishing Limited, 2009; 211–26.
- [29] Olivia, Monita, and Hamid Nikraz. "Properties of fly ash geopolymer concrete designed by Taguchi method." *Materials & Design* 36 (2012): 191-198.
- [30] Popovics S., Simeonov Y., Bozhinov G., Barovsky N.; Durability of reinforced concrete in sea water. In: Crane AP, editor. *Corrosion of reinforcement in concrete construction*. Chichester: Elish Horwood Ltd., 1983; 19–37.

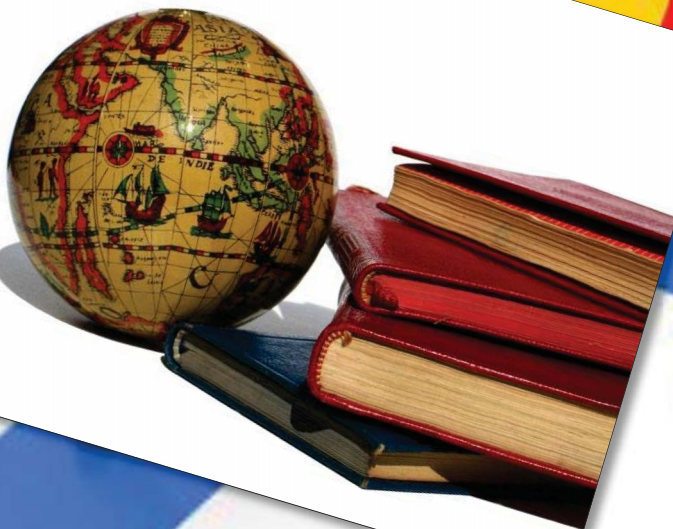
- [31] Wallah, S. E., and B. Vijaya Rangan. "Development and Properties of Low-Calcium Fly Ash-based Geopolymer Concrete." Res. Report-GC1, Curtin University, Australia (2005).
- [32] Sofi, M., et al. "Engineering properties of inorganic polymer concretes (IPCs)." *Cement and Concrete Research* 37.2 (2007): 251-257.
- [33] Diaz-Loya, Elvan, Erez N. Allouche, and Saiprasad Vaidya. "Mechanical properties of fly-ash-based geopolymer concrete." *ACI Materials Journal* 108.3 (2011): 300-306.
- [34] Palankar, Nitendra, AU Ravi Shankar, and B. M. Mithun. "Studies on eco-friendly concrete incorporating industrial waste as aggregates." *International Journal of Sustainable Built Environment* 4.2 (2015): 378-390.
- [35] Castel, Arnaud, and Stephen J. Foster. "Bond strength between blended slag and Class F fly ash geopolymer concrete with steel reinforcement." *Cement and Concrete Research* 72 (2015): 48-53.
- [36] Sarker, Prabir Kumar. "Bond strength of reinforcing steel embedded in fly ash-based geopolymer concrete." *Materials and structures* 44.5 (2011): 1021-1030.
- [37] Zain, Muhammad Fauzi Mohd, et al. "Prediction of splitting tensile strength of high-performance concrete." *Cement and Concrete Research* 32.8 (2002): 1251-1258.
- [38] Davidovits, Joseph. "Geopolymers." *Journal of thermal analysis* 37.8 (1991): 1633-1656.
- [39] Van Jaarsveld, Johan GS. "The physical and chemical characterisation of fly ash based geopolymers." (2000).
- [40] Davidovits, J., *Geopolymer Chemistry and Properties*. Proceedings of Geopolymer '88, First European Conference on Soft Mineralurgy, The Geopolymer Institute, Compiègne, France, 1988, pp. 25-48.
- [41] Rees, C., Lukey, G. C., and Van Deventer.; The role of solid silicates on the formation of geopolymers derived from coal ash, International Symposium of Research Students on Material Science and Engineering, India, December 2004, 20-22.

- [42] Lee, W. K. W., and JS J. van Deventer. "Effects of anions on the formation of aluminosilicate gel in geopolymers." *Industrial & engineering chemistry research* 41.18 (2002): 4550-4558.
- [43] Salih, Moslih Amer, Abang Abdullah Abang Ali, and Nima Farzadnia. "Characterization of mechanical and microstructural properties of palm oil fuel ash geopolymer cement paste." *Construction and Building Materials* 65 (2014): 592-603.
- [44] Temuujin, J., R. P. Williams, and A. Van Riessen. "Effect of mechanical activation of fly ash on the properties of geopolymer cured at ambient temperature." *Journal of Materials Processing Technology* 209.12 (2009): 5276-5280.
- [45] Partha, Sarathi Deb, Nath Pradip, and Kumar Sarker Prabir. "Strength and permeation properties of slag blended fly ash based geopolymer concrete." *Advanced Materials Research*. Vol. 651. Trans Tech Publications, 2013.
- [46] Giasuddin, Haider M., Jay G. Sanjayan, and P. G. Ranjith. "Strength of geopolymer cured in saline water in ambient conditions." *Fuel* 107 (2013): 34-39.
- [47] De Vargas, Alexandre Silva, et al. "The effects of Na<sub>2</sub>O/SiO<sub>2</sub> molar ratio, curing temperature and age on compressive strength, morphology and microstructure of alkali-activated fly ash-based geopolymers." *Cement and concrete composites* 33.6 (2011): 653-660.
- [48] Somna, Kiatsuda, et al. "NaOH-activated ground fly ash geopolymer cured at ambient temperature." *Fuel* 90.6 (2011): 2118-2124.
- [49] Zhang, Min-Hong, and Jahidul Islam. "Use of nano-silica to reduce setting time and increase early strength of concretes with high volumes of fly ash or slag." *Construction and Building Materials* 29 (2012): 573-580.
- [50] Riahi, Shadi, and Ali Nazari. "The effects of nanoparticles on early age compressive strength of ash-based geopolymers." *Ceramics International* 38.6 (2012): 4467-4476.
- [51] Phoo-ngernkham, Tanakorn, et al. "The effect of adding nano-SiO<sub>2</sub> and nano-Al<sub>2</sub>O<sub>3</sub> on properties of high calcium fly ash geopolymer cured at ambient temperature." *Materials & Design* 55 (2014): 58-65.





## Chapter- 2..



**REVIEW & LITERATURE**



## 2.0 General view

This chapter presents the background on the development of fly ash based geopolymer concrete in brief. This chapter also discusses the current research work on the development of modified geopolymer concrete and their application, including its structural behaviour and antibacterial activity such of concrete.

### 2.1 History of Geopolymer:

The term 'geopolymer' is coined in the 1970s by *Prof. Joseph Davidovits*, to describe a family of mineral binders with a chemical composition similar to zeolite but with an amorphous structure [1]. Geopolymers are a member of the family of inorganic polymers, and are a chain structures formed on a backbone of Al and Si ions. The polymerisation of on Si-Al minerals is a very fast chemical reaction in presence of highly alkaline condition, which forms a three dimensional polymeric chain and ring structure consists of Si-O-Al-O [2]. The three known chemical units in the geopolymer structure are: (i) Si-O-Al-O, or polysialate group, (ii) Si-O-Al-O-Si-O, or poly (sialate - siloxo) group, and (iii) Si-O-Al-O-Si-O –Si-O, or poly (sialate – disiloxo) group [3]. This polymeric chain binds the inert aggregate to form geopolymer concrete.

#### 2.1.1. Source Materials:

This inorganic polymer cements is synthesised by alkali activation of any materials that contains Silicon (Si) and Aluminium (Al) in amorphous form to produce an alternative of Portland cement [4]. Several minerals and industrial by-product materials have been investigated in the last two decades. Metakaolin or Calcined Kaolin, ASTM Class F fly ash, GGBFS, natural Al-Si minerals, combination of calcined mineral and non calcined materials, combination of fly ash and metakaolin, and combination of granulated blast furnace slag and metakaolin are generally investigated as source materials [5 - 10]. The research works relate to other source materials used in geopolymer composites are now discussed.

Besides the above mentioned materials, a new type of geopolymer composite is synthesized from industrial wastes, red mud (RM) and rice husk ash (RHA), at varying mixing ratios of raw materials. Strength, stiffness and ductility of this geopolymer composite showed better performance at higher rice husk ash to red mud ratios. The compressive strength ranges

from 3.2 to 20.5 MPa for the synthesized geopolymer with nominal Si/Al ratios of 1.68–3.35. Microstructural and compositional analyses by X-ray Diffraction (XRD) and Field Emission Scanning Electron Microscope (FESEM), showed that the final products are mainly composed of amorphous geopolymer binder with both inherited and neo-formed crystalline phases as fillers [11].

*Hajjaji et al.* (2013) developed an innovative geopolymer by alkali activation of metakaolin along with iron oxide and red mud mixtures. The presence of red mud will not affect the physical properties of geopolymer, as geopolymer samples exhibited high values of water absorption and low apparent density. The mechanical strength of such geopolymer was influenced by the presence red mud in the geopolymer mix [12].

*R. H. Kupaie et al.* (2013) established the light weight geopolymer concrete, which was synthesised from locally available waste materials such as fly ash (FA) and oil palm shell (OPS) [13]. Compressive strength of such fly ash based oil palm shell geopolymer lightweight concrete was influenced by processing parameters such as quantity of fly ash, fly ash /sand/oil palm shell ratio, dosage of alkaline activator and amount of water in the mixture. The density of oil palm shell geopolymer concrete was about 1800 kg/m<sup>3</sup> can be produced using the waste material OPS as light weight aggregate. It was also observed that the OPS based geopolymer concrete showed improved compressive strength at higher molar concentration of alkali activator.

The reactivity of volcanic ashes enhanced by alkali fusion and balancing the Na/Al ratio through metakaolin addition has been used as an alternative geopolymer material was reported by *H. T. Kouamo et al.* (2013) [14]. XRD pattern of fused volcanic ash showed that the presence of significant amount of muscovite, anorthoclase and diopside that were converted into soluble alumino-silicates and enhanced the geopolymerisation process. However, the addition of metakaolin with fused volcanic ash geopolymer mortars exhibited low setting time, low shrinkage and high compressive strength.

*Yang et al.* (2008, 2009) produced geopolymer concrete by using recycled aggregates as partial replacement for the fresh ones and mixture of waste concrete powder and metakaolin along with silica fume as the source materials for the geopolymeric binder. Their study

indicated that the content of metakaolin and silica fume and the rise in alkalinity lead to increase in compressive strength [15, 16].

*Allahverdi and Kani (2009)* investigated the geopolymerization of a mixture of finely ground waste brick and concrete in different mix proportions. They demonstrated that the presence of higher finely ground brick content and higher alkalinity of activated fluid in the geopolymer concrete resulted in stronger geopolymeric binder [17].

The ground waste concrete (GWC) and class F fly ash (FA) was used to develop an innovative geopolymeric binder. The addition of GWC up to 50 % increased the compressive strength of such modified geopolymer concrete. The geopolymer concrete with 1:1 ratio of ground waste concrete (GWC) and fly ash content with 10 molar NaOH activated solution showed better compressive strength. The SEM with EDX, XRD and FTIR analyses of such geopolymer concrete confirmed the presence of calcium in GWC that enhances the strength. The strength enhancement was mainly due to the formation of low calcium semi-crystalline CSH gel which was coexisted with the geopolymer gel and the incorporation of  $\text{Ca}^+$  into the geopolymer network [18].

*A. N. Murri et al. (2015)* reported about the acid or alkali activation of metakaolin, calcium phosphate and alumino - silicate compounds based vegetal, animal biomass ashes used as an innovative geopolymer composites [19]. It was observed that alkaline calcium alumino-silicate gels coexisted and embedded the calcium phosphate crystalline phases in the geopolymer matrix due to alkali activation of such biomass ashes based geopolymer composite. The composite exhibited higher mechanical strength. Although, it was reported that biomass ashes based geopolymer composite showed lower water and environmental stability in the long run, due to the effect of carbonation of Ca-based binding phases and subsequent dissolution of derived water soluble salts.

The geopolymer mortar synthesised from heat activation of volcanic scoria and kaolin in presence of alkaline solution (mixture of NaOH and  $\text{Na}_2\text{SiO}_3$ ). It was reported that the presence of the volcanic scoria in the geopolymer mortar enhanced the degree of geopolymerization and increased the compressive strength [20].

### 2.1.2 Activator solution:

Activator solution played an important role for the development of strength and durability of geopolymer concrete. Sodium hydroxide (NaOH) and sodium silicate ( $\text{Na}_2\text{SiO}_3$ ) solution are the most common alkali activator used for geopolymerisation [2]. Although potassium hydroxide (KOH) and potassium silicate ( $\text{K}_2\text{SiO}_3$ ) have been used as an activator fluid by several researcher [21, 22].

*Palomo et al.* (1999) reported that geopolymeric reactions occur at a high rate when the alkaline activator contains soluble silicate, either sodium or potassium silicate, compared to the use of only alkaline hydroxides [7]. The addition of sodium silicate solution to the sodium hydroxide solution as the alkaline activator enhanced the reaction between the source material and the solution. Furthermore, after a study of the geopolymerisation of sixteen natural Al-Si minerals, they found that generally the NaOH solution caused a higher extent of dissolution of minerals than the KOH solution.

*Palomo et al.* (1999) also reported the mechanism of activation of fly ash with highly alkaline solution of sodium hydroxide (NaOH), potassium hydroxide (KOH) and water glass and their combinations [23]. Fly ash activated with 8 – 12 molar concentration of NaOH solution, cured at 85°C for 24 hours produced the geopolymer composite with a compressive strength between 35 and 40 MPa, this strength can be increased to nearly 90 MPa with the addition of water glass to the NaOH ( $\text{SiO}_2 / \text{Na}_2\text{O} = 1.23$ ).

Molar concentration of sodium hydroxide and the ratio of NaOH to  $\text{Na}_2\text{SiO}_3$  are the important aspect for the development of geopolymer mortar/ concrete. *Hardjito et al.* (2005) reported that compressive strength is increased at higher molar concentration of NaOH and higher ratio of  $\text{Na}_2\text{SiO}_3/\text{NaOH}$  [24].

*Xu and van Deventer* (2000) reported that the proportion of alkaline solution to alumino-silicate powder by mass should be approximately 0.33 to allow the geopolymeric reactions to occur. Alkaline solutions formed a thick gel instantaneously upon mixing with the alumino-silicate powder. Geopolymer mortar specimen of 20 × 20 × 20 mm size showed the maximum compressive strength achieved was 19 MPa after 72 hours of curing at 35°C [25].

Similarly, *Chindaprasirt et al.* (2007) reported that the use of a low NaOH concentration of 5 M gives geopolymer mortars with relatively low strength about 24 MPa. Higher strengths of 35 and 33 MPa are obtained with the use of 10M and 15M NaOH at NaOH to Na<sub>2</sub>SiO<sub>3</sub> ratio 1.50 [26].

The compressive strength of kaolin based geopolymers depends on solid to liquid ratio and Na<sub>2</sub>SiO<sub>3</sub> / NaOH ratio. It was reported that the solid to liquid ratio of 1.00 and Na<sub>2</sub>SiO<sub>3</sub> / NaOH ratio of 0.32 were the optimum ratios for kaolin based geopolymers. It exhibited maximum compressive strength when Al<sub>2</sub>O<sub>3</sub> / Na<sub>2</sub>O and SiO<sub>2</sub> /Na<sub>2</sub>O ratio were 1.09 and 3.58 respectively [27].

*Van Jaarsveld et al.* (1998) reported that the mass ratio of the solution to the powder of about 0.39 of a geopolymer matrix showed the maximum compressive strength [28]. The compressive strength of geopolymer mortar cube specimen of size of 50 × 50 × 50 mm with 57 % fly ash and 15 % showed 75 MPa.

*G. S. Ryu et al.* (2013) reported that geopolymer concrete delivered high early strength at higher molar concentration of 9M and 12M NaOH alkali activator solution [29]. The geopolymer concrete showed a remarkable compressive strength development at the NaOH to Na<sub>2</sub>SiO<sub>3</sub> ratio of 1: 1 and SiO<sub>2</sub> to Na<sub>2</sub>O ratio of 8.0.

*G. Görhan and G. Kürklü* (2014) reported that geopolymer concrete activated with 6M NaOH and cured at 65°C showed better compressive strength than geopolymer concrete activated with 9M NaOH solution and cured at 85°C. The reductions in the strength values of the samples activated with 9 M NaOH due to increase in the coagulation of silica [30].

*Barbosa et al.* (2000) reported that the geopolymeric reaction of metakaolinite with sodium silicate solution in a highly alkaline environment with Al: Si ratio of 1: 2, showed crushing compressive strength of 48.1 MPa [31].

*Rahim et al.* (2015) reported that geopolymer samples using sodium hydroxide (NaOH) exhibited the higher compressive strength compared to KOH without addition of silicate solution. The highest compressive strength obtained for NaOH is 65.28 MPa while KOH recorded 28.73 MPa. It was also reported in FESM study that NaOH produced more crystalline structure in a well-structured form compared to KOH [32].

### 2.1.3 Curing Conditions:

Heat activation is a much desirable activity for geopolymerization for the development of strength of geopolymer concrete. Most of the research works on fly ash based geopolymer are on the mix proportion and strength variation of geopolymer concrete cured at different temperatures. The compressive strength of heat cured geopolymer concrete is generally higher than normal temperature geopolymer concrete. At early age within 7 days, heat cured geopolymer concrete achieved maximum compressive strength, whereas the compressive strength of normal temperature cured geopolymer concrete increased after 7 days to 28 days [33, 34].

*Chindaprasirt et al.* (2013) established that microwave radiation effectively enhanced the geopolymerization of fly ash based geopolymer mortar. Early-stage of microwave radiation promoted the dissolution of Si and Al species and enhanced the gel formation of geopolymer and stimulated the breaking of hydrogen bonds in water molecules. The microwave radiation (98W) for 5 min followed by 6.0 hour at 60°C resulted in the densification of the matrices and increase in the bulk density and compressive strength of the samples. The micro wave radiation followed by conventional heat curing reduced the heat curing time and energy [35].

*Bakharev* (2005) reported the influence of elevated temperature curing types of activator on phase composition, microstructure and strength development in geopolymer materials using Class F fly ash and sodium silicate and sodium hydroxide solutions [36]. Long pre-curing of geopolymer concrete / mortar at room temperature before application of heat was beneficial for strength development than 1 month of curing at elevated temperature. The importance of elevated temperature curing particularly for the samples exposed to 2 to 5 hours curing, where a significant increase in strength was observed at 85°C as compared to 65°C. Also, this study investigated of the effect of different curing regimes and types of activator on the strength development and hydration products of fly ash activated by alkali activated solution.

*Hardijito and Rangan* (2004) observed that heat curing at higher temperature increased the compressive strength of geopolymer concrete up to 60°C, beyond this temperature did not increase the compressive strength. It was also reported that heat activation of geopolymer concrete at 60°C for 24 hours showed optimum strength development [37]. Similarly, *Škvára*



*et al.* (2005) reported alkali activated geopolymer concrete achieved the maximum of strength after 6 – 12 hours of heat activation at a temperature of 60 - 80°C [38].

*J.C. Swanepoel et al.* (2002) conveyed that the compressive strength of geopolymer concrete after 28 days of curing (Fig. 2.1) indicated that the geopolymerization reaction occurred in the samples heated to 60 and 70°C for 48 hours, as the sample remained at the same strength after heating for longer time periods of 72 hours. Also, to the samples heated at the lower temperatures, 40°C and 50°C showed a decrease in strength for longer heating times. The changes that occurred in the samples heated at 40 and 50°C seems to be the result of mainly physical changes, while changes in the samples heated at 60 and 70°C seem to be more of a permanent chemical nature [8].

*Mishra et al.* (2008) reported that compressive strength of geopolymer concrete was increased with the increase of curing time 24 to 48 hours at 60°C. It was also reported that when curing time further increased from 48 hours to 72 hours, no significant variation in compressive strength was observed (Fig 2.2) [39].

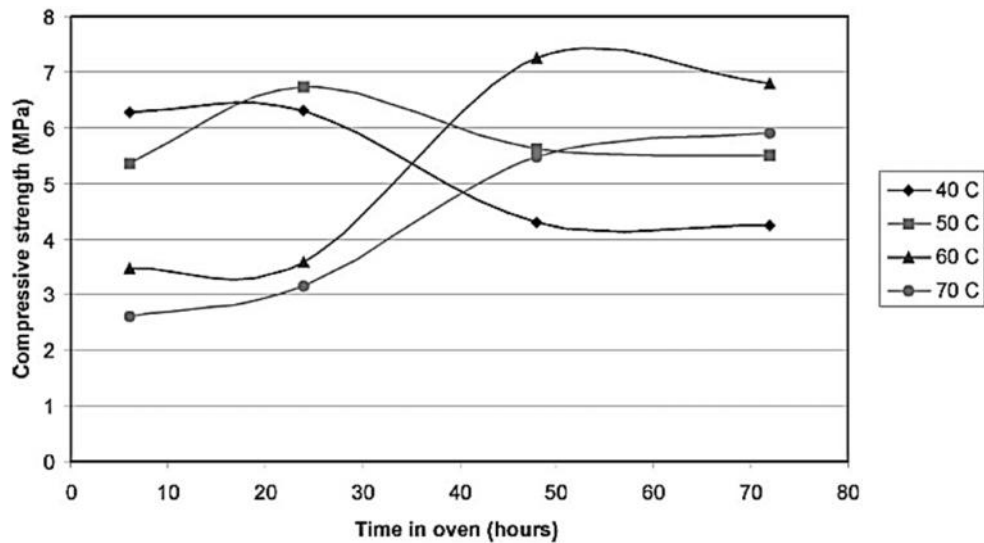


**Figure – 2.1: Compressive strength of geopolymer concrete after 28day at different temperature (Swanepoel, 2002).**

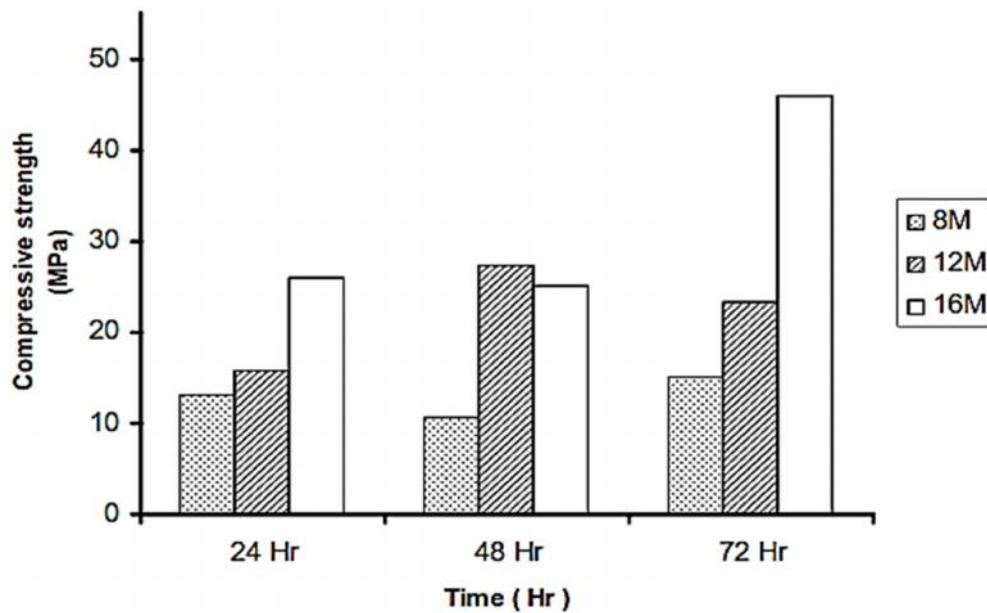


Figure – 2.2: Variation of compressive strength with curing time (*Mishra, 2008*).

## 2.2 Current trend of research on fly ash based geopolymer concrete:

Towards the beginning of 21<sup>st</sup> century, the most of research works on geopolymer concrete are on the mix proportion, molar concentration, curing time and compressive strength only [23 – 40]. However, studies on the engineering properties of geopolymer concrete for practical application is very limited. In order to use geopolymer concrete in structural engineering applications, a comprehensive evaluation of these properties is essential.

### 2.2.1 Properties fresh and hardened geopolymer concrete:

It is already reported in previous studies that there are so many parameters that influenced the compressive strength of heat activated geopolymer concrete. Beside the compressive strength further studies conducted by several researcher on compressive strength, elastic constant, stress strain behaviour, split tensile strength, bond strength and the behaviour of heat activated reinforced geopolymer concrete beams and columns etc.

*Sathonsaowaphak et al.* (2009) reported that workability of lignite bottom ash geopolymer concrete was more at low sodium silicate/sodium hydroxide ratios of 0.4 – 1.5 (Fig 2.3) [41].

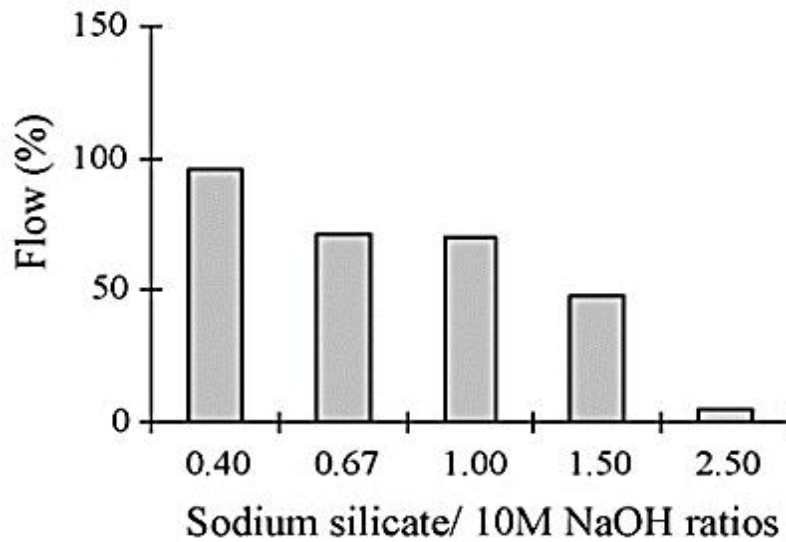


**Figure – 2.3: Workability of lignite bottom ash geopolymer concrete at different sodium silicate to 10M sodium hydroxide ratio (Sathonsaowaphak, 2009).**

Partha Sarathi Deb *et al.* (2014) noticed that the spherical shape of fly ash particles combined with lubricating effect of the alkaline activator solution showed flow ability of the fresh geopolymer concrete [42]. The use of the sodium silicate ( $\text{Na}_2\text{SiO}_3$ ) and sodium hydroxide (NaOH) solutions, which were more viscous than water, usually makes geopolymer concrete more cohesive and sticky than OPC concrete. However, a higher slump of geopolymer concrete indicated a less stickiness and higher workability of the mixture. It was also reported that the geopolymer mixture R2.5S20 with 20% slag and 80% fly ash showed a slump value of 195 mm as compared to 250 mm slump showed by the mixture of 90% fly ash and 10% slag (Fig 2.4).

Nguyen Van Chanh *et al.* (2008) reported that the setting time of geopolymer mortar depends on many factors such as types of fly ash, composition of alkaline liquid and ratio of alkaline liquid to fly ash by mass [43]. Figure 2.5 showed the effect of curing temperature on setting time. As the curing temperature increased, the setting time decreased. The effect of curing temperature on initial setting and final setting time was similar to setting time.

Hardjito *et al.* (2005) reported that the slump value decreased when the mixing time increased (Fig 2.6). Longer mixing time produced higher compressive strength and higher density. This suggests that the extended mixing time resulted in better polymerisation process, and hence enhanced properties of hardened concrete [44].

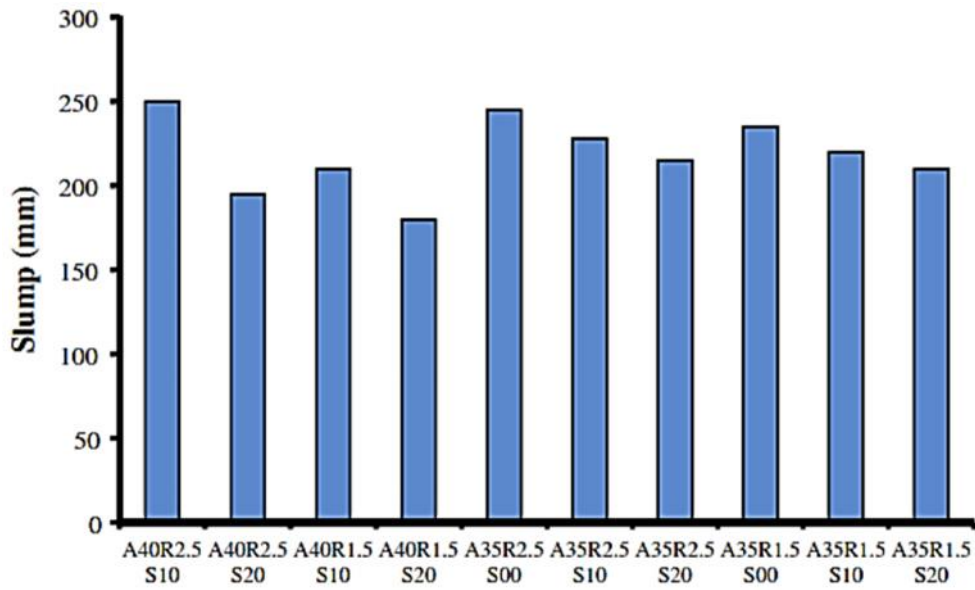


Figure – 2.4: Slump of different geopolymer concrete with different slag content (Deb, 2014).

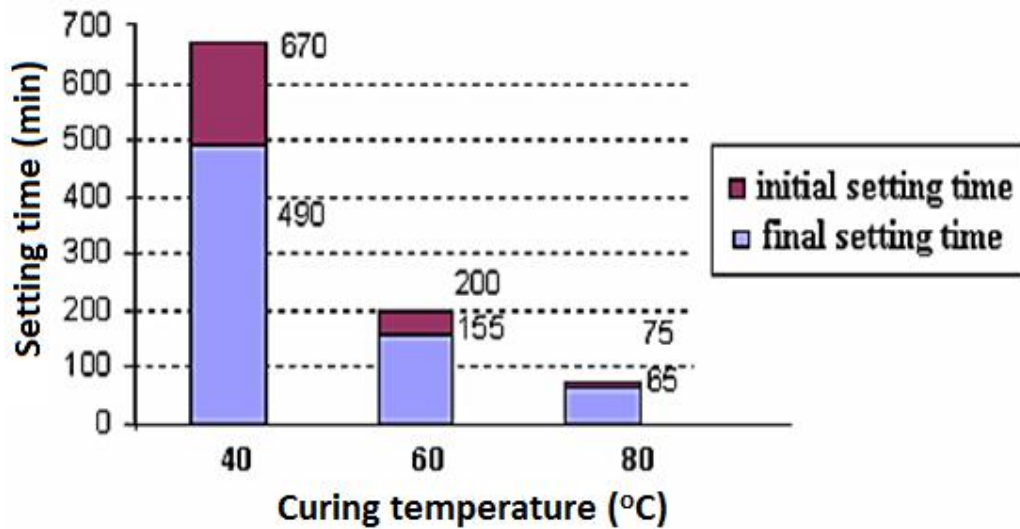


Figure – 2.5: Effect of curing temperature on setting time of geopolymer concrete (Chanh, 2008).

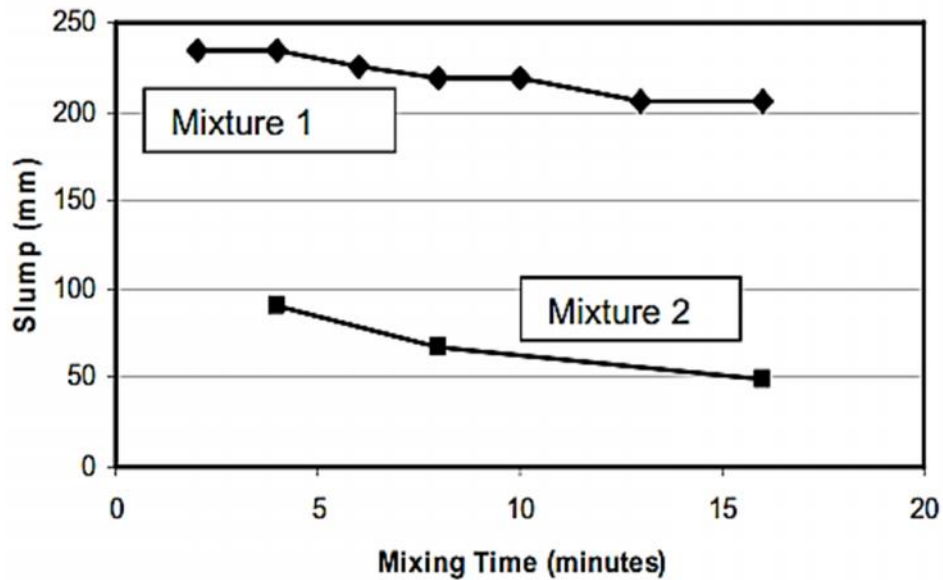


Figure – 2.6: Mixing time vs. slump value of geopolymer concrete (Hardjito, 2005).

### 2.2.1.1 Compressive strength:

The compressive strength of conventional Portland cement based concrete is the most important parameter in the mix design of concrete. The target compressive strength of conventional concrete depends upon the cement content and water / cement ratio of the mix. Similarly, compressive strength of geopolymer mortar/concrete depends upon several factors such as fluid / fly ash ratio, molar concentration of NaOH, NaOH / Na<sub>2</sub>SiO<sub>3</sub> ratio, heat activation time and temperatures, mix proportion etc.

Higher concentration (in terms of molar) of sodium hydroxide solution results in higher compressive strength of geopolymer concrete. Chindapasirt *et al.* (2009) showed that heat cured geopolymer concrete at low NaOH concentration of 5M reached 24 MPa compressive strength, whereas higher compressive strength of 35 and 33 MPa obtained with the use of 10M and 15M NaOH solution respectively (Fig 2.7). It was also reported that at higher molar concentration of NaOH fly ash based geopolymer concrete showed maximum compressive strength than that of bottom ash geopolymer concrete [45].

Palomo *et al.* (1999) reported that higher molar concentration (up to 12M) of alkali activator solution increased the geopolymerisation process and subsequently increased compressive strength [23]. Similarly, Alvarez-Ayuso *et al.* (2008) reported higher compressive

strength values were attained at curing time of 48 h, having curing temperature of 80°C and 12M NaOH solutions as activation media (Fig 2.8) [46].

The higher the ratio of sodium silicate to sodium hydroxide solution and solid to liquid ratio of activated fluid by mass, the higher the compressive strength of geopolymer concrete [47].

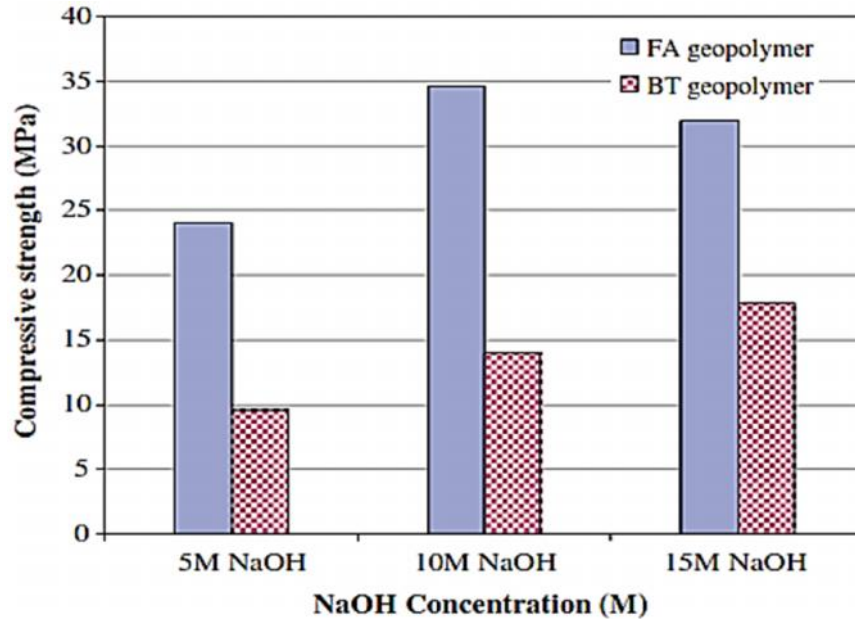


Figure – 2.7: Compressive strength of fly ash and bottom ash based geopolymer at different molar concentration (Chindaprasirt, 2009).

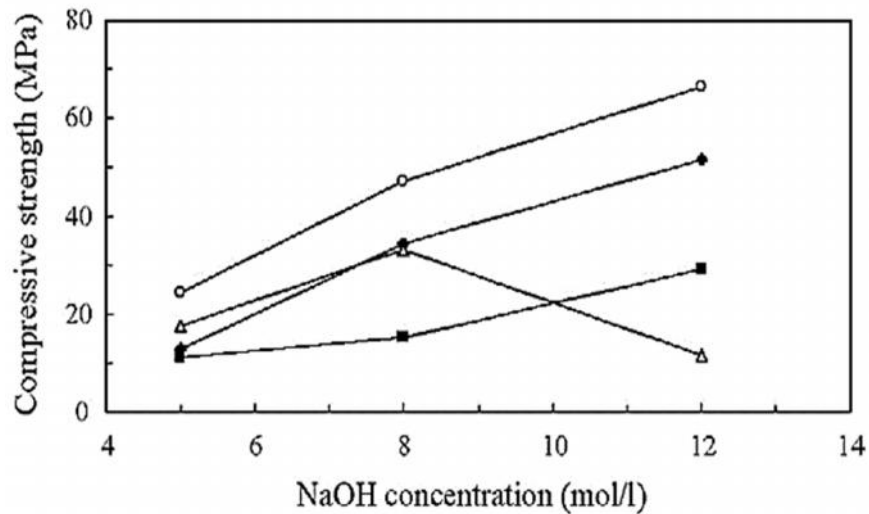


Figure – 2.8: Compressive strength of based geopolymer at different molar concentration (Ayuso, 2008).

Chindaprasirt *et al.* (2007) reported that compressive strength of geopolymer mortar with sodium silicate to sodium hydroxide ratio of 0.67 and 1.00 were significantly higher than  $\text{Na}_2\text{SiO}_3 / \text{NaOH}$  ratio of 1.5 and 3.0. The variation in the ratio of sodium silicate to sodium hydroxide ratio affects the pH conditions and affects on the strength development of the geopolymer mortar [26] (Fig 2.9).

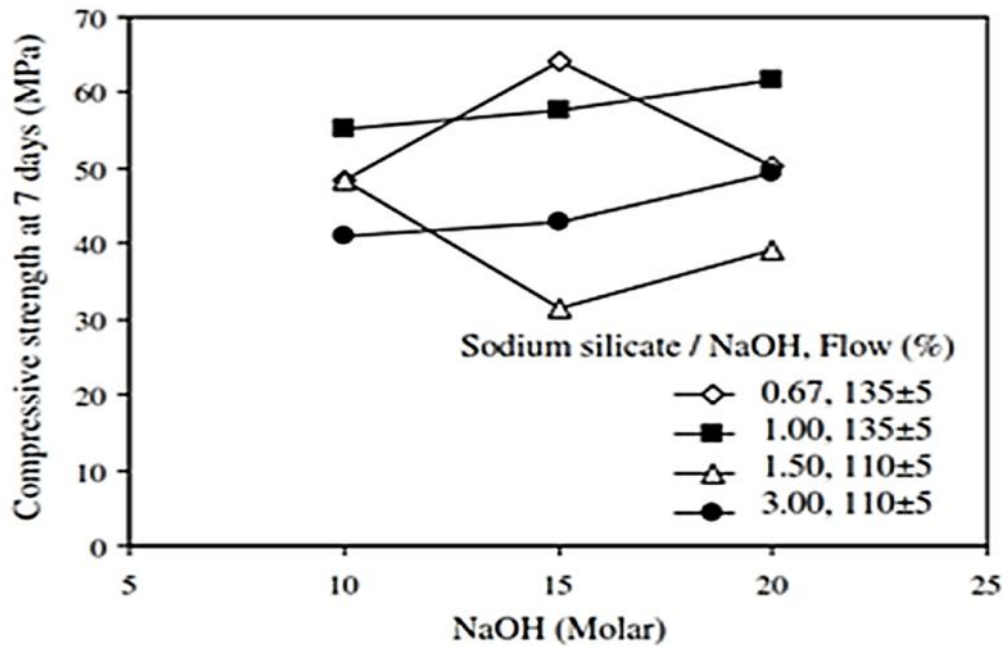


Figure – 2.9: Compressive strength of geopolymer concrete at different molar concentration (Chindaprasirt, 2007).

Salih *et al.* (2014) showed the relation between compressive strength and solid to liquid ratio of geopolymeric mixes. The compressive strength was increased by increasing the sodium silicate ( $\text{Na}_2\text{SiO}_3$ ) to sodium hydroxide ( $\text{NaOH}$ ) ratio. The increment in the  $\text{Na}_2\text{SiO}_3/\text{NaOH}$  ratio increased the amount of sodium silicate in the activator solution and increased geopolymerization (Fig 2.10). The maximum compressive strength observed at sodium silicate to sodium hydroxide ratio of 2.50 [48]. Sathonsaowaphak *et al.* (2009) observed compressive strength of geopolymer mortar increased up to sodium silicate to  $\text{NaOH}$  ratio of 1.5 (Fig 2.11) [41].

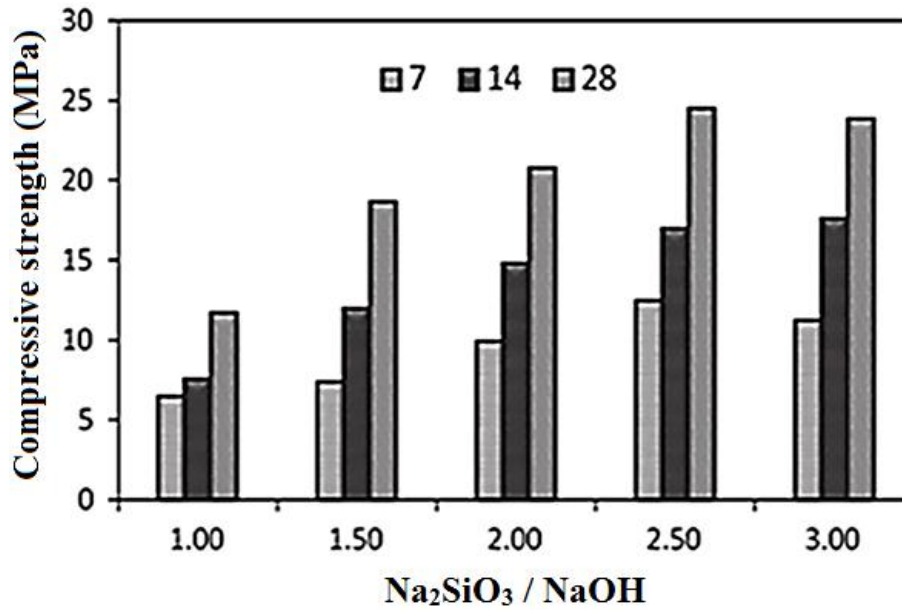


Figure – 2.10: Compressive strength of geopolymer concrete at different SS/SH ratio (Salih, 2014).

The compressive strength of geopolymer concrete also depends on  $\text{H}_2\text{O}$  to  $\text{Na}_2\text{O}$  molar ratio. Barbosa *et al.* (1999) reported that the compressive strength of geopolymer concrete was decreased with the increase of  $\text{H}_2\text{O}$  to  $\text{Na}_2\text{O}$  molar ratio [49, 50].

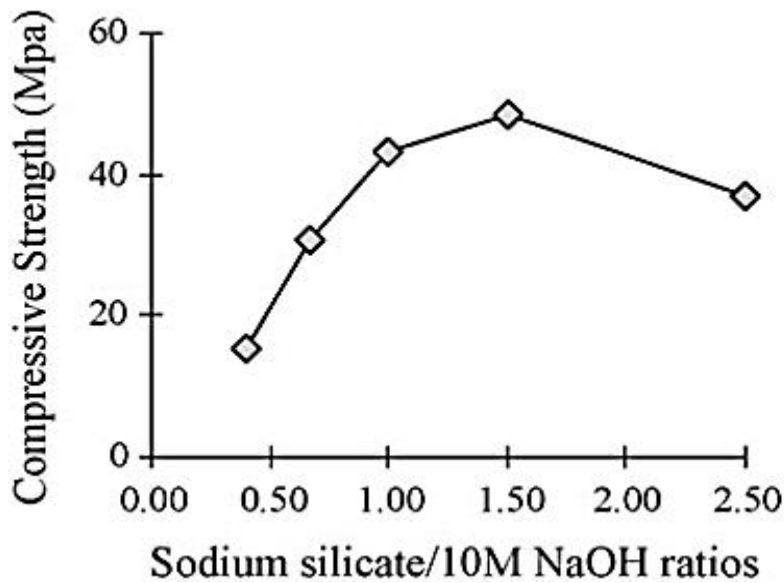


Figure – 2.11: Compressive strength of bottom ash geopolymer mortar (Sathonsaowaphak, 2009).



Longer curing time and higher curing temperature increases the compressive strength of geopolymer concrete. *Palomo et al.* (1999) reported compressive strength of geopolymer cured at 85°C was higher than the samples cured at 65°C. Longer curing time of the samples showed maximum average compressive strength [23]. Geopolymer concrete cured at 40°C disclosed very low compressive strength due to slow polymerisation process. Curing time played a positive role on the compressive strength performance of geopolymer concrete. Geopolymer concrete heat cured at 80°C for 24h showed optimum compressive strength [46]. *Rovnaník* (2012) reported that compressive strength of geopolymer concrete was the function of curing temperature and curing time (Fig 2.12). Geopolymer concrete cured at 60°C and 80°C showed better compressive strength than geopolymer concrete cured at 40°C for 4h [51].

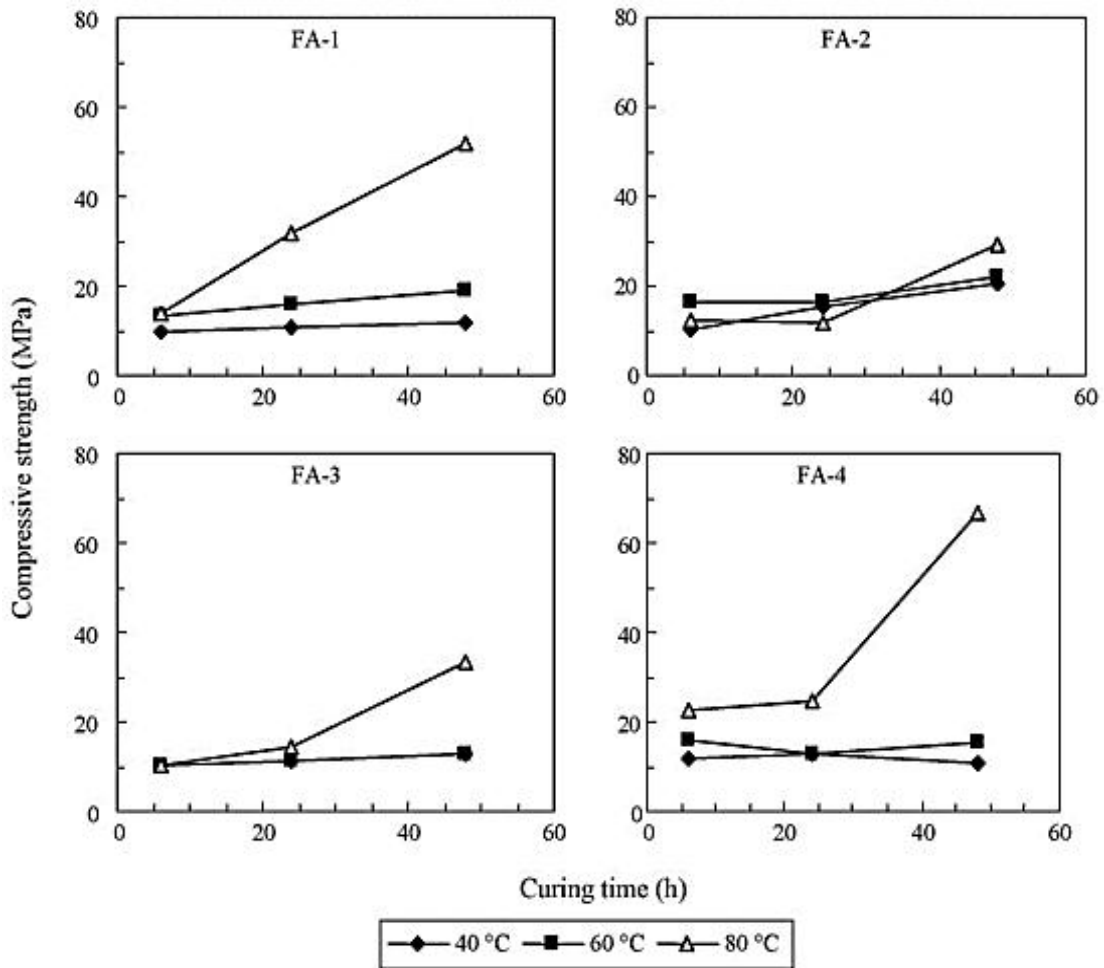


Figure – 2.12: Compressive strength of geopolymer at different curing temperature and curing time (*Rovnaník, 2012*).

### 2.2.1.2 Modulus of elasticity:

The modulus of elasticity of concrete is a function of the modulus of elasticity of the aggregates and the cement matrix and their relative proportions. To design concrete structures, the elastic modulus  $E_c$  is a fundamental parameter that needs to be defined. *Hardjito et al.* (2004) reported the stress-strain relations of fly ash based geopolymer concrete and compared with OPC concrete [52].

*Sofi et al.* (2007) reported that the compressive strength ( $f_{cm}$ ) and density ( ) of geopolymer concrete had an influence on the modulus of elasticity (Fig 2.13). They have reported an empirical relations as given in Eq. (1) and Eq. (2). The modulus of elasticity of geopolymer concrete was determined by the Eq. (1) for compressive strength  $f_{cm} < 40$  MPa and Eq. (2) for  $f_{cm} > 40$  MPa based on Figure 2.13 [53].

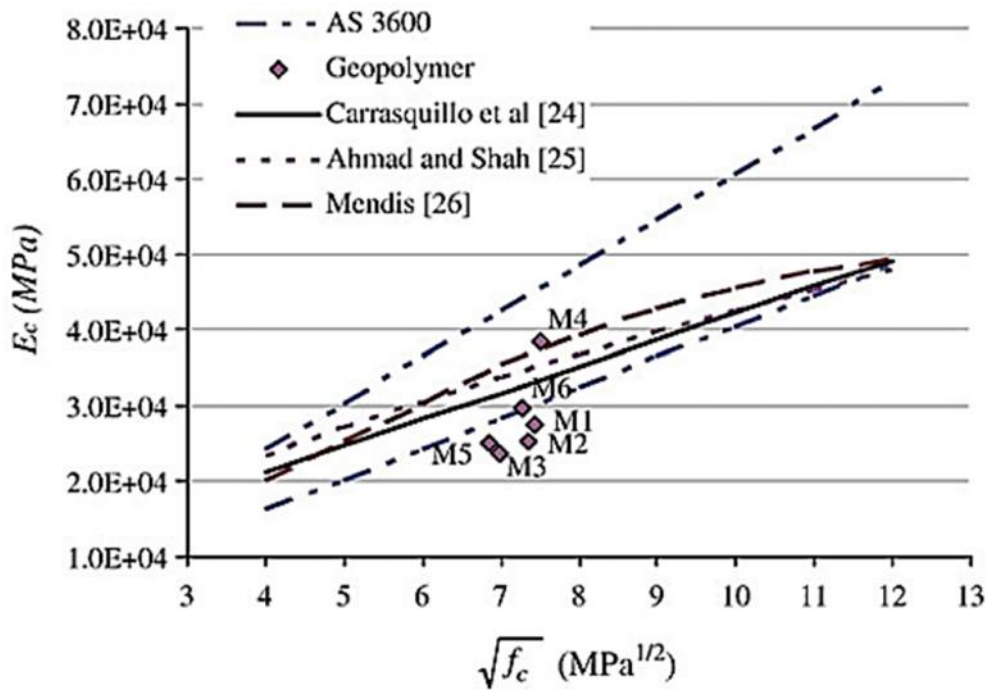


Figure – 2.13: Modulus of elasticity of geopolymer concrete (*Sofi, 2007*).

$$E_c = 0.0 \times \rho^{1.5} \times \sqrt{f_c} \pm 2 \% \dots\dots\dots(1)$$

$$E_c = [ 0.0 \times \sqrt{f_c} + 0.1 ] \rho^{1.5} \dots\dots\dots(2)$$

*Olivia et al.* reported that modulus of elasticity of fly ash geopolymer concrete designed by **Taguchi method** are 14.9 – 28.8% lower than that of conventional cement concrete. It was also reported that higher silicate content in the geopolymer concrete mix increase the modulus of elasticity [54]. *Zejak et al.* (2013) conveyed that modulus of elasticity of geopolymer paste/mortar was related to the molar concentration of NaOH solution and compressive strength of the sample. The geopolymer paste/mortar showed maximum Young’s modulus of elasticity using 10 M NaOH solution. The modulus of elasticity was reduced with the increase at the alkaline dosage of 13 M NaOH (Fig 2.14). It was also reported that geopolymer paste/mortar achieved the maximum value of the Young’s modulus at the  $\text{Na}_2\text{SiO}_3 / \text{NaOH}$  ratio of 1.5 (Fig 2.15) [55]. *Ganesan et al.* (2014) reported that the modulus of elasticity of geopolymer concrete was 50% higher than PCC of similar compressive strength [56].

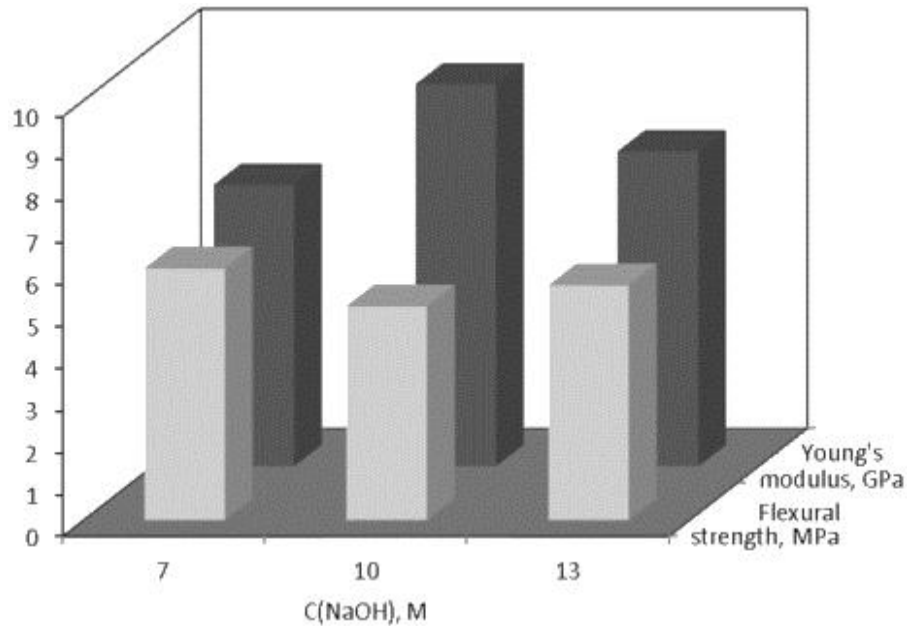


Figure – 2.14: Modulus of elasticity as a function of NaOH Concentration (*Zejak, 2013*).

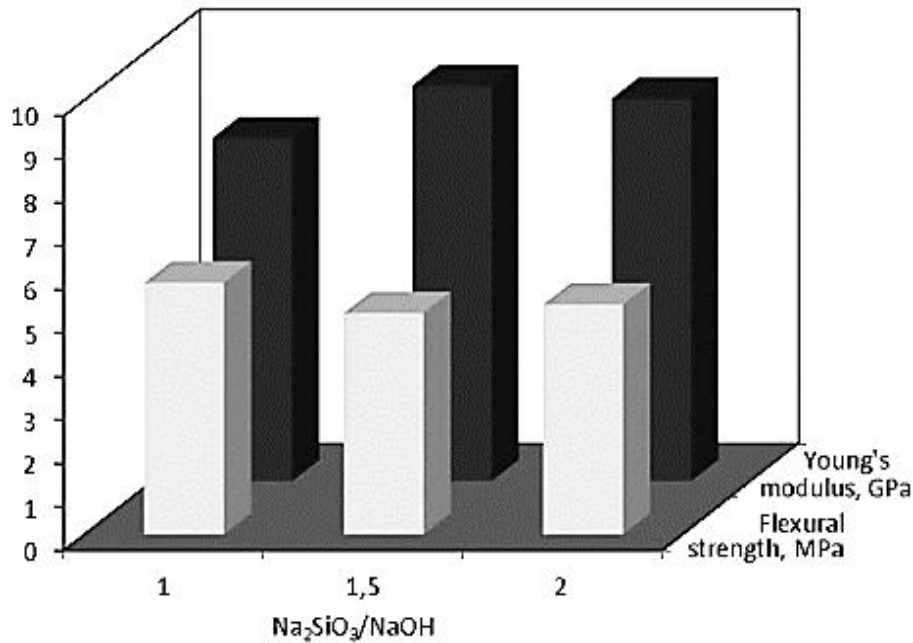


Figure – 2.15: Modulus of elasticity as a function of Na<sub>2</sub>SiO<sub>3</sub>/NaOH ratio (Zejak, 2013).

### 2.2.1.3 Tensile strength:

The tensile strength is one of the basic and important properties of the concrete. The concrete is not usually expected to resist the direct tension because of its low tensile strength and brittle nature. However, the determination of tensile strength of concrete is necessary to determine the load at which the concrete members may crack. The cracking is a form of tension failure.

The tensile splitting strength (indirect tensile strength) of geopolymer concrete is only a fraction of the compressive strength, as in the case of Portland cement concrete [24]. It was also reported that indirect tensile strength of fly ash-based geopolymer concrete is larger than the values recommended by the draft Australian Standard AS3600 (2005) and Neville (2000) for Portland cement concrete. Several researcher proposed the empirical formula to express the relationship between compressive strength and split tensile strength.

$$f_s = k \times f_c^n \dots\dots\dots (3)$$

Where  $f_{sp}$  was split tensile strength (MPa),  $f_c$  the compressive strength of concrete (MPa) and  $k$  and  $n$  were constant. Based on the above basic equation, ACI and CEB-FIP suggested the equation (4) and (5) to formulate the relationship between compressive strength

and split tensile strength of conventional cement concrete [57, 58]. In addition, several researchers have proposed other formulae on geopolymer concrete in the form of equation (6)–(8) to express this relationship [59, 60]:

$$\text{ACI363R-92: } f_s = 0.5 \sqrt{f_c} \dots\dots\dots (4)$$

$$\text{CEB-FIP: } f_s = 0.3 \times f_c^{0.6} \dots\dots\dots (5)$$

$$\text{Gardner et al: } f_s = 0.6 \times f_c^{2/3} \dots\dots\dots (6)$$

$$\text{Raphael et al: } f_s = 0.2 \times f_c^{0.7} \dots\dots\dots (7)$$

Sarkar (2011) reported that split tensile strength of fly ash based geopolymer concrete was higher than OPC concrete of same compressive strength (Fig 2.16). The reason behind higher split tensile strength was due to the use of soluble silicates in geopolymers producing a denser Interfacial Transition Zone (ITZ) between aggregates and geopolymer matrix as compared to that with cement matrix [61].

$$\text{Ryu et al: } f_s = 0.1 \times f_c^{3/4} \dots\dots\dots (8)$$

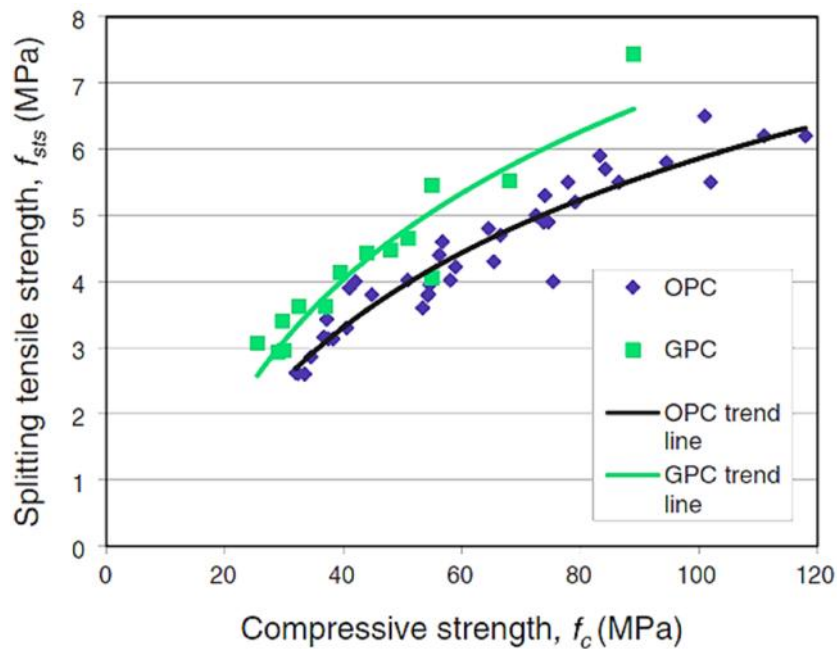
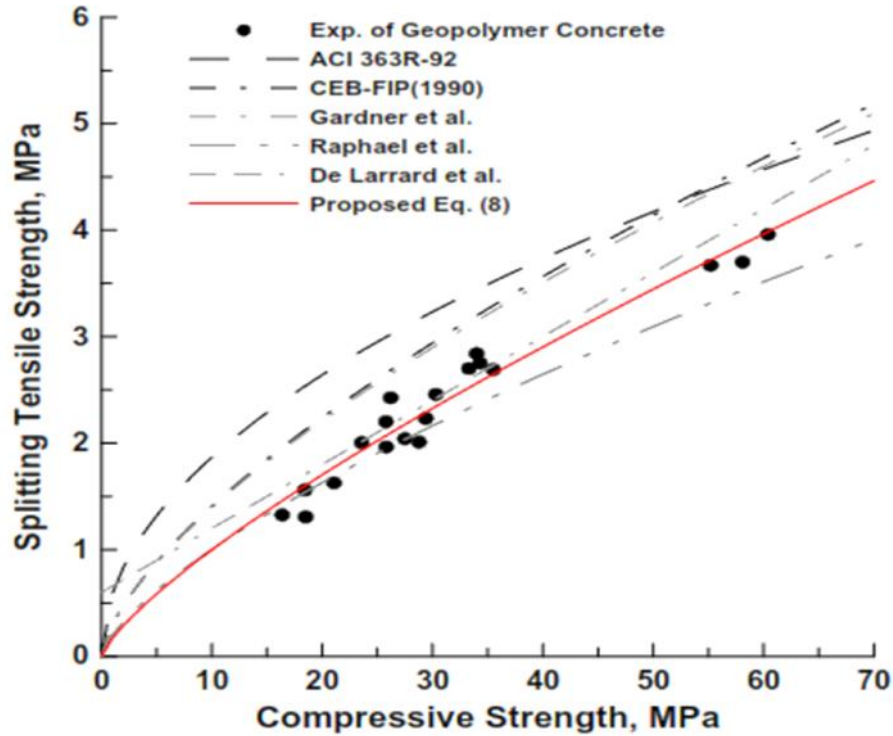


Figure – 2.16: Split tensile strength with compressive strength of GPC (Sarkar, 2011).

Ryu *et al.* (2013) reported a model to describe the relationship between compressive strength and split tensile strength of geopolymer concrete with the mix of 9 M NaOH and sodium silicate at mass ratio of 1:1 and cured at 60°C for 24h (Fig 2.17 & Eq. 8) [29].



**Figure – 2.17: Relation between compressive strength and split tensile strength of concrete (Ryu, 2013).**

Yellaiah *et al.* (2014) conveyed that direct tensile strength of geopolymer mortar cured at 30°C and 60°C was 0.11 and 0.14 times of compressive strength at activator liquid to fly ash ratio of 0.30. It was also reported that the tensile strength of geopolymer mortar was more at lower curing temperature and was less for higher curing temperature for lower activator fly ash ratio due to insufficient alkaline liquid for complete polymerization (Fig 2.18 & 2.19) [62].

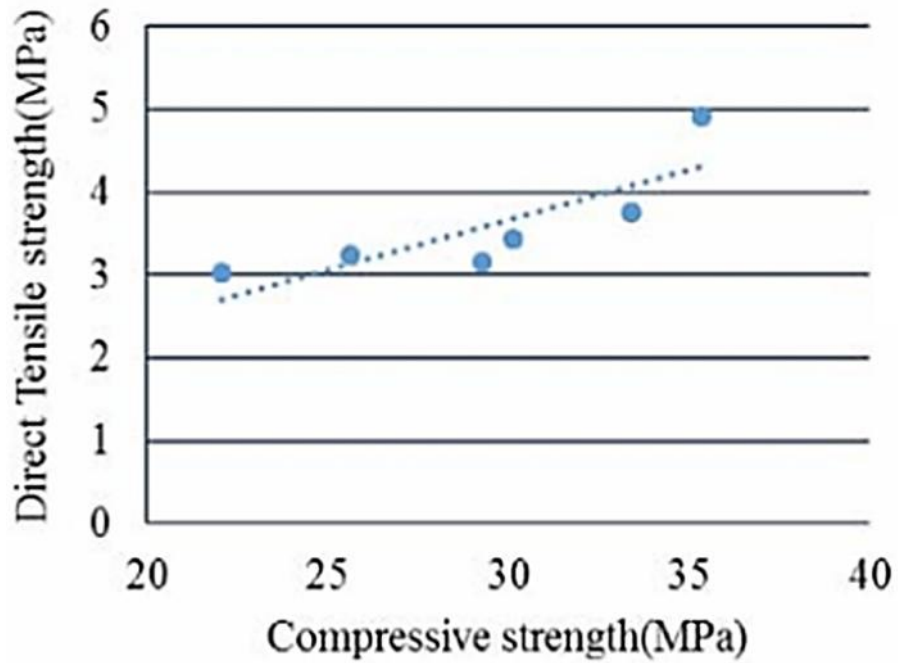


Figure – 2.18: Variation of direct tensile strength with compressive strength of geopolymer (Yellaiah, 2014).

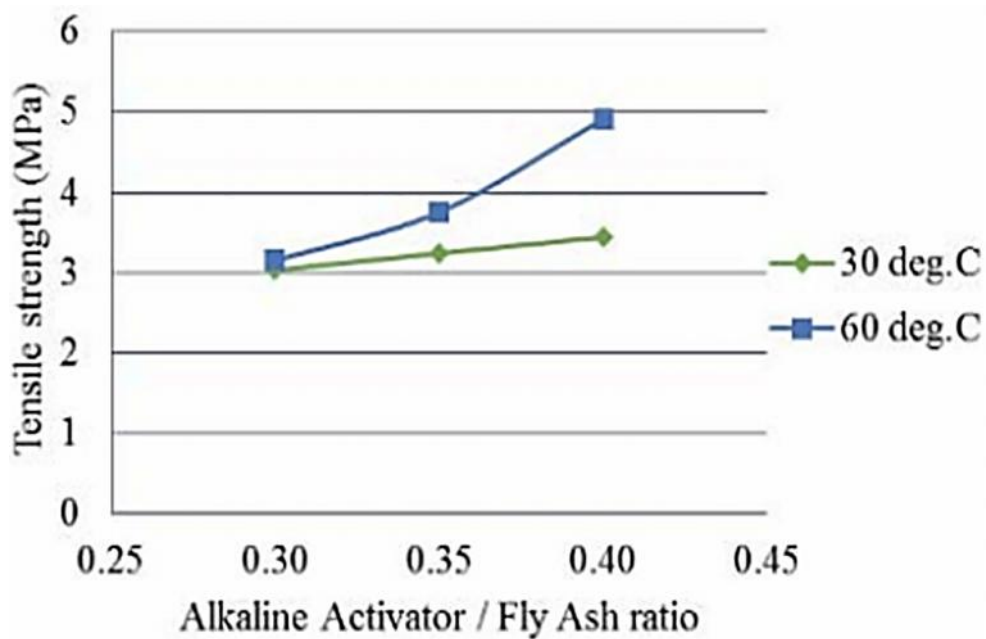


Figure – 2.19: Variation of tensile strength with alkali activator and fly ash ratio (Yellaiah, 2014).

**2.2.1.4 Flexural strength:**

Flexural strength is one measure of the tensile strength of concrete. It is a measure of an unreinforced concrete beam or slab to resist failure in bending. *Sofi et al.* (2007) reported that flexural strength of  $100 \times 100 \times 300$  mm steam cured prisms at  $30^{\circ}\text{C} - 35^{\circ}\text{C}$  for 24h was more than OPC concrete prism. It was also informed that the difference between splitting tensile and flexural strength of geopolymer concrete mixes had been found to be approximately 2.0 MPa [53].

*Olivia et al.* (2012) reported that the flexural strength of  $100 \times 100 \times 400$  mm geopolymer concrete block steam cured at  $60^{\circ}\text{C}$ ,  $70^{\circ}\text{C}$  and  $75^{\circ}\text{C}$  for 24h were 1 – 1.4 times higher than that of the OPC concrete at 28 and 91 days [54].

*Yellaiah et al.* (2014) reported that flexural strength of  $70.6\text{mm} \times 70.6\text{mm} \times 141.2\text{mm}$  prism moulds cured at  $30^{\circ}\text{C}$  and  $60^{\circ}\text{C}$  for 24h increased with the increase of alkaline activator to fly ash ratio. The maximum flexural strength of fly ash based geopolymer was achieved at  $60^{\circ}\text{C}$  for 24h curing (Fig 2.20) [62].

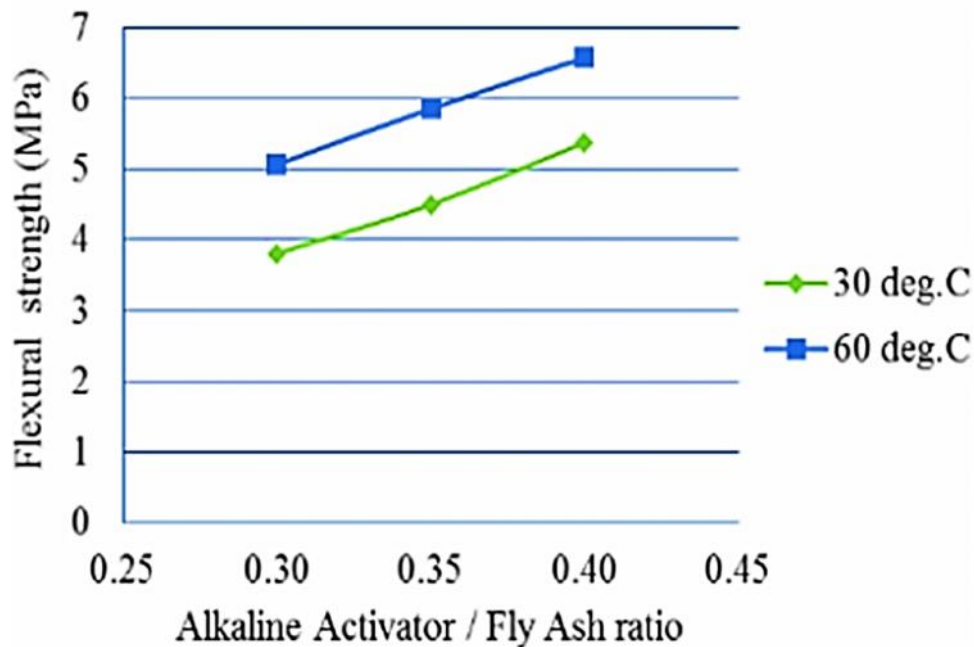


**Figure – 2.20: Variation of modulus of rupture with alkaline activator / fly ash ratio for different curing temperature (Yellaiah, 2014).**



### 2.2.1.5 Bond strength:

The performance of reinforced concrete depends on the combined action of the concrete and its embedded reinforcement as a construction material. This composite action is governed by the bond stress at the interface of the two materials. It is well established that bond strength of normal concrete depended on following major factors:

- a) Adhesion between the concrete and the reinforcing elements.
- b) Gripping effect resulting from the drying shrinkage of the surrounding concrete and the shear interlock between the bar deformations and the surrounding concrete.
- c) Frictional resistance to sliding and interlock as the reinforcing element is subjected to tensile stress.
- d) Effect of concrete quality and its strength in tension and compression.
- e) Mechanical anchorage effect of the ends of bars through development length, splicing, hooks, and crossbars.
- f) Diameter, shape, and spacing of reinforcement as they affect crack development.

For the use of geopolymer concrete it is necessary to study the bond strength between geopolymer concrete and reinforcement bar.

*Sofi et al.* (2007) investigated bonding performance of geopolymer concrete with reinforcement by beam-end specimens and direct pull out type specimens. The results of direct pull out tests were in general more conservative than those of beam-end specimens. The normalised bond strengths obtained from the beam-end specimen showed that the bond strengths of beam-end specimens were somewhat lower than those of the direct pull-out tests (Fig 2.21) [53]. The bond performance of geopolymer mixes are comparable to OPC based concrete and therefore geopolymer concrete and steel could be used as a composite material to resist tension in addition to compression.

*Sarkar* (2011) investigated the bond strength of fly ash based geopolymer concrete with reinforcing steel. The experiment was carried out on 24 geopolymer concrete and 24 ordinary Portland cement (OPC) concrete beam-end specimens, and the bond strengths of the two types of concrete were compared. It was reported that bond strength increased with the increase of compressive strength for both type of concrete (Fig 2.22). It was also noted that the bond strength of geopolymer concrete was higher than that of OPC concrete of similar compressive

strength. The split tensile strength of geopolymer concrete was higher than OPC concrete was the main reason behind the better bond strength of geopolymer concrete. It was observed from study that the use of soluble silicates in geopolymers results in a denser interfacial transition zone (ITZ) between aggregates and geopolymer matrix, contributed to the higher splitting tensile strength and bond strength of geopolymer concrete [61].

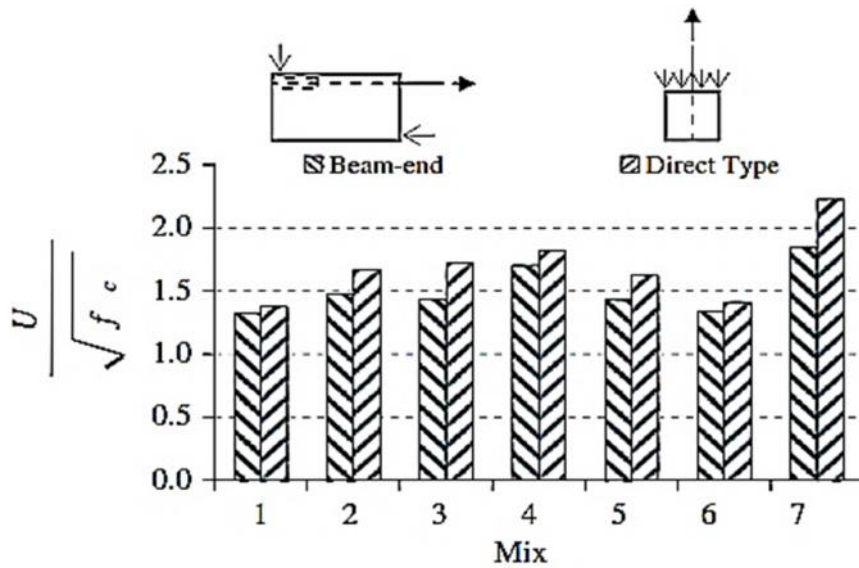


Figure – 2.21: Normalised bond strengths of beam-end and direct type specimens (Sofi, 2007).

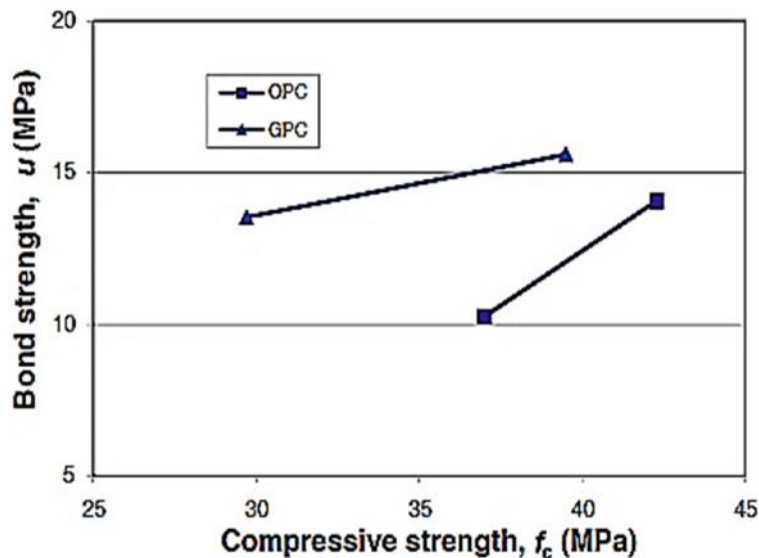
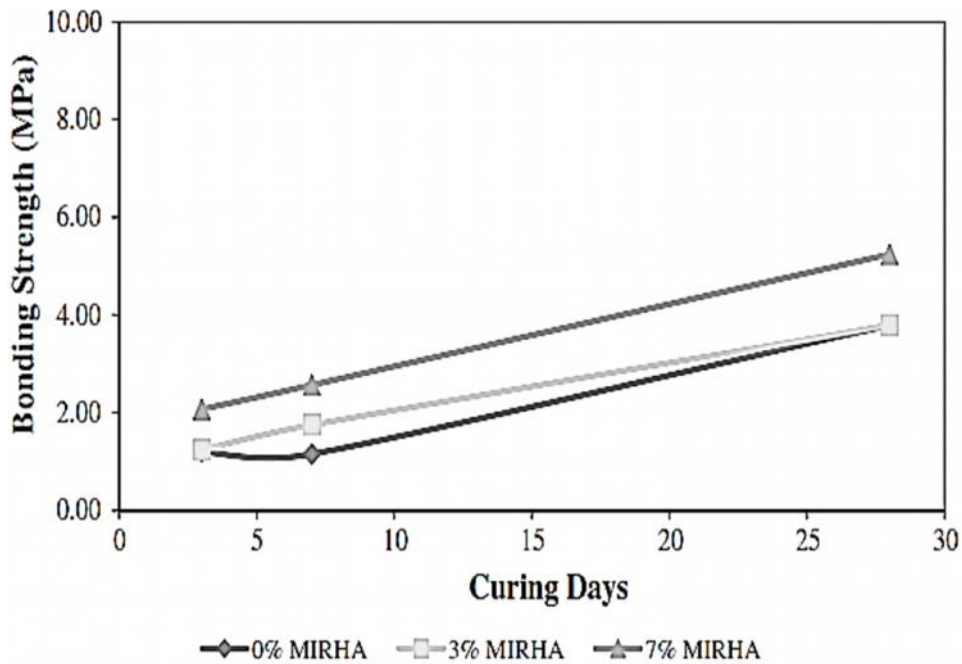


Figure – 2.22: Variation of bond strength with concrete compressive strength for 20 mm bar and 45 mm cover (Sarkar, 2011).

*Kusbiantoro et al.* (2012) investigated the bond strength of fly ash based geopolymer concrete with the addition of different percentages of microwave incinerated rice husk ash and were exposed to three different conditions (a) which were ambient ( $35 \pm 1^\circ\text{C}$ ), (b) external exposure ( $55 \pm 1^\circ\text{C}$ ), (c) oven curing ( $65 \pm 1^\circ\text{C}$ ). The addition of 3 % microwave incinerated rice husk ash (MIAHA) with fly ash based geopolymer concrete had significantly improved the bonding strength between geopolymer matrix and steel reinforcement bar up to 38.31% higher than control specimen without MIRHA inclusion (Fig 2.23). Bond strength of externally exposed MIAHA based geopolymer specimen at  $55 \pm 1^\circ\text{C}$  was 73.23% higher than normal temperature cured geopolymer concrete (Fig 2.24). It was also reported that heat cured fly ash geopolymer concrete with the addition 3% microwave incinerated rice husk ash showed maximum bond strength between concrete and reinforcement bar with in week (Fig 2.25). It was reported that the densification of geopolymer gel at elevated temperature was the main reason behind the bond strength of geopolymer concrete and reinforcement bar [64].



**Figure – 2.23: Bonding strength of fly ash–MIRHA based geopolymer concrete in ambient curing (*Kusbiantoro, 2012*).**

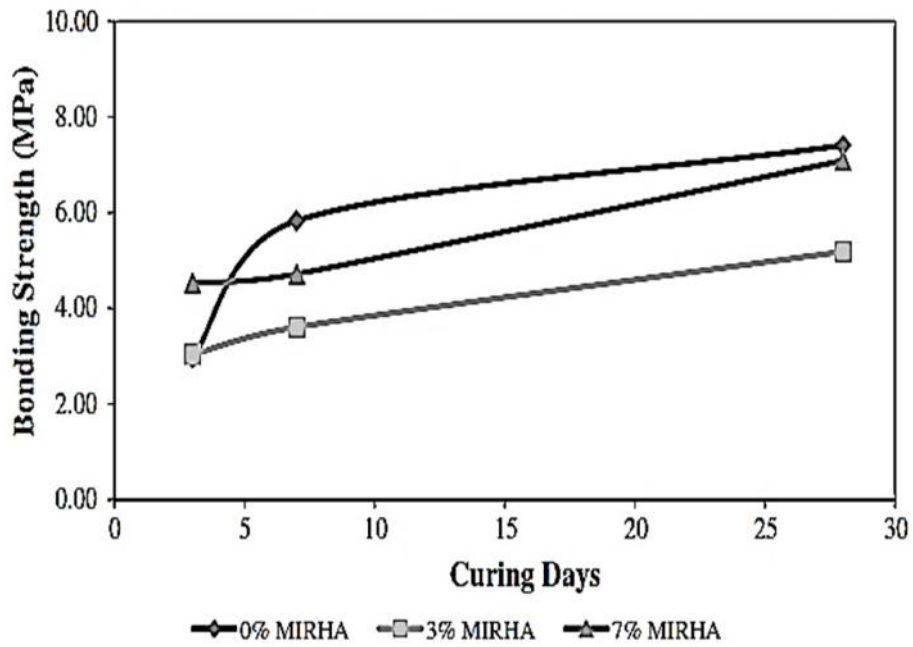


Figure – 2.24: Bonding strength of fly ash–MIRHA based geopolymer concrete in external exposure curing (Kusbiantoro, 2012).

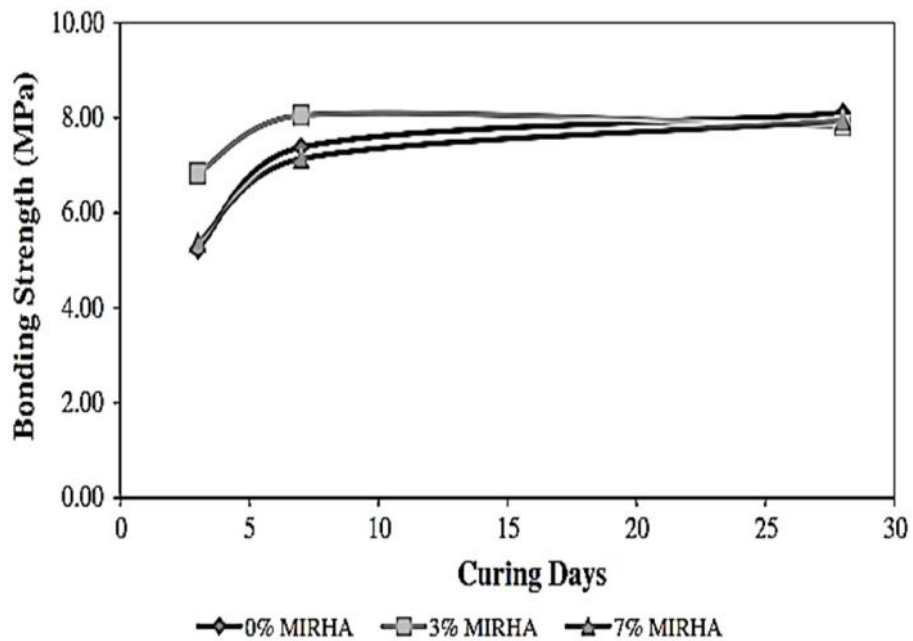


Figure – 2.25: Bonding strength of fly ash–MIRHA based geopolymer concrete in oven curing (Kusbiantoro, 2012).

Castel *et al.* (2015) reported the bond performance of geopolymer concrete composed of low calcium fly ash and ground granulated blast furnace slag (GGBFS) with both deformed and smooth reinforcing steel bars. They investigated using the standard RILEM pull-out test. It was conveyed that for equivalent compressive strength, bond strength of geopolymer concrete was 10 % more than OPC based concrete for ribbed bar (Fig 2.26). However, the bond strength of geopolymer concrete using smooth bar showed that the chemical adhesion of geopolymer concrete to the steel surface is similar to the OPC concrete. High early bond strength achieved by providing an intensive period of heat curing. The bond strength geopolymer specimen cured at 40°C and 80°C for 24 hours were reported as 6 MPa and 18 MPa at 28 days [65].

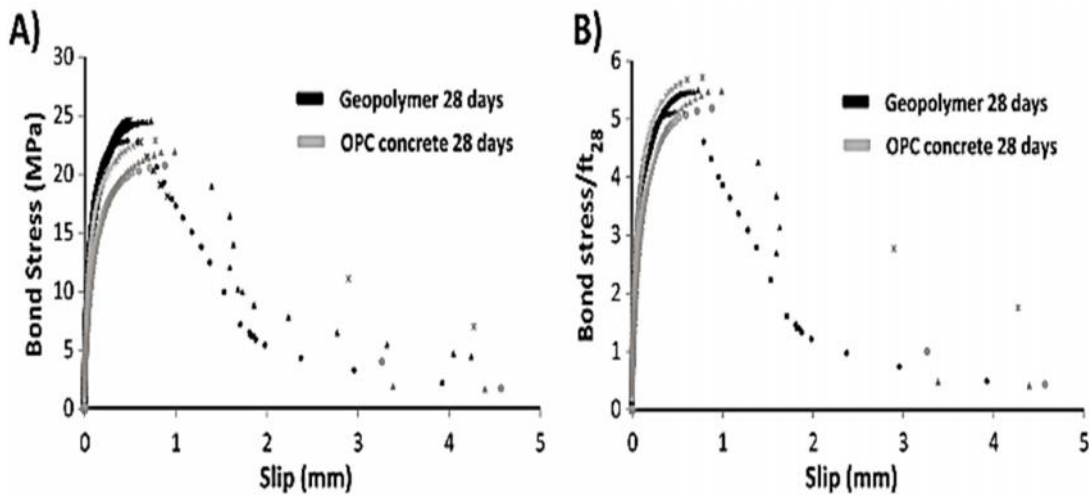


Figure – 2.26: The bond stress–slip curves of geopolymer and OPC concretes after 28 days curing (Castel, 2015).

### 2.2.1.6 Flexural behaviour of reinforced beam:

There are almost no literatures on structural behaviour of reinforced geopolymer concrete beams and column. For use of geopolymer concrete as a structural member, behaviour of reinforced geopolymer concrete needs special attention. Chang *et al.* (2007) studied the shear and bond strength of reinforced geopolymer concrete beams. The failure modes and crack patterns observed for reinforced geopolymer concrete beams were similar to those reported in the literature for reinforced Portland cement concrete beams. The design provisions contained in the Australian Standard for Concrete Structures AS3600-09 and American Concrete Institute Building Code ACI318-08 are found to give conservative predictions for the shear strength and

bond strength of reinforced geopolymer concrete beams. These design provisions are, therefore, applicable to design of reinforced geopolymer concrete beams [66].

*Sumajouw et al.* (2006) reported the flexural behaviour of twelve numbers of 200 mm wide by 300 mm deep by 3300 mm long rectangular doubly reinforced geopolymer concrete beams. The flexural capacity of the beams was influenced by the longitudinal tensile reinforcement ratio and the compressive strength of geopolymer concrete. As the longitudinal tensile reinforcement ratio increased, the flexural capacity of the beams increased significantly (Fig 2.27). Because the test beams were under reinforced, the flexural capacity increased only marginally when the compressive strength of concrete increased.

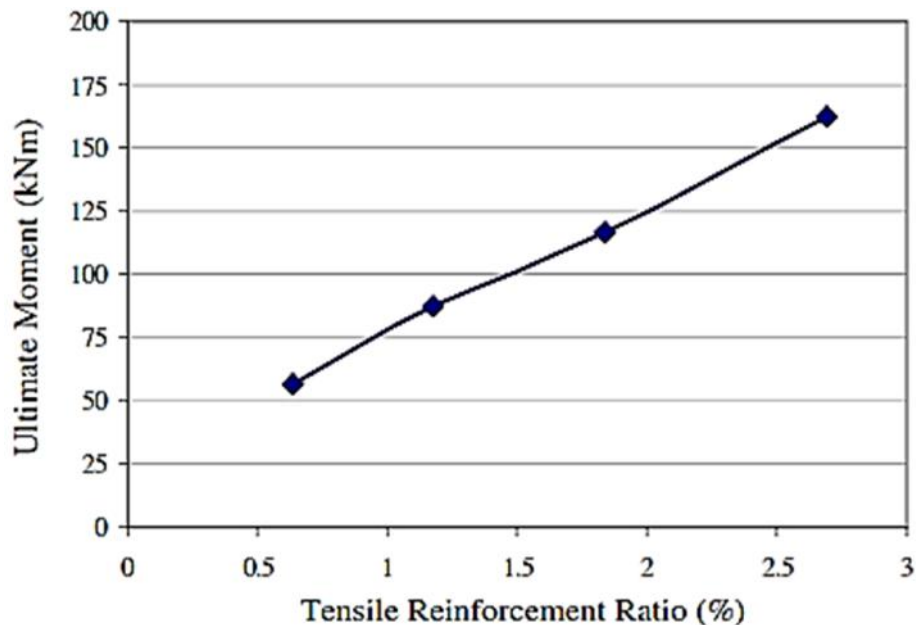


**Figure – 2.27: Effect of percentages of tensile reinforcement on the flexural capacity of beam (*Sumajouw, 2006*).**

The cracking moment of geopolymer concrete increased as the concrete compressive strength increased for geopolymer concrete. The similar behaviour was observed for normal concrete beam (Fig 2.28). It is also noted that the ductility of reinforced geopolymer concrete beams, as indicated by the ratio of mid-span deflection at ultimate moment to mid-span deflection at yield moment, increased as the tensile reinforcement ratio decreased. Similar results are observed in case of reinforced geopolymer concrete column. The load carrying capacity of geopolymer column was also influenced by the longitudinal reinforcement ratio, concrete compressive strength, and the load-eccentricity. The failure load of test columns increased as the load-

eccentricity decreased, and as the longitudinal reinforcement ratio and concrete compressive strength increased [67].

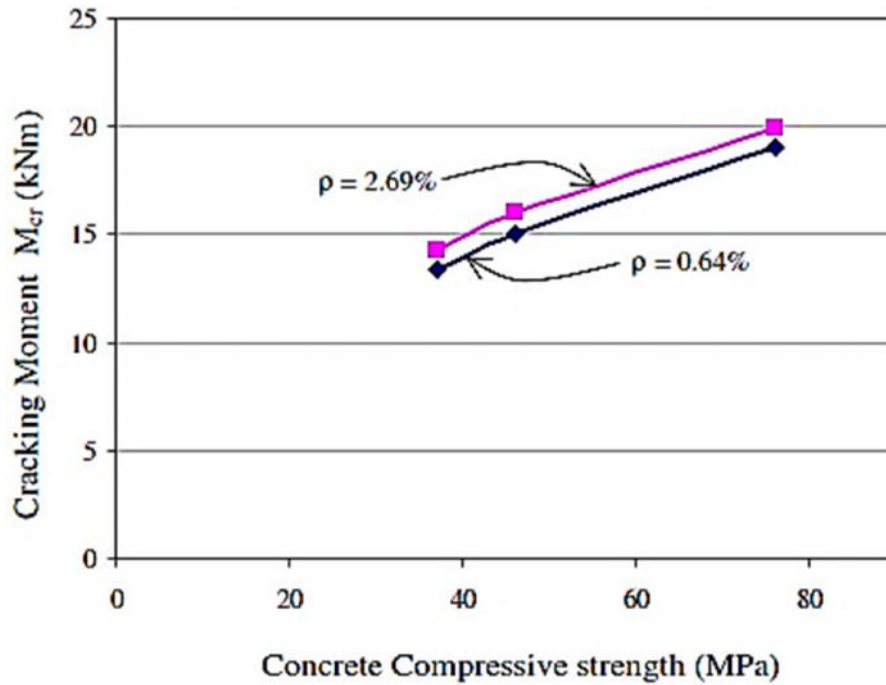


Figure – 2.28: Effect of concrete compressive strength on cracking moment (Sumajouw, 2006).

Ambily *et al.* (2012) reported the experimental and analytical investigations on shear behaviour of reinforced geopolymer concrete beams. The load deflection characteristics at mid span of reinforced geopolymer concrete beams and OPC concrete beam is almost similar. The GPC beams showed slightly more deflections at the same load than the OPC concrete beams. The ultimate load carrying capacity of reinforced geopolymer concrete beams is 15% more than that of OPC concrete beam in spite of a 20% higher compressive strength [68].

## 2.2.2 Microstructure analysis of geopolymer concrete

A brief outline about the microstructures of geopolymer matrix relevant to the present research is presented in this section.

### 2.2.2.1 X-ray Diffraction analysis:

XRD analysis is based on constructive interference of monochromatic X-rays and crystalline sample. The X-rays are generated by a cathode ray tube, filtered to produce monochromatic radiation, collimated to concentrate, and directed towards the sample. The interaction of incident rays with the sample produces constructive interferences. The constructive interference of X-rays diffracted from the planes of atoms within the solid give rise to a characteristic diffraction peak or a sequence of peaks that are unique to a particular material. Thus, XRD may be a useful tool for the present study even though the amount of information which can be obtained is limited due to the substantial amorphous nature of geopolymers.

XRD analysis confirmed that in the presence of alkali activated solution and heat activation of amorphous compounds present in fly ash transform into semi crystalline and semi crystalline compound. The peaks of hematite, quartz, and mullite have been distinctly observed and the hump denotes presence of amorphous silica in the geopolymer matrix as shown in diffractogram [69, 70].

Alvarez-Ayuso et al. (2008) reported from XRD study that the fly ash with glass content, yielded geopolymers with the greatest compressive strength. The higher the content of the glassy constituent in the fly ash, the higher the degree of geopolymeric reaction. They concluded that the compressive strength of geopolymer mortar/concrete increased due to present of excess amount of crystalline compound transformed from fly ash [46].

*T. Bakharev* (2005) had reported that the phases of geopolymer matrix were amorphous, and only in the case of materials prepared with sodium hydroxide solution were semi crystalline zeolitic phases. The peaks were observed in XRD analysis of heat activated geopolymer matrix due to quartz, mullite and hematite of the crystalline component of the fly ash (Fig 2.29). The broad peak in the region  $20 - 32^\circ = 2\theta$  arising from the glassy phase of the fly ash and broad peaks in the region  $6 - 10^\circ$  and  $12 - 16^\circ = 2\theta$  arising from alumino-silicate gel [36].



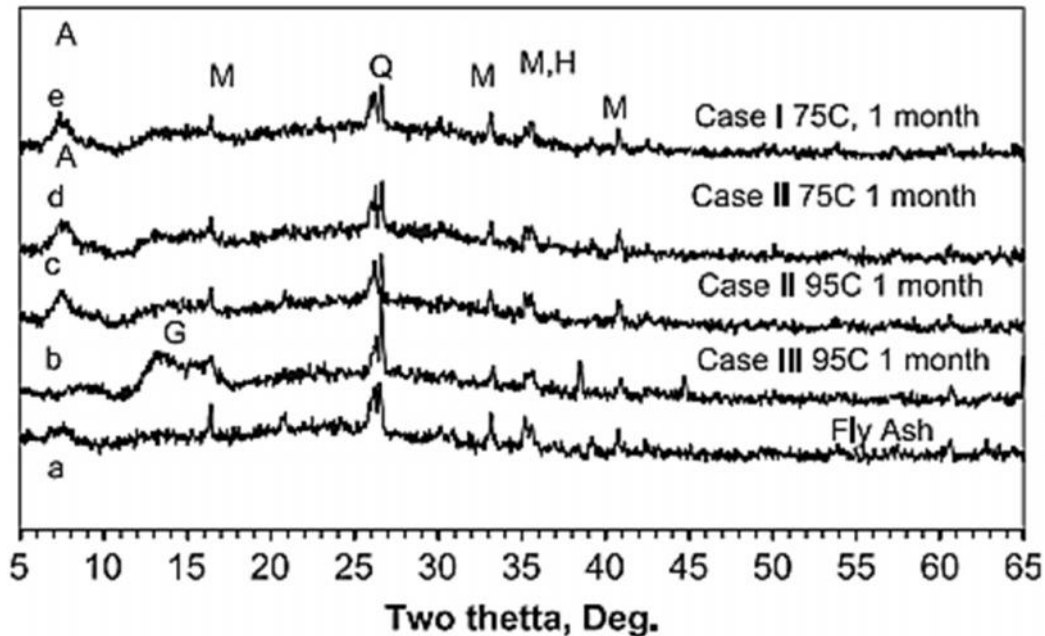


Figure – 2.29: XRD analysis fly ash based geopolymers concrete, A = poorly crystalline, G = poorly crystalline alumino-silicate gel, Q = quartz, M = mullite, H = hematite (Bakharev, 2005).

Yubin Jun and Jae Eun Oh (2014) reported that the activated geopolymers show quartz, mullite and hematite as major crystalline in XRD analysis, but also illustrated the formation of new phases such as chabazite, zeolite A-Na as well as C-S-H. The alkali-activated fly ash sample containing Al-rich chabazite phase showed much higher compressive strength than the samples with zeolite A-Na [71].

XRD analysis results of fly ash based geopolymers concrete/mortar depends on molar concentration and heat activation. The alumina-silicate substances with amorphous structure are the main products generated by geopolymerization through the alkali-activation process. Finding the patterns of the products in amorphous phase by XRD is very difficult. There were numerous peaks of mullite ( $3\text{Al}_2\text{O}_3, \text{SiO}_2$ ) and quartz ( $\text{SiO}_2$ ) in the crystalline phase was observed (Fig 2.30) [29].

Chindaprasirt *et al.* (2013) reported that peaks of crystalline quartz ( $\text{SiO}_2$ ), calcium sulfate ( $\text{CaSO}_4$ ) and calcium oxide ( $\text{CaO}$ ) were observed in the XRD analysis of high calcium fly ash based geopolymers paste under microwave radiation followed by heat curing for 3h, 6h and 12h at  $65^\circ\text{C}$ . The broad hump at  $22 - 38^\circ$  observed in XRD analysis of geopolymers matrix, indicated the presence semi crystalline phase with high amount of amorphous gel. It was also

reported that the calcium silicate compounds from the reaction between high calcium fly ash, silica and silicate solution. Microwave radiation cured geopolymer paste exhibited the sharp peaks of crystalline phases with high degree of amorphous phase of the semi-crystalline geopolymer (Fig 2.31) [35].

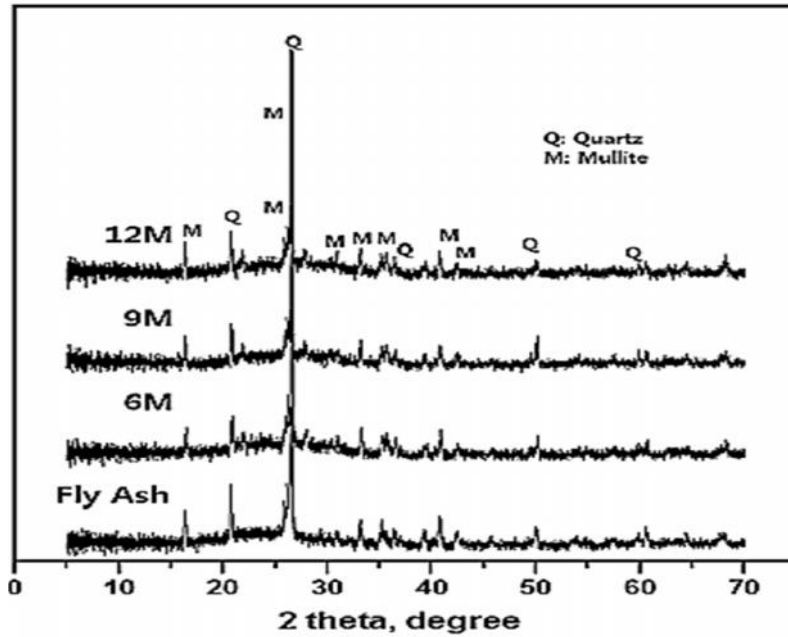


Figure – 2.30: XRD analysis of fly ash and geopolymer matrix (Ryu, 2013).

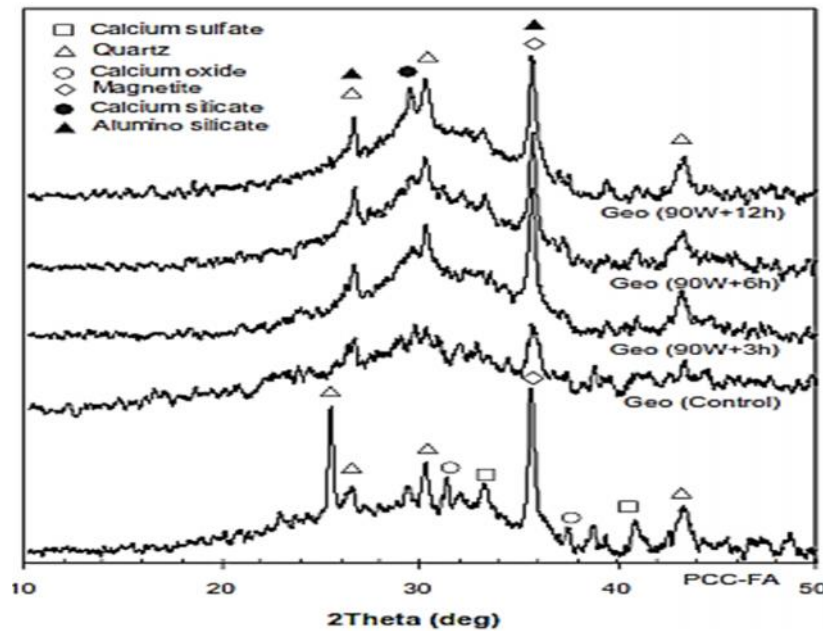


Figure - 2.31: XRD patterns of geopolymer pastes with microwave radiation and additional 65°C heat curing (Chindapasirt, 2013).

### 2.2.2.2 Scanning Electron Microscopy (SEM) and Energy Dispersive X-ray (EDX):

The scanning electron microscope (SEM) uses a focused beam of high energy electrons to generate variety of signals at the surface of solid sample. The high energy electron carry a significant amount of kinetic energy and this energy dissipated as a variety of signals produced by electron-sample interaction. These signals include secondary electron, backscattered electron and X-rays provide the information about SEM. The secondary product is readily interpretable images of the surface to determine sample morphology. The emitted X-ray has an energy characterization of the parent element. The detection and measurement of energy permits elemental analysis.

Ryu *et al.* (2013) observed that fly ash particles polymerized in presence of alkali activator produced amorphous, semi crystalline and crystalline product. The un-reacted fly particle is also observed in spherical shape. The un-reacted fly Ash particle in the matrix do not act as filler, but instead increase the strength of the matrix with age through the bonding strength provided by the complex reaction between the surfaces of the particles (Fig 2.32A & B) [29] .

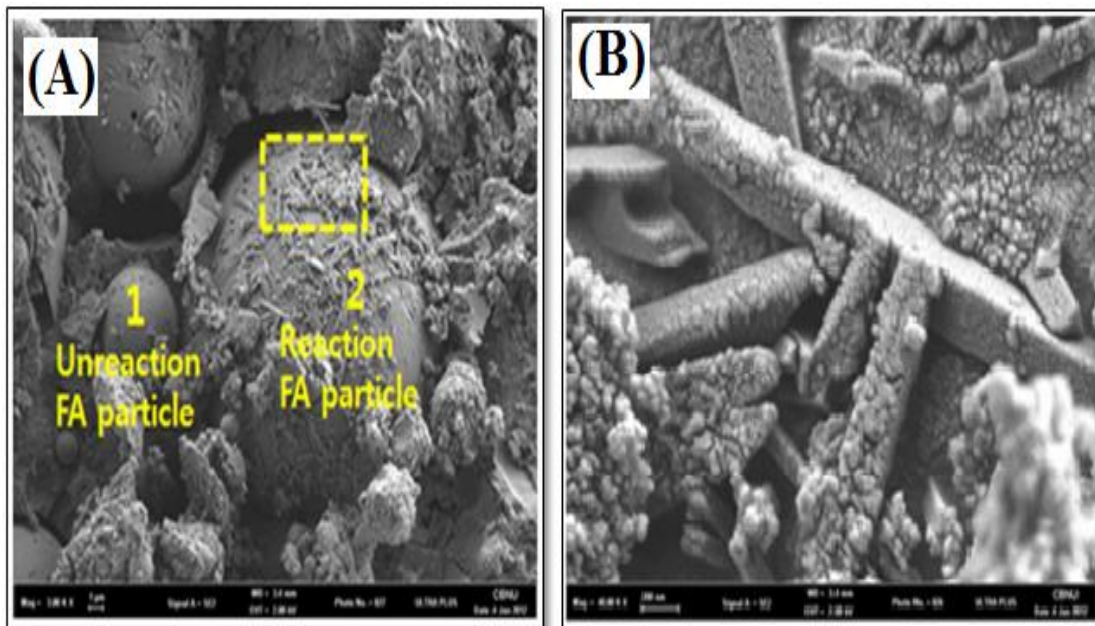
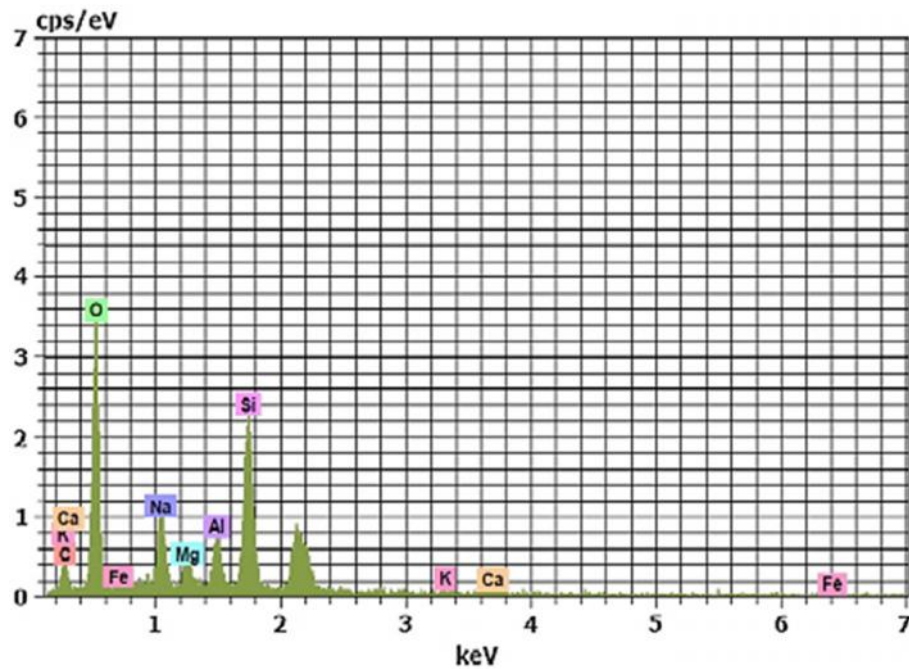


Figure – 2.32: (a) Unreacted fly ash and (b) reaction product after polymerization (Ryu, 2013).



**Figure – 2.33: EDX analysis of the geopolymer matrix (Ryu, 2013).**

Also EDX results are presented in figure 2.33 of alkali activated fly ash geopolymer matrix. It is clearly observed that most of the reactant is composed of silica and alumina. The sodium is observed due to presence of alkali activator ( $\text{NaOH} + \text{Na}_2\text{SiO}_3$ ) in geopolymerization process. These reactants in turn combine with the Na ions dissociated from the external NaOH, causing the reaction products to agglomerate and enabling the strength to develop through combinations of fly ash particles [29].

*Chindaprasirt et al.* (2013) reported the SEM images of un-reacted spherical fly ash, partially reacted grains of fly ash particles of microwave cured geopolymer mortar (Fig 2.33). Gel formation on fly ash particles showed the dissolution of glassy phase in the alkaline solution as showed in Figure 2.34A & 2.34C. A large number of gels were formed on the fly ash particles owing to the promoted dissolution of Si and Al species from fly ash with microwave radiation. It was found in FESM study that the Interfacial Transition Zone (ITZ) between aggregates and concrete matrix in heat cured geopolymer matrix stronger than that in cement concrete. The stronger ITZ contributed to the higher splitting tensile strength and bond strength of geopolymer concrete [35].

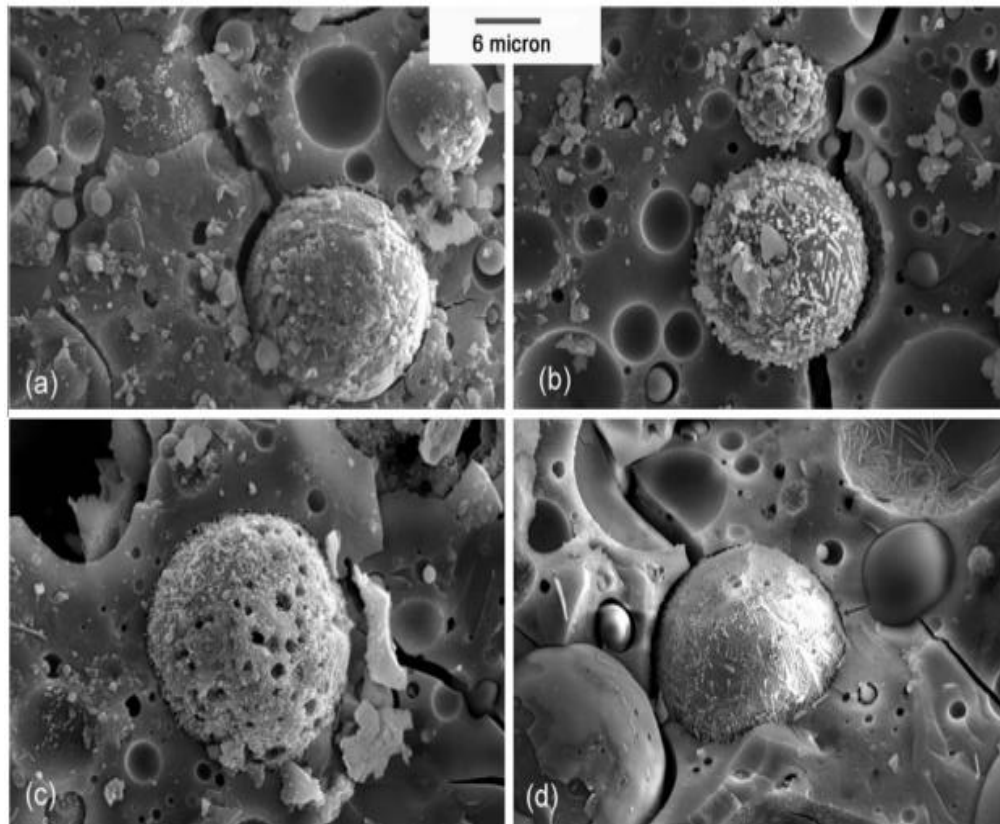


**Figure – 2.34: Microstructure of geopolymer pastes with microwave radiation and additional 65°C heat curing; (a) 3h, (b) 6h, (c) 12h, and (d) Control (Chindaprasirt, 2013).**

*Chindaprasirt et al.* (2009) compared in SEM images of fly ash and bottom ash based geopolymer matrix. Both SEM images showed a continuous mass of alumino-silicate with unreacted, partially reacted ash particles. The ratio of Si/Al for of bottom ash geopolymer matrix was higher than that of fly ash based geopolymer as observed in EDX analysis. The higher ratio of Si/Al results in geopolymers with lower strength and higher elasticity (Fig 2.35) [45]. *Fletcher et al.* (2005) also reported that the compressive strength of geopolymer mortar / concrete increased with the increased in amount of crystalline compound transformed from fly ash (Fig 2.36) [72].

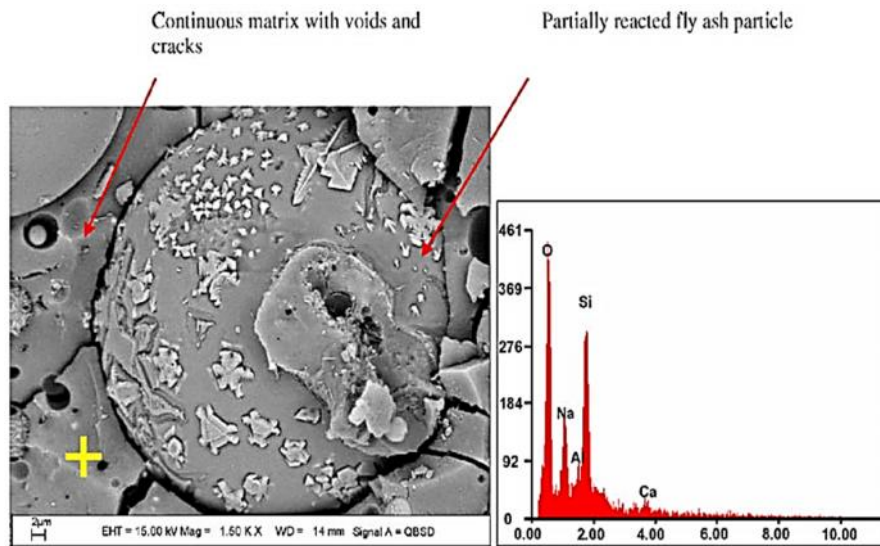


Figure – 2.35: SEM-EDX analysis of fly ash based geopolymer (Chindaprasirt, 2009).

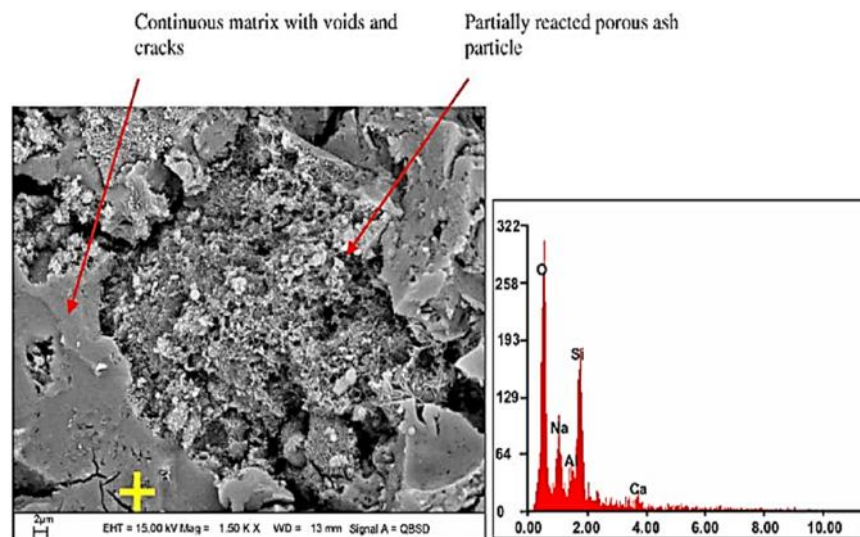
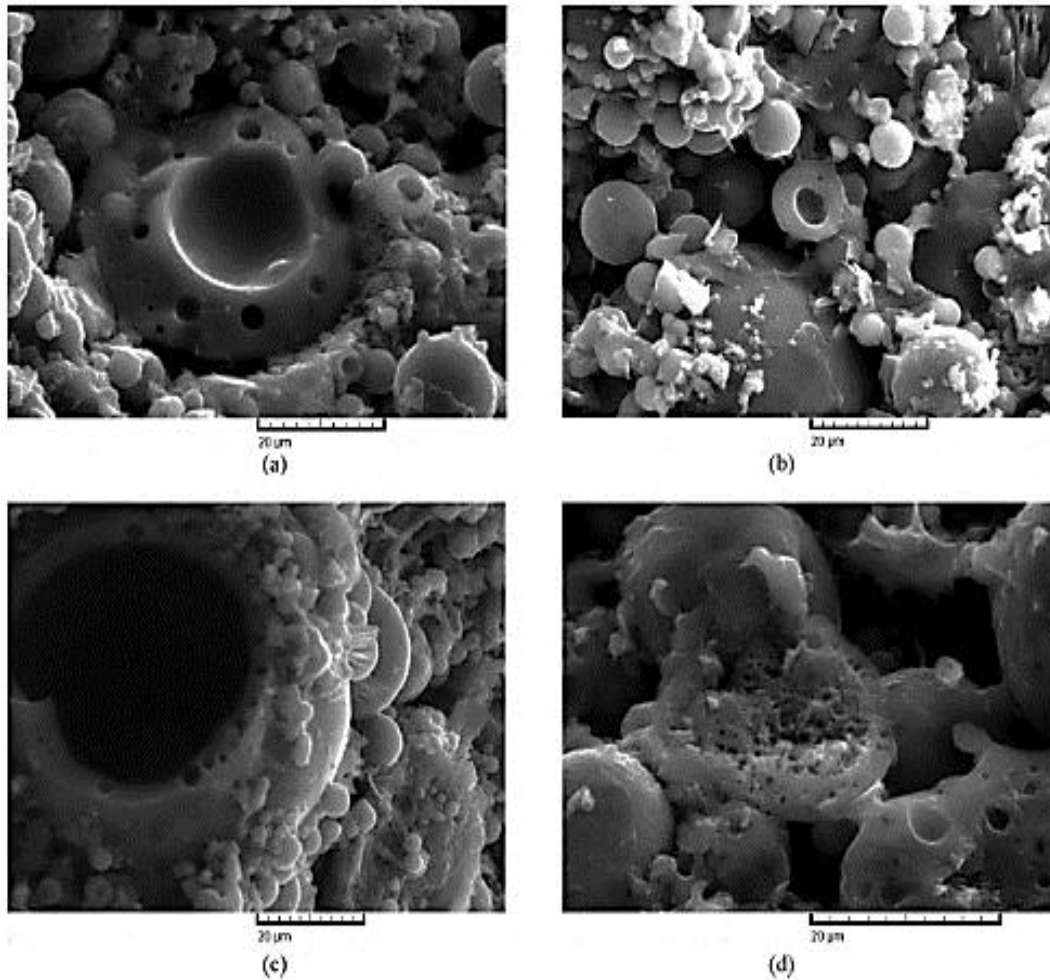


Figure – 2.36: SEM-EDX analysis of bottom ash based geopolymer (Fletcher, 2005).

Muek *et al.* (2012) observed that the sodium silicate gel was the majority product, along with the unreacted fly ash particles, during the aging time up to 28 days. The microstructure was highly inhomogeneous and the matrix was full of loosely structured fly ash grains of different sizes. Numerous circular cavities belonging to fly ash particles are evident in the gel. Cavities surroundings consist of tubular vitreous network (Figs 2.37a-c). The considerable amount of unreacted spheres, as well as the presence of pores in the geopolymer matrix (Fig 2.35d) indicated an incomplete reaction in the system and could explain why the alkali activated fly ash samples showed a lower degree of reaction. Figure 2.37 clearly showed

inhomogeneous glass-like matrix of the amorphous aluminosilicate gel. The unreacted spheres of fly ash indicate an uncompleted reaction in the systems investigated [73].



**Figure – 2.37: SEM micrographs of the hardened alkali activated fly ash samples (Muek, 2012).**

EDX analysis of geopolymeric gel showed that the gel was mostly consists of the phases containing Na-Si-Al in the bulk region suggesting the formation of silicate-activated gel by polymerization throughout the inter particles volume. Sodium, silica, alumina, small amount of iron, calcium, potassium and magnesium were observed in the gel by Energy Dispersive X-Ray Analysis (EDX) (Fig 2.36). These elements (Fe, Ca, K, Mg) was obviously represented the fly ash phases, which for various reasons, did not dissolve during alkali activation [73]. *Lloyd et al.* (2009) suggested that during alkaline activation these remnants may even disperse through the gel [74]. According to *Muek et al.* (2012) and *Lloyd et al.* (2009)

different solubility of phases in the aluminosilicate gel formed determines the distance of these remnants from the surface of fly ash particle (Fig 2.38).

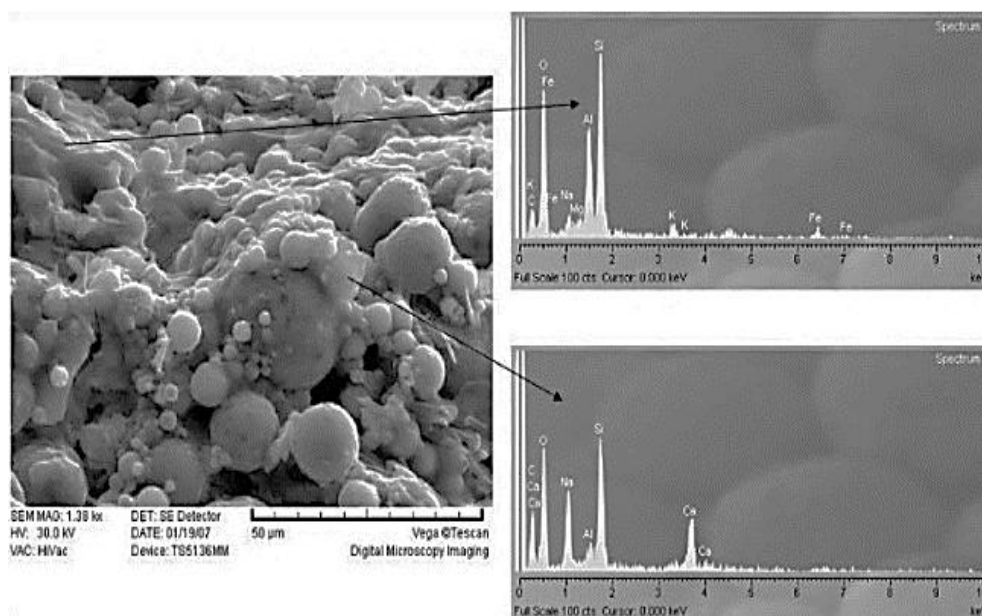


Figure – 2.38: SEM and EDX analysis of alkali activated fly ash sample (Lloyd, 2009).

### 2.2.2.3. Fourier Transform Infra-Red Spectroscopy (FTIR):

FTIR (Fourier Transform Infra-Red Spectroscopy) is a sensitive technique particularly for identifying organic chemicals in a whole range of applications although it can also characterise some inorganic chemicals. FTIR relies on the fact that the most molecules absorb light in the infra-red region of the electromagnetic spectrum. This absorption corresponds specifically to the bonds present in the molecule.

The distinct band of O-Si-O bending near  $460\text{ cm}^{-1}$  and Si-O-Si stretching vibration at wave number range  $950 - 1200\text{ cm}^{-1}$  were observed in FTIR study of geopolymer paste (Fig 2.39). The Si-O-Si stretching vibration was more prominent than the O-Si-O bending mode as in Figure 2.39. Si-O-Si vibration is used to indicate the degree of geopolymerization. It is observed that the peak near  $750 - 850\text{ cm}^{-1}$  may refer to symmetric stretching vibration of Si-O-Si. An asymmetric stretching vibration band of Si-O-T (T=Al, Si) have been described as a strongest band in the region of  $950 - 1250\text{ cm}^{-1}$  [31].



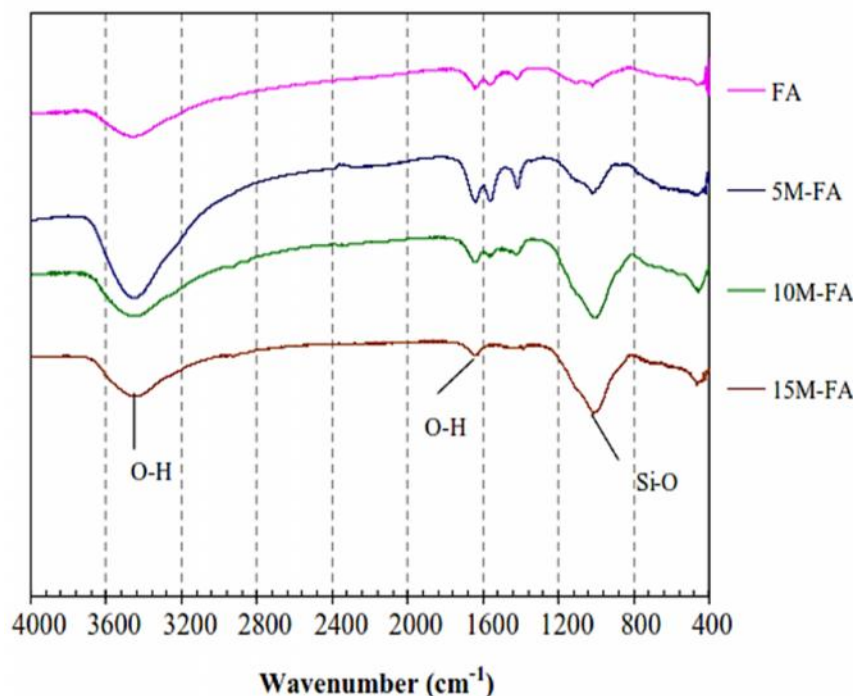


**Figure – 2.39: FTIR spectra of fly ash based geopolymer (Barbosa, 2000).**

*T. Bakharev* (2005) observed the FTIR spectrum of the alkali-activated fly ash samples showed some differences when compared to the raw fly ash. The band at  $800\text{ cm}^{-1}$  due to  $\text{AlO}_4$  vibrations disappeared and a new band at around  $700\text{ cm}^{-1}$  appeared. Also, the band at  $1200\text{ cm}^{-1}$  due to asymmetric stretching  $\text{Si-O-Si}$  and  $\text{Al-O-Si}$  in fly ash shifts to lower frequencies ( $960\text{--}1000\text{ cm}^{-1}$ ) after geopolymeric reaction. The shift was higher in the fly ash activated by sodium hydroxide than in the fly ash activated by sodium silicate. In all geopolymeric materials, new bands appeared in the regions of  $1600$  and  $3450\text{ cm}^{-1}$ , which were attributed to bending vibrations ( $\text{H-O-H}$ ) and stretching vibration ( $-\text{OH}$ ), respectively. These changes were consistent with the formation of the alumino-silicate network in a polymer structure (Fig 2.40) [36].

*Muek et al.* (2012) reported the FTIR spectra for all the AAFA systems, as well as the spectrum for the original fly ash. The main broad band at  $1086.39\text{ cm}^{-1}$  in the original FA, corresponding to asymmetric stretching vibrations of  $\text{Si-O-Si}$  and  $\text{Al-O-Si}$  developed sharper and shifts toward lower frequencies ( $\sim 1074\text{ cm}^{-1}$ ) due to new reaction products. The formation of this new amorphous alumino-silicate gel phase was suggested depolymerisation and structural reorganization of the amorphous phases in the AAFA materials. The new band

appeared in the region of  $1600\text{ cm}^{-1}$  and  $3450\text{ cm}^{-1}$  were attributed to bending vibrations (H–O–H) and stretching vibrations (–OH, H–O–H) (Fig 2.41) [73].

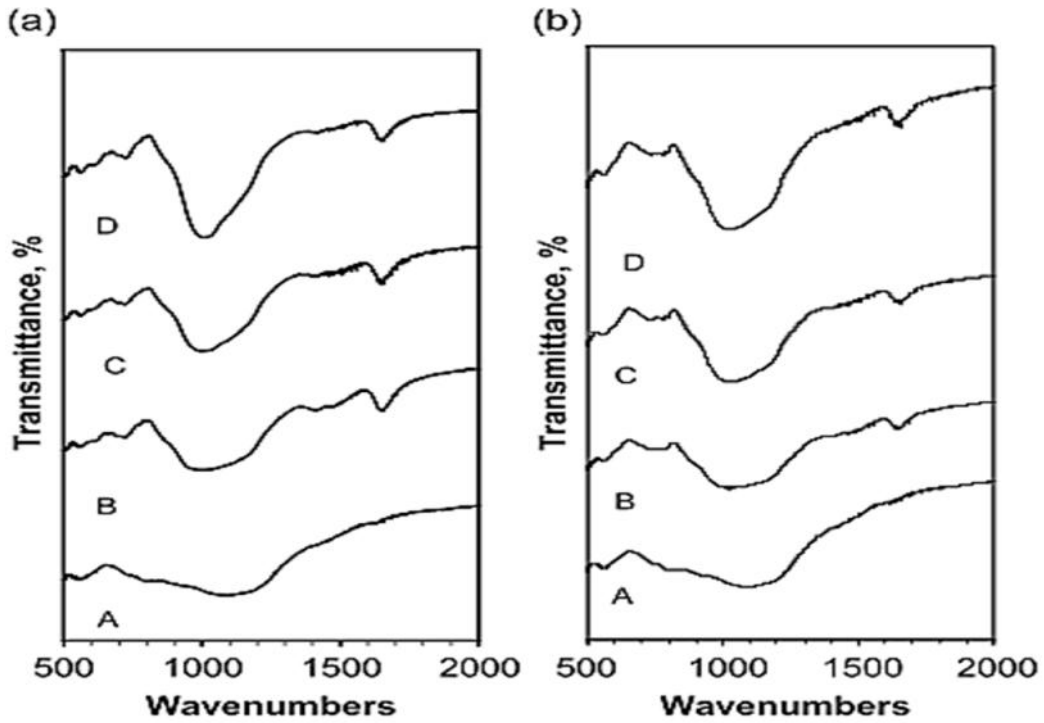


Figure - 2.40: FTIR study of fly ash with (a) sodium hydroxide (b) sodium silicate activator (Bakharev, 2005).

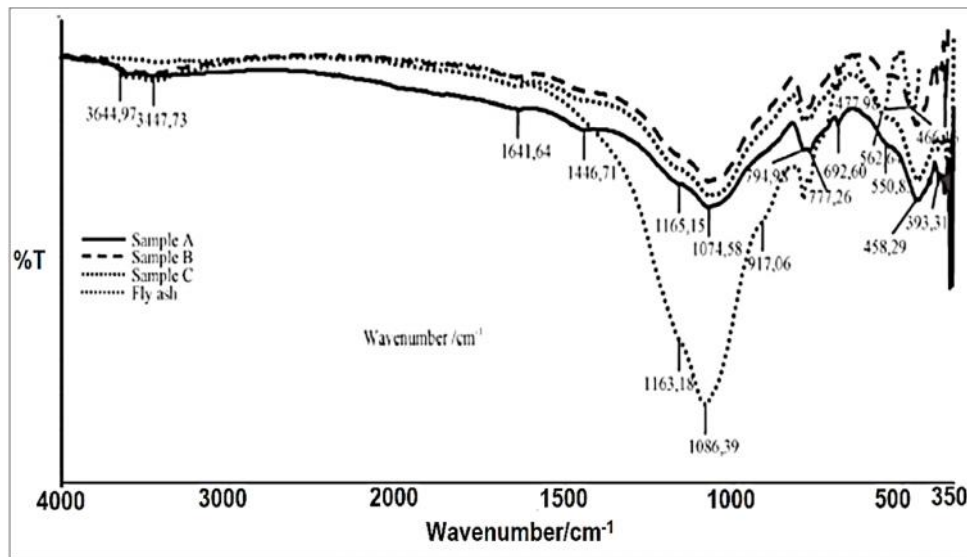


Figure - 2.41: FTIR spectra for the original FA and AAFA systems (Muek, 2012).

### 2.3 Applications of geopolymer mortar/concrete:

Most applications of geopolymer mortar/concrete to date have been in the precast industry using accelerated curing. However, geopolymers have various other areas of applications from civil engineering field to automobile and aerospace industries. *Rangan et al.* (2005) have identified various economic benefits of using fly ash based geopolymer concrete, by taking into account that the cost of purchasing fly ash (excluding transportation) is relatively low. Therefore, after taking into account the cost of activator liquids, it was estimated that the production of fly ash-based geopolymer concrete may be 10 – 30% cheaper than that of Portland cement concrete. This is not the case though in practice, as the large cement companies usually control the supply of raw materials, including fly ash, which is often locked up by long term agreements [75]. Some of the applications of geopolymers based on their Si/Al ratio were tabulated by *Wallah and Rangan*, as follows [76]:

Since geopolymers are considered as two-component systems (reactive solid components alkaline activation solution) they can be used as suitable binders in precast industry for the manufacture of reinforced products such as large-diameter pipes and roofing tiles [77]. Immobilization techniques are used for the treatment of large amounts of heavy metals and radioactive wastes, thus geopolymerisation has received over the years significant attention due to its low cost, flexibility and increased durability versus time [1, 2].

**Table – 2.1 Application of geopolymer mortar/concrete:**

Si:Al ratio	Applications
1	- Bricks - Ceramics - Fire protection
2	- Low CO <sub>2</sub> cements and concretes - Radioactive and toxic waste encapsulation
3	- Fire protection fibre glass composite - Foundry equipment - Heat resistant composites, 200°C to 1000°C - Tooling for aeronautic titanium processing
>3	- Sealants for industry, 200°C to 600°C - Tooling for aeronautics SPF aluminium
20 - 35	- Fire resistant and heat resistant fibre composites

## 2.4 Modified Geopolymer concrete without heat activation:

The scope of geopolymer concrete is limited to the precast member due to requirement of heat activation after casting. Most of the research works on fly ash based geopolymer are on the mix proportion and strength variation of geopolymer concrete cured at different temperature range of 45 °C to 80 °C for about 2 -3 hours [35, 72 – 82]. It is well-known that the geopolymer mortar provides poor strength at ambient temperature of about  $27 \pm 2$  °C curing due to slow polymerization process. There are limited literatures on available on geopolymer to eliminate the shortcomings of ambient temperature curing. The literate available on these areas are now presented. There were several technique has been adopted for the development of strength and durability of ambient temperature cured geopolymer concrete.

*Xie et al.* (2015) reported an experimental study on the behaviour fly ash, bottom ash and blended fly and bottom ash-based geopolymer concrete cured at ambient temperature. The workability of the coal ash-based GPCs was directly related to the mass ratio of fly ash-to-bottom ash (Fly Ash: Bottom Ash) and the liquid-to-binder ratio (l/b), and mixes with a higher fly ash content and l/b ratio exhibited a better workability. Compressive, flexural and modulus of elasticity of coal ash based (Bottom ash and Fly ash) geopolymer concrete increased with a decreased in liquid to binder ratio, or in an increased fly ash to bottom ash ratio (Fig 2.42). SEM micrographs showed that the density and homogeneity of the GPC increased with an increased in the mass ratio of fly ash to-bottom ash. This indicated that fly ash undergoes a higher degree of geopolymerization compared to that of bottom ash (Fig 2.43). The ambient temperature cured coal ash-based GPCs exhibited a higher drying shrinkage compared to that of OPCs due to the large amount of unreacted coal ash particles in the hardened GPC structure due to lower degree of geopolymerization at ambient temperature curing [83].

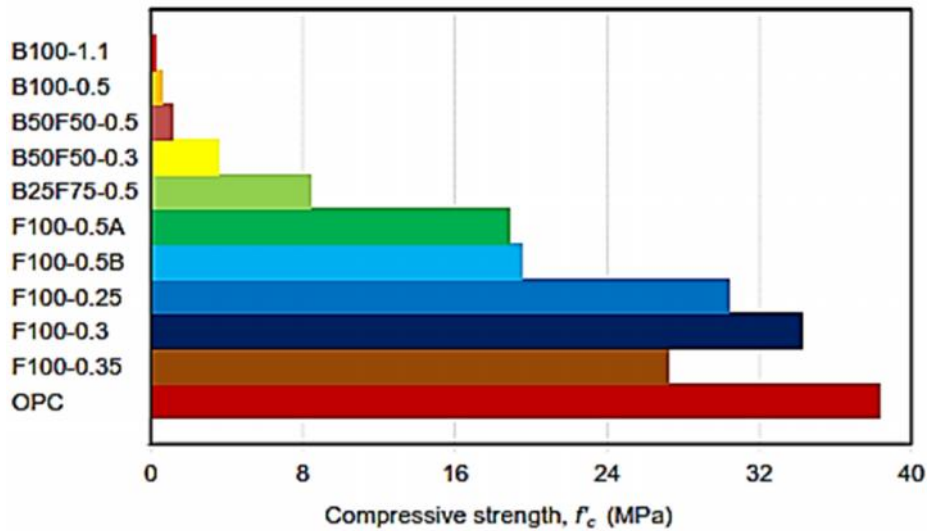


Figure – 2.42: Compressive strength of bottom ash, fly ash and mix of fly ash and bottom ash geopolymer concrete (Xie, 2015).

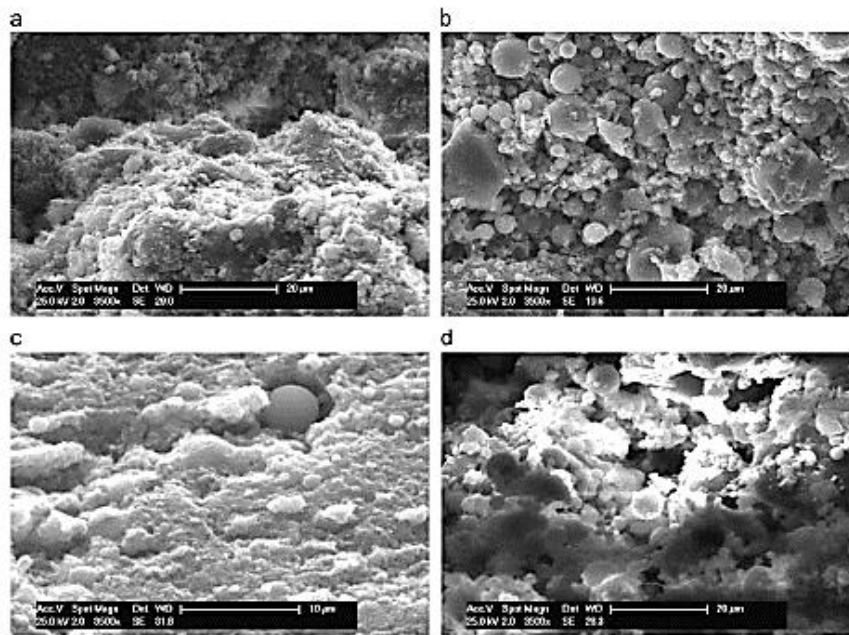


Figure – 2.43: FESM image of (a) 100% BA, (b) 50 % BA + 50% FA, (c) 25% BA + 75% FA, (d) 100% FA geopolymer concrete (Xie, 2015).

Temuujin *et al.* (2009) reported the mechanical activation of the fly ash results in particle size and morphology changes with concomitant increase in reactivity with alkaline liquid. Mechanical activation of fly ash in a vibration mill with milling media to powder ratio of 10:1 leads to a reduction of particle size and change in particle shape but little change in mineralogical composition. Mechanically activated ash based geopolymer paste cured at ambient temperature showed 80 % increase in compressive strength than raw fly ash based

geopolymer paste. The main contribution to increased compressive strength of the geopolymer is attributed to reduction of particle size and change in morphology allowing a higher dissolution rate of the fly ash particles [84].

*Wongpa et al.* (2010) reported that an ambient temperature cured inorganic polymer concretes (IPCs) can be produced from rice husk–bark ash (RHBA) combined with fly ash (FA). The compressive strength of RHBA and FA modified geopolymer concrete cured at ambient temperature were influenced by the ratios between the paste content and the aggregate content and the weight ratio between the solution content (S) and the ash content (A). The solution to ash ratio was the most important factor that controlled the rate of reduction in compressive strength of IPCs while paste to aggregate ratio had the less influence. The higher the S/A ratio, the lower the compressive strength. On the other hand, for the same solid to ash, the mixtures containing higher paste to aggregate ratio produced lower compressive strength than that with lower paste to aggregate ratio (Fig 2.44). It was stated that the geopolymer mix of paste to aggregate ratio 0.34 and solid to ash content ratio 0.63 showed the highest compressive strength at ambient temperature curing [85].

*Somna et al.* (2011) reported that ground fly ash synthesised with hydroxide for 5 minutes cured at room temperature produced more strength than ordinary fly ash based geopolymer paste. The ground fly ash had the higher surface area than ordinary fly ash, resulted in a significant improvement compressive strength at ambient temperature. XRD results of NaOH activated ground fly ash showed the presence of more amorphous and crystalline phase of quartz ( $\text{SiO}_2$ ) and hematite ( $\text{Fe}_2\text{O}_3$ ) than ordinary fly ash geopolymer matrix [86].

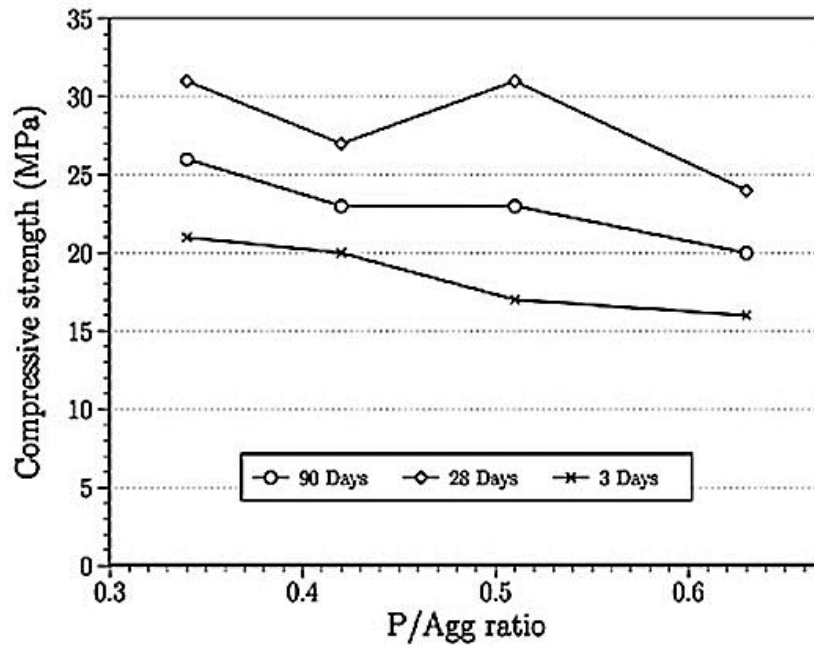


**Figure – 2.44: Relation between compressive strength and paste to aggregate ratio of IPCs (Wongpa, 2010).**

Nath *et al.* (2012) reported that the inclusion of slag up to 30 % of total binder in the fly ash based geopolymer mixture decreased the setting time and increased the compressive strength up to 55MPa at 28days of normal temperature cured geopolymer mortar. With the increase of alkaline activator solution in the mix from 35% to 45% of total binder, the setting time increased and compressive strength decreased (Fig 2.45). The improvement of strength of fly ash and slag blended geopolymer concrete was due to the increase of calcium bearing compound in the dissolute binder which produced reaction product from both alkali activated fly ash and slag. The higher Si/Al ratio of slag incorporated mixes also contributed to harden fast and develop strength [87].

Application of nano particle is an important area of research for development of normal temperature cured geopolymer concrete. It has been noted that an important additive materials to concrete specimens to acquire higher strengths is nanoparticle such as SiO<sub>2</sub> and Al<sub>2</sub>O<sub>3</sub>. Nanoparticles can act as heterogeneous nuclei for cement pastes, further accelerating cement hydration because of their high reactivity, as nano-reinforcement, and as nano-filler, densifying the microstructure, thereby, leading to a reduced porosity.

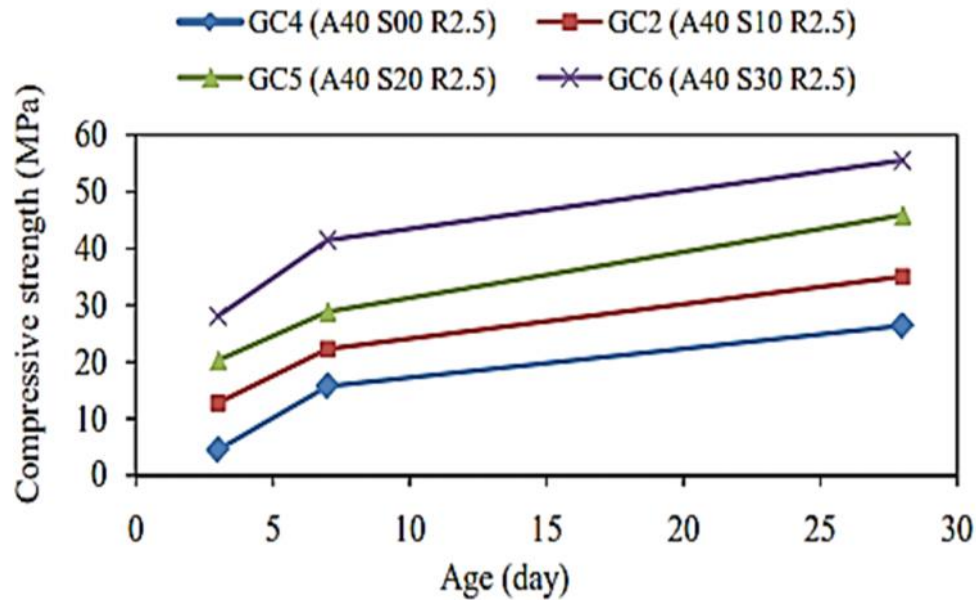


**Figure – 2.45: Compressive strength of the geopolymer concrete at different percentage of GBFS (Nath, 2012).**

*Khater et al.* (2012) studied the effect of nano-silica on alkali activated water-cooled slag geopolymer cured at ambient temperature. It was reported that the addition of nano silica results enhanced the compressive strength of alkali activated water cooled geopolymer concrete cured at ambient temperature compared with specimens without nano silica. Nano silica with its amorphous and high specific surface area increases geopolymerization process. It was observed in XRD analysis that due to transformation of the amorphous component in the geopolymer into crystalline one with increase of nano-silica content which is positively reflected on their microstructural and mechanical properties [88].

*Tanakorn Phoo-ngernkham et al.* (2014) reported that the effect of adding nano-SiO<sub>2</sub> and nano-Al<sub>2</sub>O<sub>3</sub> on the properties of high calcium fly ash geopolymer pastes. The compressive strength and flexural strengths of geopolymer pastes containing nano-SiO<sub>2</sub> and nano-Al<sub>2</sub>O<sub>3</sub> were higher than that of control paste. At 90 days, the compressive strengths of pastes containing 2% nano-SiO<sub>2</sub> and nano-Al<sub>2</sub>O<sub>3</sub> increased to 51.8 and 56.4 MPa, respectively compared with 39.4 MPa of the control paste. At 90 days, the flexural strengths of pastes containing 2% nano-SiO<sub>2</sub> and nano-Al<sub>2</sub>O<sub>3</sub> were 5.98 and 5.92 MPa compared with 4.31 MPa of the control paste. It was also reported that the compressive strengths at 90 days of 3% of nano-SiO<sub>2</sub> and nano-Al<sub>2</sub>O<sub>3</sub> reduced to 48.1 and 46.1 MPa which informed that the properties



of high calcium FA geopolymer could be enhanced with addition of 2% nano-SiO<sub>2</sub> and nano-Al<sub>2</sub>O<sub>3</sub> by weight. The SEM and XRD analysis indicated that the microstructures of geopolymer pastes containing 1–2 % nano-SiO<sub>2</sub> and nano-Al<sub>2</sub>O<sub>3</sub> were enhanced with denser matrix and increased reaction products. The addition of nano-SiO<sub>2</sub> as additive to high calcium fly ash geopolymer paste resulted in the decrease of setting time due to the formation of CSH which accelerated the setting and hardening of geopolymer pastes. While, the addition of same amount of nano-Al<sub>2</sub>O<sub>3</sub> resulted in only a slight reduction in setting time. Mechanical strength of high calcium fly ash based geopolymer concrete cured at ambient temperature increased with addition of nano-SiO<sub>2</sub> and nano-Al<sub>2</sub>O<sub>3</sub> due to the formation of additional CSH or CASH and NASH gels in geopolymer matrix [89].

*Shadi Riahi et al.* (2012) reported that with the addition of 3% nano SiO<sub>2</sub> in the fly ash based geopolymer concrete showed better compressive strength at early ages than geopolymer concrete without nano SiO<sub>2</sub>. It was also reported that nano Al<sub>2</sub>O<sub>3</sub> had no effect on the strength development of geopolymer mortar [90].

## **2.5 Antibacterial activity of conventional concrete and geopolymer concrete:**

Deterioration of concrete generally occur when any environmental agent can break the inorganic bonds of the cement binder. Acids, sulphates, ammonium and magnesium salts, alkalis, organic esters, and carbon dioxide can destroy a binder over time. The deterioration of concrete by different is also an important research area. Sources of sulphate which can cause sulphate attack include groundwater, seawater, wastewater oxidation of sulphide minerals in clay adjacent to the concrete, pollution from industrial waste and masonry [91].

Sulphate deterioration of concrete materials is bio-corrosion – the process caused by presence and activities of microorganisms producing sulphuric acid. The biogenic sulphuric acid is generated by complex mechanisms and various microbial species, particularly ferrous and sulphur oxidizing bacteria genera *Acidithiobacillus*. There are five species of *Acidithiobacillus sp.* that play important roles on corroded and corroding concrete: *T. thioparus*, *T. novellus*, *T. neapolitanus*, *T. intermedius* and *Ac. thiooxidans*. The first four species listed are neutrophilic sulfur-oxidizing microorganisms (NSOM). The last species listed is an acidophilic sulphur-oxidizing microorganism (ASOM) [92].

Concrete has a typical pH of approximately 11 or 12, depending upon the mix design. This high pH is the result of the formation of calcium hydroxide  $[Ca(OH)_2]$  as a by-product of the hydration of cement. A surface pH of 11 or 12 does not allow the growth of any bacteria. The pH of this concrete is slowly lowered over time due to carbon dioxide ( $CO_2$ ) and hydrogen sulphide gas ( $H_2S$ ). These gases are known as "acid" gases because they form relatively weak acid solutions when dissolved in water. Carbon dioxide produces carbonic acid and  $H_2S$  produces thiosulfuric and poly thionic acid. They dissolve in the water on the moist surfaces above the sewage flow and react with the calcium hydroxide to reduce the pH of the surface. Eventually the surface pH is reduced to a level ( $pH < 9$ ), which supports the growth of bacteria. At this point, the contest between the durability of the concrete or mortar and the deterioration from acids produced by the *Thiobacillus* bacteria begins and the time line toward serious corrosion and even line collapse has started. Biological colonization occurs around pH 9. Over 60 different species of bacteria are known to regularly colonize wastewater pipelines and structures above the water line (Fig 2.46). Most species of bacteria in the genus *Thiobacillus* have the unique ability to convert hydrogen sulphide gas to sulphuric acid in the presence of oxygen. Because each species of bacteria can only survive under a specific set of environmental conditions, the particular species inhabiting the colonies change with time. The production of sulphuric acid from hydrogen sulphide is an aerobic-biological process and occurs on surfaces exposed to atmospheric oxygen [93].



**Figure – 2.46: Bacterial attack on concrete.**

Generally, the methods commonly used for the concrete structures protection from bio-deterioration include modifications of concrete mix design coatings that may be sprayed, painted or rolled onto the concrete surface and liners. The concrete mix modification usually

involves increasing the alkalinity, since the corrosion rate is inversely proportional to concrete alkalinity. The concrete that we expect to expose on the biological attack should indicate the water-to-cement ratio  $w/cm = 0.45$ , and depth of the water penetration  $< 2.0$  cm, and should contain specific additives including polypropylene or other fibers, and biocides. The additives may be prepared as bacteriostatic composite systems protecting concrete for a long time [93]. Biocides selection must always depend on the microorganisms that will settle the concrete stone. Simultaneous usage of the biocide and the protective coating as well as the biocides addition to the coating are more frequently recommended.

There are almost no literature on antibacterial activity of geopolymer concrete. *Hashimoto et al.* (2015) reported that about the antimicrobial activity of geopolymer made from metakaolin and an alkali solution samples immersion in copper chloride solution for 24h and ion-exchanged with copper ions [94]. The effect of the amount of copper ions eluted from geopolymer particles ion-exchanged inside the saw-tooth oak sawdust on antimicrobial activity, the sawdust plus mushroom hyphae was mixed with copper chloride solutions of 0.01, 0.05, or 0.10 mol/L concentrations. The samples composed of sawdust with oyster mushroom hyphae treated with the copper chloride solutions after zero and seven days. At greater copper ion concentrations, the colour of the samples did not change from brown to white, indicating suppression of growth of the oyster mushroom hyphae. *Nies* (1999) reported that a copper ion concentration of 1 mmol/L was the minimum concentration that exhibited antimicrobial activity against microorganisms (*Escherichia coli*) [95]. In the present study, 8mL of a 0.01, 0.05, or 0.10 g/mL copper chloride solution was mixed with 25g of sawdust containing 7.5 g (30 mass %) of water. Therefore, the actual copper chloride concentrations in the 0.01, 0.05, and 0.1 g/mL solutions were 5, 25 and 50 mmol/L, respectively. When the copper chloride concentration was greater than 25 mmol/L, antimicrobial activity against oyster mushroom growth was complete. However, at 5 mmol/L, antimicrobial activity was slight compared to that for the sample without geopolymer particles (Fig 2.47). At a copper chloride concentration of 5 mmol/L, the concentration of copper ions was approximately 300 ppm. It was also reported that the concentration of copper ions

greater than 300 ppm possessed antimicrobial activity that completely suppressed the growth of oyster mushroom hyphae.

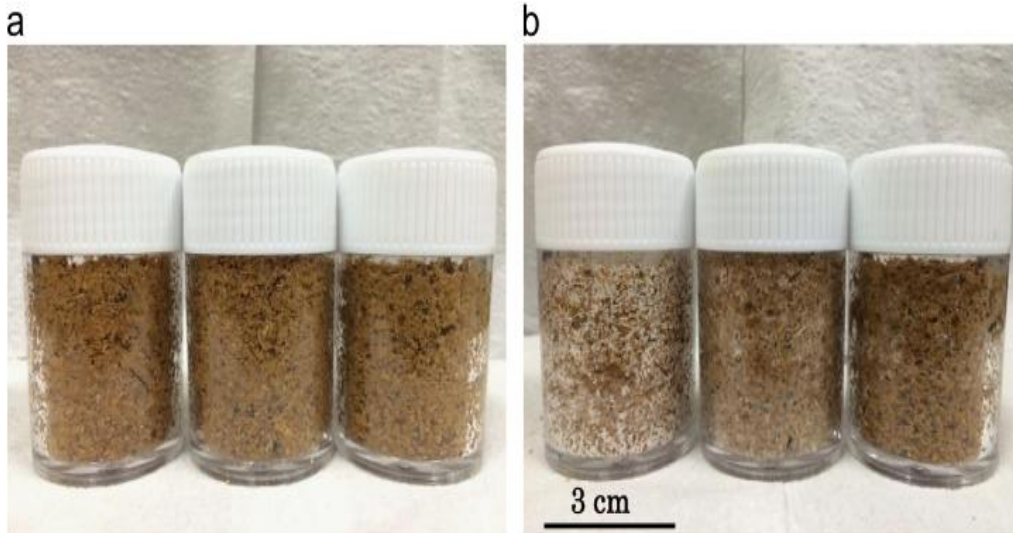


**Figure – 2.47: Optical photograph of samples of snow dust with oyster mushroom hyphae and copper chloride solution at various concentration (Nies, 1999).**

## 2.6 Aim of the study:

Based on the review of literature on the geopolymer mortar/concrete, a comprehensive experimental programme has been taken up on fly ash based geopolymer mortar and subsequently geopolymer concrete. The basic aim is to develop geopolymer mortar/concrete using low calcium fly ash (abundantly available in India) without heat activation for practical purpose. This has been made in the present study (I) by the addition of appropriate amount of nano silica and (II) by the modification of process of heat cured geopolymer mortar/concrete. The structural performance of such modified geopolymer concrete has been also studied. Finally, an attempt has been made to improve the antibacterial activity of geopolymer mortar using silver-silica nano composite. The details of the study are as follows:

- ✓ To develop nano silica modified geopolymer mortar/concrete cure at ambient temperature at different molar concentrations of activated fluid.
- ✓ To determine the mechanical strength and durability performance in terms of RCPT and water absorption of nano silica modified geopolymer mortar (cured at ambient temperature) and compare to the heat cured geopolymer mortar and control cement mortar.

- ✓ To access the antibacterial property of geopolymer mortar with silver-silica nano composite cured at ambient temperature.
- ✓ To study the structural behaviours (compressive, split tensile, bond strength, modulus of elasticity and flexural behaviour) study of nano silica modified geopolymer concrete and compare with heat cured geopolymer concrete and OPC concrete.
- ✓ To develop an energy efficient process for geopolymer mortar at different fluid to fly ash ratio, cured at ambient temperature after casting for practical purpose.
- ✓ To study mechanical strength and durability study of process modified geopolymer mortar and compare with conventional heat cured geopolymer and control cement mortar.
- ✓ To determine the structural behaviour of process modified geopolymer concrete and compare with conventional heat cured geopolymer concrete.

## REFERENCES:

---

- [1] Davidovits, J. (1988, June). Geopolymer chemistry and properties. In *Geopolymer* (Vol. 88, No. 1, pp. 25-48).
- [2] Davidovits, J. (1999, June). Chemistry of geopolymeric systems, terminology. In *Geopolymer* (Vol. 99, pp. 9-40).
- [3] Provis JL, van Deventer J. S. J, editors. *Geopolymers, structure, processing, properties and industrial applications*. Oxford: Woodhead Publishing Limited, 2009; 211–26.
- [4] Duxson, P., Fernández-Jiménez, A., Provis, J. L., Lukey, G. C., Palomo, A., & Van Deventer, J. S. J. Geopolymer technology: the current state of the art. *Journal of Materials Science*, 42(9) (2007): 2917-2933.
- [5] Barbosa, V. F., & MacKenzie, K. J. Synthesis and thermal behaviour of potassium sialate geopolymers. *Materials Letters*, 57(9) (2003): 1477-1482.
- [6] Teixeira-Pinto, A., Fernandes, P., & Jalali, S. (2002, October). Geopolymer manufacture and application-Main problems when using concrete technology. In *Geopolymers 2002 International Conference*. Melbourne, Australia, Siloxo Pty Ltd.
- [7] Palomo, A., Blanco-Varela, M. T., Granizo, M. L., Puertas, F., Vazquez, T., & Grutzeck, M. W. Chemical stability of cementitious materials based on metakaolin. *Cement and Concrete Research*, 29(7) (1999): 997-1004.
- [8] Swanepoel, J. C., & Strydom, C. A. Utilisation of fly ash in a geopolymeric material. *Applied Geochemistry*, 17(8) (2002): 1143-1148.
- [9] Xu, H., & Van Deventer, J. S. J. The geopolymerisation of alumino-silicate minerals. *International Journal of Mineral Processing*, 59(3) (2000): 247-266.
- [10] Cheng, T. W., & Chiu, J. P. Fire-resistant geopolymer produced by granulated blast furnace slag. *Minerals Engineering*, 16(3) (2003): 205-210.
- [11] He, J., Jie, Y., Zhang, J., Yu, Y., & Zhang, G. Synthesis and characterization of red mud and rice husk ash-based geopolymer composites. *Cement and Concrete Composites*, 37 (2013): 108-118.
- [12] Hajjaji, W., et al. "Composition and technological properties of geopolymers based on metakaolin and red mud." *Materials & Design*, 52 (2013): 648-654.

- 
- 
- [13] Kupaei, Ramin Hosseini, et al. "Mix design for fly ash based oil palm shell geopolymer lightweight concrete." *Construction and Building Materials*, 43 (2013): 490-496.
- [14] Kouamo, H. Tchakoute, et al. "Synthesis of volcanic ash-based geopolymer mortars by fusion method: Effects of adding metakaolin to fused volcanic ash." *Ceramics International*, 39.2 (2013): 1613-1621.
- [15] Yang, Z. X., et al. "Geopolymer concrete fabricated by waste concrete sludge with silica fume." *Materials Science Forum*, 620 (2009).
- [16] Yang, Z. X., et al. "The performance of geopolymer based on recycled concrete sludge." *Ceramic Materials and Components for Energy and Environmental Applications: Ceramic Transactions*, 210 (2010): 221.
- [17] Allahverdi, A., and E. Najafi Kani. "Construction wastes as raw materials for geopolymer binders." *Int J Civil Eng*, 7.3 (2009): 154-160.
- [18] Ahmari, Saeed, et al. "Production of geopolymeric binder from blended waste concrete powder and fly ash." *Construction and Building Materials*, 35 (2012): 718-729.
- [19] Murri, Annalisa Natali, et al. "Production and characterization of geopolymer blocks based on hydroxyapatite rich biomass ashes." *Ceramics International*, 41.10 (2015): 12811-12822.
- [20] Hervé Kouamo Tchakouté, Sakeo Kong, Jean Noël Yankwa Djobo, Leonel Noubissié Tchadjié, Daniel Njopwouo, A comparative study of two methods to produce geopolymer composites from volcanic scoria and the role of structural water contained in the volcanic scoria on its reactivity, *Ceramics International*, 41 (2015): 12568–12577.
- [21] Andini, S., et al. "Coal fly ash as raw material for the manufacture of geopolymer-based products." *Waste management*, 28.2 (2008): 416-423.
- [22] Kong, Daniel LY, Jay G. Sanjayan, and Kwesi Sagoe-Crentsil. "Factors affecting the performance of metakaolin geopolymers exposed to elevated temperatures." *Journal of Materials Science*, 43.3 (2008): 824-831.
- [23] Palomo, A., M. W. Grutzeck, and M. T. Blanco. "Alkali-activated fly ashes: a cement for the future." *Cement and concrete research*, 29.8 (1999): 1323-1329.

- 
- 
- [24] Hardjito D, Rangan BV. Development and properties of low-calcium fly ash based geopolymer concrete. Research report GC1. Perth (Australia): Faculty of Engineering Curtin University of Technology; 2005.
- [25] Xu, Hua, and Jannie SJ Van Deventer. "Geopolymerisation of multiple minerals." *Minerals Engineering*, 15.12 (2002): 1131-1139.
- [26] Chindaprasirt, P., T. Chareerat, and Vute Sirivivatnanon. "Workability and strength of coarse high calcium fly ash geopolymer." *Cement and Concrete Composites*, 29.3 (2007): 224-229.
- [27] Heah, C. Y., et al. "Study on solids-to-liquid and alkaline activator ratios on kaolin-based geopolymers." *Construction and Building Materials*, 35 (2012): 912-922.
- [28] Van Jaarsveld, J. G. S., J. S. J. van Deventer, L. Lorenzen. Factors Affecting the Immobilization of Metals in Geopolymerized Fly Ash. *Metallurgical and Material Transactions B*, 29B (1998): 283-291.
- [29] Ryu, Gum Sung, et al. "The mechanical properties of fly ash-based geopolymer concrete with alkaline activators." *Construction and Building Materials*, 47 (2013): 409-418.
- [30] Görhan, Gökhan, and Gökhan Kürklü. "The influence of the NaOH solution on the properties of the fly ash-based geopolymer mortar cured at different temperatures." *Composites part b: engineering*, 58 (2014): 371-377.
- [31] Barbosa, Valeria FF, Kenneth JD MacKenzie, and Clelio Thaumaturgo. "Synthesis and characterisation of materials based on inorganic polymers of alumina and silica: sodium polysialate polymers." *International Journal of Inorganic Materials*, 2.4 (2000): 309-317.
- [32] R.H. Abdul Rahim, T. Rahmiati, K. A. Azizli, Z. Man, M.F. Nuruddin, L. Ismail, Comparison of using NaOH and KOH Activated Fly Ash-based Geopolymer on the Mechanical Properties, *Materials Science Forum*, 803 (2015), 179-184.
- [33] Pal Santanu, Mandal Saroj. "Different Thermal activation effect on fly ash Based Geo-polymer Concrete". *Indian Concrete Institute Journal*, 12 (2011): 23-25.
- [34] Vijai, K., R. Kumutha, and B. G. Vishnuram. "Effect of types of curing on strength of geopolymer concrete." *International Journal of the Physical Sciences*, 5.9 (2010): 1419-1423.



- 
- 
- [35] Chindaprasirt, Prinya, Ubolluk Rattanasak, and Sompop Taebuanhuad. "Role of microwave radiation in curing the fly ash geopolymer." *Adv Powder Technol*, 24 (2013): 703-707.
- [36] Bakharev, T. "Geopolymeric materials prepared using Class F fly ash and elevated temperature curing." *Cement and Concrete Research*, 35.6 (2005): 1224-1232.
- [37] Hardjito, Djwantoro, et al. "On the development of fly ash-based geopolymer concrete." *ACI Materials Journal-American Concrete Institute*, 101.6 (2004): 467-472.
- [38] Škvára, František, Tomáš Jílek, and Lubomír Kopecký. "Geopolymer materials based on fly ash." *Ceram.-Silik*, 49.3 (2005): 195-204.
- [39] Mishra, Anurag, et al. "Effect of concentration of alkaline liquid and curing time on strength and water absorption of geopolymer concrete." *ARPJ Journal of Engineering and Applied Sciences*, 3.1 (2008): 14-18.
- [40] Lloyd N, Rangan B. Geopolymer concrete with fly ash. In: Second international conference on sustainable construction materials and technologies, 3(2010): 1493–504.
- [41] Sathonsaowaphak, Apha, Prinya Chindaprasirt, and Kedsarin Pimraksa. "Workability and strength of lignite bottom ash geopolymer mortar." *Journal of Hazardous Materials*, 168.1 (2009): 44-50.
- [42] Deb, Partha Sarathi, Pradip Nath, and Prabir Kumar Sarker. "The effects of ground granulated blast-furnace slag blending with fly ash and activator content on the workability and strength properties of geopolymer concrete cured at ambient temperature." *Materials & Design*, 62 (2014): 32-39.
- [43] Van Chanh, Nguyen, Bui Dang Trung, and Dang Van Tuan. "Recent research geopolymer concrete." The 3rd ACF International Conference-ACF/VCA, Vietnam. 2008.
- [44] Hardjito, D., et al. "Introducing fly ash-based geopolymer concrete: manufacture and engineering properties." 30th Conference on our World in Concrete and Structures. 2005.
- [45] Chindaprasirt, Prinya, et al. "Comparative study on the characteristics of fly ash and bottom ash geopolymers." *Waste Management*, 29.2 (2009): 539-543.

- 
- 
- [46] Álvarez-Ayuso, E., et al. "Environmental, physical and structural characterisation of geopolymer matrixes synthesised from coal (co-) combustion fly ashes." *Journal of Hazardous Materials*, 154.1 (2008): 175-183.
- [47] Davidovits J. "Geopolymers: inorganic polymeric new materials." *J Therm Anal*, 37 (1991): 1633–1656.
- [48] Salih, Moslih Amer, Abang Abdullah Abang Ali, and Nima Farzadnia. "Characterization of mechanical and microstructural properties of palm oil fuel ash geopolymer cement paste." *Construction and Building Materials*, 65 (2014): 592-603.
- [49] Barbosa, V.F.F., K MacKenzie, K.J.D. and Thaumaturgo, C. "Synthesis and Characterisation of Sodium Polysialate Inorganic Polymer Based on Alumina and Silica", Geopolymer '99 International Conference, France, 1999.
- [50] Djwantoro Hardjito, Chua Chung Cheak & Carrie Ho Lee Ing, Strength and Setting Times of Low Calcium Fly Ash-based Geopolymer Mortar, *Modern Applied Science*, 2 (2008): 4.
- [51] Rovnaník, Pavel. "Effect of curing temperature on the development of hard structure of metakaolin-based geopolymer." *Construction and Building Materials*, 24.7 (2010): 1176-1183.
- [52] Hardjito, D., Wallah, S. E., Sumajouw, D. M. J. & Rangan, B. V., 2004, 'The Stress-Strain Behaviour of Fly Ash-Based Geopolymer Concrete', in *Development in Mechanics of Structures & Materials*, vol. 2, Eds. A.J. Deeks and Hong Hao, A.A. Balkema Publishers - The Netherlands, pp. 831-834.
- [53] Sofi, M., et al. "Engineering properties of inorganic polymer concretes (IPCs)." *Cement and Concrete Research*, 37.2 (2007): 251-257.
- [54] Olivia, Monita, and Hamid Nikraz. "Properties of fly ash geopolymer concrete designed by Taguchi method." *Materials & Design*, 36 (2012): 191-198.
- [55] Radomir Zejak, Irena Nikoli, Dragoljub Ble, Vuk Radmilovi, Velimir Radmilovi, Mechanical and microstructural properties of the fly-ash-based geopolymer paste and mortar, *Materials and technology*, 47 (2013) 4, 535–540.
- [56] Ganesan, N., et al. "Stress–strain behaviour of confined Geopolymer concrete." *Construction and Building Materials*, 73 (2014): 326-331.
- [57] ACI 363R-92. State-of-the-art report on high-strength concrete. ACI committee report 363. American Concrete Institute, Detroit, 363R1–363R55; 1992.

- 
- 
- [58] Committee Euro-International du Beton (CEB-FIP). CEB-FIP model code 1990, Thomas Telford, London; 1993.
- [59] De Larrard F, Malier Y., "Engineering properties of very high performance concrete." In: Malier Y, editor. High performance concrete: from material to structure. London: E & FN Spon; 1992. p. 85–114.
- [60] Gardner, N. J., and S. M. Poon. "Time and temperature effects on tensile, bond, and compressive strengths." *Journal Proceedings*. Vol. 73. No. 7. 1976.
- [61] Sarker, Prabir Kumar. "Bond strength of reinforcing steel embedded in fly ash-based geopolymer concrete." *Materials and structures*, 44.5 (2011): 1021-1030.
- [62] P. Yellaiah, Sanjay Kumar Sharma, T. D. Gunneswara Rao, "Tensile strength of fly ash based geopolymer mortar." *ARPJ Journal of Engineering and Applied Sciences*, 9 (2014).
- [63] Sofi, M., et al. "Bond performance of reinforcing bars in inorganic polymer concrete (IPC)." *Journal of Materials Science*, 42.9 (2007): 3107-3116.
- [64] Kusbiantoro, Andri, et al. "The effect of microwave incinerated rice husk ash on the compressive and bond strength of fly ash based geopolymer concrete." *Construction and Building Materials*, 36 (2012): 695-703.
- [65] Castel, Arnaud, and Stephen J. Foster. "Bond strength between blended slag and Class F fly ash geopolymer concrete with steel reinforcement." *Cement and Concrete Research*, 72 (2015): 48-53.
- [66] Chang, Ee Hui, et al. "Bond behaviour of reinforced fly ash-based geopolymer concrete beams." 24th Biennial Conf. of the Concrete Institute of Australia. Vol. 10. Concrete Institute of Australia, Luna Park, Sydney, 2009.
- [67] Rangan, B. Vijaya, et al. "Reinforced low-calcium fly ash-based geopolymer concrete beams and columns." 31st conference on our world in concrete & structures. 2006.
- [68] Ambily, P. S., et al. "Experimental and analytical investigations on shear behaviour of reinforced geopolymer concrete beams." *International Journal of Civil & Structural Engineering*, 2.2 (2011): 682-697.
- [69] Shigemoto, N., et al. "Characterization of Na-X, Na-A, and coal fly ash zeolites and their amorphous precursors by IR, MAS NMR and XPS." *Journal of materials science*, 30.22 (1995): 5777-5783.

- 
- 
- [70] Gomes, S., et al. "Characterization of magnetite in silico-aluminous fly ash by SEM, TEM, XRD, magnetic susceptibility, and Mössbauer spectroscopy." *Cement and Concrete Research*, 29.11 (1999): 1705-1711.
- [71] Jun, Yubin, and Jae Eun Oh. "Mechanical and microstructural dissimilarities in alkali-activation for six Class F Korean fly ashes." *Construction and Building Materials*, 52 (2014): 396-403.
- [72] Fletcher, Ross A., et al. "The composition range of aluminosilicate geopolymers." *Journal of the European Ceramic Society*, 25.9 (2005): 1471-1477.
- [73] Mužek, Mario Nikola, Jelica Zeli , and Dražan Jozi . "Microstructural characteristics of geopolymers based on alkali-activated fly ash." *Chemical and Biochemical Engineering Quarterly*, 26.2 (2012): 89-95.
- [74] Lloyd, Redmond R., John L. Provis, and Jannie SJ van Deventer. "Microscopy and microanalysis of inorganic polymer cements. 1: remnant fly ash particles." *Journal of materials science*, 44.2 (2009): 608-619.
- [75] Rangan, B. Vijaya, et al. "Studies on fly ash-based geopolymer concrete." *Proceedings of the World Congress Geopolymer, Saint Quentin, France*. Vol. 28. 2005.
- [76] Wallah, S. E., and B. Vijaya Rangan. "Low-calcium fly ash-based geopolymer concrete: long-term properties." *Res. Report-GC2, Curtin University, Australia*. pp (2006): 76-80.
- [77] Buchwald, Anja. "What are geopolymers? Current state of research and technology, the opportunities they offer, and their significance for the precast industry." *Betonwerk und Fertigteil-Technik* 72.7 (2006).
- [78] Kong, Daniel LY, and Jay G. Sanjayan. "Effect of elevated temperatures on geopolymer paste, mortar and concrete." *Cement and concrete research*, 40.2 (2010): 334-339.
- [79] He, Peigang, et al. "Thermal evolution and crystallization kinetics of potassium-based geopolymer." *Ceramics International*, 37.1 (2011): 59-63.
- [80] Hussin, M. W., et al. "Performance of blended ash geopolymer concrete at elevated temperatures." *Materials and Structures*, 48.3 (2015): 709-720.
- [81] Vijai, K., R. Kumutha, and B. G. Vishnuram. "Effect of types of curing on strength of geopolymer concrete." *International Journal of the Physical Sciences*, 5.9 (2010): 1419-1423.

- 
- 
- [82] Guo, Xiaolu, Huisheng Shi, and Warren A. Dick. "Compressive strength and microstructural characteristics of class C fly ash geopolymer." *Cement and Concrete Composites*, 32.2 (2010): 142-147.
- [83] Xie, Tianyu, and Togay Ozbakkaloglu. "Behavior of low-calcium fly and bottom ash-based geopolymer concrete cured at ambient temperature." *Ceramics International*, 41.4 (2015): 5945-5958.
- [84] Temuujin, J., R. P. Williams, and A. Van Riessen. "Effect of mechanical activation of fly ash on the properties of geopolymer cured at ambient temperature." *Journal of Materials Processing Technology*, 209.12 (2009): 5276-5280.
- [85] Wongpa, J., et al. "Compressive strength, modulus of elasticity, and water permeability of inorganic polymer concrete." *Materials & Design*, 31.10 (2010): 4748-4754.
- [86] Somna, Kiatsuda, et al. "NaOH-activated ground fly ash geopolymer cured at ambient temperature." *Fuel*, 90.6 (2011): 2118-2124.
- [87] Nath, Pradip, and P. K. Sarker. "Geopolymer concrete for ambient curing condition." Australasian Structural Engineering Conference 2012: The past, present and future of Structural Engineering. Engineers Australia, 2012.
- [88] Khater, H. M., et al. "Effect of nano-silica on alkali activated water-cooled slag geopolymer." *ARPJ Journal of Science and Technology*, 2 (2012): 2.
- [89] Phoo-ngernkham, Tanakorn, et al. "The effect of adding nano-SiO<sub>2</sub> and nano-Al<sub>2</sub>O<sub>3</sub> on properties of high calcium fly ash geopolymer cured at ambient temperature." *Materials & Design*, 55 (2014): 58-65.
- [90] Riahi, Shadi, and Ali Nazari. "The effects of nanoparticles on early age compressive strength of ash-based geopolymers." *Ceramics International*, 38.6 (2012): 4467-4476.
- [91] Ghoualem, H. "Assessment of a Wastewater and Treatment by the Lagoon Process." *Chemical Engineering* 17 (2009).
- [92] Nica, D., et al. "Isolation and characterization of microorganisms involved in the biodeterioration of concrete in sewers." *International bio deterioration & biodegradation*, 46.1 (2000): 61-68.
- [93] Shook, William E., and Leonard W. Bell. "Corrosion control in concrete pipe and manholes." *Water Environmental Federation Orlando, Florida* (1998).
- [94] Hashimoto, Shinobu, et al. "Antimicrobial activity of geopolymers ion-exchanged with copper ions." *Ceramics International*, 41.10 (2015): 13788-13792.

- [95] Nies, Dietrich H. "Microbial heavy-metal resistance." *Applied microbiology and biotechnology*, 51.6 (1999): 730-750.



Chapter- 3...

**Instruments  
&  
Apparatus**





### **3.0 General**

The usual mechanical strength properties such as compressive strength and split tensile strength of mortar/concrete have been determined as per Indian Standard codes IS 516 (1958) and IS 5816 (1999) respectively. The different specimens have been prepared for the above test and tested accordingly. To determine the bond strength of geopolymer concrete with reinforcement, a special arrangement has been made as per IS 2770 (1997) and discussed here. The flexural strength of reinforced geopolymer concrete and the Rapid Chloride Ion Penetration Test (RCPT) of geopolymer concrete /mortar (as per ASTM C1202) have been discussed. For microstructure analysis Field Emission Scanning Electron Microscope (FESM) with Energy-dispersive X-ray Spectroscopy (EDS), Transmission Electron Microscope (TEM), X-Ray Diffraction (XRD) and Fourier Transform Infrared Spectroscopy (FTIR). The working principal and important features of some of these instruments are described briefly.

### **3.1 Bond strength:**

The load carrying capacity of reinforced concrete structure is generally influence by the interaction between the concrete and reinforcement. The stress is transferred between reinforcement and concrete in the longitudinal direction of the bars through bond. An essential feature of the reinforced concrete is the bond behavior between steel and concrete. The bond strength is determined by pull out test on the concentric deformed rebar or mild steel rebar embedded on cubical specimens. A special type of mould is designed to prepare the concrete specimen with reinforcement bar. The test specimen is then mounted in a Universal Testing Machine in such a manner that the bar is pulled axially from the cube. The end of the bar at which the pull is applied is projected from the top face of the cube. The movement between the reinforcing bar and the concrete cube, as indicated by the dial micrometers is noted at a sufficient number of intervals throughout the test. The graph load corresponding to the slip is plotted for determination of bond strength. The bond stress values are calculated as per IS 2770 (Part – I): 2007.



**Figure 3.1: Bond strength testing arrangement.**

### **3.2. Flexural strength (Reinforced concrete beam):**

Load deflection behavior and flexural strength of reinforced concrete beam is an important parameter to design a concrete structures. The test specimen is mounted in a beam testing load frame of 500 kN capacity. All the beams are simply supported and subjected to two point concentrated loads placed symmetrically on the span. The load is applied on two points and deflection is measured by dial gauge of 0.001mm least count under the load points and at mid span. The load on the beam is increased by the load cell attached with the frame. The deflection of beam at different location with respect to certain incremental load is noted. The experiment is carried out until the crack are observed. The flexural strength and moment carrying capacity of the concrete specimen with different percentages of tensile, compression and shear reinforcement is measured. The bending moment capacity of the concrete beam is determined as per IS 456: 2000.



**Figure 3.2: Flexural strength test setup for reinforced concrete beam.**

### **3.3. Chloride Ion Permeability Test (RCPT):**

According to ASTM C1202 [3], this tests has been performed using 50 mm long, 100 mm diameter water saturated cylindrical specimens cut from the long cylinder of 100 mm diameter and 200 mm length. The specimen is placed in the testing apparatus where one end of the specimen is exposed to a solution containing sodium chloride (NaCl) 3% by mass and the other end is exposed to a solution containing sodium hydroxide (NaOH) of 0.30 (N). The negative terminal is connected to the electrode in the reservoir with the NaCl solution and the positive terminal is connected to the electrode in the NaOH solution. The negatively charged chloride ions will migrate towards the positive terminal. To increase the rate of chloride penetration into the specimen, thus speeding up the test, a constant 60 V potential is applied across the specimen. The more permeable is the concrete, the more chloride ions will migrate through the specimen, and a higher current will be measured.

It will be provided with rubber gasket and washers for achieving leak proof. Stainless steel bolts with washers and nuts will be provided to hold the specimen rigidly. The power supply will be applied to each cell through banana sockets and the current will be distributed through the brass mesh. Each cell will be provided with openings in top for pouring

chemicals and the temperature sensors. The openings can be closed with lids. The volume of chemicals within the chamber shall be 250ml.

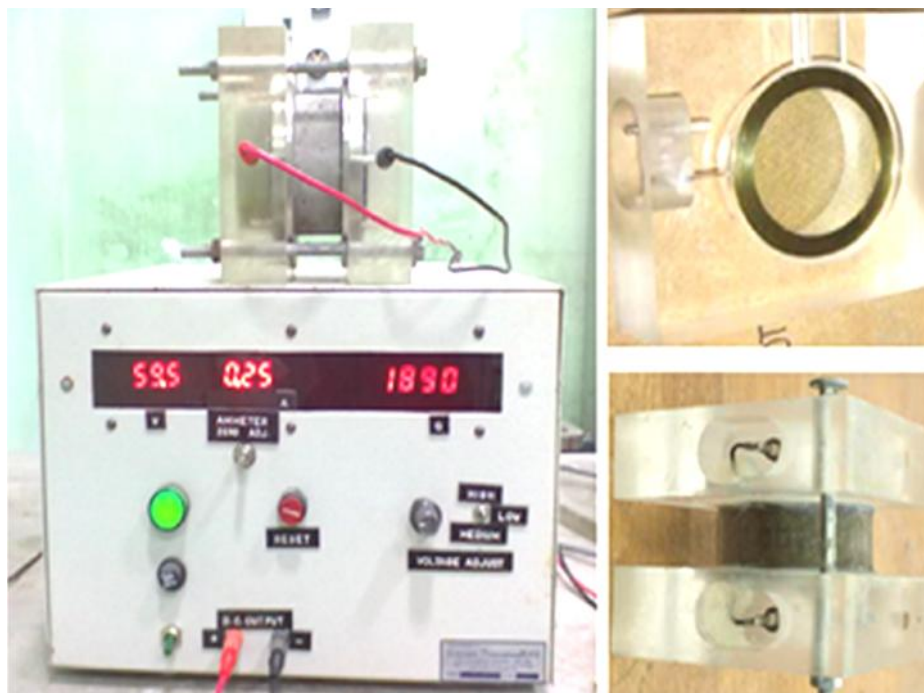


**Figure 3.3: RCPT arrangement.**

### **3.4. Field Emission Scanning Electron Microscope (FESEM):**

The scanning electron microscopy is a versatile, non-destructive technique that reveals detailed information about the morphology and the composition of natural and manufactured materials. In a scanning electron microscope, the specimen is exposed to a narrow electron beam from an electron gun, which rapidly moves over or scans the surface of the specimen. The electrons interact with the atoms that make up the sample producing signals that contain information about the sample's surface topography, composition and electrical conductivity. The types of signals produced by the FESEM include secondary electrons, back-scattered electrons (BSE), characteristic X-rays, light (cathodoluminescence), specimen current and transmitted electrons. Secondary electron detectors are standard equipment in all FESEMs, but it is rare that a single machine would have detectors for all possible signals. The signals result from interactions of the electron beam with atoms at or near the surface of the sample. In the most common or standard detection mode, secondary

electron imaging or SEI, can produce very high-resolution images of a sample surface, revealing details less than 1 nm in size. Due to the very narrow electron beam, SEM micrographs have a large depth of field yielding a characteristic three-dimensional appearance useful for understanding the surface structure of a sample.

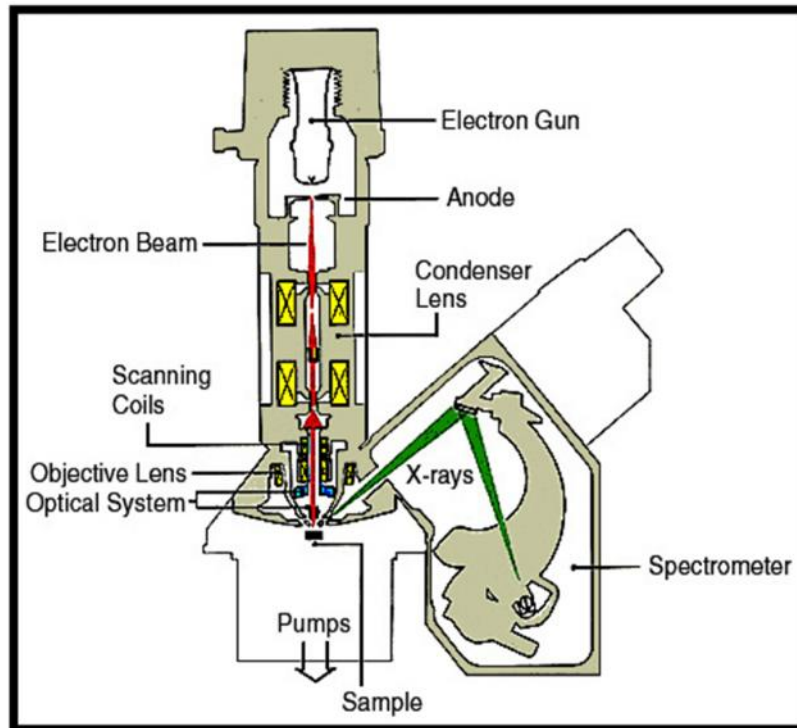


**Figure 3.4A: Graphical presentation of FESEM setup.**

INSPECT F50 SEM (FEI Europe BV, The Netherlands) has been used to characterize morphology and microstructural analysis of cementitious materials. FESEM specimens are dried, then gold coated & stored in the desiccators prior to examination using an INSPECT F50. Back-scattered electrons (BSE) are reflected from the sample by elastic scattering. BSE are often used in analytical FESEM along with the spectra made from the characteristic X-rays, because the intensity of the BSE signal is strongly related to the atomic number ( $Z$ ) of the specimen. BSE images can provide information about the distribution of different elements in the sample. Characteristic X-rays are emitted when the electron beam removes an inner shell electron from the sample, causing a higher-energy electron to fill the shell and release energy. These characteristic X-rays are used to identify the composition and measure the abundance of elements in the sample.



**Figure 3.4B: FESEM laboratory test arrangement.**

### **3.5. HI-Resolution Transmission Electron Microscope (HRTEM):**

Basic principle of HRTEM is quite similar to their optical counterparts, the optical microscope. The major difference is that in HRTEM, a focused beam of electrons instead of light is used to form image to achieve information about the structure and composition of the specimen. An electron source usually named as the “Gun” produces a stream of electrons which is accelerated towards the specimen using a positive electrical potential. This stream is then focused using metal apertures and magnetic lenses called “condenser lenses” into a thin, focused, monochromatic beam. Beam strikes the specimen and a part of it gets transmitted through it. Generally the electron beam is much more energetic than the beam used in SEM (100-300 kV in HRTEM compared to 1-30 kV in SEM). Thus the beam may pass through the sample. Samples with smaller thickness (< 100 nm) can give good images in HRTEM than in SEM. The advantages of HRTEM are due their high resolution, easy particle size measurement and the ability to determine crystallinity easily. So, the very small crystals can be identified and their crystal structures can be determined easily. From a selected area of electron diffraction pattern, a useful crystallographic data can be obtained. TEM imaging can

be combined with several material analysis techniques like Electron Energy Loss Spectroscopy (EELS), Energy Filtered TEM (EFTEM) and Energy Dispersive X-ray (EDX).

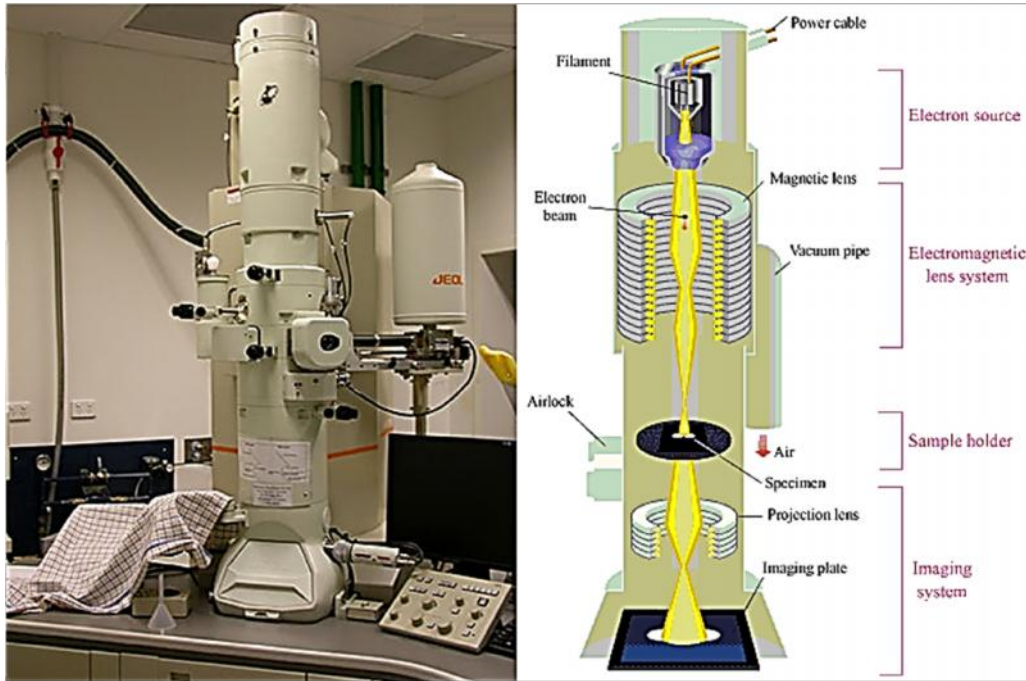


**Figure 3.5: HRTEM test setup.**

In this research study a transmission electron microscope (Model JEM-2100, JEOL, Japan) has been used to characterize the morphology of geopolymers composite and cement composite. It has three independent condenser lenses and produces the highest probe current for any given probe size which allows for improved analytical and diffraction capabilities. The JEM-2100 offers a number of pumping options including full dry pumped/Turbo-pumped versions for lab environments that do not allow for oil-based or rotary pumps. The instrument has a guaranteed resolution of 0.1 nm. The resolution attained during routine measurements is 8–10 Å. The magnification in this instrument could be varied from 50 X to 1,500,000 X with accelerating voltage 200 kV. Samples have been prepared by dropping the suspension of the sample onto a carbon coated copper grid and allowing the solvent to evaporate.

### 3.6. X-RAY Diffraction (XRD):

X-ray diffraction is now a common technique for the study of crystal structures and atomic spacing. X-ray diffraction is based on constructive interference of monochromatic X-rays and a crystalline sample. These X-rays are generated by a cathode ray tube, filtered to produce monochromatic radiation, collimated to concentrate, and directed toward the sample. The interaction of the incident rays with the sample produces constructive interference (and a diffracted ray) when conditions satisfy Bragg's Law ( $2d \sin \theta = n\lambda$  where  $n =$  an integer,  $\lambda =$  wavelength in angstroms,  $d =$  inter atomic spacing in angstroms,  $\theta =$  the diffraction angle in degrees). This law relates the wavelength of electromagnetic radiation to the diffraction angle and the lattice spacing in a crystalline sample. These diffracted X-rays are then detected, processed and counted. By scanning the sample through a range of  $2\theta$  angles, all possible diffraction directions of the lattice are to be attained due to the random orientation of the powdered material.

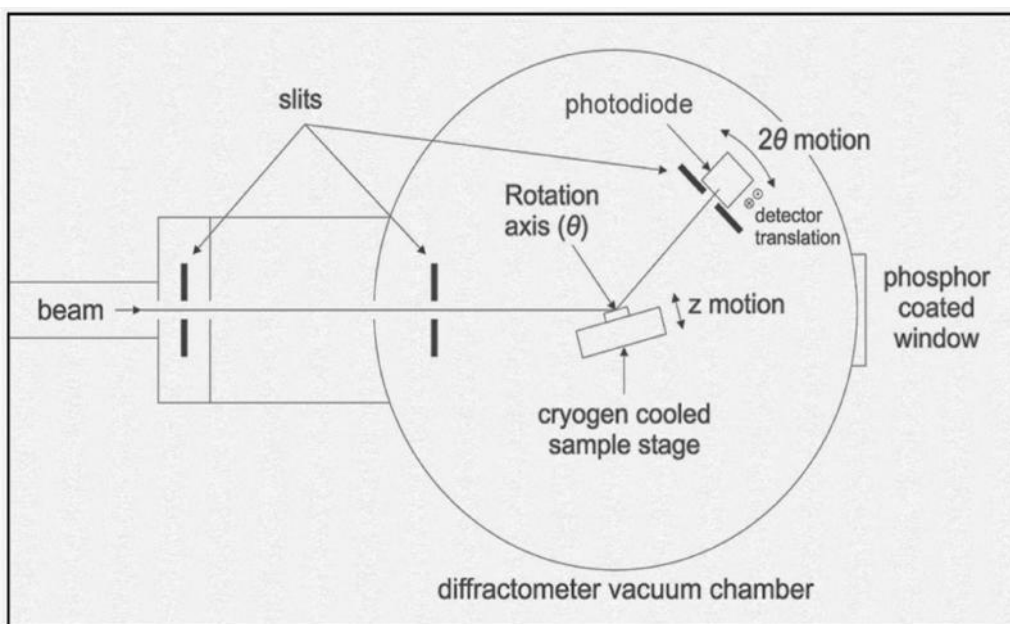


**Figure 3.6A: Graphical presentation of XRD test.**

Conversion of the diffraction peaks to d-spacings allows the identification of the mineral because each mineral has a set of unique d-spacings. Files of d-spacings for hundreds of thousands of inorganic compounds are available from the International Centre for Diffraction Data as the Powder Diffraction File (PDF). Many other sites contain d-spacings of



minerals such as the American Mineralogist Crystal Structure Database. BRUKER D8 ADVANCE instrument is used for present study for XRD analysis of geopolymer composites and control cement matrix.



**Figure 3.6B: XRD test arrangement.**

### **3.7. Fourier Transform Infra-red Spectroscopy (FTIR):**

FTIR (Fourier Transform Infra-red Spectroscopy) is a sensitive technique particularly for identifying organic chemicals in a whole range of applications although it can also characterise some inorganics. Examples include paints, adhesives, resins, polymers, coatings and drugs. A common FTIR spectrometer consists of a source, interferometer, sample compartment, detector, amplifier, A/D convertor, and a computer. The source generates radiation which passes the sample through the interferometer and reaches the detector. Then

the signal is amplified and converted to digital signal by the amplifier and analog-to-digital converter, respectively. Eventually, the signal is transferred to a computer in which Fourier transform is carried out.

FTIR relies on the fact that the most molecules absorb light in the infra-red region of the electromagnetic spectrum. This absorption corresponds specifically to the bonds present in the molecule. The frequency range is measured as wave numbers typically over the range  $4000 - 600 \text{ cm}^{-1}$ .

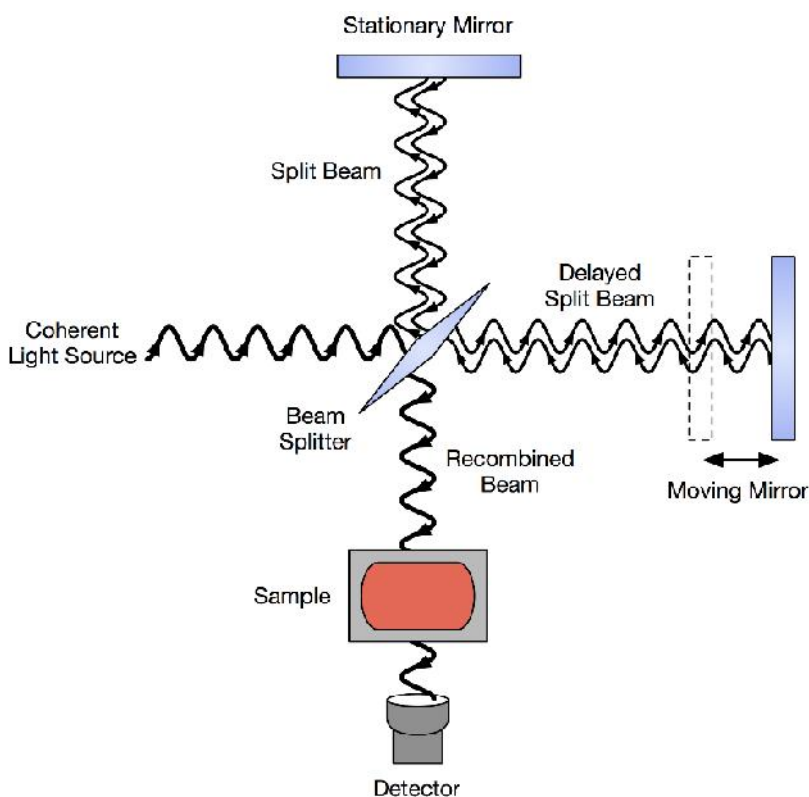


**Figure 3.7: Graphical presentation of FTIR working principal.**

The background emission spectrum of the IR source is first recorded, followed by the emission spectrum of the IR source with the sample in place. The ratio of the sample spectrum to the background spectrum is directly related to the sample's absorption spectrum. The resultant absorption spectrum from the bond natural vibration frequencies indicates the presence of various chemical bonds and functional groups present in the sample. FTIR is particularly useful for identification of organic molecular groups and compounds due to the range of functional groups, side chains and cross-links involved, all of which will have characteristic vibrational frequencies in the infra-red range.

### 3.8. Fluorescence Microscopy:

Fluorescence is a phenomenon that takes place when a substance absorbs light at a given wavelength and emits light at another wavelength. Fluorescence occurs as an electron, which has been excited to a higher and more unstable energy state, relaxes to its ground state and gives off a photon of light. The light that is responsible for excitation, or moving the electron to a higher energy state, is of shorter wavelength and higher energy than the fluorescence emission, which has a longer wavelength, lower energy, and different color. Fluorescence microscopy combines the magnifying properties of the light microscope with fluorescence technology that allows the excitation and detection of emissions from fluorophores - fluorescent chemical compounds. With fluorescence microscopy, scientists can observe the location of specific cell types within the tissues or the molecules of cells.

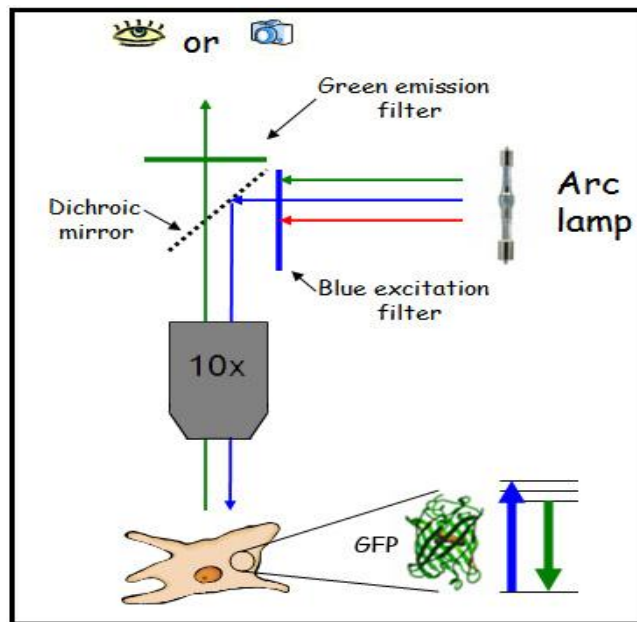


**Figure 3.8A: Graphical presentation Fluorescence Microscopy.**

The principle behind fluorescence microscopy is simple. As light leaves the arc lamp it is directed through an exciter filter, which selects the excitation wavelength. This light is reflected toward the sample by a special mirror called a dichroic mirror, which is designed to reflect light only at the excitation wavelength. The reflected light passes through the objective where it is focused onto the fluorescent specimen. The emissions from the specimen are in turn, passed back up through the objective where magnification of the image occurs and now through the dichroic mirror. This light is filtered by the barrier filter, which selects for the

emission wavelength and filters out contaminating light from the arc lamp or other sources that are reflected off of the microscope components. Finally, the filtered fluorescent emission is sent to a detector where the image can be digitized, or it's transmitted to the eyepiece for optical viewing. The exciter filter, dichroic mirror, and barrier filter can be assembled together into a component known as the filter cube. Different filter cubes can be changed during specimen viewing to change the excitation wavelength, and a series of diaphragms can be used to modify the intensity of excitation.

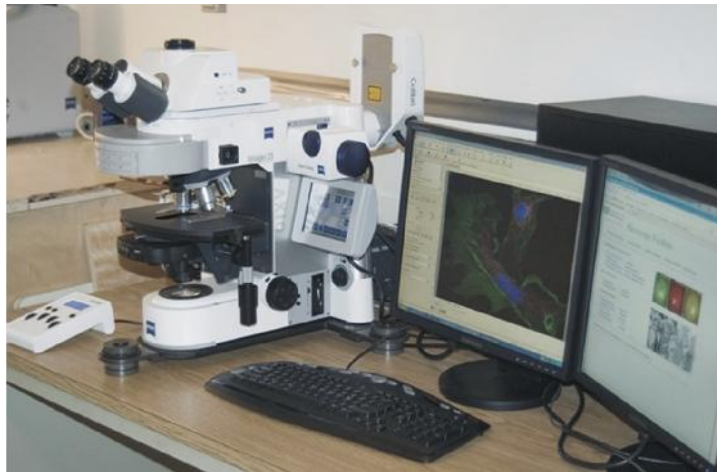


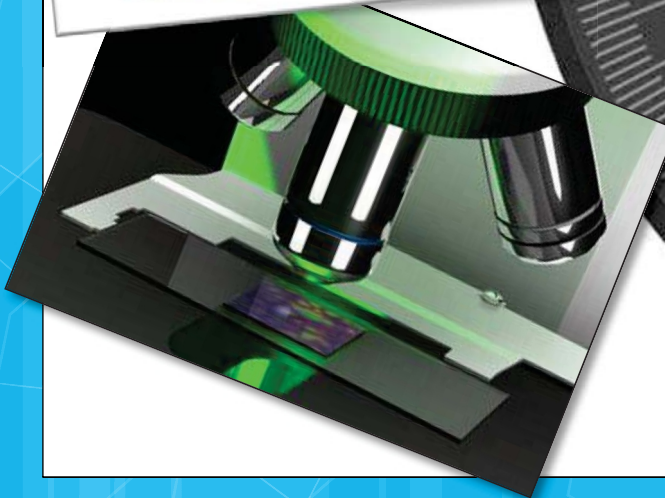
**Figure 3.8B: Fluorescence Microscopy laboratory setup.**

**List of BIS Standards:**

- ❖ IS 456 – 2000: Plain and Reinforced Concrete Code of Practice, Bureau of Indian Standards, New Delhi, India.
- ❖ IS 2770 (Part-1) – 2007: Method of Testing Bond in Reinforced Concrete; Bureau of Indian Standard, New Delhi, India.
- ❖ IS 4031 (Part – VI) – 1988: Method of Physical Test of Hydraulic Cement, Bureau of Indian Standards, New Delhi, India.
- ❖ IS 10080 – 1982: Specification for Vibration Machine, Bureau of Indian Standards, New Delhi, India.
- ❖ IS 5816 – 1999: Splitting Tensile Strength of Concrete Method of Test, Bureau of Indian Standards, New Delhi, India.
- ❖ IS 516 – 1959: Method for Test for Strength of Concrete, Bureau of Indian Standards, New Delhi, India.



Chapter- 4....



**M  
A  
T  
E  
R  
I  
A  
L  
S  
&  
M  
E  
T  
H  
O  
D  
S**



#### 4.0. EXPERIMENTAL DETAILS

The experimental studies have been conducted mainly at the Concrete Technology and Structural Engineering laboratory of Civil Engineering Department, Jadavpur University, Kolkata, India. At first, the details of all materials and chemicals used in this study are presented in section 4.1. The next two sections (4.2 & 4.3) include the experimental programme to study the effect of nano-silica on geopolymer mortar and geopolymer concrete respectively. In section 4.4, the experimental programme to study the effect of the addition of silver-silica nano composite on geopolymer mortar against bacterial action has been presented. Finally, experimentation on process development of conventional geopolymer mortar and concrete have been presented in section 4.5 and 4.6 respectively.

#### 4.1. MATERIALS & CHEMICALS.

The materials for the study include low calcium Class F fly ash (National Thermal Power Corporation Ltd, Farakka, India), Ordinary Portland Cement (43 grade), locally available river sand (Specific gravity 2.52, water absorption 0.50%, and fineness modulus of 2.38) and coarse aggregate (Specific gravity 2.78, water absorption 0.42%, and fineness modulus of 4.89) [1]. The basic physical and chemical properties of fly ash have been tested before the experimental work and are presented in Table – 4.1 and 4.2.

**Table – 4.1. Chemical analysis report of fly ash:**

Material	Chemical composition (in percentage)								
Fly Ash	SiO <sub>2</sub>	Al <sub>2</sub> O <sub>3</sub>	Fe <sub>2</sub> O <sub>3</sub>	CaO	MgO	Na <sub>2</sub> O	K <sub>2</sub> O	SO <sub>4</sub>	LOI
	64.97	26.64	5.69	0.33	0.85	0.49	0.33	0.25	0.45

**Table – 4.2. Particle size analysis report of fly ash:**

Material	Particle size distribution						
Fly Ash	>500μ	300-500μ	150-300μ	150-90μ	90-45μ	< 45μ	Specific Gravity
	NIL	1.42	11.67	48.06	31.98	6.87	2.05

Locally available Sodium hydroxide (NaOH) pellet of 99% purity and liquid sodium silicate (Na<sub>2</sub>SiO<sub>3</sub>) (specific gravity 1.53) having 45% solid content has used as an activator fluid. The colloidal nano silica (Bee Chemicals, India), Nutrient Broth (NB) media ingredients like peptone, beef extract, Yeast extract, agar (Hi-media Pvt. Ltd., India), silver nitrate (Merck Germany), deionized water, carbonic acid, *E. coli* (MTCC 1652 strain), *S. aureus* (MTCC 96 strain) bacteria have been used for this study. The basic properties of colloidal nano silica as provided by suppliers is described in Table – 4.3.

**Table – 4.3. Properties of colloidal nano silica:**

Colloidal Nano-silica	Properties of colloidal nano silica				
<b>CemSynXLP</b>	Average particle size (nm)	Solid content (Wt. %)	Viscosity (PaS)	pH	Solid density (gm/cc)
	4 to 30 nm	30%	8.5	9.0 - 9.6	2.37



## **4.2. GEOPOLYMER MORTAR WITH NANO-SILICA AND CONTROL MORTAR:**

) Preparation of geopolymer mortar (with / without nano silica) and control cement mortar.

Three different molar concentration of NaOH such as 8 (M), 10 (M) and 12 (M) have been mixed with Na<sub>2</sub>SiO<sub>3</sub> solution in the proportion of 1:1.75 (by weight) to make alkali activator fluid. The molar concentration and the ratio have been fixed on the previous study. Colloidal nano silica with 4%, 6%, 8% and 10% of fly ash by weight has been also added to the activator fluid. It may be mentioned here that water present in the colloidal nano silica is adjusted from the activator solution during the preparation. The ratio of fly ash: sand and activator fluid (with / without nano silica) to fly ash have been fixed at 1:3 (by weight) and 0.40 respectively.

The nano-silica modified geopolymer mortar samples have been prepared by thoroughly hand mixing dry fly ash and sand (by weight) with activator solution (with nano-silica). Table vibrator have been used for proper compaction. After that, the geopolymer mortar specimens with nano silica have been removed from the mould after one day of casting and are placed at ambient temperature ( $27 \pm 20$  °C) before testing.

For the preparation of conventional geopolymer mortar fly ash and sand (by weight) has been dry mixed (hand mixing) for two minutes and the appropriate amount of activator fluid of different molar concentrations is added and mixed thoroughly. Table vibrator have been used for proper compaction. The conventional geopolymer mortar specimens have been cured at 60°C temperature for 48h within the hot air oven and after 2 days of casting the specimen are kept at ambient temperature until testing. For the preparation of controlled mortar sample, Ordinary Portland Cement of 43 Grades (IS 8112) has been mixed with sand (hand mixing) [2]. However, conventional water curing has been made for the normal cement mortar specimens after one day of casting. The details of all the mixtures are shown in Table – 4.4.

### **4.2.1. Compressive Strength of mortar:**

The standard mortar cube specimen size of 70.6 mm × 70.6 mm × 70.6 mm have been prepared for compressive strength study [3, 4]. The cube specimens have been tested at 3 days, 7 days, and 28 days after casting to determine the compressive strength of both types of

geopolymer (with / without nano silica) mortar and control cement mortar. For each category eighteen numbers of samples have been tested and taken the average value. The breaking loads of the samples have been determined by compressive strength testing machine.

**Table – 4.4. Mix proportion varying molar concentration, percentage of nano silica and curing condition.**

Mix Mark	Fly ash : Sand	Molar concentration	% of nano-silica w.r.t fly ash	Curing conditions
<b>Control (CM)</b>	1:3 Cement: Sand	N.A	N.A	Conventional water curing
<b>8GM0H</b>	1:3	8.0	0.0	Heat cured at 60°C for 48h.
<b>8GM4</b>	1:3	8.0	4.0	Ambient temp.(27±2 <sup>0</sup> C) curing
<b>8GM6</b>	1:3	8.0	6.0	Ambient temp.(27±2 <sup>0</sup> C) curing
<b>8GM8</b>	1:3	8.0	8.0	Ambient temp.(27±2 <sup>0</sup> C) curing
<b>8GM10</b>	1:3	8.0	10.0	Ambient temp.(27±2 <sup>0</sup> C) curing
<b>10GM0H</b>	1:3	10.0	0.0	Heat cured at 60°C for 48h.
<b>10GM4</b>	1:3	10.0	4.0	Ambient temp.(27±2 <sup>0</sup> C) curing
<b>10GM6</b>	1:3	10.0	6.0	Ambient temp.(27±2 <sup>0</sup> C) curing
<b>10GM8</b>	1:3	10.0	8.0	Ambient temp.(27±2 <sup>0</sup> C) curing
<b>10GM10</b>	1:3	10.0	10.0	Ambient temp.(27±2 <sup>0</sup> C) curing
<b>12GM0H</b>	1:3	12.0	0.0	Heat cured at 60°C for 48h.
<b>12GM4</b>	1:3	12.0	4.0	Ambient temp.(27±2 <sup>0</sup> C) curing
<b>12GM6</b>	1:3	12.0	6.0	Ambient temp.(27±2 <sup>0</sup> C) curing
<b>12GM8</b>	1:3	12.0	8.0	Ambient temp.(27±2 <sup>0</sup> C) curing
<b>12GM10</b>	1:3	12.0	10.0	Ambient temp.(27±2 <sup>0</sup> C) curing

\*\* (xGM<sub>y</sub>, Where “GM – Geopolymer mortar”, “x – Molar concentration”, “y – percentages of nano-silica” and “0H – Heat cured without nano silica”).

#### **4.2.2. Split tensile strength test of mortar:**

The split tensile strength of nano-silica modified geopolymer, heat cured geopolymer and control cement mortar cylinder specimen of size 100 mm diameter x 200 mm height have been cast for different mixes. All the nano silica modified geopolymer mortar specimens have been tested after 28 days of air curing. The cylinder has placed horizontally between the loading surfaces of compression testing machine and the load is applied to the perpendicular to the axis of the cylinder. Plywood has been used as a packing material to avoid any sudden slip. The maximum load has been applied to the specimen recorded to calculate the split tensile strength of the specimen as per IS: 5816 (1999) [5].

#### **4.2.3. Flexural strength of mortar:**

The flexural strength tests have been carried out on beam specimens of size 100×100×200 mm under standard two point loading for all types of mortar mixes. The beam specimens have been tested in flexural testing machine under a uniform rate of loading after 28 days of curing. The test procedure has been followed according to ASTM C293 [6]. All the test results has been reported in this experimental work represent the average value obtained from a minimum of three specimens.

#### **4.2.4. Rapid Chloride Penetration Test (RCPT) of mortar:**

For chloride ion penetration, test cylinder specimen (100 mm diameter × 200 mm height) has been sliced into core specimens of thickness 50 mm. The current is passing through the specimen at 60 Volt has been recorded at 30 minutes interval over a period of six hours and total charge in Coulombs is calculated [7].

#### **4.2.5. Water absorption test on mortar:**

Water absorption capacity of mortar samples has been also determined as per Neville's method [8]. The pore structure of concrete is known to be of high importance for the durability of the material. A characterization of this pore structure by means of a simple test is often investigated, in order to find a very simple compliance criterion with respect to concrete durability. The mortar cube of dimension 70.6mm x 70.6mm x 70.6 mm have been used for this experiment. After 28 days curing, the mortar samples have been dried at 52 °C for 72 h. Then the mass of these specimens have been noted by using weighing machine. The samples

have been immersed in water for 30 min and 24h. The mass of the immersed samples mass have been recorded. This led to measure the increase in mass as a percentage of dry mass.

#### **4.2.6. Microstructure analysis of mortar:**

##### **4.2.6.1. X-Ray Diffraction analysis:**

The geopolymer mortar (with/without nano silica) and control mortar samples possessing acceptable results of compressive strength of different mixtures (12GM6, 12GM0H, CM) have been dried and sieved to make the size less than 5 $\mu$ m for X-ray diffraction analysis in powder X-ray diffractometer (Bruker AXS Inc, Model D8, WI, USA) with a scan speed 0.5 s/step at 40 KV. The XRD spectrum has been analyzed in the range  $2\theta = 10^\circ - 70^\circ$  and the peak positions are marked and compared from Joint Committee on Powder Diffraction standards (JCPDs) file.

##### **4.2.6.2. Field Emission Scanning Electron Microscopy analysis:**

For FESEM analysis, the fine powder of geopolymer and cement mortar specimens have been diluted with ethanol (99.9%) to make a film on carbon tape and then kept under vacuum desiccators for evaporation. Finally, the dried samples have been gold coated for field emission scanning electron microscope FESEM (HITACHI S-4800, JAPAN) analysis.

Based on the results of nano-silica modified geopolymer mortar, the experimental program has been taken on geopolymer concrete with / without nano-silica.

### 4.3. GEOPOLYMER CONCRETE WITH NANO SILICA:

The experimental study on geopolymer concrete (with / without nano-silica) has been grounded on the best results of nano-silica modified geopolymer mortar with 6% nano-silica at 12 molar concentration of NaOH activated solution at fluid to fly ash ratio 0.40.

J) Preparation of geopolymer concrete (with / without nano silica) and control cement concrete.

The NaOH solution (12M) has been mixed with Na<sub>2</sub>SiO<sub>3</sub> solution in the proportion of 1:1.75 (by weight) to make alkali activator fluid for both geopolymer concrete with or without nano-silica. Colloidal nano-silica with 6% of fly-ash (by weight) has been also added to the activator fluid. The amount of water present in the colloidal nano-silica is adjusted from the activator solution during the preparation. The details of the various mixes have been shown in Table – 4.5. The nano-silica modified geopolymer concrete (12GC6) specimens have been removed from the mould after 24h of casting and are placed at ambient temperature (27 ± 2°C) until the testing. However, the geopolymer concrete without nano-silica (12GC0H) specimens has been cured at a 60°C temperature for 48h within the hot air oven. After 2 days of heat curing, the samples have been kept at ambient temperature until the test. The conventional water cured cement concretes (CC) of similar compressive strength of 12GC0H have been prepared by the addition of 0.1% ViscoCrete -10R admixture and are taken as control specimens. Tilting drum has been used for proper mixing and for compaction table vibrator has been used.

**Table – 4.5: Details of nano-silica modified geopolymer (12GC6), conventional heat cured geopolymer (12GC0H) concrete and control cement concrete (CC) mix.**

Mix Mark	Cement (Kg/m <sup>3</sup> )	Fly ash (Kg/m <sup>3</sup> )	F.A (Kg/m <sup>3</sup> )	C.A (Kg/m <sup>3</sup> )	Fluid : Fly ash	% of nano silica	Curing condition
12GC6	0.0	440	723	1085	0.40	6.0	Ambient temp. curing.
12GC0H	0.0	440	723	1085	0.40	0.0	Heat curing 60°C for 48h.
CC	400.0	Nil	690	1205	0.40 (W/C)	0.0	Conventional water curing

\*\* (xGCy, Where “GC – Geopolymer concrete”, “x – Molar concentration”, “y – percentages of nano-silica”, “0H – Heat cured without nano silica”, “CC – Conventional concrete” and “W/C – Water / Cement”).

#### **4.3.1. Compressive strength tests of concrete:**

The standard cube specimens of size 150 mm × 150 mm × 150 mm dimension have been prepared for three mixes (12GC6, 12GC0H & CC) to determine the compressive strength of concrete samples. The compressive strength of each category samples has been analyzed at different ages (3, 7 & 28 days) of curing [9].

#### **4.3.2. Split tensile strength and modulus of elasticity:**

The split tensile strength testing has been carried out on 150 mm (diameter) × 300 mm geopolymer (12GC6 & 12GC0H) and control cement concrete cylinder specimen of three mixes as per IS 5816 (1999) after 28 days of curing [5]. Also, the cylinder specimen of 150 mm diameter and 300 mm height have been also prepared for the modulus of elasticity determination by using strain controlled machine (YAW3000A, China). The cylindrical samples have been capped with sulphur blinder on their two opposite flat faces and the load is continued up to about 70% of their peak stress to determine the modulus of elasticity.

#### **4.3.3. Bond strength:**

The bond strength of geopolymer (12GC6 & 12GC0H) and control cement concrete (CC) have been determined by pull out test on the concentric deformed rebar or mild steel rebar embedded on cubical specimens of 150 mm × 150 mm × 150 mm. During casting and subsequent compaction, the concentrically placed steel bars have been held in position using a specially designed steel mould arrangement. The specimens for each category have been tested after 28 days of curing. The experiment has been completed when pull-out failure of reinforcement bar (deformed; 0.2% proof stress = 500 MPa & mild steel; yield stress = 250 MPa) occurred. The slip corresponding to the load has been noted and the corresponding bond strength between reinforcement and concrete is determined as per IS 2770 [10].

#### **4.3.4. Flexural strength test on reinforced concrete beam:**

The reinforced concrete beam specimens for three mixes have been 100 × 150 mm in cross section and length of 1200mm, simply supported over an effective span of 900mm. The nominal cover to rebar of the beam has been 15mm. The details of three different percentages of tensile, compression and shear reinforcement are shown in Table – 4.6. The load has been

applied on two points each 150 mm away from the centre of the beam towards the support (Fig 4.1 & 4.2). The deflections at the centre and at the load point have been measured against the load applied at intervals of 1.0 KN. The maximum experimental bending moment is calculated at mid span is  $M_{the} = P \times (L/3)$ , where 'P' is the load applied at equal distance with respect to mid-point of the beam and 'L' is the clear span of the beam. The theoretical bending moment ( $M_{exp}$ ) of the beam has been calculated as per IS 456 (2000) [11]. The bending moment capacity of reinforced geopolymer concrete (with / without nano-silica) beam and control cement concrete beam have been determined.

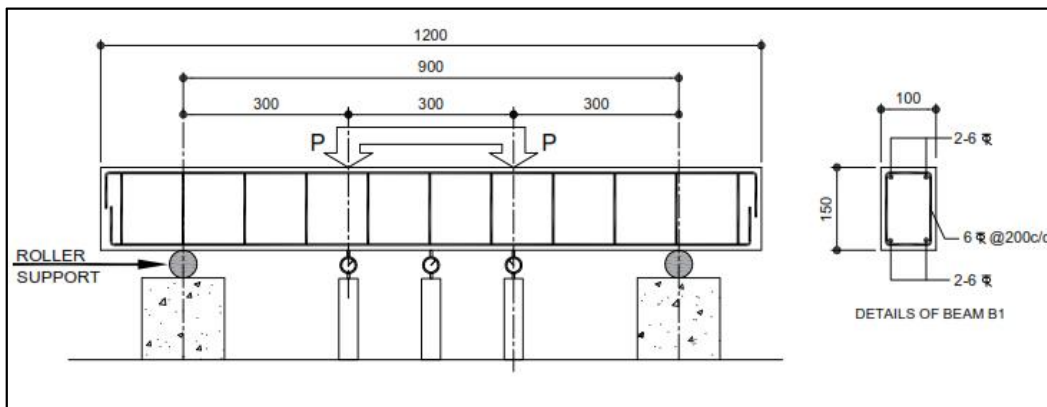


**Figure 4.1: Typical beam details and loading arrangement.**



**Figure 4.2: Flexural strength test setup for reinforced concrete beam.**

**Table – 4.6: Reinforcement details of nano-silica modified geopolymer (A1 to A7), conventional geopolymer (B1 to B7) concrete and control concrete (C1 to C7) beam.**

Beam Mark	Length (mm)	Reinforcement		% of reinforcement		Shear Spacing(6 )
		(Bottom)	(Top)	(p <sub>t</sub> )	(p <sub>c</sub> )	
A1	1200	2 - 6	2 - 6	0.45	0.45	200 mm
A2	1200	3 - 6	2 - 6	0.67	0.45	200 mm
A3	1200	2 - 8	2 - 6	0.81	0.45	200 mm
A4	1200	2 - 8	3 - 6	0.81	0.67	200 mm
A5	1200	2 - 8	2 - 8	0.81	0.81	200 mm
A6	1200	2 - 8	2 - 6	0.81	0.45	150 mm
A7	1200	2 - 8	2 - 6	0.81	0.45	100 mm
B1	1200	2 - 6	2 - 6	0.45	0.45	200 mm
B2	1200	3 - 6	2 - 6	0.67	0.45	200 mm
B3	1200	2 - 8	2 - 6	0.81	0.45	200 mm
B4	1200	2 - 8	3 - 6	0.81	0.67	200 mm
B5	1200	2 - 8	2 - 8	0.81	0.81	200 mm
B6	1200	2 - 8	2 - 6	0.81	0.45	150 mm
B7	1200	2 - 8	2 - 6	0.81	0.45	100 mm
C1	1200	2 - 6	2 - 6	0.45	0.45	200 mm
C2	1200	3 - 6	2 - 6	0.67	0.45	200 mm
C3	1200	2 - 8	2 - 6	0.81	0.45	200 mm
C4	1200	2 - 8	3 - 6	0.81	0.67	200 mm
C5	1200	2 - 8	2 - 8	0.81	0.81	200 mm
C6	1200	2 - 8	2 - 6	0.81	0.45	150 mm
C7	1200	2 - 8	2 - 6	0.81	0.45	100 mm



#### **4.3.5. Microstructural study of concrete:**

##### **4.3.5.1. XRD analysis:**

The micro-structural properties of nano-silica modified geopolymer (12GC6), heat cured geopolymer (12GC0H) and control cement concrete (CC) fragments have been collected after the strength investigation. The fragments have been crushed into fine powder by pestle-mortar are dried and sieved to make the size less than 5 $\mu$ m for X-ray diffraction analysis by using the powder X-ray diffractometer (Bruker AXS Inc, Model D8, WI, USA) with a scan speed 0.5 s/step at 40 KV. The XRD spectrum has been taken from  $2\theta = 20^\circ$  to  $80^\circ$ . The peaks in the new positions of the spectrum have been marked, match up to and identified from the Joint Committee on Powder Diffraction Standards (JCPDs) data file.

##### **4.3.5.2. SEM with EDS analysis:**

For EDS study, a pinch of powder sample has been taken and dispersed in absolute ethyl alcohol on double coated carbon tape and dried in vacuum desiccators for 15 min. The dried powdered sample has been examined in Field Emission Scanning Electron Microscope, FESEM (INSPECT F50 SEM, FEI Europe BV, The Netherlands) for EDS analysis using QUANTAX ESPRIT 1.9 software.

##### **4.3.5.3. Fourier Transform Infrared Spectroscopic analysis:**

Fourier transform infrared spectroscopy (FT-IR410 JASCO, U.S.A.) has been used to determine the presence of various chemical bonds and functional groups in the nano-silica modified geopolymer and conventional heat cured geopolymer concrete. Samples have been prepared by using the KBr pellet (97% KBr) technique for the IR analysis.

#### 4.4. SILVER-SILICA MODIFIED GEOPOLYMER MORTAR

A silver-silica nano composite had been developed by simple adsorption of silver in a suitable amount of colloidal silica suspension for anti-bacterial property development. Low Calcium Class F dry fly ash, locally available sand, alkali activator fluid (mixture of sodium hydroxide, sodium silicate and deionized water) have been used as basic ingredients of geopolymer mortar [1]. For control cement mortar, Ordinary Portland Cement (OPC) and deionized water has been used. Nutrient Broth (NB) media ingredients like peptone, beef extract, Yeast extract, NaCl, agar (Hi-media Pvt. Ltd., India), silver nitrate (Merck Germany), deionized water, carbonic acid, *E. coli* (MTCC 1652 strain), *S. aureus* (MTCC 96 strain) bacteria have been used. All reagents have been prepared with milli-Q ultra-pure water. The basic properties of colloidal nano silica are mentioned in Table – 4.3.

##### 4.4.1. Preparation of silver silica nano composite:

For preparation of silver nanoparticles (Ag NPs) on the surface of colloidal silica nanoparticles (SiO<sub>2</sub> NPs), 100 mM colloidal silica NPs water solution has been taken and the 5 mM silver nitrate (AgNO<sub>3</sub>) is added drop-wise under vigorous stirring at ambient temperature for 6h, 24h [12].

##### 4.4.2. Confirmative test for silver-silica nano composite:

The silver-silica nano solution has been lyophilized (EYELA FDU-1200, Japan) and crushed to make a uniform fine powder. The surface morphology of the synthesized nano structured samples have been evaluated using High Resolution Transmission Electron Microscopy (HRTEM; JEOL, JEM 2100). The surface charges and size distribution of silica NPs and silver-silica nano composite have been determined by using Zeta Potential Analyzer (Brookhaven Instruments Corp. Holtsville, USA). XRD analysis has been performed (Bruker AXS, Inc., Model D8, WI, USA) with mono-chromatised Cu-K $\alpha$  radiation of wavelength 1.5406 Å at 55 kV and 40 mA. The sample has been examined at 2 $\theta$  from 10° to 80° and identified by referring to data of Joint Committee on Powder Diffraction Standards (JCPDS) files.

#### 4.4.3. Preparation of mortar samples:

Two different fly-ash based geopolymer mortars ( $GM_{Si}$ ,  $GM_{Ag-Si}$ ) and a conventional control mortar (CM) have been prepared for the present study. The activator fluid to fly ash ratio has been taken at 0.40. The activator fluid has been made by mixing 12M NaOH with  $Na_2SiO_3$  at weight ratio of 1:1.75. This solution has been mixed with colloidal nano silica solution (activator 1) for the preparation of  $GM_{Si}$  geopolymer specimens. For preparation of  $GM_{Ag-Si}$  geopolymer mortar, activator 2 has been prepared by 12M NaOH and  $Na_2SiO_3$  at same weight ratio with nano silver-silica solution. The amount of nano silica and silver-silica nano composite in the respective activator 1 and activator 2 solutions has been 6% (w/w) of fly ash used. For the preparation of control mortar sample (CM), OPC of 43 grade sand and distilled water have been used. Details of all mixes are shown in Table – 4.7. For determination of mechanical strength (compressive strength, flexural and split tensile strength) and durability (RCPT), the samples of mix  $GM_{Si}$  and  $GM_{Ag-Si}$  have been removed from the mould after 24 h and kept in ambient temperature and tested after 3, 7 and 28 days of air curing. Conventional water curing has been made for the CM specimens until the test. It may be mentioned here that the mix  $GM_{Si}$  is same as 12GM6. The mix  $GM_{Ag-Si}$  is the modified mix of  $GM_{Si}$  with silver nano particle.

**Table – 4.7. Nano silica modified geopolymer ( $GM_{Si}$ ), silver silica modified geopolymer mortar ( $GM_{Ag-Si}$ ) and control mortar (CM), mix proportions:**

Mix Mark	Fly ash : sand	Activator solution	% of $SiO_2$ NPs	% of Ag- $SiO_2$ NPs	Curing condition
$GM_{Si}$	1:3	Activator 1 (NaOH + $Na_2SiO_3$ + $SiO_2$ NPs)	6.0	Nil	Air curing at room temperature.
$GM_{Ag-Si}$	1:3	Activator 2 (NaOH + $Na_2SiO_3$ + Ag- $SiO_2$ NPs)	Nil	6.0	Air curing at room temperature.
CM	1:3 (Cement : Sand)	Water	Nil	Nil	Water Curing

#### **4.4.4. Mechanical strength and durability study:**

The standard mortar cube specimens of dimension 70.6 mm × 70.6 mm × 70.6 mm have been prepared for different mixes to determine the compressive strength of mortars. All the specimens have been tested at 3 days, 7 days, and 28 days after casting to determine the compressive strength. Flexural strength testing has been carried out on mortar bars (50 mm × 50 mm × 200 mm) for all (GM<sub>Si</sub>, GM<sub>Ag-Si</sub>, CM) samples. The center point loading method has been adopted for the determination of flexural strength (ASTM C293) [5]. Cylinder specimens (100 mm diameter × 200 mm height) have been tested for split tensile strength test for each category after 28 days from the date of casting. Rapid Chloride ion Penetration Test (RCPT) has been adopted for the durability assessment of different mortar mixes. Test cylinder specimens (100 mm diameter × 200 mm height) have been sliced into core specimens of thickness 50 mm and subjected to RCPT by impressing 60V [7]. All the specimens have been tested after 28 days of casting.

#### **4.4.5. Antibacterial Study:**

##### **4.4.5.1. Bacterial kinetics study:**

Bacterial kinetics of mortar samples from GM<sub>Si</sub>, GM<sub>Ag-Si</sub> and CM have been investigated against *S. aureus* (gm +ve) and *E. coli* (gm -ve) bacterial strains distinctly. From an overnight growing fresh culture of both bacteria, a volume of culture approximately representing ~10<sup>7</sup> CFU/ml (Colony Forming Unit / ml) has been washed and suspended in Phosphate buffer (PBS). The fresh culture has been then diluted by 5 ml nutrient broth (0.5% peptone, 0.1% beef extract, 0.2% Yeast extract, 0.5% NaCl, pH 7) at a final cell concentration of 10<sup>4</sup> CFU/ml and incubated at 37 °C. For anti-bacterial assay, 2 mg/ml (~2 × Minimum Inhibitory Concentration) of each dry dust samples (pH < 9) (GM<sub>Si</sub>, GM<sub>Ag-Si</sub> and CM) have been used to treat the inoculated broth separately. Time dependent killing has been determined by plating the culture from the treated geopolymer mortar samples and control cement mortar sample in agar plate (15%) after different time of incubation (0, 2, 4, 6, 8, 12, 24 h). Plates have been incubated at 37 °C and the numbers of colonies are counted after 24 h. The whole experiment has been repeated trice.

#### **4.4.5.2. Minimum Inhibitory Concentration (MIC) and Minimum Bactericidal Concentration (MBC) test of Mortar samples**

Using batch culture process, the Minimum Inhibitory Concentration (MIC) has been observed by the varying concentration of different geopolymer samples [13]. Growth medium containing initial cell concentration ( $10^7$  CFU/ml) of each strain has been taken distinctly. The different mortar powders ( $GM_{Si}$ ,  $GM_{Ag-Si}$  and CM) have been added in the growth medium distinctly and inoculated at 37 °C on a rotary shaker. In 5ml NB, the powder samples (0.1% - 5.0 % w/v) of each category have been added separately in several marked tubes. The growth inhibitions ( $GM_{Si}$  and  $GM_{Ag-Si}$  treated bacterial cells) have been measured against control at 620 nm by a UV-visible Spectrophotometer (ELICO, SL 196 Spectropharm) [14 & 15].

Minimum bactericidal concentration (MBC) is defined as the lowest concentration of silver nanoparticles present in  $GM_{Ag-Si}$  samples that kills 99.9% of the bacteria. The presences of viable microorganisms have been examined and lowest concentrations causing bactericidal effect are reported as MBC for the growth inhibitory concentrations [16]. The experiment has been performed by plating (Nutrient Agar plate 15%) the bacterial cultures with upper amounts above the MIC. The agar plates have been inoculated at 37 °C for 24 h. All the experiments have been carried out in triplicate.

#### **4.4.5.3. Fluorescence Microscopic analysis:**

The intensity of fluorescence is proportional to the level of intracellular reactive oxygen species. The working solution of 10 µl each of SYBR Green dimethyl sulphoxide (DMSO) solution (1:100 v/v) and PI water solution (1mg/ml) have been taken in to 1 ml of each treated  $GM_{Si}$  &  $GM_{Ag-Si}$  and CM samples. After incubation at 37 °C for 30 min, each sample has been mounted immediately over slides and pictures are captured by the fluorescence microscope for this experiment [17].

#### **4.4.5.4. Morphological investigation for bacterial strains:**

Certain volume of nutrient broth (NB) medium and powder samples of the three different mortar specimens ( $GM_{Si}$ ,  $GM_{Ag-Si}$  & CM) have been added separately to 5 ml cultures of each bacteria resulting in final concentration of 1mg/ml samples and bacterial concentration of

$10^8$  CFU/ml. This experiment has been performed for both bacteria (*E. coli* & *S. aureus*) and for three different test samples separately. For morphological analysis, bacterial growth medium in mid exponential phase and with the same cell density have been treated with samples (GM<sub>Si</sub>, GM<sub>Ag-Si</sub> and CM) for 6h at 37 °C. The bacterial samples have been then washed with milli-Q water, fixed with 2% glutaraldehyde and placed on a silicon platelet (Plano, Wetzlar, Germany). A series of ethanol dehydration steps have been carried out followed by staining with 3% uranyl acetate in 25% ethanol. Finally, the samples have been washed with buffer solution (0.1 M sodium phosphate, pH 7.2) and investigated using FESEM (INSPECT F50 SEM, The Netherlands).

## **4.5. PROCESS DEVELOPMENT FOR GEOPOLYMER MORTAR**

### J Preparation of process modified geopolymer and conventional geopolymer concrete.

Low Calcium Class F (American Society for Testing and Materials 2001) dry fly ash and activator solution consists of sodium hydroxide (NaOH) and sodium silicate (Na<sub>2</sub>SiO<sub>3</sub>) have been used as the base material for present study. The properties of fly ash, sodium hydroxide (NaOH) and sodium silicate (Na<sub>2</sub>SiO<sub>3</sub>) have been described in para 4.1. NaOH of 8 molar concentration has been mixed with Na<sub>2</sub>SiO<sub>3</sub> solution in the proportion of 1:1.75 (by weight) to make alkali activator fluid. The ratio of fly ash: sand has been fixed at 1:3 (by weight) and activator fluids to fly ash ratio of 0.35, 0.40 and 0.45 have been considered in for both the process.

In Process – I (Refer. Fig 4.3), fly ash has been mixed with appropriate quantity of activated fluid and stirred in a hot air oven for 45 minutes at different temperatures of 40°C, 60°C and 80°C. River sand has been mixed immediately with the hot mixture of activated fluid and fly ash thoroughly for two minutes before casting. Finally, the mortar specimens have been removed from the mould after 10-12 hours of casting and are placed at ambient temperature (27 ± 20 °C) until testing.

In Process – II (Refer. Fig 4.3), sand and fly ash has been dry mixed for 2 minutes and the appropriate quantity of activator fluid is added and mixed thoroughly at ambient laboratory temperature. After one hour of casting, the mortar specimens along with the mould have been cured at three different temperatures of 40°C, 60°C and 80°C within the hot air oven for 48 hours [18-21]. Finally, the specimens have been kept at ambient temperature after removing from the mould until testing. The details of all the mixtures are shown in Table – 4.8.

### **4.5.1. Mechanical strength:**

For both the process (Process – I & II), mortar cubes of size 70.7 mm x 70.7 mm x 70.7 mm have been prepared for determination of compressive strength and mortar bar of size 50 mm x 50 mm x 200 mm are prepared for flexural strength measurement. The split tensile strength of geopolymer mortar (both the process) have been determined by using cylinder samples of size 100 mm diameter x 200 mm height. Compressive strength of the mortar cubes

has been determined at 3 days, 7 days, and 28 days. Flexural strength on mortar bar and tensile strength on cylinders have been determined at 28 days for the different mixes. All strength values are based on the average of three specimens.

#### **4.5.2. Durability test:**

For chloride ion penetration test, cylinder specimen has been sliced into core specimen of thickness 50 mm at the age of 28 days for all the mixes. The sliced specimens have been then subjected to RCPT by impressing 60V [7]. Cube specimen having fluid to fly ash ratio of 0.35 have been immersed in water for 30 minutes and 24 hours for water absorption test. Also cube specimens have been immersed in sulphate solution for one month for sulphate test.

#### **4.5.3. Micro-structural study:**

##### **4.5.3.1. Field Emission Scanning Electron Microscopy (FESEM) with EDS:**

For FESEM (Field Emission Scanning Electron Microscopy) analysis, EDS (Energy dispersive spectroscopy) and XRD (X-ray Diffraction test) analysis, the broken samples of maximum compressive strength at 28 day for both process (Process – I and Process – II) have been dried and sieved to make the size less than 5 $\mu$ m. Fine powder has been diluted with ethanol (99.9%) to make a film on carbon tape and then kept under vacuum desiccators for evaporation. Finally, the dried samples have been gold coated for FESEM and EDS (HITACHI S-4800, JAPAN) analysis.

##### **4.5.3.2. X-Ray Diffraction Analysis:**

For X-ray diffraction analysis in powder X-ray diffractometer (Bruker AXS Inc, Model D8, WI, USA) with a scan speed 0.5 s/step at 40 KV. The XRD spectrum has been analyzed in the range  $2\theta = 10^\circ$  to  $2\theta = 70^\circ$  and the peak positions are marked and compared from JCPDS file.



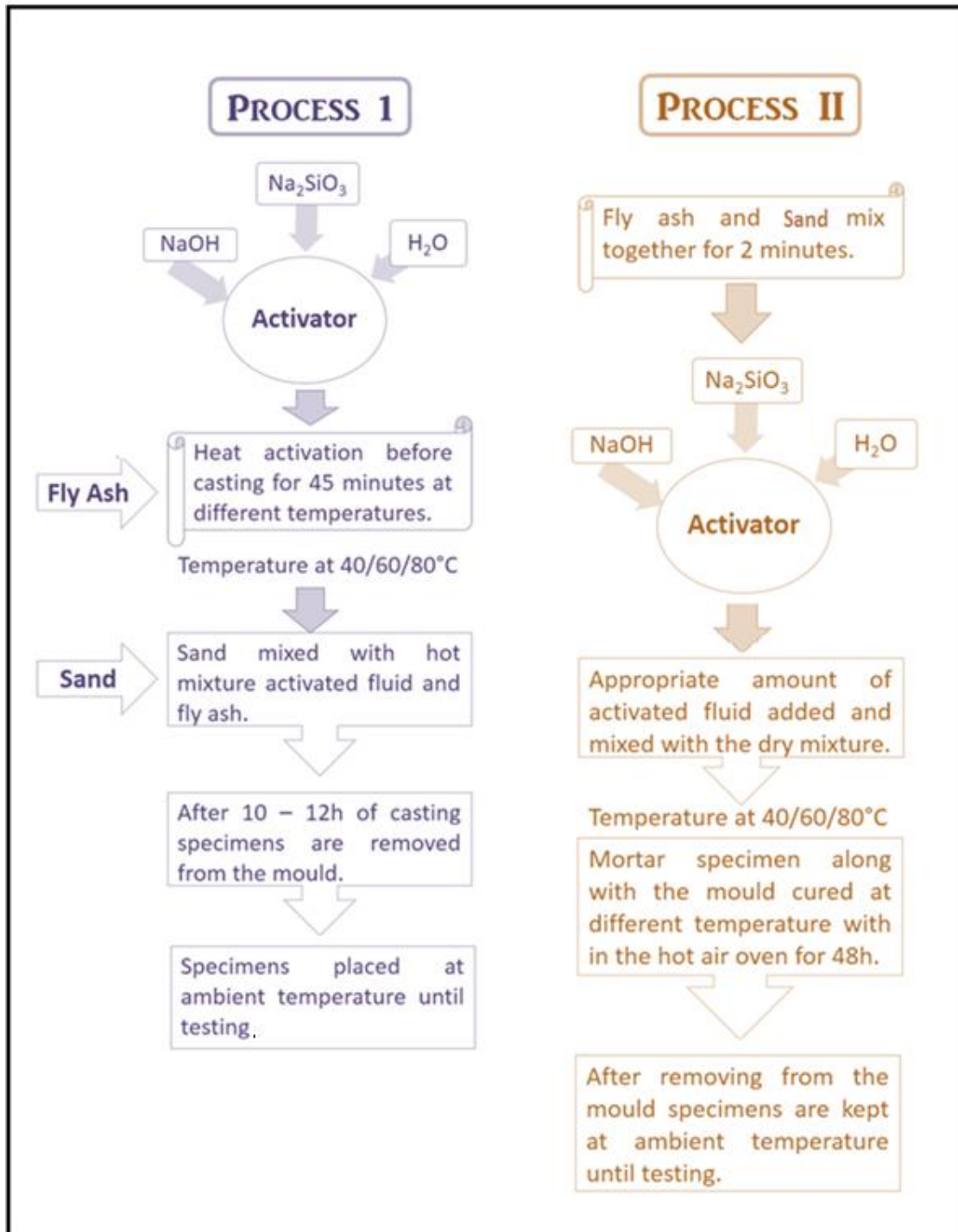


Figure – 4.3: Details of Process – I and Process – II geopolymer mortar.

**Table – 4.8. Mix proportion for different process (Process – I and Process – II):**

Mix No	Fluid : Fly Ash	Process type	Temperature °C	Heat curing Process
<b>G1</b>	0.35	Process-I	40	Heat curing of fly ash and activated fluid for 45 minutes before casting at different temperatures.
<b>G2</b>			60	
<b>G3</b>			80	
<b>G4</b>	0.35	Process-II	40	Heat curing of samples after casting for 48 hours at different temperatures.
<b>G5</b>			60	
<b>G6</b>			80	
<b>G7</b>	0.40	Process-I	40	Heat curing of fly ash and activated fluid for 45 minutes before casting at different temperatures.
<b>G8</b>			60	
<b>G9</b>			80	
<b>G10</b>	0.40	Process-II	40	Heat curing of samples after casting for 48 hours at different temperatures.
<b>G11</b>			60	
<b>G12</b>			80	
<b>G13</b>	0.45	Process-I	40	Heat curing of fly ash and activated fluid for 45 minutes before casting at different temperatures.
<b>G14</b>			60	
<b>G15</b>			80	
<b>G16</b>	0.45	Process-II	40	Heat curing of samples after casting for 48 hours at different temperatures.
<b>G17</b>			60	
<b>G18</b>			80	

#### 4.6. PROCESS DEVELOPMENT FOR GEOPOLYMER CONCRETE

Based on the performance of Process –I and Process – II geopolymer mortar at fluid to fly ash ratio 0.35 and processed at 60°C, the structural behavior of process modified geopolymer concrete (GPC – I & GPC – II) have been studied. The basics properties of fly ash, sodium hydroxide and sodium silicate have been described in para 4.1. The preparation of GPC – I (Process – I) and GPC – II (Process – II) geopolymer concrete specimen have been described in figure -3. The compressive, flexural and tensile strength along with modulus of elasticity of this geopolymer concrete have been studied to understand its structural behavior. Additionally, micro-structural properties of the concrete have been assessed by FESEM with EDS, FTIR and XRD analysis. The detail of the mix for GPC – I and GPC – II geopolymer concrete have been presented in Table – 4.9.

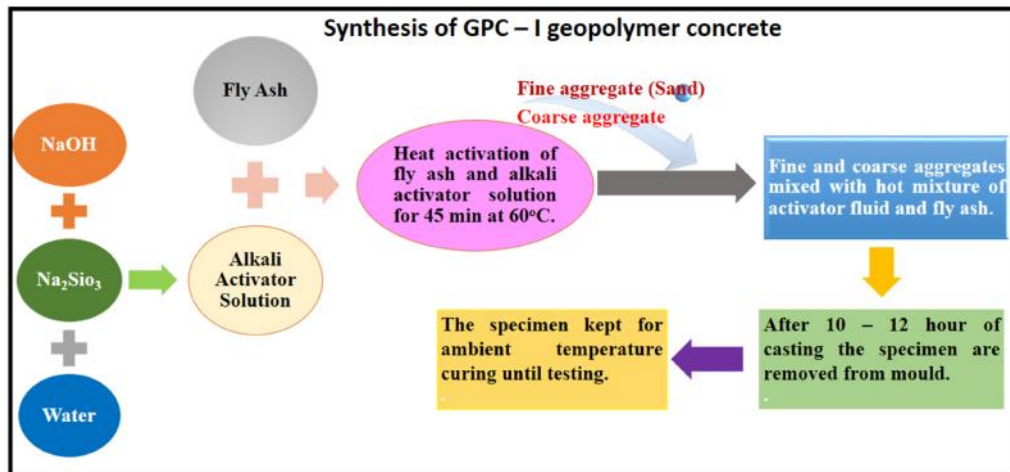


Figure – 4.4: Graphical presentation of synthesis of process modified geopolymer concrete (GPC – I).

##### 4.6.1. Mechanical strength of process developed geopolymer concrete

The geopolymer cube specimens of size 150 mm × 150 mm × 150 mm dimension have been prepared to determine the compressive strength of GPC – I & GPC – II concrete samples. The compressive strength of each category samples has been analyzed at different ages (3, 7 & 28 days) of curing [9]. The split tensile strength of geopolymer concrete for both process – I & II have been tested using concrete cylinder of size 100 mm (diameter) × 200 mm (height) after 28 days of curing. The modulus of elasticity of geopolymer concrete cylinders of 150 mm diameter and 300 mm height have been determined by using strain controlled machine

(YAW3000A, China) for the both process. The flexural strength of GPC – I and GPC – II geopolymer concrete beam of size 100 × 100 × 500 mm have been determined as per ASTM C293 [6]. The bond strength between geopolymer concrete of both process and reinforcement bar (yield stress = 250 MPa & 0.2 % of proof stress = 500) have been determined as per IS 2770 (Part 1) [10]. The experimental method to determine the bond strength have been described in para 4.3.3.

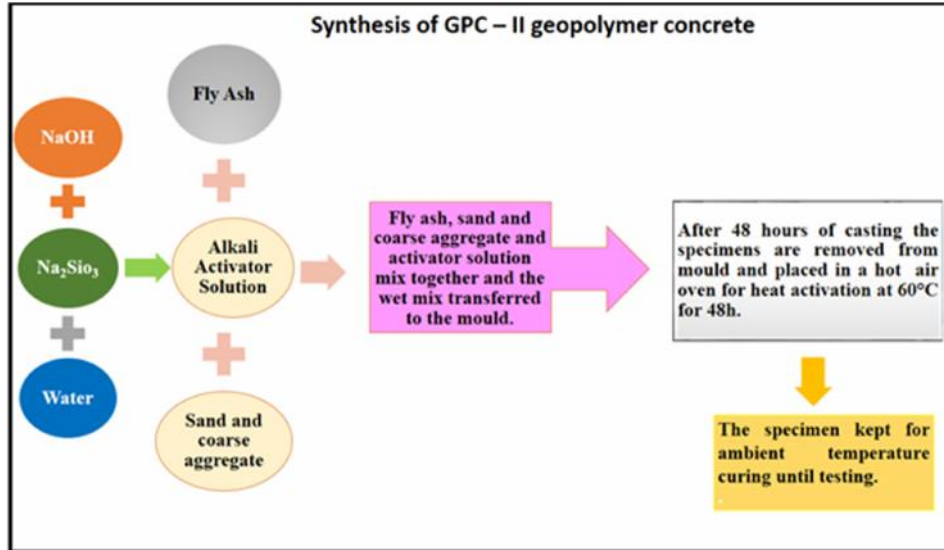


Figure – 4.5: Graphical presentation of synthesis of conventional heat cured geopolymer concrete (GPC – II).

Table – 4.9: Details of GPC – I and GPC – II (conventional heat cured) geopolymer concrete mix:

Mix type	Process	Fly ash (Kg/m <sup>3</sup> )	Fine Agg. (Kg/m <sup>3</sup> )	Coarse Agg. (Kg/m <sup>3</sup> )	Fluid : Fly ash	Curing condition
GPC-I	Process - I	440	723	1085	0.35	Heat curing of fly ash and activated fluid for 45 minutes at 60°C.
GPC-II	Process - II	440	723	1085	0.35	Heat curing of samples after casting for 48 hours at 60°C.

\*\* “GPC – I - Geopolymer concrete of Process – I”, “GPC – II – Geopolymer concrete of Process – II”.

#### **4.6.2. Microstructural study of process developed geopolymer concrete**

The micro-structural properties of both GPC – I and GPC – II geopolymer concrete have been analyzed by FESM with EDS and XRD analysis. The methods adopted to analyze the micro-structural properties have been described in para 4.4.3.

##### **4.6.2.1. X-Ray Diffraction analysis**

The micro-structural properties of GPC – I (Process – I) geopolymer concrete and GPC – I (Process – II) geopolymer concrete fragments have been collected after the strength investigation. The fragments have been crushed into fine powder by pestle-mortar are dried and sieved to make the size less than 5 $\mu$ m for X-ray diffraction analysis by using the powder X-ray diffractometer (Bruker AXS Inc, Model D8, WI, USA) with a scan speed 0.5 s/step at 40 KV. The XRD spectrum has been taken from  $2\theta = 20^\circ$  to  $80^\circ$ . The peaks in the new positions of the spectrum have been marked, match up to and identified from the JCPDS data file.

##### **4.6.2.2. SEM with EDS analysis**

A pinch of powder concrete sample has been taken and dispersed in absolute ethyl alcohol on double coated carbon tape and dried in vacuum desiccators for 15 min. The dried powdered sample has been examined in Field Emission Scanning Electron Microscope, FESEM (INSPECT F50 SEM, FEI Europe BV, The Netherlands) for EDS analysis using QUANTAX ESPRIT 1.9 software.

## REFERENCES:

---

- [1] ASTM C618: Standard Specification for Coal Fly Ash and Raw or Calcined Natural Pozzolan for Use in Concrete; ASTM International, West Conshohocken, PA, 2012.
- [2] IS 8112 – 1989: Specification for 43 grade ordinary Portland cement. CED 2: Cement and Concrete.
- [3] IS 4031 (Part – VI) – 1988: Method of Physical Test of Hydraulic Cement, Bureau of Indian Standards, New Delhi, India.
- [4] IS 10080 – 1982: Specification for Vibration Machine, Bureau of Indian Standards, New Delhi, India.
- [5] IS 5816 – 1999: Splitting Tensile Strength of Concrete Method of Test, Bureau of Indian Standards, New Delhi, India.
- [6] ASTM C293: Standard Test Method for Flexural Strength of Concrete (Using Simple Beam with Centre-Point Loading); ASTM International, West Conshohocken, PA, 2008.
- [7] ASTM C1202: Standard Test Method for Electrical Indication of Concretes Ability to Resist Chloride Ion Penetration; ASTM International, West Conshohocken, PA, 2000.
- [8] Neville A. M.; Properties of concrete. 4th Ed. Pearson Higher Education, Prentice Hall, Englewood Cliffs. 1996.
- [9] IS 516 – 1959: Method for Test for Strength of Concrete, Bureau of Indian Standards, New Delhi, India.
- [10] IS 2770 (Part-1) – 2007: Method of Testing Bond in Reinforced Concrete; Bureau of Indian Standard, New Delhi, India.
- [11] IS 456 – 2000: Plain and Reinforced Concrete Code of Practice, Bureau of Indian Standards, New Delhi, India.
- [12] V. Pol, D. N. Srivastava, O. Palchik, V. Palchik, M. A. Slifkin and A. M. Weiss, Sonochemical Deposition of Silver Nanoparticles on Silica Spheres, Langmuir, 2002, 18, 3352–3357.

- [13] L. Qi, Z. Xu, X. Jiang, C. Hu and X. Zou, Preparation and antibacterial activity of chitosan nanoparticles, *Carbohydr Research*, 2004, 339, 2693–700.
- [14] J. Ruparelia, A. Chatterjee, S. P. Duttagupta and S. Mukherji, Strain specificity in antimicrobial activity of silver and copper nanoparticles, *Acta-Biomaterial*, 2008, 4, 707–716.
- [15] G. Ren, D. Hu, C. Cheng, M. A. Vargas-Reus, P. Reip, R. P. Allaker, Characterisation of copper oxide nanoparticles for antimicrobial applications, *International Journal of Antimicrobial Agents*, 2009, 33, 587-590.
- [16] M. R. Avadia, A. M. M. Sadeghib, A. Tahzibic, Kh. Bayati, M. Pouladzadeh, Z. Mehr and M. R. Thehrani, Diethyl Methyl Chitosan as an Enhancing Agent for Colon Drug delivery I: Synthesis, Characterization, *European Polymer Journal*, 2004, 40, 1355–1361.
- [17] S. Barbesti, S. Citterio, M. Labra, M. D. Baroni, M. G. Neri and S. Sgorbati, Two and three-color fluorescence flow cytometric analysis of immunoidentified viable bacteria, *Cytometry*, 2000, 40, 214–218.
- [18] Vijai K, Kumutha R, Vishnuram B G. Effect of types of curing on strength of geopolymer concrete, *International Journal of the Physical Sciences*, 2010; Vol. 5(9).
- [19] Guo X, Shi H, Dick WA. Compressive strength and microstructural characteristics of class C fly ash geopolymer, *Cement and Concrete Composites*, 2010; 32; 2.
- [20] Gorhan G, Kurklu G. The influence of the NaOH solution on the properties of the fly ash based geopolymer mortar cured at different temperature, *Composites*, 2014; Part B 58; page 371-377.
- [21] Barbosa F. F. V, Mackenzie J D K, Thaumaturgo C. Synthesis and characterisation of materials based on inorganic polymers of alumina and silica: sodium polysialate polymers, *International Journal of Inorganic Materials*, 2000; 309-317.





# Chapter- 5.....

MAKE THINGS HAPPEN!



**RESULTS &  
DISCUSSION**



## **5.0. GENERAL**

At first, the experimental results on the nano-silica based geopolymer mortar and concrete have been presented in section 5.1 and 5.2 respectively and critically discussed. Further, the results of antibacterial properties of nano silver-silica modified geopolymer mortar have been discussed in 5.3. Finally, the experimental results of the process modified geopolymer mortar and concrete have been discussed in 5.4 and 5.5 respectively.

### **5.1. NANO-SILICA BASED GEOPOLYMER MORTAR:**

The aim of this study is to eliminate the much needed heat activation for the preparation of conventional geopolymer mortar along with appropriate mechanical strength and durability. Figure 5.1 summarises the compressive strength of fly ash based geopolymer mortar samples having molar concentration of 8 (M) without nano silica (heat cured) and with 4%, 6%, 8% and 10% of nano silica addition (without heat curing). The compressive strength of controlled sample (cement mortar) made with OPC cement marked as “CONTROL” is also presented for comparison. Similarly, Figure 5.2 and 5.3 show the similar results of compressive strength of geopolymer mortars for molar concentration of 10 (M) and 12 (M) respectively. It has been noted that the 28 days compressive strength of 8(M) geopolymer mortars without nano silica cured at 60°C for 48 hours and nano silica modified geopolymer mortar cured at ambient temperature are less than that of cement mortar (Refer Fig. 5.1). However, at higher molar concentration (10M and 12M), the 28 days compressive strengths of geopolymer mortars (with/without nano silica) are comparatively higher than control cement mortar (Refer Fig. 5.2 & 5.3). This may be due to the lesser polymerization of Al-Silica at low alkali content in lower molar concentration and more polymerization at higher molar concentration.

It is also noted that the addition of nano silica in the geopolymer mortar up to 6% of fly ash (replacement mode) seems to provide sufficient 28 days compressive strength at ambient temperature curing for 10M and 12M NaOH solution as shown in Figure 5.2 and 5.3. However, beyond 6% of nano silica addition, there is no such improvement in compressive strength of geopolymer mortar (cured at ambient temperature) at all ages.

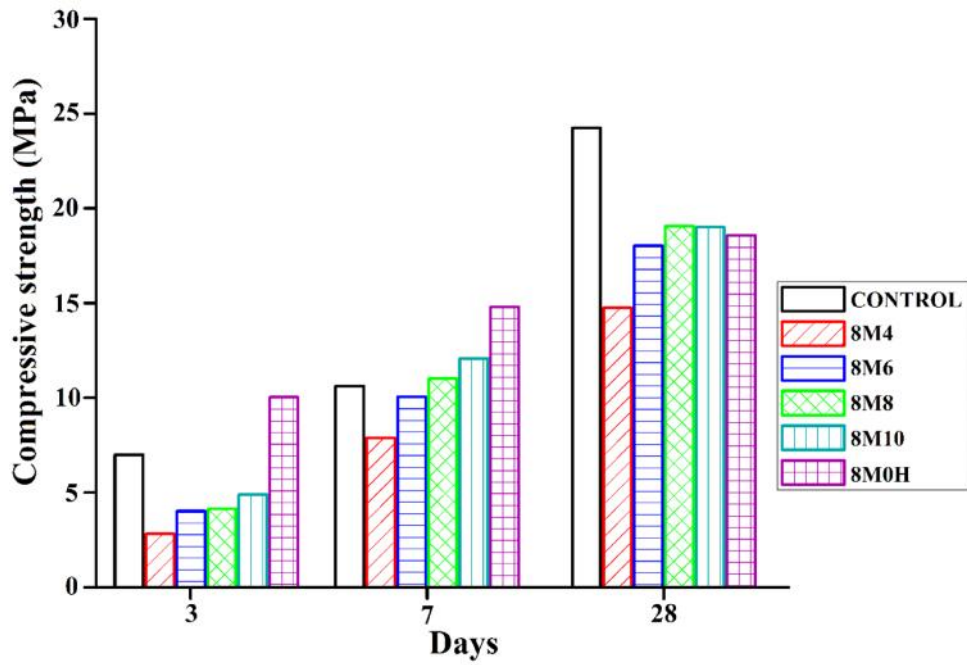


Figure –5.1: Compressive strength of 8(M) geopolymer mortar and cement mortar samples.

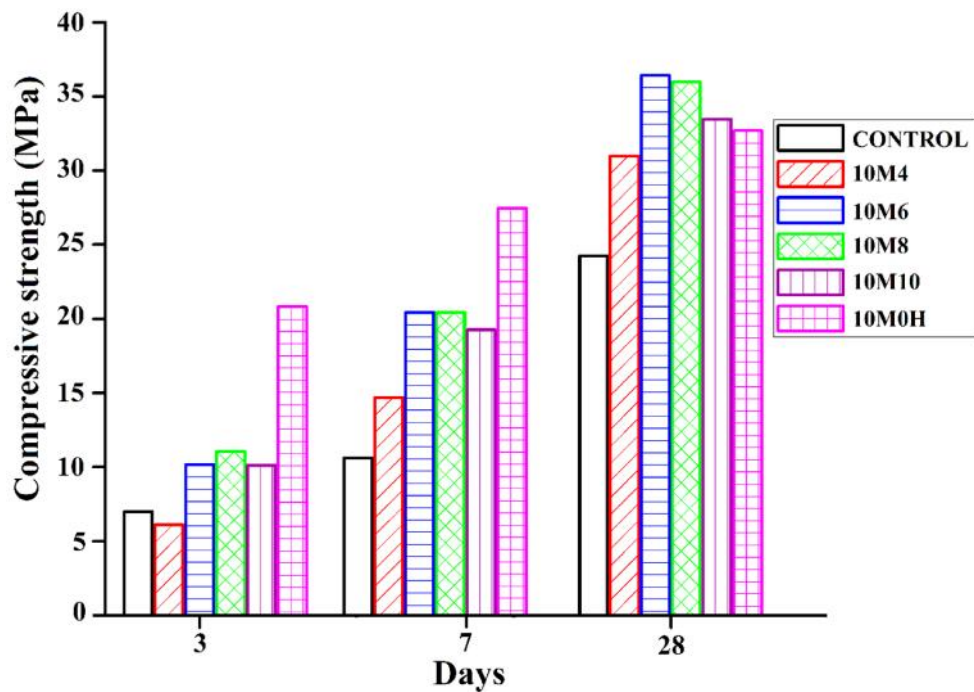
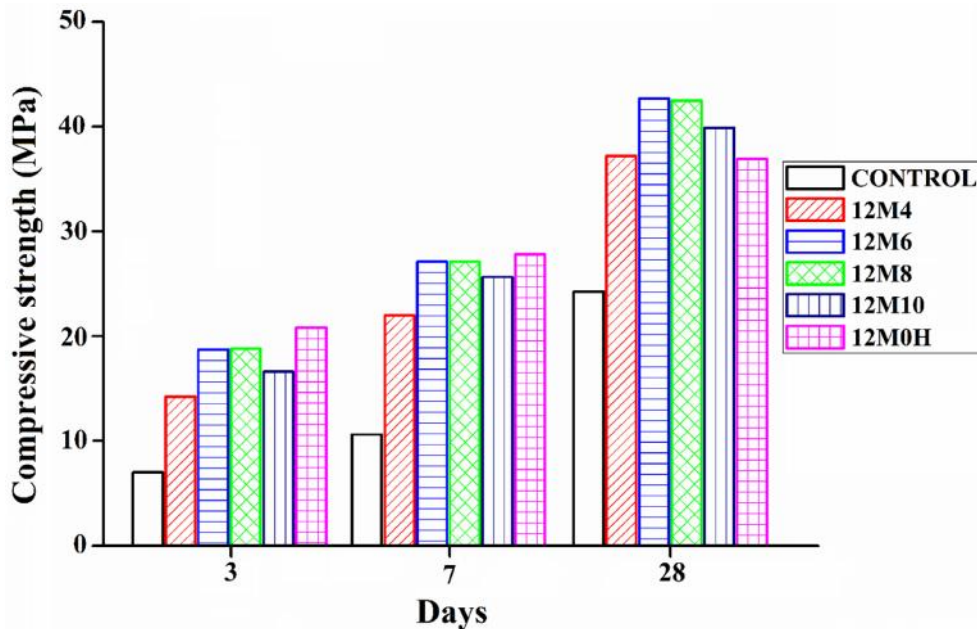


Figure – 5.2: Compressive strength of 10(M) geopolymer and cement mortar samples.

*(Published in Construction and Building Materials; 2014)*

It seems that the 6% of nano silica addition is the optimum for the present study. The decrease in compressive strength of mortar containing more than 6% nano silica can be attributed to the agglomeration of nano silica in wet mixture. Nanoparticles, due to their small size, have high inter-particle van der Waal's forces causing the nanoparticles to agglomerate [1–3]. Hence, the nanoparticles will form agglomerates about hundreds of times larger than the primary nanoparticle causing them to lose the desirable surface area to volume ratio. Due to its higher van der Waal's forces, the size of the nano silica agglomerate becomes more than that of the basic geopolymer material, fly ash. The effect of nano silica on the compressive strength of conventional mortar/concrete and its role in dispersion in the matrix has been also reported by several researcher [4, 5]. It may be concluded that the strength of geopolymer mortar with more than 6% colloidal nano silica is reduced due to agglomeration of nano silica, which reduces the surface area of nano silica and decreases polymerisation process. Thus, the 6% nano-silica addition in geopolymer mortar has been considered here for further studies.



**Figure – 5.3: Compressive strength of 12(M) geopolymer and cement mortar samples.**  
*(Published in Construction and Building Materials; 2014)*

It is also noted in Figure 5.1, 5.2 and 5.3 that the compressive strength of heat cured geopolymer mortar (without nano silica) is more than ambient temperature cured geopolymer mortar (with nano silica) at early ages (3days & 7days). The increase in compressive strength

of geopolymer mortar with nano silica and cured at ambient temperature is not so satisfactory at an early ages. Similar results are reported for geopolymer mortar with fly ash (3%) and rice husk ash (93%) and with different percentage (1, 2, 3% by weight) of nano-SiO<sub>2</sub> and nano-Al<sub>2</sub>O<sub>3</sub> addition under oven cured for 2, 4 and 8 hours at temperature of 25°C, 70°C and 90°C [6]. This indicates that incomplete polymerization of geopolymer matrix at the early ages cured at ambient temperature. However, at later ages (28days) the results are quite satisfactory for geopolymer mortar with 6% nano silica cured at ambient temperature.

Figure 5.4 shows that the 28 days compressive strength of geopolymer mortar with/without nano silica is almost same at 8M concentration. However, the 28 days compressive strength of 10M and 12M geopolymer mortar with 6% of nano silica is about 11% and 13% more than that of geopolymer mortar (heat cured) without nano silica respectively. This may be due to the availability of more alkali in the mix for polymerization. Therefore, it may be concluded that the 6% colloidal nano silica addition to geopolymer mortar increases the polymerization rate due to its high specific surface area and provides an optimum 28 days strength without any heat curing for activation particularly for 10M and 12M concentration.

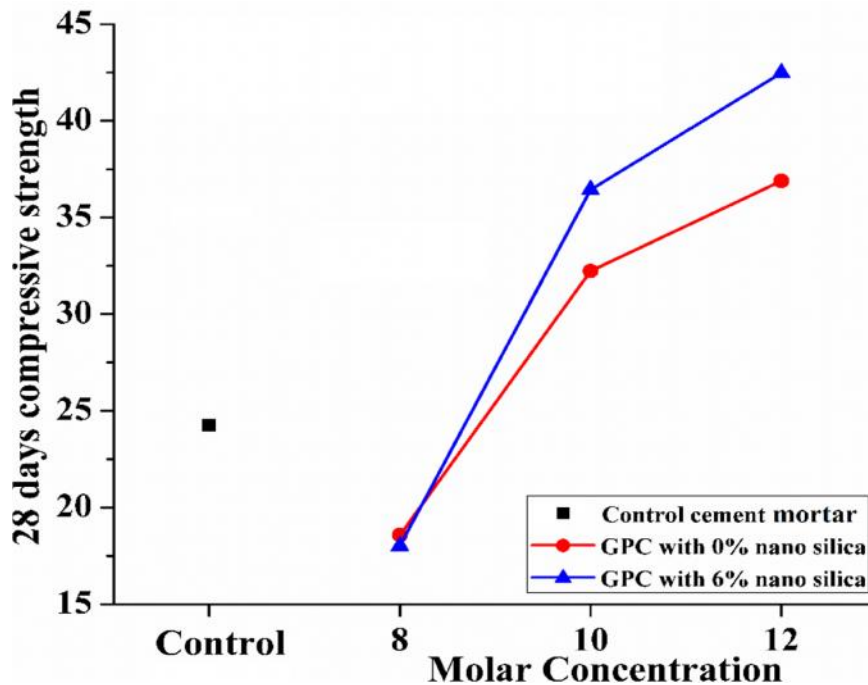
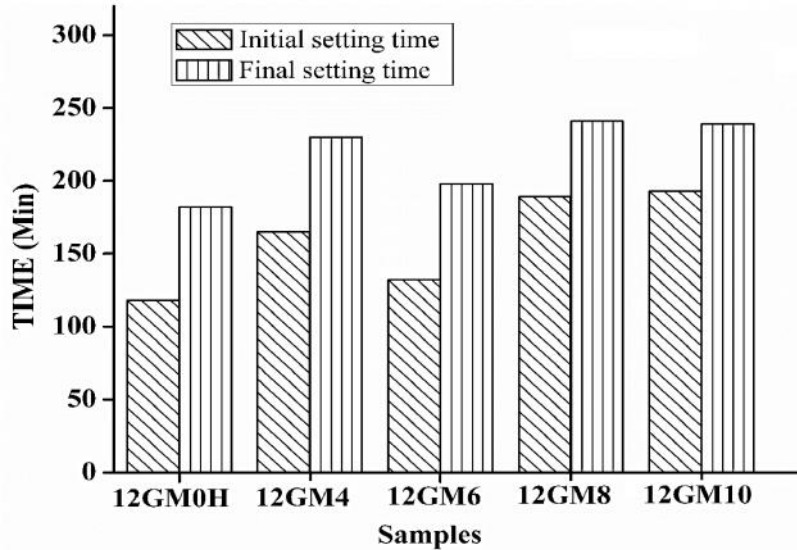


Figure – 5.4: Compressive strength of geopolymer mortar & cement mortar at 28 days.

It has been also observed that the initial and final setting time of 12 (M) geopolymer mortar (heat activated) without nano silica is comparatively less than that of geopolymer mortar (cured at ambient temperature) with nano silica (Fig 5.5). It is also observed that with the increase in percentage of nano silica in the geopolymer mortar, the initial and final setting time of the geopolymer mixes is generally increased.



**Figure – 5.5: Initial and final setting time of geopolymer mortar (with / without nano silica).**

The flexural strength and split tensile strength of geopolymer mortar (with/without nano silica) and control cement mortar at 28 days are shown in Figure 5.6 and 5.7. It is noted that both the flexural strength and split tensile strength (28 days) of geopolymer mortar specimen increase with the increase in molar concentration of activator solution mainly due to the availability of more alkali in the mix. It is also noted that the flexural strength and split tensile strength of 8(M) geopolymer (with/without nano silica) less than Control cement mortar at 28 days. At 10M and 12M concentration, the geopolymer mortar with the addition of 6% nano silica and cured at ambient temperature shows better flexural and tensile strength than that of geopolymer mortar without nano silica (with heat curing) and the corresponding CONTROL cement mortar. The results are almost similar to the corresponding 28 days compressive strength of the mix.

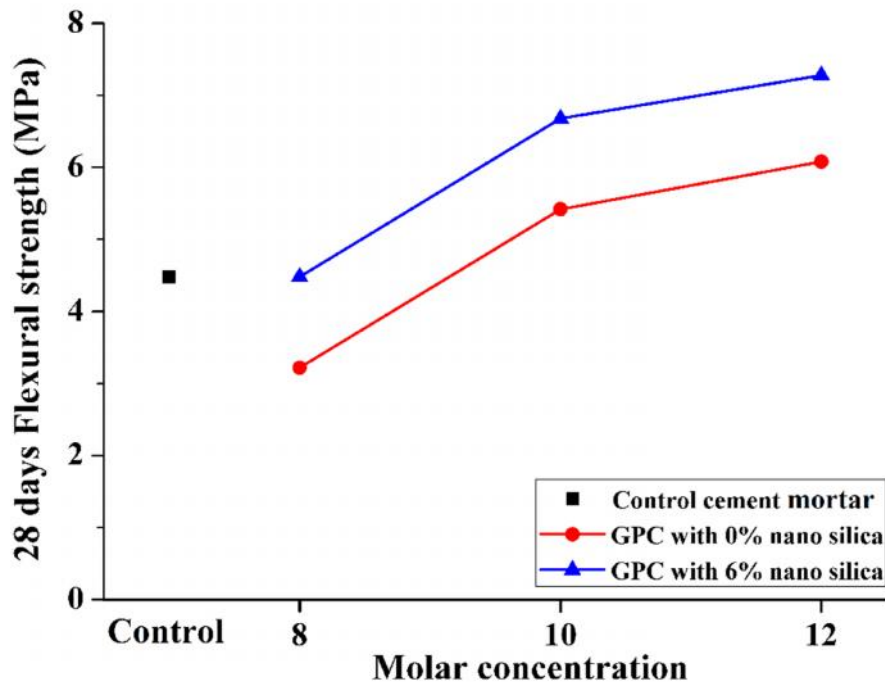


Figure – 5.6: Flexural strength of fly ash based geopolymer and cement mortar samples.

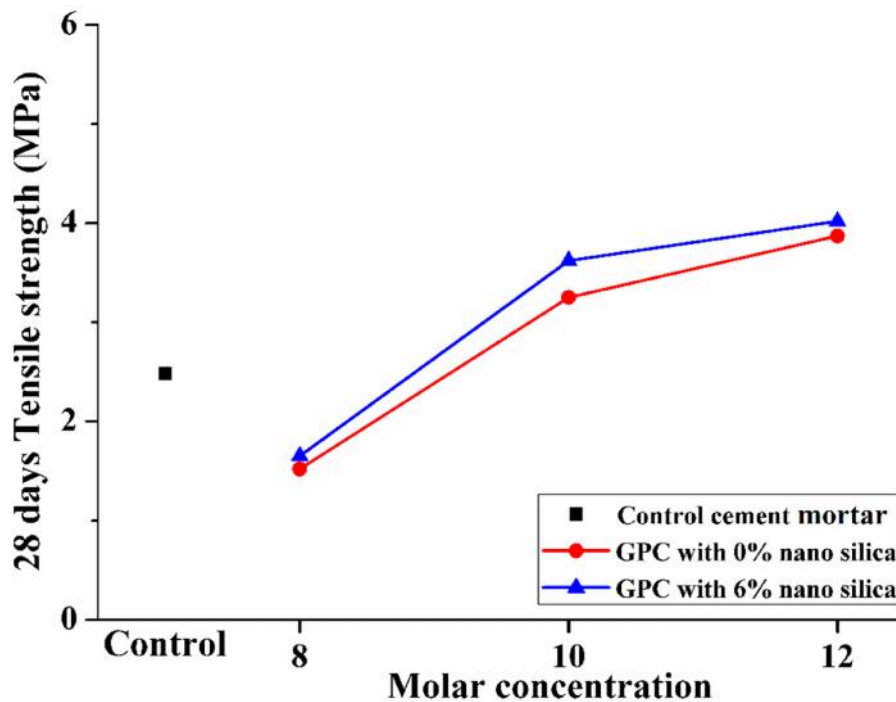


Figure – 5.7: Tensile strength of fly ash based geopolymer and cement mortar samples.

*(Published in Construction and Building Materials; 2014)*



A comparison of experimental test results of Rapid Chloride Ion Penetration Test (RCPT) for both geopolymer mortar with 6% of nano silica and without nano silica at different molar concentration (8M, 10M and 12M) and conventional cement mortar samples are presented in Figure 5.8. It may be mentioned here that for a particular molar concentration of geopolymer mortar with or without nano silica, the concentration of NaOH in the samples remains same, thus the difference in RCPT values for such case might be compared without any interference. It is noted that a lesser amount of charge is passed through geopolymer mortar with nano silica (ambient temperature curing) compared to the geopolymer mortar without nano silica (heat cured). This indicates that the diffusion coefficient will be less in the nano silica modified geopolymer matrix due to presence more amount of crystalline compound and thereby improvement in the durability is expected. It has been also observed that large amount of charge passes through 8(M) geopolymer mortar (with/without nano silica) than control cement mortar indicating less polymerization at low alkali content.

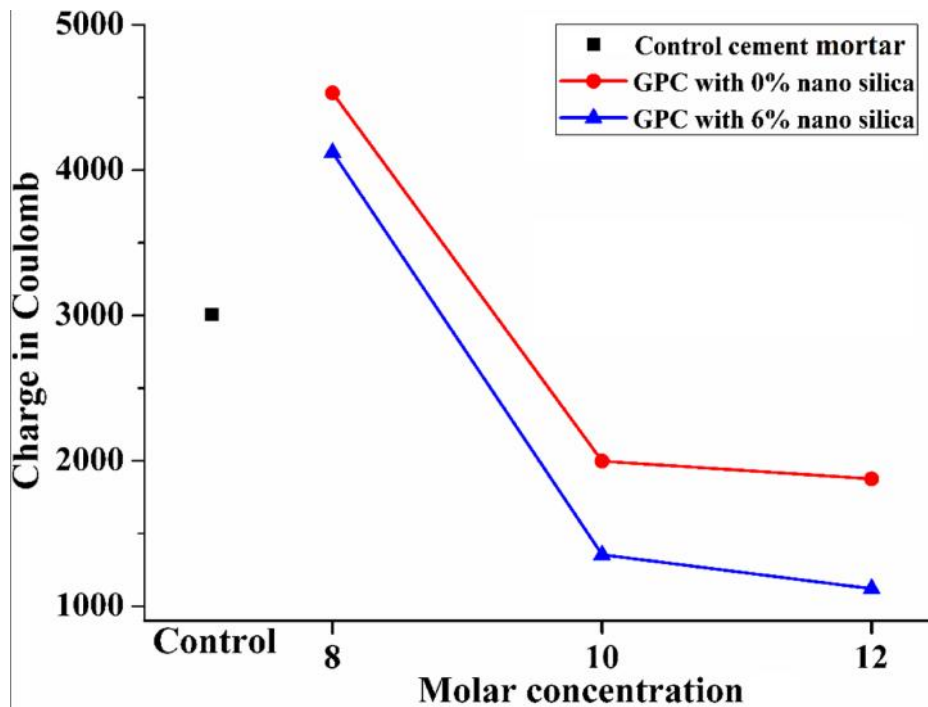


Figure – 5.8: Charge passed through geopolymer mortar samples (with / without nano silica) at different molar concentration and cement mortar samples.

The results of saturated water absorption on mortar specimens (Mix No - 8GM0H, 10GM0H, 12GM0H, 8GM6, 10GM6, 12GM6 and Control) after 28 days curing are presented in Figure 5.9. The water absorption indirectly indicates the durability of the geopolymer mortar. It is observed a lesser percentage of water absorption in geopolymer mortar having 6% nano silica (8GM6, 10GM6 and 12GM6) than that of heat cured geopolymer mortar without nano silica (8GM0H, 10GM0H, 12GM0H) and control mortar.

Therefore, it may be concluded that 6% nano silica addition in geopolymer mortar is optimum for better pore structure modification in the geopolymer mortar [7]. The strength durability performance of geopolymer mortar is optimum at 6% nano silica addition for the present matrix.

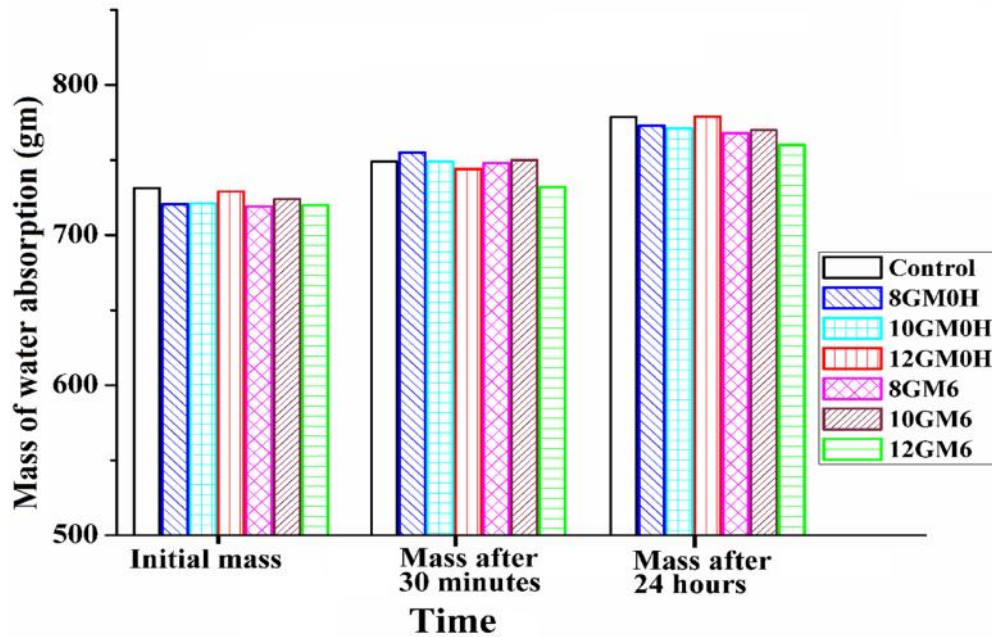
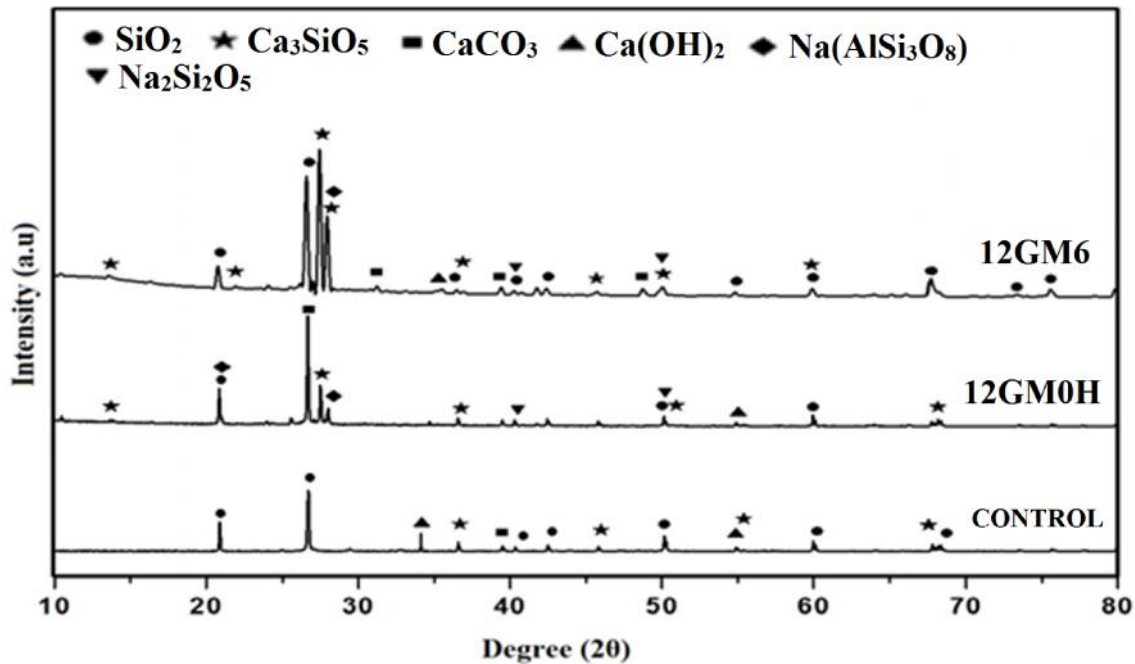


Figure – 5.9: Water absorption test on geopolymer mortar (with / without nano silica) of different molar concentration and cement mortar samples.

Figure 5.10 represents the X-Ray Diffraction analysis of geopolymer mortar without nano silica (12GM0H), with 6% nano silica (12GM6) and conventional cement mortar (Control). In geopolymer mortar having 6% nano silica, some specific extra peak positions are noticed compared to the geopolymer mortar without nano silica (12GM0H). It indicates the formation of new phase quartz ( $\text{SiO}_2$ ), alite ( $\text{Ca}_3\text{SiO}_5$ ), albite ( $\text{Na}(\text{AlSi}_3\text{O}_8)$ ), and  $\text{CaCO}_3$  in geopolymer mortar with 6% nano silica samples. Although, there are a few numbers of

peak of only  $\text{SiO}_2$ ,  $\text{Ca}_3\text{SiO}_5$  and  $\text{Ca}(\text{OH})_2$  present in case of controlled sample. As per XRD analysis, the crystalline phase is easily detected in the region of  $2\theta = 26^\circ - 32^\circ$  in the geopolymer mortar with 6% nano silica, which may be due to the formation of crystalline compound in geopolymer matrix. Therefore, it may be concluded that the strength of 12GM6 sample (with nano silica) is more than 12GM0H (without nano silica) sample due to presence of more amount of crystalline compounds [7].



**Figure – 5.10: XRD Analysis of fly ash based geopolymer mortar sample (12GM0H and 12GM6) and cement mortar (CM) samples.**

*(Published in Construction and Building Materials; 2014)*

The morphology of the geopolymer mortar samples with (0% & 6%) nano silica addition and conventional cement mortar is examined by the Field Emission Scanning Electron Microscope (FESEM) as shown in Figure 5.11A, 5.11B and 5.11C respectively. The conventional cement mortar matrix and geopolymer mortar sample without nano silica (12GM0H) are comparatively less dense than the geopolymer mortar with 6% nano silica (12GM6). Also, the geopolymer mortar sample without nano silica (12GM0H) has more numbers of unreacted fly ash particles than 12GM6 sample as shown in Figure 5.11A, 5.11B. The presence of nano silica in geopolymer mixes provides an extra enhancement on the polymerisation process due to its amorphous property and high specific surface area.

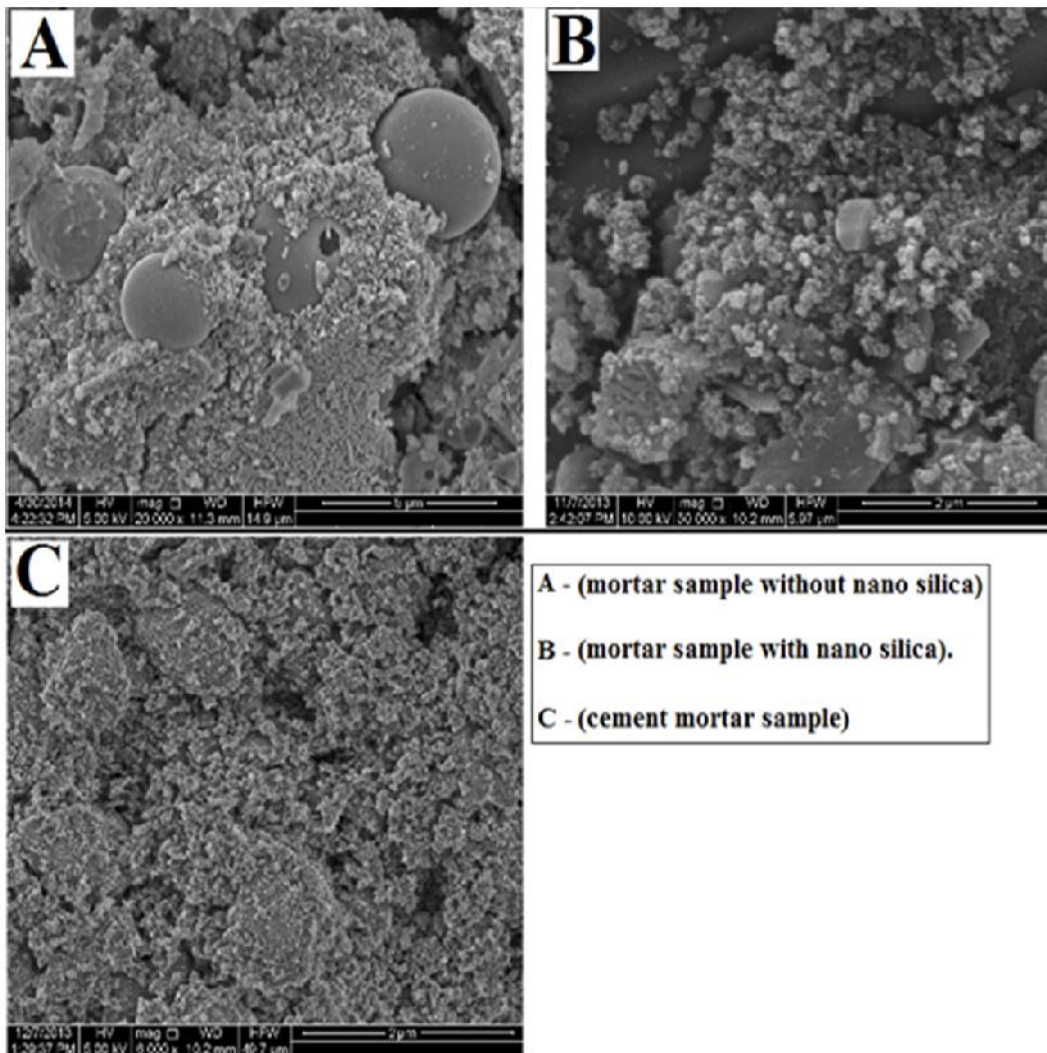


**Figure 5.11: FESEM image of (A) 12GM0H geopolymer mortar sample (B) 12M6 geopolymer mortar sample (C) CM sample**  
*(Published in Construction and Building Materials; 2014)*

Therefore, it is concluded that the geopolymer mortar with 6% nano-silica provides better strength as well as enhanced durability in terms of water absorption and RCPT values. It may be mentioned here that no heat activation is needed for this geopolymer mortar. Therefore, the results of geopolymer mortar with 6% nano-silica have been further extended to geopolymer concrete with 6% nano-silica addition at 12(M) NaOH activator fluid in the next section.

## 5.2. NANO-SILICA MODIFIED GEOPOLYMER CONCRETE:

Based on the performance of nano silica in geopolymer mortar, the similar effect of nano silica on geopolymer concrete has been now studied. The study has been limited to geopolymer concrete (with 6 % nano-silica) at 12(M) NaOH activator solution only. This is due to the remarkable performance of geopolymer mortar with 6% nano silica at 12(M) concentration of activator solution. Figure 5.12 demonstrates the compressive strength of geopolymer concretes with and without nano silica (12GC6 & 12GC0H) and control concrete (CC) samples at 3, 7 and 28 days. Based on the results, it is noted that the compressive strength of heat cured geopolymer concrete and control concrete samples are almost similar as designed. However, the compressive strength of geopolymer concrete with nano silica (12GC6) samples is comparatively higher than that of other geopolymer concrete without nano silica (12GC0H) concrete. The improvement in compressive strength of nano silica modified geopolymer concrete is about 14 % than both the heat cured geopolymer concrete and control cement concrete at 28 days.

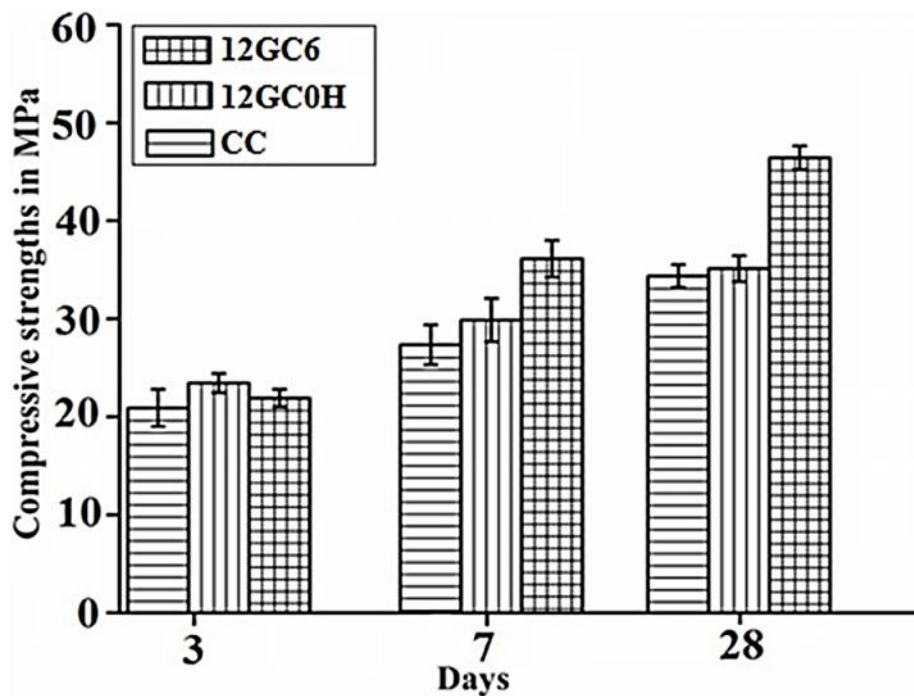


Figure – 5.12: Compressive strength of 12GC6, 12GC0H geopolymer concrete and control cement concrete (CC) at 3, 7 and 28 days.

*(Published in Construction and Building Materials; 2017)*

It has been observed that the fresh concrete properties such as slump test value and compacting factor test value of nano-silica modified geopolymer concrete are almost similar to conventional heat cured geopolymer concrete as well as control cement concrete (Table – 5.1).

The 28 days split tensile strength of geopolymer concrete with /without nano silica (12GC6 & 12GC0H) and control cement concrete (CC) are presented in Table – 5.1. It is noted that the split tensile strength of 12GC0H is more than that of CC concrete. These results are quite similar to the results of compressive strength results at 28 days. Also, the modified geopolymer concrete with 6% nano silica (12GC6) shows better split tensile strength than geopolymer concrete without nano silica (12GC0H) and the corresponding CC samples at 28 days. Geopolymer concrete with the addition of nano silica increases the dissolution rate of Si and Si–Al phases, which strongly affects the rate of polymerization. Also, the presence of nano silica in geopolymer mixture is the key factor to enhance the polymerisation process for its amorphous property and the high specific area [7].

It is also noted that the modulus of elasticity of 12GC0H geopolymer concrete is less than control cement concrete at equivalent compressive strength (Refer Table – 5.1). However, the Modulus of Elasticity of geopolymer concrete with nano silica (12GC6) is obtained as 37.28 GPa at a compressive strength of 46.43 MPa (Fig. 5.13). Therefore, the deformation behaviour of nano silica based geopolymer concrete is quite less compared to other two mix.

**Table – 5.1: Fresh concrete and harden concrete properties of different mixes:**

Mix Type	Slump (mm)	Compacting factor	Compressive strength at 28d (MPa)	Split tensile strength at 28d (MPa)	E <sub>c</sub> at 28d (GPa)	Bond strength at 28d (MPa)
<b>12GC6</b>	120	0.90	46.43	4.33	37.28	5.16© 3.12®
<b>12GC0H</b>	110	0.89	35.11	3.39	30.81	4.11© 2.67®
<b>CC</b>	105	0.87	34.77	2.78	32.58	3.56© 2.26®

© - Deformed steel rebar (0.2 % proof stress = 500 MPa),

® - Mild steel rebar (yield stress = 250 MPa).

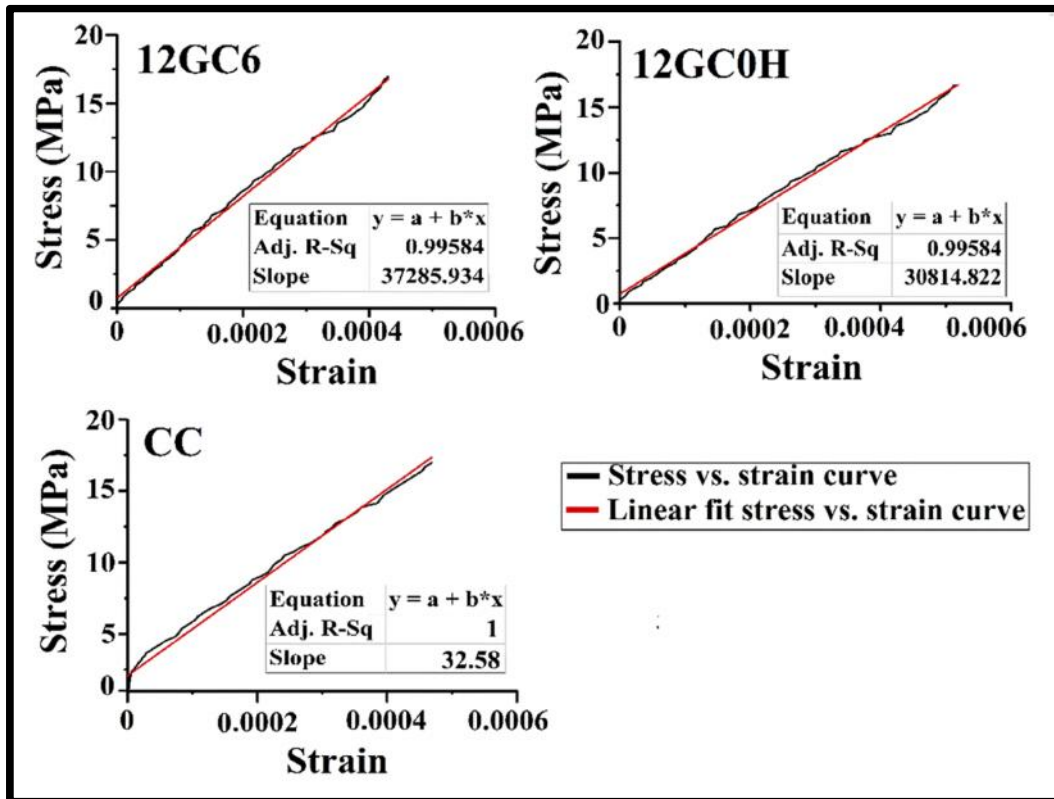


Figure – 5.13: Stress-strain curve of 12GC6, 12GC0H geopolymer concrete and CC concrete.

*(Published in Construction and Building Materials; 2014)*

Figure 5.14 and table 5.2 demonstrates the bond stress vs. slip curves of 20mm diameter reinforcement bars (High Yield Strength Deformed bar; 0.2% proof stress = 500 MPa and mild steel bar; yield stress = 250 MPa) for both types of geopolymer concrete (12GC6 & 12GC0H) and control cement concrete (CC) after 28 days of curing. The main thrust is to check the bond characteristics of geopolymer concrete with /without nano silica compared to conventional cement concrete. The result shows that the geopolymer concretes (12GC6 & 12GC0H) possess better bond strength than control concrete samples both for deformed and mild steel bars. Again, the geopolymer concrete (12GC6) with nano silica shows higher bond strength than 12GC0H geopolymer concrete for both deformed and mild steel reinforcement bars. All the samples are failed by the pull-out load of the reinforcement bar. It is also observed, that the slip for plain bars are more compared to that of deformed bar at equal pull-out load (Refer Fig. 5.14).

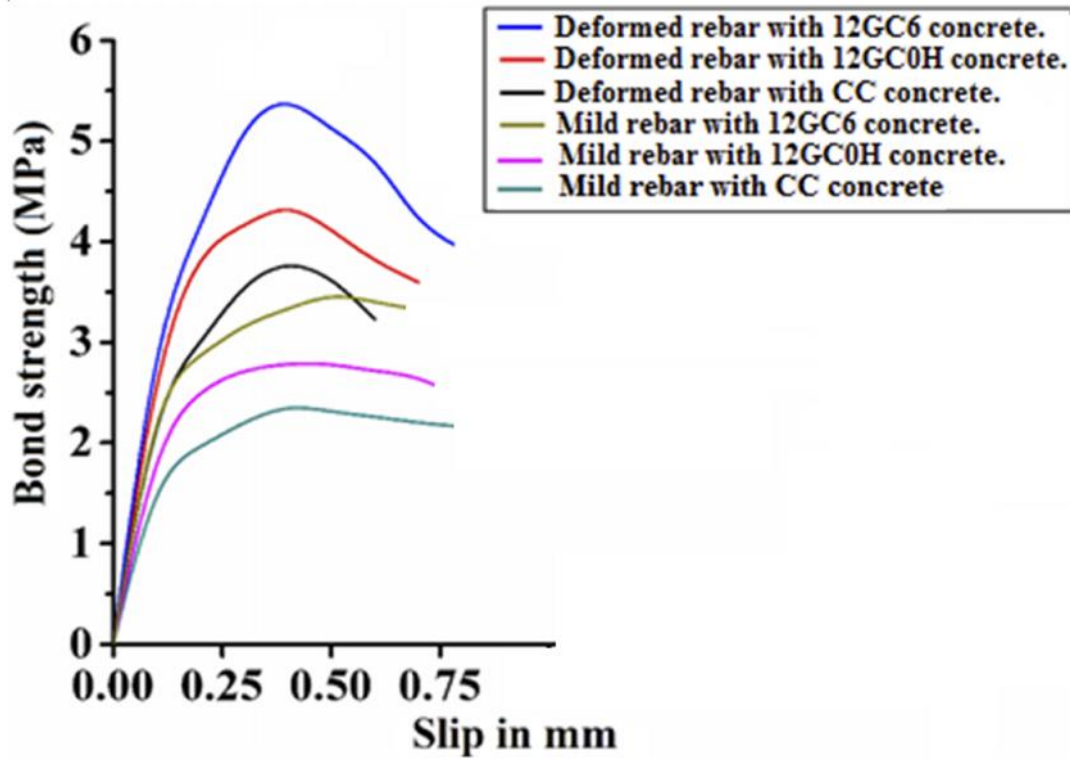


Figure – 5.14: Bond strength vs. slip curve of geopolymer concrete (12GC6 & 12GC0H) and control cement concrete (CC) with deformed and mild steel bar.

The bond strength of geopolymer concrete with 6% nano silica (12GC6) is more than geopolymer concrete without nano silica (12GC0H) and CC concrete, as the split tensile strength nano-silica modified geopolymer concrete (12GC6) is also higher than the other concretes [8, 9]. The presence of soluble silicates in geopolymer concrete produce a denser or stronger interfacial transition zone (ITZ) between aggregates and geopolymer matrices as compared to the cement matrices which causes the better bond strength between geopolymer concrete and reinforcement bar [10 – 12].

Table – 5.2: Details of bond stress test result of 12GC6, 12GC0H and CC reinforced concrete:

Rebar type	12GC6 (MPa)		12GC0H (MPa)		CC (MPa)	
	At failure load	At 0.25 mm slip	At failure load	At 0.25 mm slip	At failure load	At 0.25 mm slip
Mild steel	3.49	3.12	2.71	2.67	2.37	2.26
Deformed steel	5.47	5.16	4.44	4.11	3.82	3.56



The load deflection behaviour of steel reinforced nano-silica modified geopolymer concrete (12GC6), conventional heat cured geopolymer concrete (12GC0H) and control cement concrete (CC) beams are shown separately in Figure 5.15, 5.16 and 5.17 respectively. As the load is increased, all the beams are started to deflect and the flexural cracks are developed near the center of the beams. All the beam specimens are ultimately failed in the similar way due to the yielding of the reinforcement bar followed by the crushing of concrete. The flexural capacity of the beams is increased significantly with the enhancement of the tensile reinforcement for all types of concrete mixes (12GC6, 12GC0H & CC). It is observed that the flexural capacity of 12GC6 concrete beams (marked as A1, A2, A3) is increased by 12%, 7% and 18% for tensile reinforcement percentage of 0.45%, 0.67% and 0.81% with respect to 12GC0H geopolymer concrete beams (marked as B1, B2, B3) respectively (Fig.5.15). Also, flexural capacity of reinforced heat cured geopolymer concrete beam is comparatively higher than control cement concrete beams of equivalent compressive strength. The flexural capacity of 12GC6 concrete beams (A1, A4, A5, A6, A7) at different percentages of compressive reinforcement (Fig. 5.16) and shear reinforcement (Fig. 5.17) are better than that of the 12M0H geopolymer concrete beam (B1, B4, B5, B6, B7) and CC concrete beam (C1, C4, C5, C6, C7).

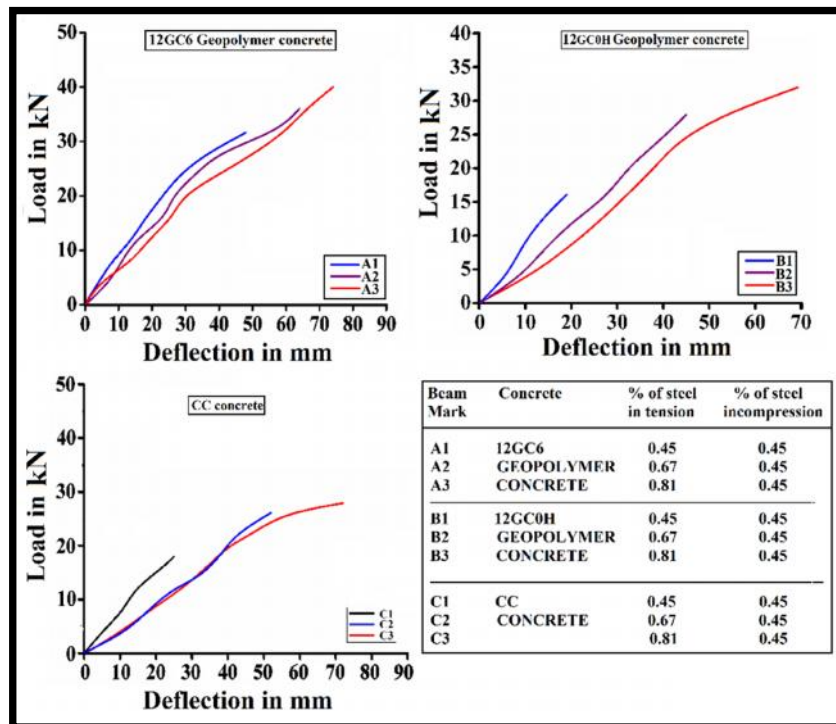


Figure – 5.15: Load vs. deflection curve capacity of 12GC6, 12GC0H and CC concrete beams with different percentages of tensile reinforcement.

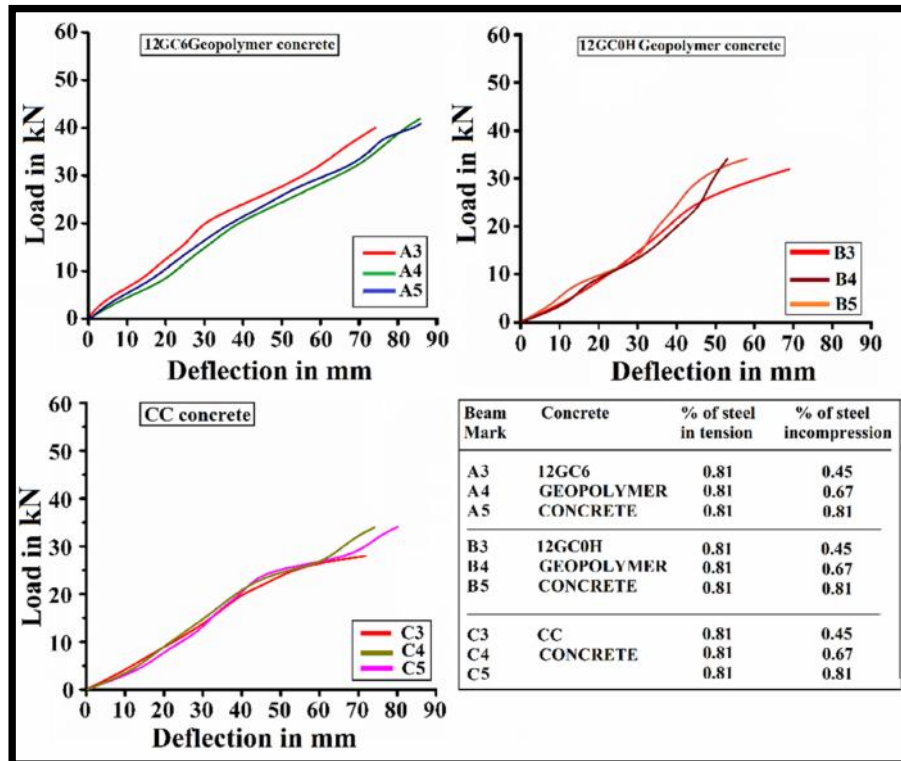


Figure – 5.16: Load vs. deflection curve of 12GC6, 12GC0H and CC concrete beams with different percentages of compressive reinforcement.

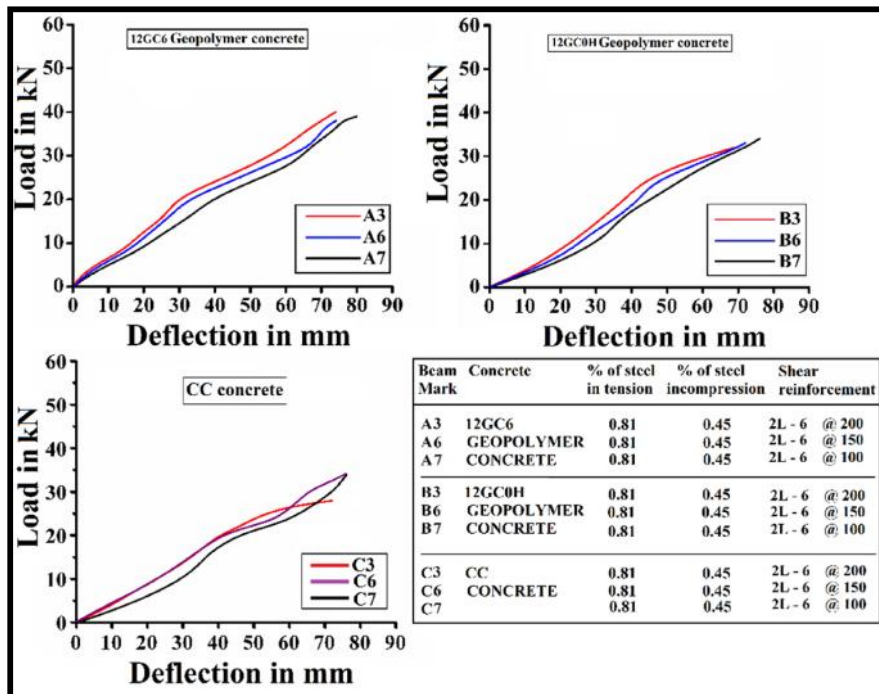


Figure – 5.17: Load vs. deflection curve of 12GC6, 12GC0H and CC concrete beams with different amount of shear reinforcement.

(Published in Construction and Building Materials; 2017)

Again, the experimental bending moment capacity of the tested reinforced concrete beams (12GC6, 12GC0H and CC) are compared with their corresponding theoretical bending moment capacity values determined as per IS 456 (2000) [13]. It may be mentioned here that the theoretical bending moment has been calculated as per clause G1.1 (b) of IS 456 (2000). Though the relationship is applicable to the cement concrete, the same formulation has been considered for geopolymer concrete. The bending moment capacity ratio,  $M_{exp} / M_{th}$  (the ratio of experimental bending moment and theoretical bending moment) of nano silica modified reinforced geopolymer concrete beam is comparatively higher than that of heat cured geopolymer and control cement concrete beam at different percentages of tensile and compressive reinforcement (Refer Table 5.3). Therefore, the design of geopolymer beams will be safer compared to normal concrete beam.

**Table – 5.3: Theoretical ( $M_{th}$ ) and experimentally ( $M_{exp}$ ) calculated bending moment (kN-m) of 12GC6, 12GC0H and CC reinforced concrete beam:**

Percentages of reinforcement		Theoretical bending moment	CC	12GC0H	12GC6
$p_t$	$p_c$	$M_{th}$	$M_{exp}$	$M_{exp}$	$M_{exp}$
0.45	0.45	2.65	2.80	2.50	4.98
0.67	0.45	3.82	4.07	4.30	5.57
0.81	0.45	4.34	4.37	5.02	5.98
0.81	0.67	4.34	4.68	5.18	6.16
0.81	0.81	4.34	4.76	5.23	6.21

$p_t$  = percentage of steel in tension (bottom),  $p_c$  = percentage of steel in compression (top).

*(Published in Construction and Building Materials; 2017)*

Therefore, the flexural behaviour of reinforced nano silica modified geopolymer concrete (12GC6) cured at ambient condition are almost similar to the heat cured geopolymer concrete (without nano silica) and control cement (CC) concrete whereas, the bending moment capacity of reinforced nano silica modified geopolymer concrete (12GC6) is significantly higher than the heat cured geopolymer concrete (without nano silica) and CC concrete beam. The higher mechanical strength of geopolymer concrete with 6% nano silica and its better bond behaviour with reinforcement bar help to provide the improvement of

flexural strength and bending moment capacity of reinforced geopolymer concrete (12GC6) beam with nano silica. Thus, the design provisions contained in the current standards and codes for the design of flexural member with conventional concrete can be used to design structural members with fly ash-based nano silica added geopolymer concrete.

The crack patterns in 12GC6, 12GC0H and CC concrete beams are shown in Figure 5.18 and it is noted that the flexure cracks are initiated in the bending zone as expected. The cracks in samples are then propagated with the further load increment and the new cracks are also developed along the span. The large numbers of narrow cracks with different widths and depths are observed with a closet space in 12GC6 concrete beams than other concrete beams. It is also observed that first cracking load of 12GC6 concrete beams was more than 12GC0H and CC concrete reinforced beams.



**Figure – 5.18: Crack patterns of 12GC6, 12GC0H and CC concrete beams.**

After the assessment of structural behaviours, the microstructural properties of 12GC6, 12GC0H and CC concrete samples are then analysed by using X-Ray Diffraction test (XRD), Fourier Transform Infrared Spectroscopy (FTIR) and Field Emission Scanning Electron Microscopy (FESEM) with Energy Dispersive X-ray (EDS). X-Ray Diffraction patterns of 12GC6 and 12GC0H geopolymer concrete and CC concrete are represented in

Figure 5.19. The intensity of quartz, mullite and hematite peaks are more in 12GC6 due to the presence of additional nano silica in the matrix. Also, some extra peaks are shown in XRD analysis of nano-silica modified geopolymer concrete, which indicates the formation of a new phase of albite ( $\text{NaAlSi}_3\text{O}_8$ ), kaolinite ( $\text{Al}_2\text{Si}_2\text{O}_5(\text{OH})_4$ ), and alite ( $\text{Ca}_3\text{SiO}_5$ ) crystalline compound compared to that of 12GC0H and CC concretes.

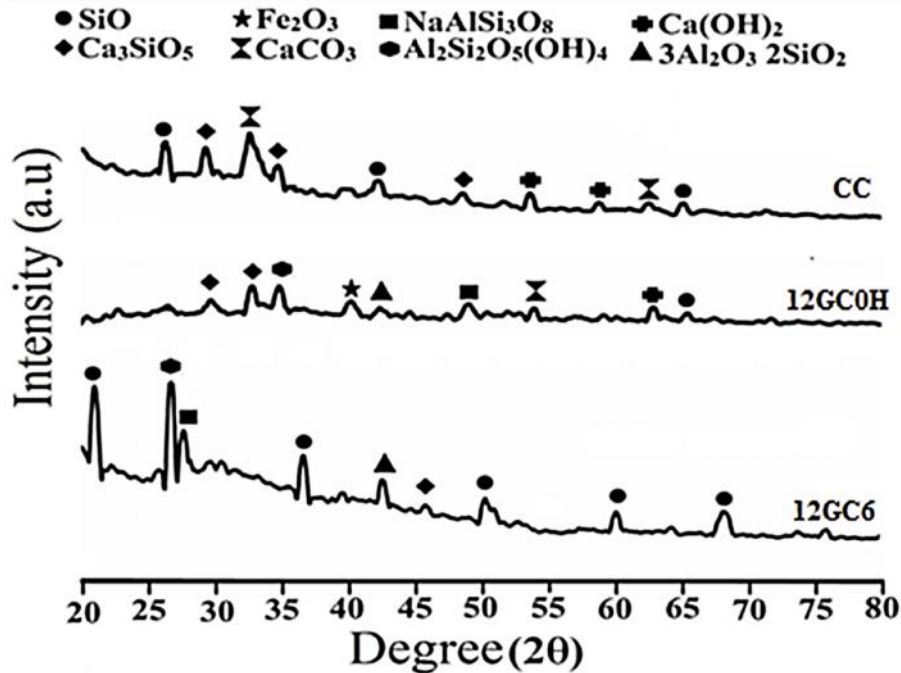


Figure – 5.19: XRD analysis of 12GC6 & 12GC0H and CC concrete.

*(Published in Construction and Building Materials; 2017)*

The wide diffraction hump is also detected around  $2\theta = 25 - 30^\circ$  which confirms the presence of crystalline phases in 12GC6 geopolymer matrix. The broad hump registered between  $2\theta = 25^\circ - 30^\circ$  in the XRD diagram of 12GC6 geopolymer concrete indicates the dissolution of the fly ash amorphous phase and the formation of a new amorphous phase and crystalline phases in the matrix [14].

The infrared spectroscopic results of 12GC6 and 12GC0H samples are shown in Figure 5.20. The distinct intensity band near  $460\text{ cm}^{-1}$  is recognised for the Si-O-Si bending vibration. The band between  $750\text{ cm}^{-1}$  to  $800\text{ cm}^{-1}$  is also observed due to the  $\text{AlO}_4$  vibration. Another peak for the asymmetric stretching at the vibration band of Si-O-T (T = Al, Si) which is described as the strongest band, registered in the region of  $950\text{ cm}^{-1} - 1050\text{ cm}^{-1}$ .

The position ( $1420\text{ cm}^{-1}$ ) of Si-O-Si in 12GC0H is basically shifted to the right position ( $1485\text{ cm}^{-1}$ ) in 12GC6. A significant band is also located at approximately  $3450\text{ cm}^{-1}$  for OH stretching bonding.

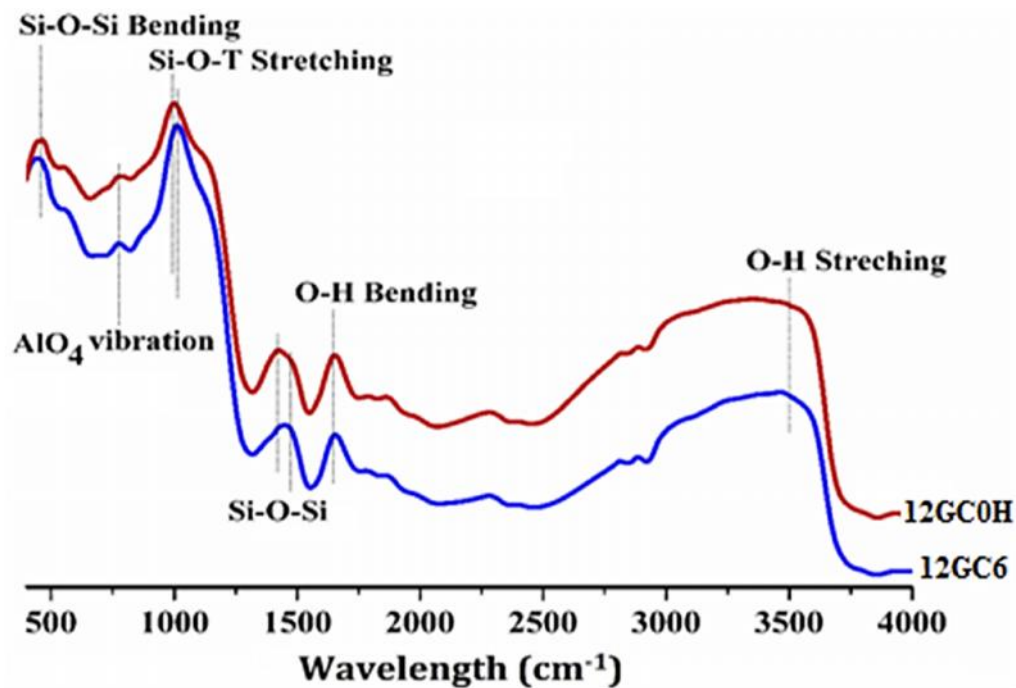


Figure – 5.20: FTIR analysis of geopolymer concrete (12GC6 & 12GC0H).

The asymmetric stretching vibration band of Si–O–T (T = Al, Si) of 12GC6 geopolymer matrix shifted to right ward with respect to 12GC0H geopolymer matrix may be associated with the formation of less polymerised structure at  $990\text{ cm}^{-1}$  and non-dissolved high polymerised structures at  $1025\text{ cm}^{-1}$ . The Si-O-Si position ( $1420\text{ cm}^{-1}$ ) in 12GC0H is shifted to the right position ( $1485\text{ cm}^{-1}$ ) in 12GC6 matrices due to the chemical changes in the geopolymer matrix with the addition of colloidal nano-silica [14, 15].

Figure 5.21 exhibits FESEM micrographs along with elemental analysis of 12GC6 and 12M0H and CC concrete matrices. In elemental analysis, the major elements are Si, Al, Ca with some amount of Fe are present in geopolymer concrete samples (12GC6& 12GC0H) and control cement (CC) concrete. As the experimental work is based on low calcium fly-ash geopolymer concrete, the presence of Ca in geopolymer concrete (12GC6& 12GC0H) is less than control cement concrete. The ratios of Si/Al for the 12GC6 and 12GC0H samples are significantly different. The ratio of Si/Al for 12GC6 geopolymer concrete is 2.60, and for

12GC0H geopolymer concrete is 1.52 (Fig. 5.21). It is also noted in FESEM image that a large amount of crystalline compound are observed in the 12GC6 matrix than that of 12GC0H concrete matrix.

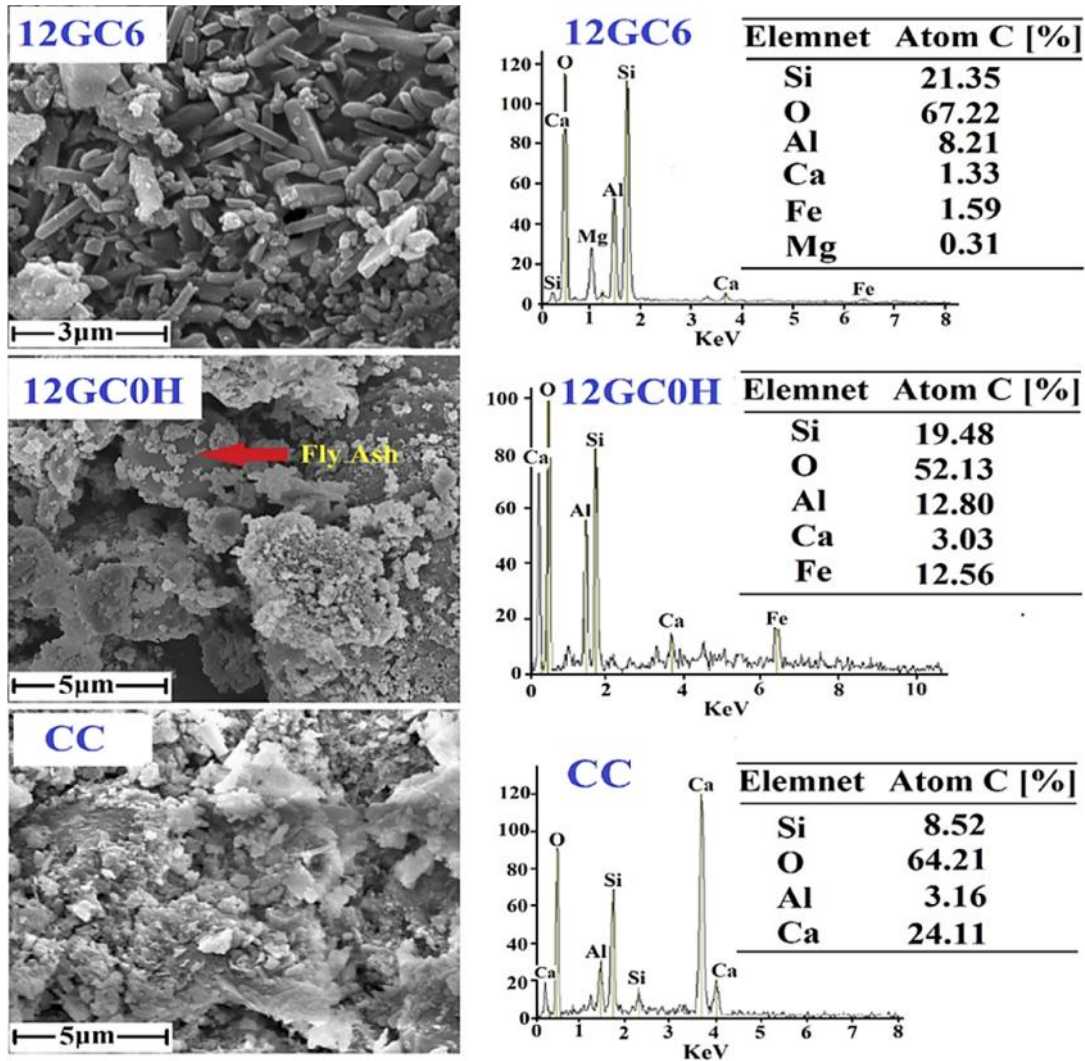


Figure – 5.21: SEM micrographs and EDX analysis of 12GC6, 12GC0H geopolymer concrete and control cement concrete (CC).

*(Published in Construction and Building Materials; 2017)*

The large amount of crystalline compounds are transformed from the amorphous phase in nano-silica modified cementitious matrix. The unreacted heterogeneous fly-ash are also present in 12GC0H matrices due to the lower polymerization rate which lead to lower mechanical strength. The augmentation of the mechanical strengths of 12GC6 geopolymer concrete is due to the large number of crystalline geopolymer plates spread all over the

surface. The alumina leaching in nano-silica modified geopolymer concrete is higher than heat cured geopolymer concrete. The ratio of Si/Al ratio of 12GC6 geopolymer matrices is higher than 12GC0H concrete, that causes the higher mechanical strength of nano silica modified geopolymer concrete [16, 17]. The higher amount of the Si/Al ratio and homogeneous texture of crystalline plates in the matrix exhibit the higher mechanical strength of nano silica modified geopolymer concrete than other concrete. Therefore, the appropriate amount of nano silica addition seems to be beneficial for the development of geopolymer mortar cured at ambient temperature.



### 5.3. ANTIBACTERIAL ACTIVITY OF SILVER-SILICA MODIFIED GEOPOLYMER MORTAR.

It has been established in section 5.1 that the nano-silica modified geopolymer mortar cured at ambient temperature shows appreciable strength and durability than conventional heat cured geopolymer mortar. Beside the strength and durability, the antibacterial properties of the same geopolymer mortar is now discussed here. To improve the antibacterial property of nano silica modified geopolymer mortar, the effect of silver nano particle has been incorporated in the study. The different types of nano-materials like copper, zinc, titanium, magnesium, gold, alginate and silver have come up but the silver nanoparticles have proved to be the most effective as it has good antimicrobial efficacy against bacteria, viruses and other eukaryotic micro-organisms [18 – 21]. The synthesis of silver nano particle has been generally achieved via various routes, including micro-emulsion technique, sonochemical reduction, photochemical technique, etc. [22]. These synthetic methods are time consuming and require expensive instruments. Also, silver (Ag) nanoparticles synthesized by these methods are easily aggregated, which causes deterioration of their chemical properties and decreases their antibacterial properties [23, 24]. In this study, the Ag nanoparticles are attached on the surface of SiO<sub>2</sub> nanoparticles are prepared by modified Stöber method. The release time of Ag can be delayed for a long time so that Ag supported materials will have great potential for antibacterial applications. The study has been limited to geopolymer mortar only.

Therefore, a silver-silica nano composite has been developed by simple adsorption of silver in a suitable amount of colloidal silica suspension for anti-bacterial property development. It may be mentioned here that the mix GM<sub>Si</sub> is same as 12GM6 (i.e. geopolymer mortar with 6% nano silica). The notations have been changed here to provide similar notation as in the published paper. Similarly, the mix GM<sub>Ag-Si</sub> represents the modified mix of GM<sub>Si</sub> with silver nano particle. The amount of nano silica and silver-silica nano particle is kept same for GM<sub>Si</sub> and GM<sub>Ag-Si</sub> geopolymer mix respectively. The mechanical strength, durability and mechanistic antibacterial activity of fly ash based silver-silica nano composite modified geopolymer mortar (GM<sub>Ag-Si</sub>) had been investigated and compared with silica modified geopolymer mortar (GM<sub>Si</sub>) and control cement mortar (CM). The preparation of silver-silica nano composite has been confirmed by several morphological studies. Transmission Electron Microscopy analysis of silica NPs and silver-silica nano composite

shows their very regular spherical shape (Fig.5.22A & 5.22B). Figure 5.22B shows the silver NPs (mean  $\pm$  SD:  $4 \pm 1$  nm) are formed on the surface of silica NPs ( $30 \pm 10$  nm).

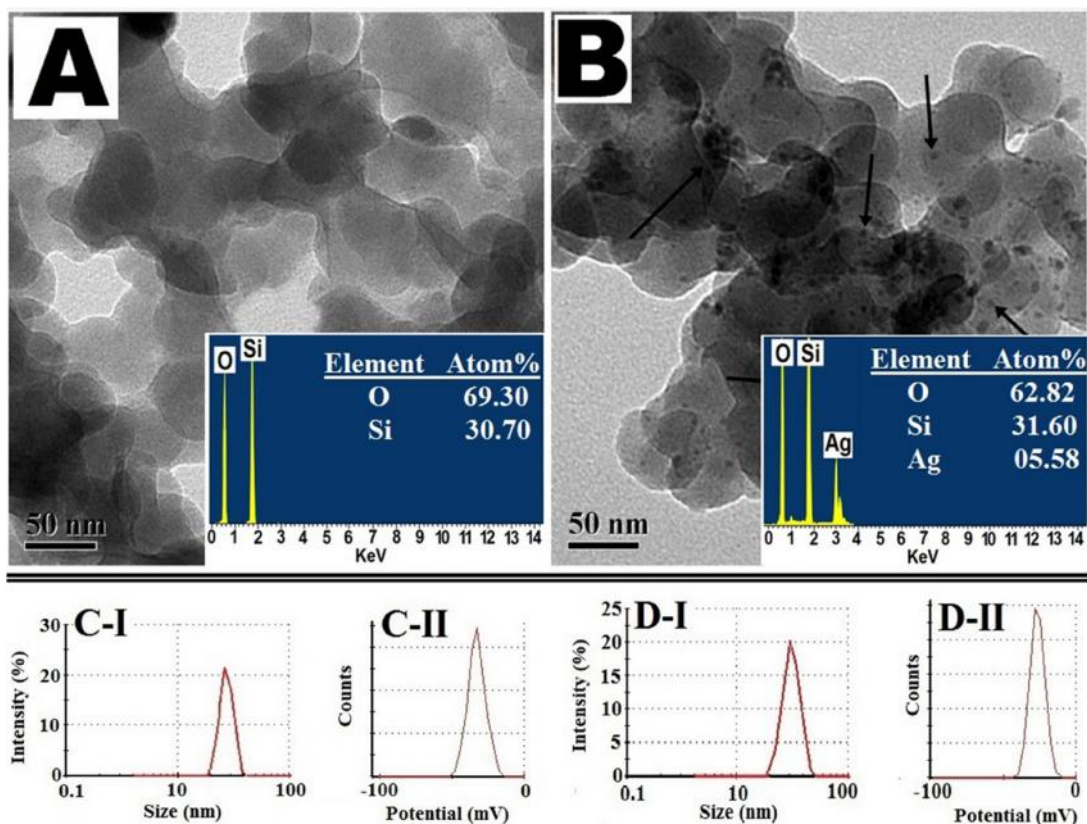


**Figure – 5.22: TEM image of (A) Silica NPs & (B) Silver-silica NPs with inset representing elemental analysis by EDS. Zeta size (C-I & D-I) and Zeta potential (C-II & D-II) distribution graph of silica NPs & silver-silica NPs respectively.**

*(Published in RSC Adv., 2015.)*

The elemental analysis of newly synthesized silica NPs and silver-silica nano composites are shown in Figure 5.22A & 5.22B (inset). The presence of the elements O and Si are observed at 0.562 KeV (O) and 1.75 KeV (Si) respectively. The Si, O and Ag peaks are clearly shown in Figure 5.22B (inset), which indicates the presence of silver nano particles. It is confirmed from the TEM images that the nano particles are pure in colloidal form but the particles are of hybrid-type in silver-silica nano composites. Also the average size of the silica NPs seems to be 20 – 40 nm as per the analysis made by Zeta size distribution graph (Fig. 5.24C-I). The silver NPs ( of size  $4 \pm 1$  nm) are attached on the surface of silica NPs as shown in Figure 5.22D-I. Also a comparatively broad peak in Figure 5.22D-I reveals the

greater size distribution of silver-silica nano composite. This is also much correlated with TEM results (Fig. 5.22B). The overall surface charge of the pure silica NPs (Fig. 5.22C-II) is negative (-50 mV) whereas silver silica nano-composite (Fig. 5.22D-II) shows some greater positive charges (>-50 mV) which has been confirmed by zeta potential analysis.

The X-ray Diffraction profiles of newly synthesized silica NPs and silver-silica nano-composite are matched up with Joint Committee on Powder Diffraction standards (JCPDs) data file (Fig. 5.23A). The XRD pattern of silver-silica NPs shows the presence of sharp peaks of Ag nano particle in Figure 5.23A (II). The peaks of silver nano particle are absent in XRD analysis of SiO<sub>2</sub> NPs as shown in Figure 5.23B (I). The sharp peaks indicate that the newly synthesized nano particles are either very small crystallite or semi-crystalline in nature. The average crystallite size of silver nano particles is estimated by Scherrer's equation for the (111), (100) and (006) diffraction peaks at  $2\theta = 38.118$ , 45.593 and 71.101 respectively. Therefore, it can be clearly confirmed that the silver-silica nano composite particles are successfully synthesized.

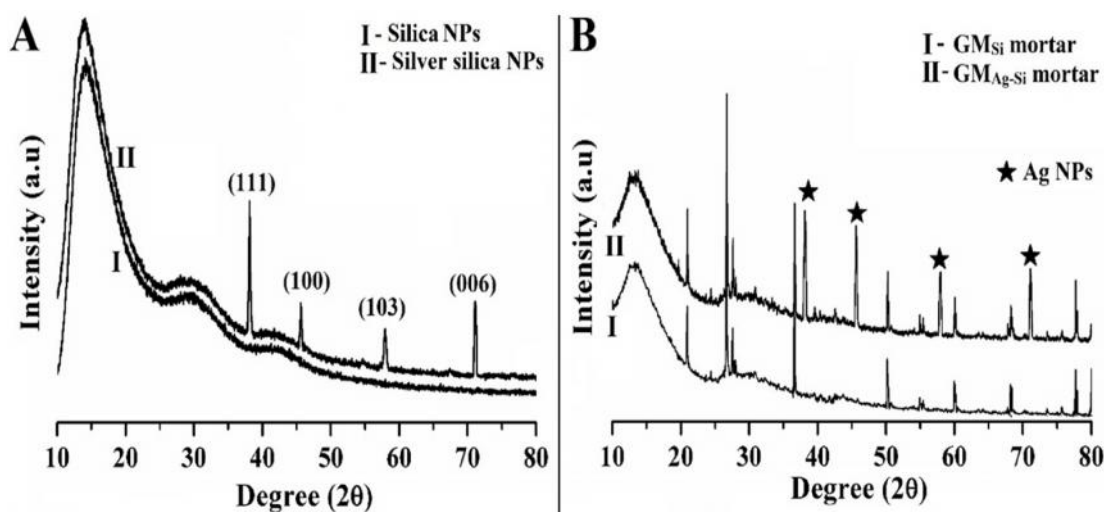


**Figure – 5.23A: XRD spectra of (I) SiO<sub>2</sub> NPs & (II) Ag-SiO<sub>2</sub> NPs.**

**Figure – 5.23B: XRD spectra of (I) GM<sub>Si</sub> and (II) GM<sub>Ag-Si</sub>.**

*(Published in RSC Adv., 2015.)*

The XRD spectra of nano silica modified geopolymer mortar (GM<sub>Si</sub>) and nano silver-silica nano composite modified geopolymer (GM<sub>Ag-Si</sub>) mortar are presented in Figure 5.25B. In case of geopolymer mortar with nano silver-silica composite, some additional peak

positions are observed at same specific positions (2 ) which confirms the presence of silver nano particles in  $GM_{Ag-Si}$  mortar.

Figure 5.24 represents the compressive strength of fly ash based nano silica modified geopolymer mortar ( $GM_{Si}$ ), nano silver-silica modified geopolymer mortar ( $GM_{Ag-Si}$ ) and control cement mortar (CM) samples at 3, 7 and 28 days. The above two types of geopolymer mortar samples are cured in air at ambient temperature. The strength of water cured control mortar samples made with OPC cement is also compared. It is noted that both the geopolymer mortar samples ( $GM_{Si}$  and  $GM_{Ag-Si}$ ) show better compressive strength than CM samples at all ages. However, geopolymer mortar with silica NPs and geopolymer mortar with silver-silica nano composite seems to provide similar compressive strength cured at ambient temperature. Therefore, it may be concluded that the presence of silver NPs attached on the surface of silica NPs does not influence the compressive strength of silver-silica modified geopolymer mortar.

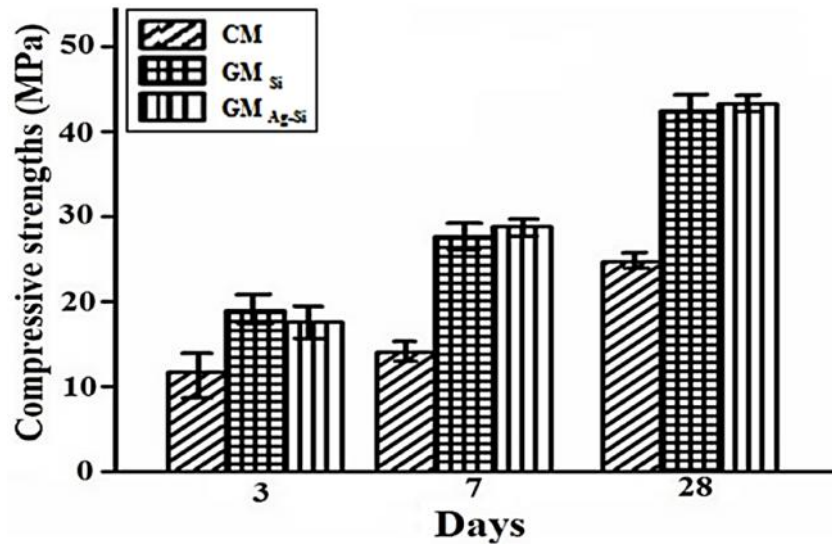


**Figure – 5.24: Compressive strength of  $GM_{Ag-Si}$ ,  $GM_{Si}$  geopolymer mortar and control cement mortar at different ages.**

*(Published in RSC Adv., 2015.)*

Similar behaviour has been also observed on flexural strength and split tensile strength of geopolymer mortars and control mortar samples at 28 days (Fig. 5.25). A comparison of RCPT value for samples of mix  $GM_{Si}$ ,  $GM_{Ag-Si}$  and CM are presented in Figure 5.26. It is observed that a lesser amount of ions has been passed through geopolymer

with nano silica / nano silver silica (i.e GM<sub>Ag-Si</sub> / GM<sub>Si</sub>) matrices compared to CM matrices. About 37% reduction in RCPT values are noted for both geopolymer mortar (with silver-silica nano composite/silica nano particle) than that of control cement mortar.

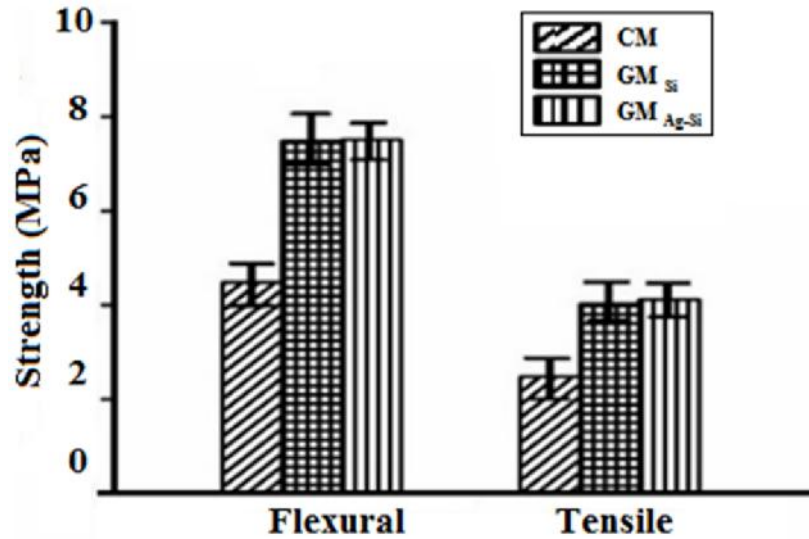


Figure – 5.25: Flexural and tensile strength of GM<sub>Ag-Si</sub>, GM<sub>Si</sub> geopolymer and CM.

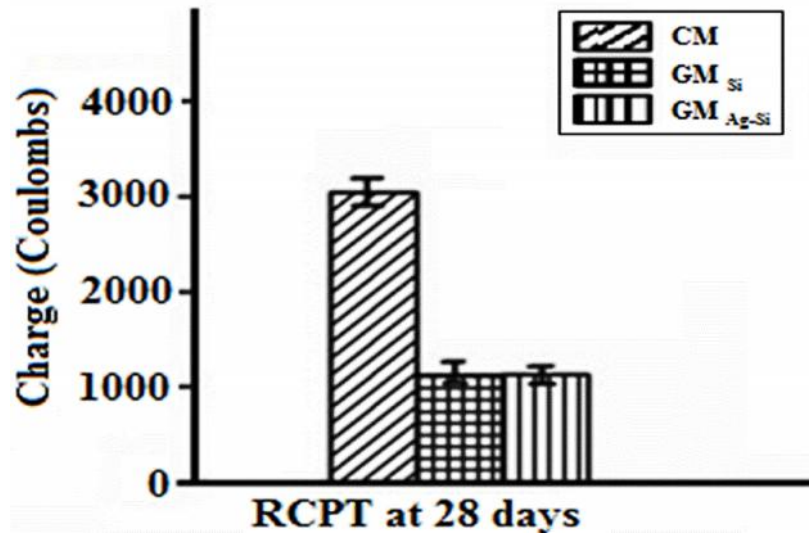


Figure – 5.26: RCPT of different mortar samples (CM, GM<sub>Si</sub> and GM<sub>Ag-Si</sub>).

In this present study, the silver NPs (3 – 5 nm) has been attached on the surface of silica NPs of 20 – 40 nm to develop the antimicrobial activity of the geopolymer mortar. In presence of positively charged silver NPs on the surface of the negatively charged silica NPs, the overall charges of silver-silica nano composite is reduced. The incorporation of this newly

formed silver NPs in the low calcium fly-ash based geopolymer mortar has improved its anti-bacterial property although the strength and durability are not affected by the presence of such silver NPs in geopolymer mortar cured at ambient temperature.

The bactericidal kinetics of exponentially growing gram negative *E. coli* and gram positive *S. aureus* bacteria are observed against samples of GM<sub>Si</sub>, GM<sub>Ag-Si</sub>, and CM specimen by time killing assay. The result reveals that the populations of *E. coli* and *S. aureus* bacteria are reduced by 99% after 8h and 6h (Fig. 5.27C & 5.27D) for GM<sub>Ag-Si</sub> respectively. The antibacterial effect has been shown by plate culture of bacteria after 8h treatment (Fig. 5.27A & 5.27B). A large number of colonies are found in GM<sub>Si</sub> and control specimens whereas such colonies are almost absent in case of GM<sub>Ag-Si</sub> sample.

The Minimum Inhibitory Concentration (MIC) and Minimum Bactericidal Concentration (MBC) values of samples of GM<sub>Ag-Si</sub> mix against gram +ve and gram -ve microorganisms are presented in tables – 5.4 and 5.5. Table – 5.4 indicates that a considerably low amount of GM<sub>Ag-Si</sub> (0.15 mg/mL) has been able to eradicate the gram (+ve) bacterial cells (>99%). Gram -ve organisms are more resistant to the growth inhibiting effect of the sample (0.10 mg/mL) compared to gram +ve bacterial cells. The antibacterial activities of GM<sub>Ag-Si</sub> geopolymer mortar samples are significantly higher than that of the other specimens (GM<sub>Si</sub> & CM sample). The MBC values for silver-silica nano composite treated cells are not more than 4 times of their respective MIC values indicating that the nano composites are bactericidal rather than bacteriostatic. The MBC value (Table – 5.5) indicates that a considerably lower amount of silver (0.43 µg/ml) has been able to eradicate the gram positive bacterial (*S. aureus*) cells. The gram negative organisms (*E. coli*) are more resistant to the growth inhibiting effect of silver NPs (0.32 µg/ml).

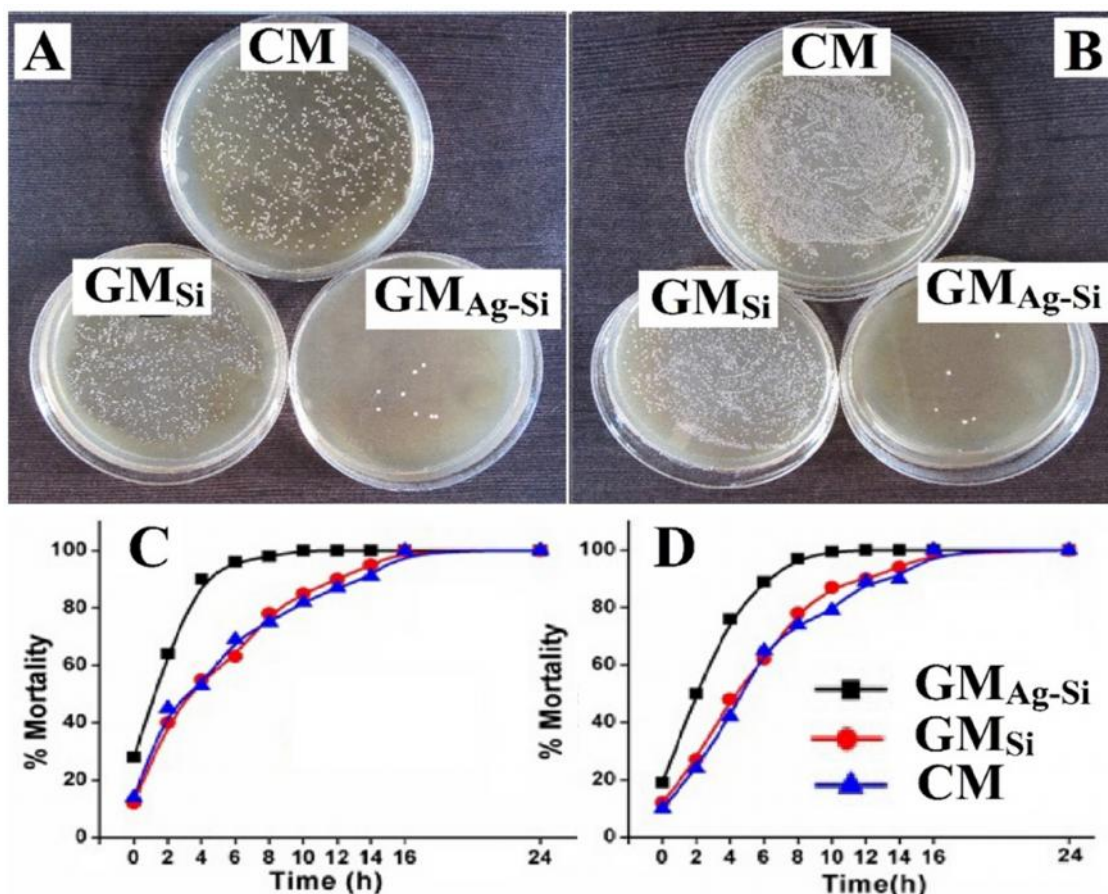


Figure – 5.27: Photographs of colonies of (A) *E. coli* & (B) *S. aureus* incubated on agar plates obtained from cultivated suspensions with (CM, GM<sub>Si</sub> & GM<sub>Ag-Si</sub>) and mortality curve of (C) Gram –ve bacteria (D) Gram +ve bacteria in presence of CM, GM<sub>Si</sub> & GM<sub>Ag-Si</sub>.

(Published in RSC Adv., 2015.)

Table – 5.4: Minimum Inhibitory Concentration (MIC) ASSAY (mg/mL):

Bacteria	Control	GM <sub>Si</sub>	GM <sub>Ag-Si</sub>
<i>E. coli</i>	NA	NA	0.10
<i>S. aureus</i>	NA	NA	0.15

Table – 5.5: Minimum Bactericidal Concentration (MBC) ASSAY (mg/mL):

Bacteria	Control	GM <sub>Si</sub>	GM <sub>Ag-Si</sub>
<i>E. coli</i>	NA	NA	0.32
<i>S. aureus</i>	NA	NA	0.43

The SYBR Green is a bacterial cell membrane permeant dye which stains both live and dead cells. The fluorescence microscopic images show that control cells and GM<sub>Si</sub> treated cells (*E. coli* and *S. aureus*) are intensely stained with SYBR Green, whereas GM<sub>Ag-Si</sub> treated cells are found to be PI positive (Fig. 5.28). The PI is an impermeant dye that stains only dead and membrane compromised cells due to loss of the plasma membrane integrity. The result of morphological analysis of GM<sub>Ag-Si</sub> treated cells represents extensive membrane destruction and disruption of cells after 8h of incubation (Fig. 5.28C) in respect to control and GM<sub>Si</sub> treated *E. coli* cells (Fig.5.28A and 5.28B) respectively. Control and GM<sub>Si</sub> treated cells show distinct spherical morphology of coccus shaped *S. aureus* (Fig. 5.28D and 5.28E respectively), whereas membrane deformation and pore formation can be seen along with cell debris in case of GM<sub>Ag-Si</sub> treated cells (Fig. 5.28F).

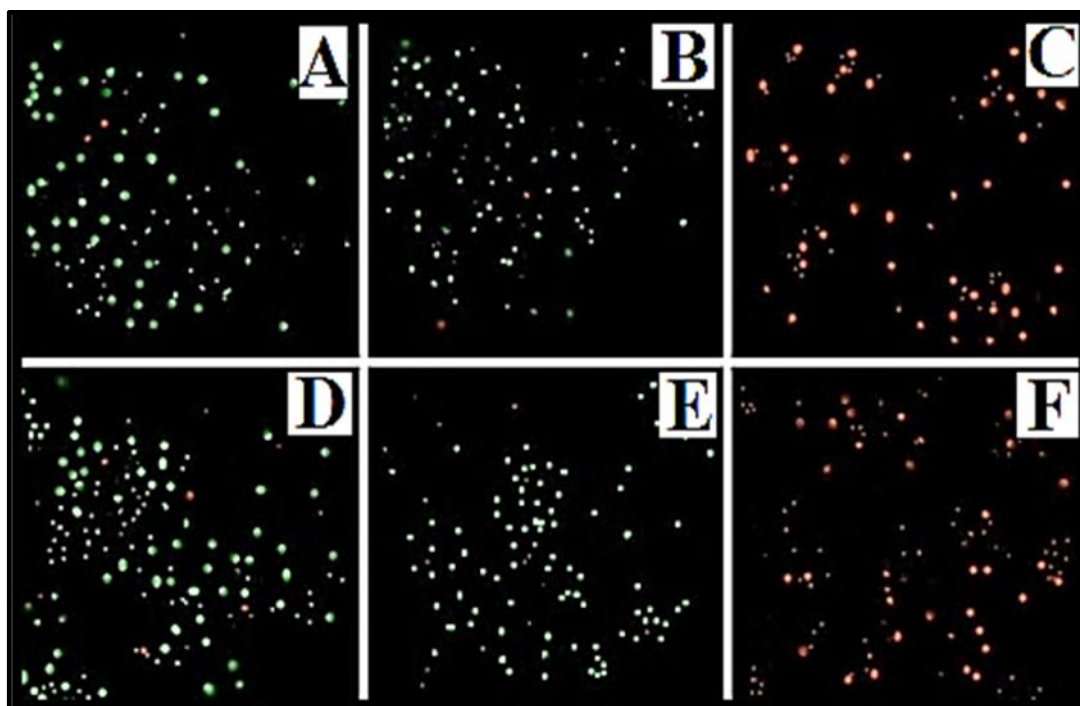


**Figure – 5.28: Fluorescence microscopic images of (A) CM treated *E. coli*, (B) GM<sub>Si</sub> treated *E. coli*, (C) GM<sub>Ag-Si</sub> treated *E. coli*, (D) CM treated *S. aureus*, (E) GM<sub>Si</sub> treated *S. aureus*, (F) GM<sub>Ag-Si</sub> treated *S. aureus* bacterial cells.**

*(Published in RSC Adv., 2015.)*



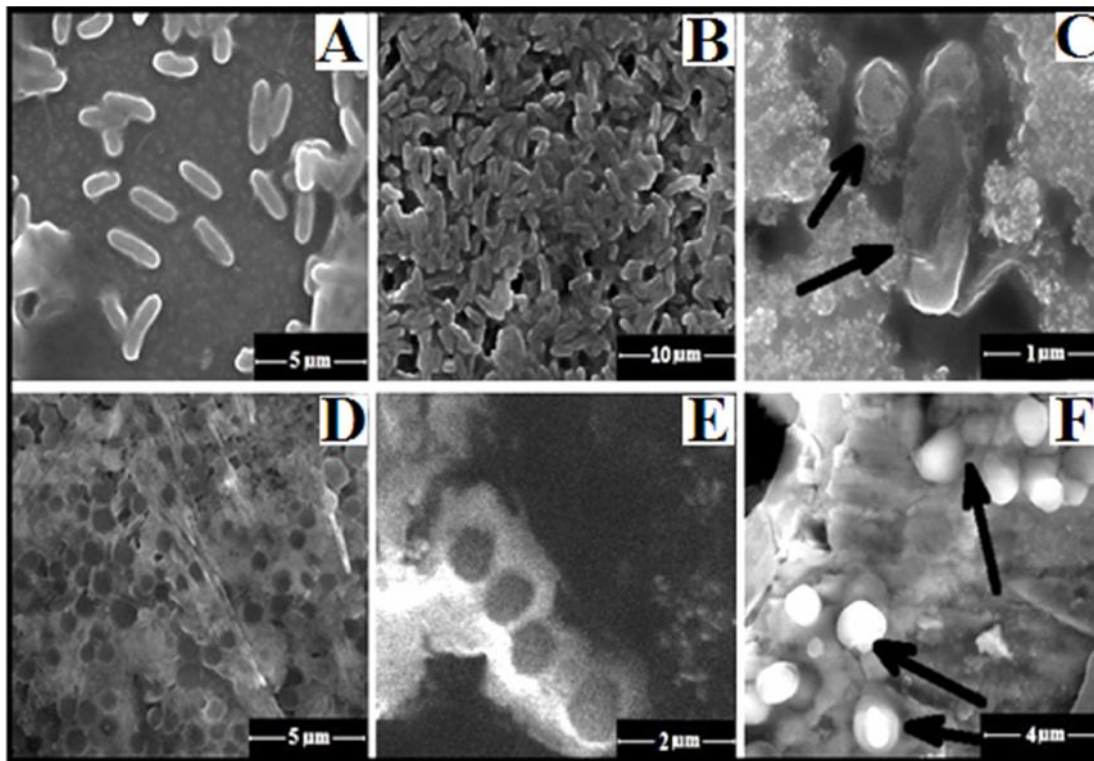


**Figure – 5.29: FESEM images of (A) CM treated *E. coli* (B) GM<sub>Si</sub> treated *E. coli* (C) GM<sub>Ag-Si</sub> treated *E. coli* (D) CM treated *S. aureus* (E) GM<sub>Si</sub> treated *S. aureus* (F) GM<sub>Ag-Si</sub> treated *S. aureus*.**

*(Published in RSC Adv., 2015.)*

The silver has the potential to kill bacteria in minimum time period. The different bacterial cell wall disruptions (Fig. 5.29) indicate that the antibacterial property has been developed in desired geopolymer mortar. Silver-silica nano composite having 6% by weight of fly ash in geopolymer mortar was sufficient to resist the bacterial growth. The growth for both types of bacteria (gram -ve / gram + ve) has been stopped within 6 – 8h only in presence of silver NPs modified GM<sub>Ag-Si</sub> geopolymer mortar. The bacterial growth population, in general, depends on numerous external factors like pH, temperature, concentration of nanoparticles [25, 26]. In various studies, it has been reported that due to the high alkali property of fresh concrete/mortar at early age, it will not allow any bacterial growth. However, the pH of concrete / mortar is slowly reduced over time by the effect of carbon dioxide and hydrogen sulphide gas and the growth of bacteria starts.

Silver silica nano composite modified geopolymer mortar shows better resistance to bacterial attack than nano silica modified geopolymer and control samples at pH less than

9.0. Silver nano particles incapacitate enzymes through binding of sulfhydryl (thiol) groups in amino acids of bacterial cell and promote the release of ions/NPs with subsequent hydroxyl radical formation [27, 28]. Gram-negative bacteria possess an outer membrane outside the peptidoglycan layer which is absent in Gram-positive organisms [29]. The outer membrane protects bacteria from harmful agents, such as detergents, drugs, toxins and degradative enzymes by functioning as selective permeability barrier. The cell wall disruption by the lower amount of silver NPs in geopolymer particle (~MIC) may be the main reason of bactericidal kinetics. Due to positive charge, silver NPs in the liquid growth medium are attracted electrostatically to the negatively charged cell wall of bacteria. A few oxidized silver ions/NPs also get attached electrostatically to the bacterial membrane and thus decreases the osmotic stability of the cell, trailed by consequent leakage of intracellular constituents. The anti-bacterial activity of  $GM_{Ag-Si}$  is developed by introducing silver NPs on the surface of silica NPs which is the main ingredients for anti-bacterial activity of geopolymer mortar. Therefore, such materials can be used in sewer concrete pipe line and other similar structures.

#### **5.4. PROCESS DEVELOPMENT FOR GEOPOLYMER MORTAR**

The nano silica addition in geopolymer mortar/concrete eliminates the heat activation to achieve an acceptable strength and durability (Refer section 5.1 and 5.2). Alternatively, a modified process (Process – I) has been also proposed to eliminate heat activation. In this proposed modified process, the heat activation has been made before casting of samples and the amount of heat energy required for polymerisation of fly ash and activator solutions is comparatively less. The main advantage of this process is that it can be mechanised for industrial purpose. The details of the process have been already presented in section 4.5 and Figure 4.3. The heat energy is applied to the mixture of fly ash and activator solution (NaOH + Na<sub>2</sub>SiO<sub>3</sub> + H<sub>2</sub>O) for better control of polymerisation. The details of the mix proportion and curing conditions are explained in table – 4.8. It is also noted that 8(M) NaOH solution used as an activator for the preparation of Process – I and Process – II geopolymer mortar.

In the preparation of Process – I geopolymer mortar (Refer. Fig 4.3), fly ash is mixed with appropriate quantity of activator fluid containing 8(M) NaOH solution, Na<sub>2</sub>SiO<sub>3</sub> solution and water. The mixture is then stirred in a hot air oven for 45 minutes at different temperatures of 40°C, 60°C and 80°C. River sand is immediately mixed with the hot mixture of activated fluid and fly ash thoroughly for two minutes before casting. Finally, the mortar specimens are removed from the mould after 10 – 12 hours of casting and are placed at ambient temperature (27 ± 20 °C) until testing.

In Process – II conventional geopolymer mortar (Refer. Fig 4.3), sand and fly ash are dry mixed for 2 minutes and the appropriate quantity of activator fluid is added and mixed thoroughly at ambient laboratory temperature. After one hour of casting, the mortar specimens along with the mould are cured at three different temperatures of 40°C, 60°C and 80°C within the hot air oven for 48 hours [30 – 32]. Then the mortar samples are kept in room temperature until testing. This process is a very common and have limitations for practical use.

The compressive strength of the process modified geopolymer mortar (Process – I) and conventional heat cured geopolymer mortar (Process – II) for a given fluid to fly ash ratio 0.35 and at the age of 3 days, 7 days and 28 days are presented in Figure 5.30. Similar test results are presented in Figure 5.31 and 5.32 for the fluid to fly ash ratio of 0.40 and 0.45 respectively. It is observed that for all the fluid to fly ash ratio, the geopolymer mortars under

Process – I show substantially higher compressive strength than similar mortar under Process – II at all ages up to 28 days. In Process – I, the maximum compressive strength at 28 days of geopolymer mortar is developed at fluid to fly ash ratio 0.35 and at activation temperature of 60°C for 45 minutes. The 28 days compressive strength of Process – I geopolymer mortar (at fluid to fly ash ratio 0.35 and activated at 60°C for 45 minutes) is about 16 % more than Process – II geopolymer mortar (at fluid to fly ash ratio 0.35 and activated at 60°C for 48 hours). Thus geopolymer mortar developed at 60°C for both Process – I and Process – II at 0.35 fluid to fly ash ratio has been considered for further study. It is also noted that the compressive strength of both Process – I and Process – II geopolymer mortar decreases with the increase of fluid to fly ash ratio as expected.

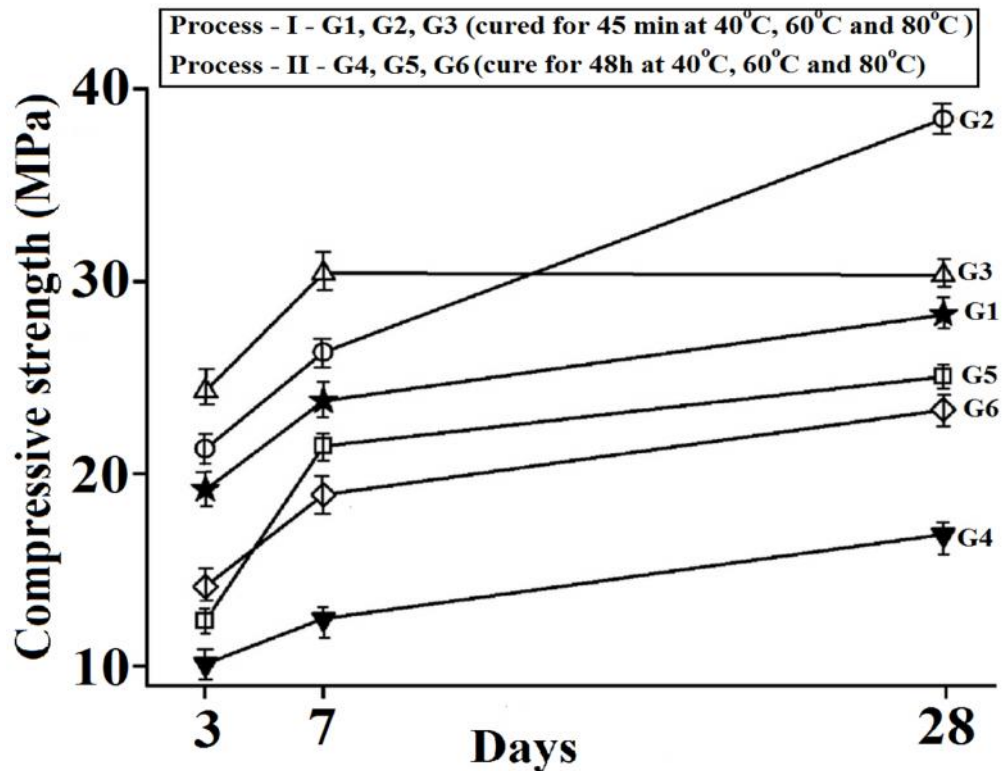


Figure – 5.30: Compressive strength of geopolymer mortar at fluid/ fly ash ratio 0.35 in Process – I and Process – II.

*(Published in Indian Concrete Journal, 2015.)*

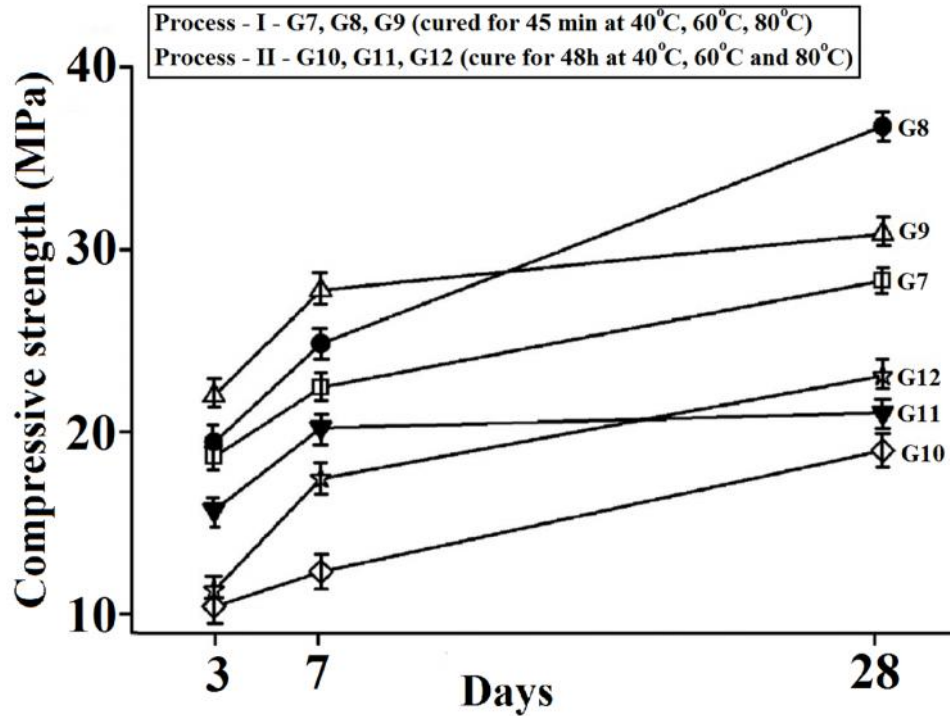


Figure – 5.31: Compressive strength of geopolymer mortar at fluid/ fly ash ratio 0.40 in Process – I and Process – II.

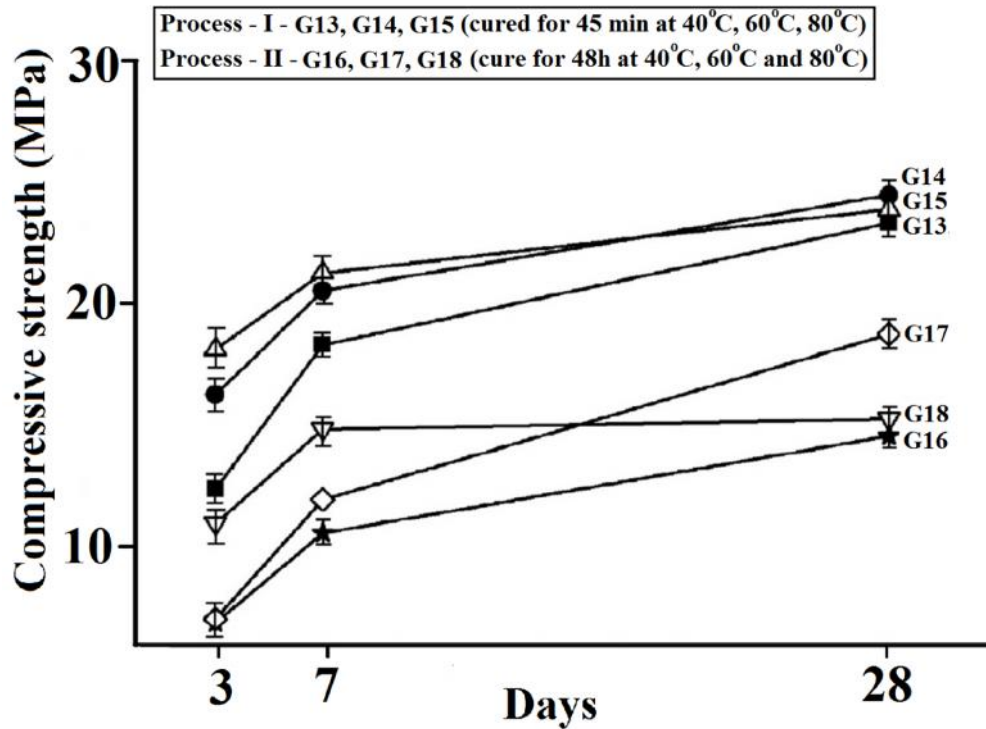


Figure – 5.32: Compressive strength of geopolymer mortar at fluid/ fly Ash ratio 0.45 in Process – I and Process – II.

The 28 days flexural strength of Process – I geopolymer mortar and Process –II geopolymer mortar specimens are shown in Figure 5.33, 5.34 and 5.35 for fluid to fly ash ratio 0.35, 0.40 and 0.45 respectively. It has been observed that the flexural strength of Process – I geopolymer mortar is more than that of Process – II geopolymer mortar. Also, the flexural strength of both Process – I and Process – II decreases with the increase of fluid to fly ash ratio.

Similarly the 28 days split tensile strength of Process – I geopolymer and Process – II geopolymer mortar specimens are shown in Figure 5.36, 5.37 and 5.38 for fluid to fly ash ratio of 0.35 0.40 and 0.45 respectively. It is observed that Process – I geopolymer mortar shows better split tensile strength than that of Process – II geopolymer mortar. It is also noted that Process – I geopolymer mortar cured at 60°C for 45 minutes shows maximum tensile strength than that of other type of geopolymer mortar at fluid to fly ash ratio 0.35.

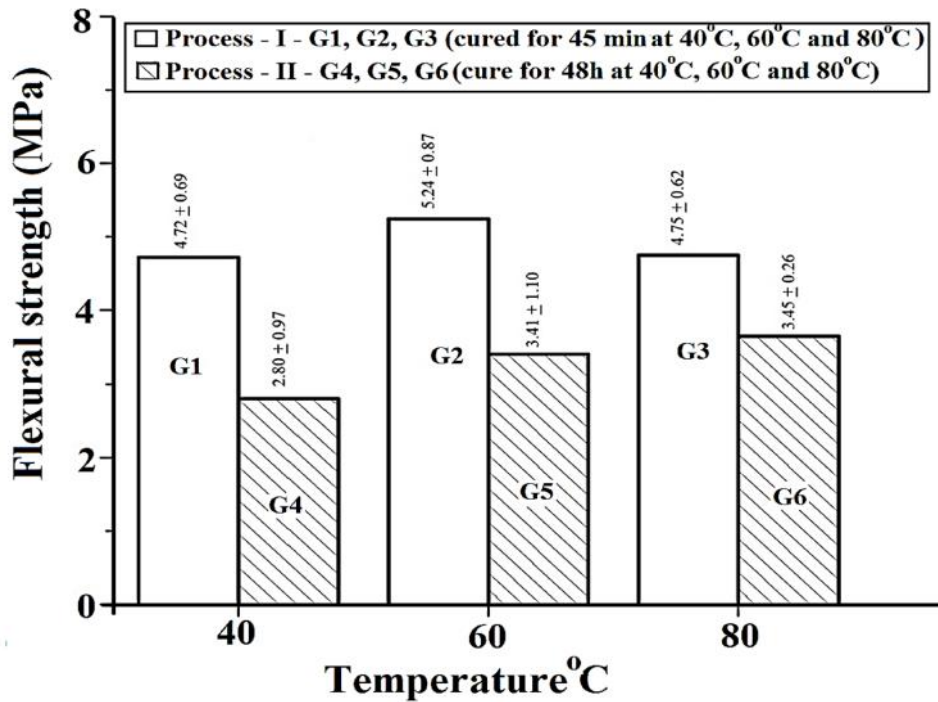


Figure – 5.33: Flexural strength of geopolymer mortar at fluid/ fly ash ratio 0.35 in Process – I and Process – II.

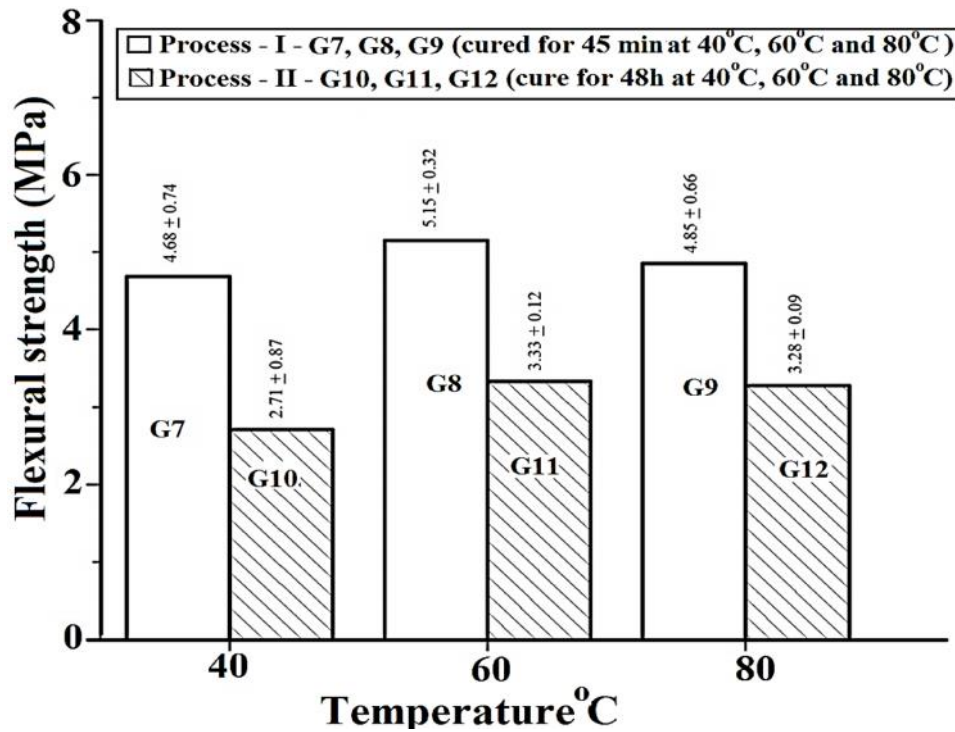


Figure – 5.34: Flexural strength of geopolymer mortar at fluid/ fly ash ratio 0.40 in Process – I and Process – II.

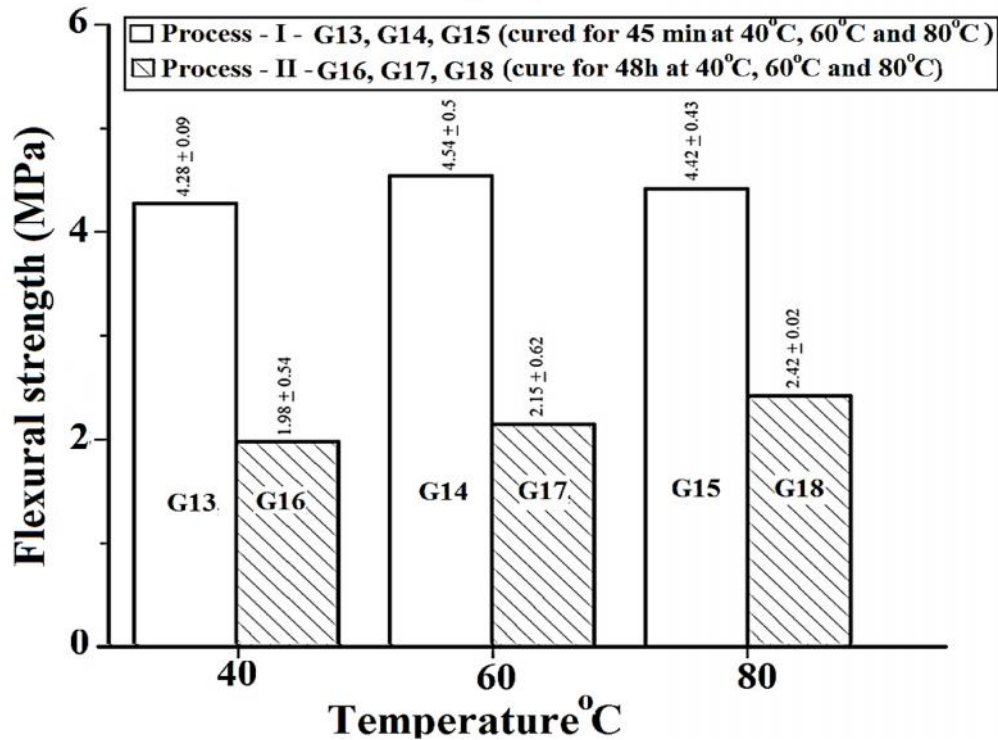


Figure – 5.35: Flexural strength of geopolymer mortar at fluid/ fly ash ratio 0.45 in Process – I and Process – II.

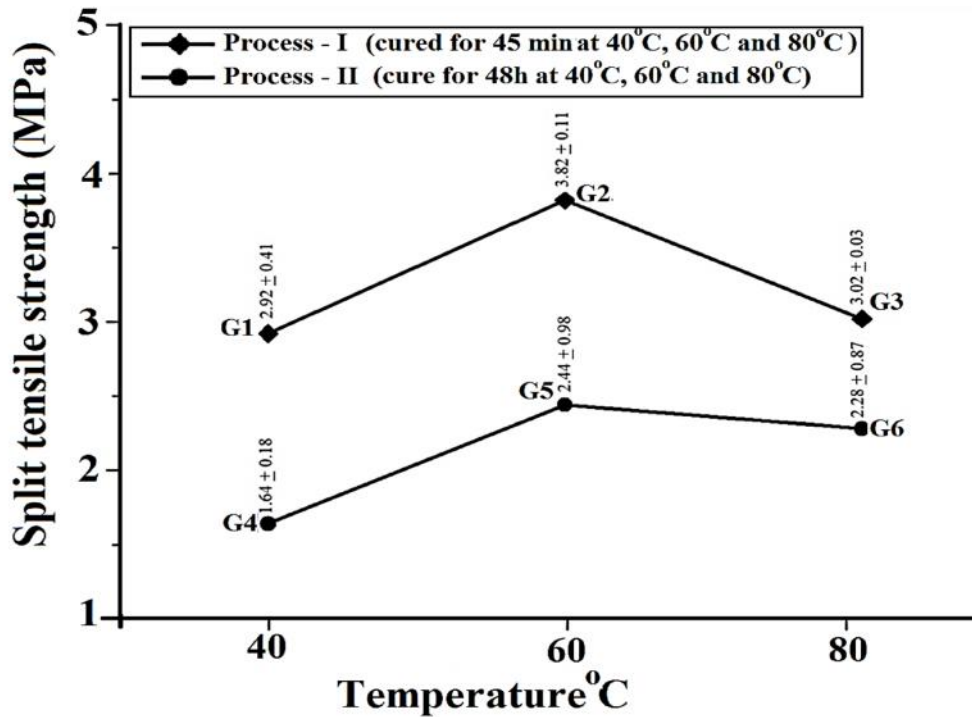


Figure – 5.36: Tensile strength of geopolymer mortar at fluid/ fly ash ratio 0.35 in Process – I and Process – II.

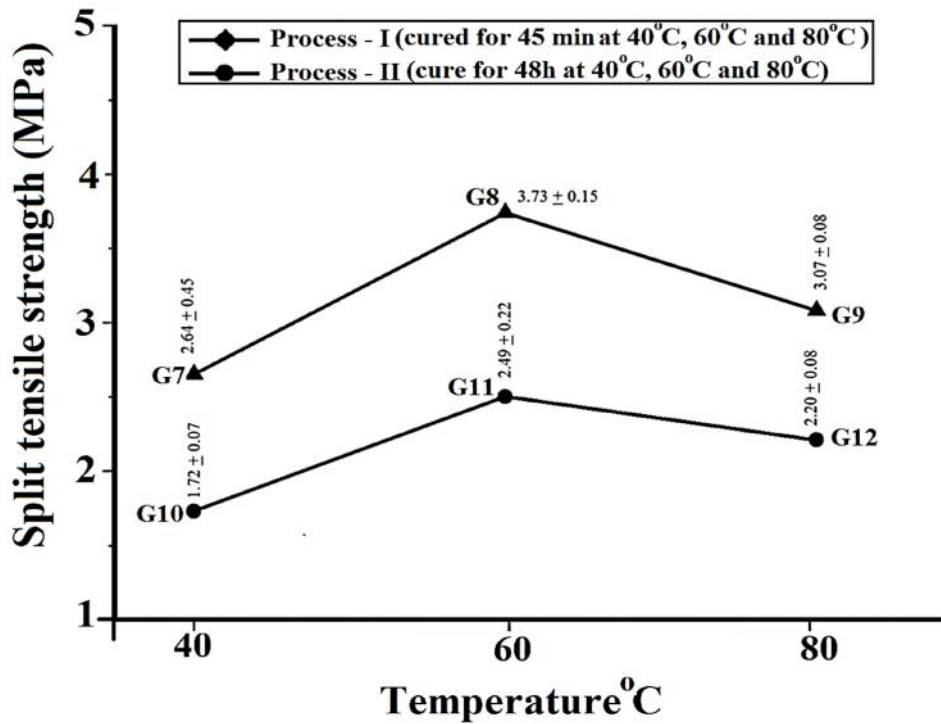


Figure – 5.37: Tensile strength of geopolymer mortar at fluid/ fly ash ratio 0.40 in Process – I and Process – II.



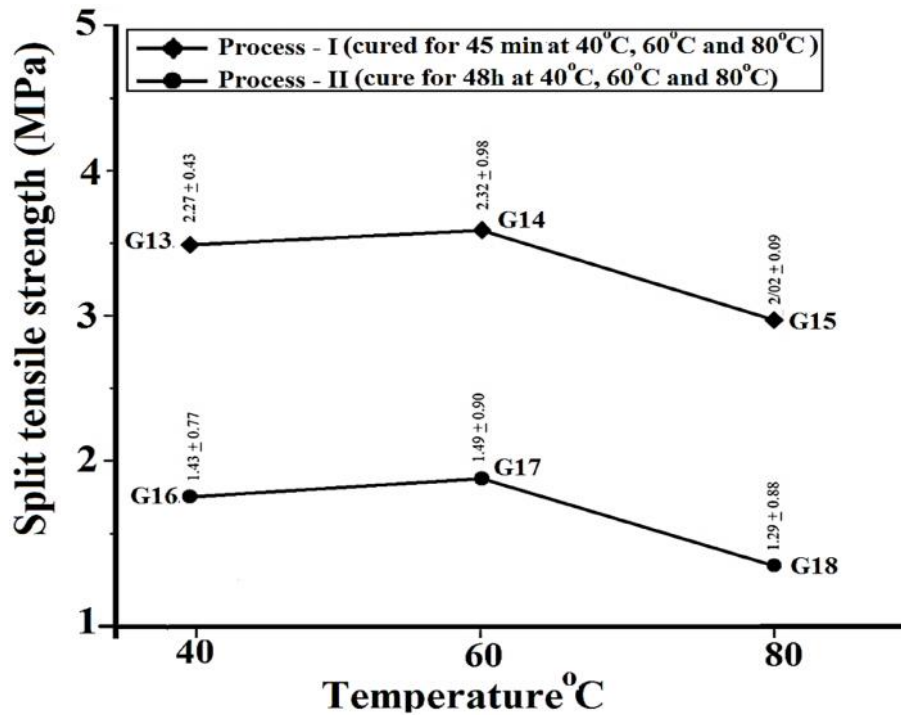


Figure – 5.38: Tensile strength of geopolymer mortar at fluid/ fly ash ratio 0.45 in Process – I and Process – II.

In general, the flexural and split tensile strength of geopolymer mortar increases with the increase of compressive strength. Both the flexural and split tensile strength of Process – I and Process– II geopolymer mortar reduces with the increase of fluid to fly ash ratio. Also, flexural and tensile strength of geopolymer mortar (Process – I & II) is optimum at fluid to fly ash ratio 0.35 and activation temperature of 60°C, due to higher rate of polymerisation at early ages.

The results of RCPT value for both Process – I and Process – II geopolymer mortar samples (28 days) are shown in Figure 5.39, 5.40 and 5.41 for three fluid to fly ash ratios of 0.35, 0.4 and 0.45 respectively. The amount of charge passed in RCPT for geopolymer mortar for both Process – I and Process – II is increased with the increase of fluid to fly ash ratio. The lesser amount of charge is passed in geopolymer mortar both for Process – I and Process – II at curing temperature of 60°C and fluid to fly ash ratio of 0.35. However, the amount of charge passing through Process – I geopolymer mortar is comparatively less than that of Process – II geopolymer mortar for other conditions remain same. This confirms that the diffusion coefficient will be less due to presence more amount of crystalline compound in Processes – I geopolymer mortar thereby improving the durability.

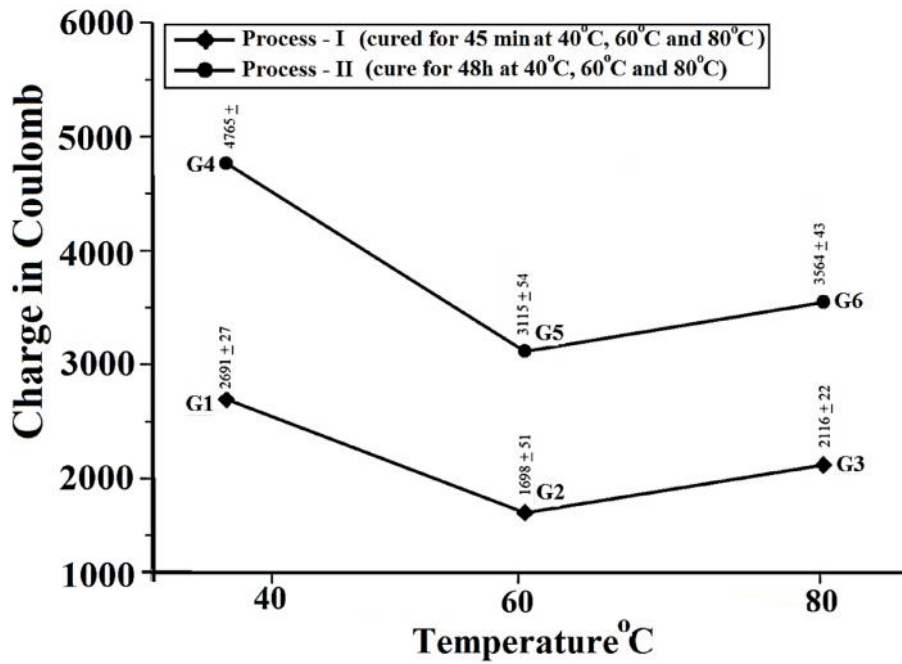


Figure – 5.39: Charge passed through geopolymer mortar at fluid/ fly ash ratio 0.35 in Process I and Process II.

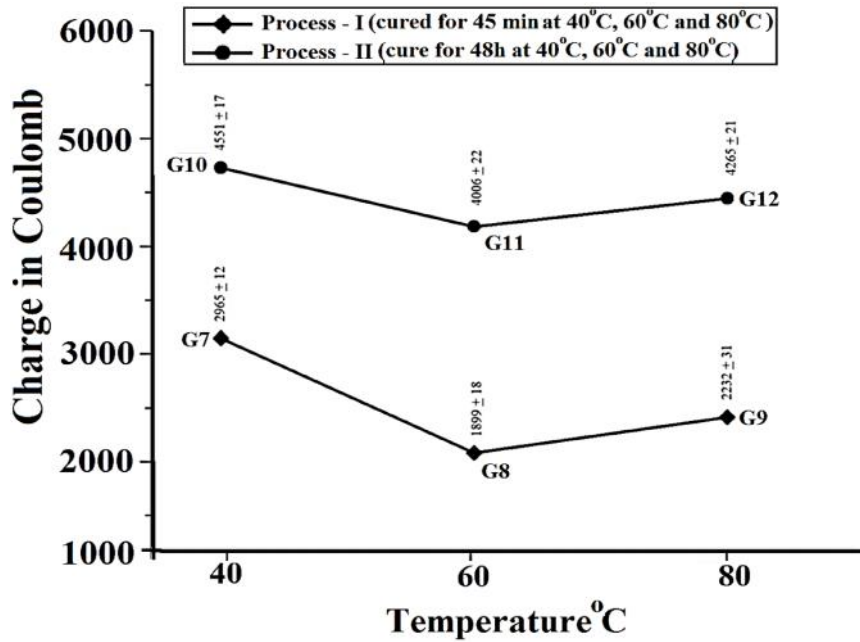


Figure – 5.40: Charge passed through geopolymer mortar at fluid/ fly ash ratio 0.40 in Process I and Process II.

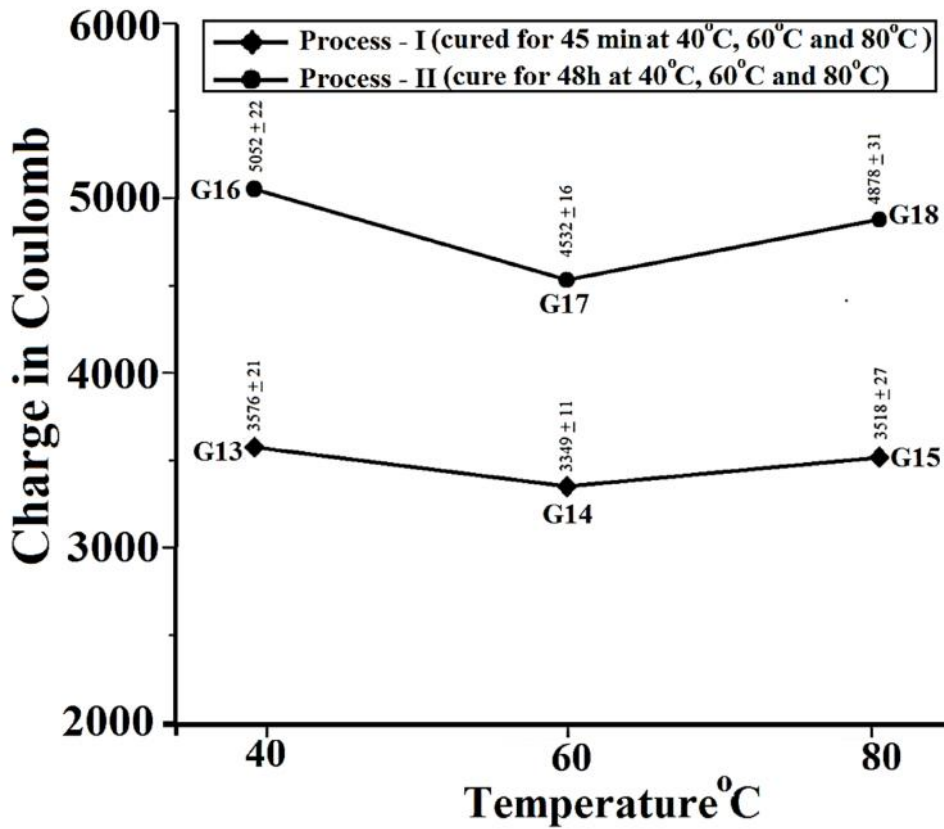


Figure – 5.41: Charge passed through geopolymer mortar at fluid/ fly ash ratio 0.45 in Process I and Process II.

Table – 5.6 shows the saturated water absorption of geopolymer cube specimens of the two process (Process – I & Process – II) after immersion in water for 30 minutes and 24 hours. Similarly sulphate test results of such geopolymer mortar are shown in table – 5.7 after immersion of specimen in sulphate solution for one month. The results indicate that the lesser water absorption and sulphate attack (in terms of weight gain) in Process – I geopolymer mortar compared to Process – II geopolymer mortar due to better pore structure modification.

**Table – 5.6: Water absorption test results of geopolymer mortar samples in Process I & II (fluid/ fly ash = 0.35):**

Mix No	Initial average mass (gm.)	Average mass after 30 min (gm.)	% increment	Average mass after 24 hours (gm.)	% increment	Remarks
<b>G1</b>	731.6	749.5	2.39	785.6	4.60	<b>Process – I</b>
<b>G2</b>	720.9	735.8	2.02	751.6	2.10	
<b>G3</b>	728.6	739.3	1.44	762.9	3.10	
<b>G4</b>	729.7	754.6	3.30	793.2	4.87	<b>Process – II</b>
<b>G5</b>	733.7	756.3	3.00	781.6	3.26	
<b>G6</b>	720.3	739.3	2.56	767.3	3.65	

**Table – 5.7: Sulphate test results of geopolymer mortar samples in process I & II (fluid/ fly ash = 0.35).**

Mix No	Initial average mass (gm.)	Average mass after Sulphate attack (gm.)	% increment	Remarks
<b>G1</b>	731.6	766.3	4.53	<b>Process – I</b>
<b>G2</b>	720.9	745.3	3.28	
<b>G3</b>	728.6	774.0	5.86	
<b>G4</b>	729.7	766.3	4.78	<b>Process – II</b>
<b>G5</b>	733.7	764.0	3.97	
<b>G6</b>	720.3	758.7	5.05	

The X-Ray Diffraction analysis of geopolymer mortars made in Process – I and Process – II are presented in Figure 5.42. Some specific extra peak positions are observed in Process – I geopolymer mortar of fluid to fly ash ratio of 0.35 and activation temperature of 60°C compared to similar Process – II geopolymer mortar. The large numbers of peaks in

geopolymer mortar in Process – I indicate the presence of more amount of semi crystalline and crystalline compounds. It is also observed that due to better polymerisation of Process – I geopolymer mortar, the formation of mullite, albite, calcite and quartz compounds are higher than that of Process – II geopolymer mortar.

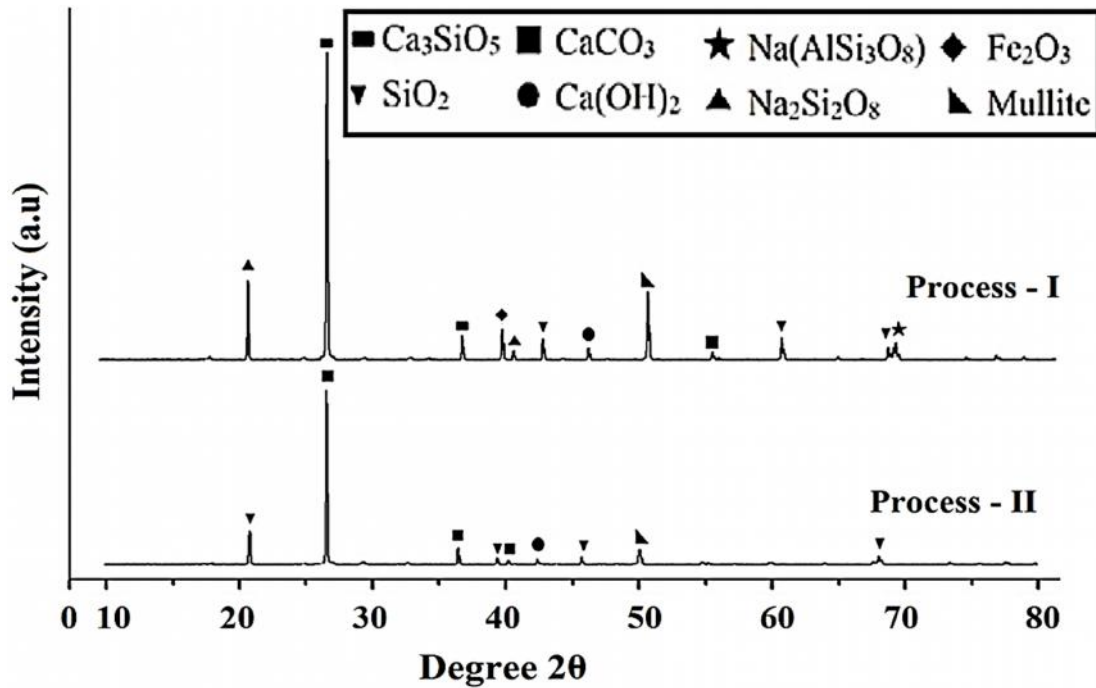


**Figure – 5.42: XRD analysis of Process – I and Process – II geopolymer mortar at fluid/fly ash ratio 0.35.**

It is also observed from FESEM images that in Process – I, the polymerisation of fly ash is more uniform within whole matrix than Process – II as shows in Figure 5.43. The presence silica compound in Process – I and Process – II was 98.87% and 81.12% respectively as summarized in elemental analysis (Fig. 5.44). The large numbers of unreacted fly ash is also observed in Process – II geopolymer mortar, which confirms that the geopolymer matrix is not fully polymerised (refer Fig. 5.43). It is noted that Si/Al ratio of Process – I geopolymer mortar is higher than Process – II geopolymer mortar.

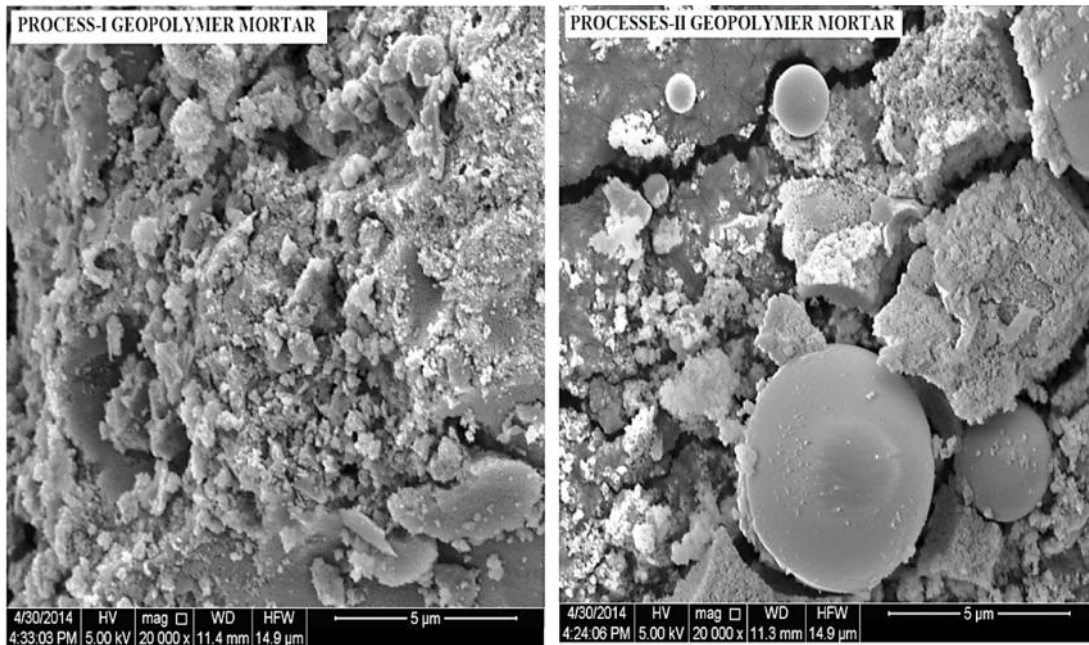


Figure – 5.43: FESEM image of Process – I and Process –II geopolymer mortar of fluid to fly ash ratio 0.35.

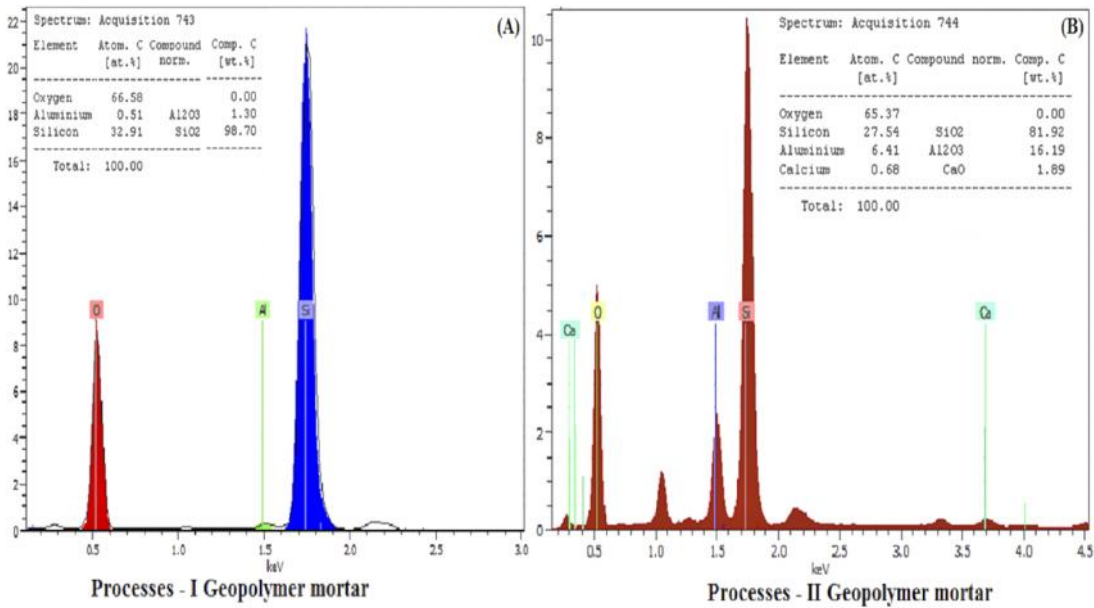


Figure – 5.44: EDS analysis of (A) Process – I and (B) Processes – II geopolymer mortar of fluid to fly ash ratio 0.35.

Based on the microstructure analysis, it is concluded that the improvement in compressive strength of Process – I geopolymer mortar compared to Process – II geopolymer mortar is due to the higher rate of polymerisation. In case of Process – I geopolymer mortar,

the fly ash is fully polymerised in presence of alkali activated solution at early age. Also XRD analysis confirms that the more amount of crystalline compound are observed in Process – I geopolymer mortar than Process – II geopolymer mortar. The FESM images also show that a large number unreacted fly ash are located in Process – II geopolymer mortar. The elemental analysis confirms the amount of crystalline compound in Process – I geopolymer mortar is higher than Process – II geopolymer mortar. The higher Si/Al ratio exhibits higher mechanical for Process – I geopolymer mortar than Process – II geopolymer mortar.

## 5.5. PROCESS DEVELOPMENT FOR GEOPOLYMER CONCRETE

Based on the performance of process modified geopolymer mortar, the study has been further extended for geopolymer concrete. The same process that used in geopolymer mortar has been followed in the process modified geopolymer concrete excepts 12mm coarse aggregate and sand has been added instead of sand only to determine the structural behavior such modified concrete. The study has been limited to processes modified geopolymer concrete of fluid to fly ash ratio 0.35 and of 8(M) NaOH activator solution only, as the performance of process modified geopolymer mortar (Process – I) with fluid to fly ash ratio 0.35 at 8(M) concentration of activator solution is quite remarkable. In this section Process – I geopolymer concrete is represented as GPC - I and Process – II (conventional heat cured) geopolymer concrete as GPC – II.

Figure 5.45 shows the compressive strength of GPC – I and GPC – II geopolymer concrete samples at 3, 7 and 28 days. The compressive strength of process modified GPC – I geopolymer concrete seems to be much higher than that of conventional heat cured GPC – II geopolymer concrete. It is noted that the compressive strength of GPC – I geopolymer concrete is about 15 % higher than GPC – II geopolymer concrete at all ages.

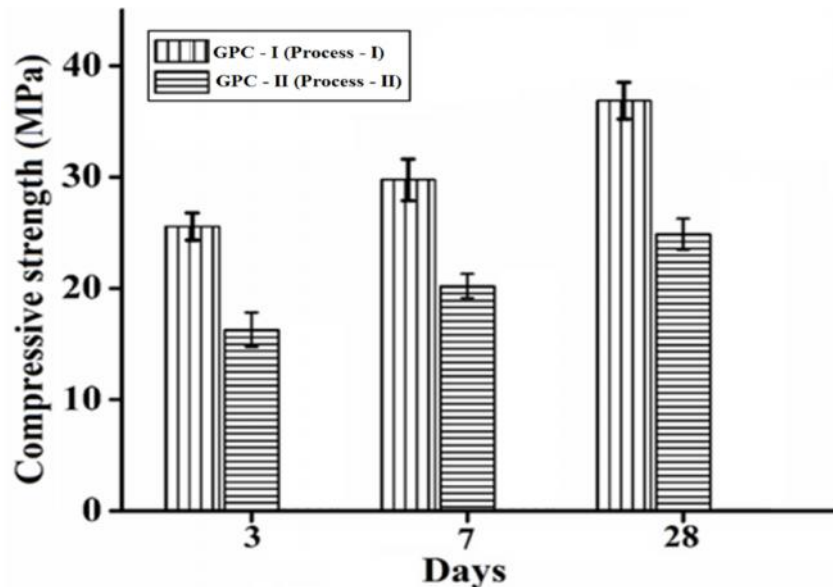
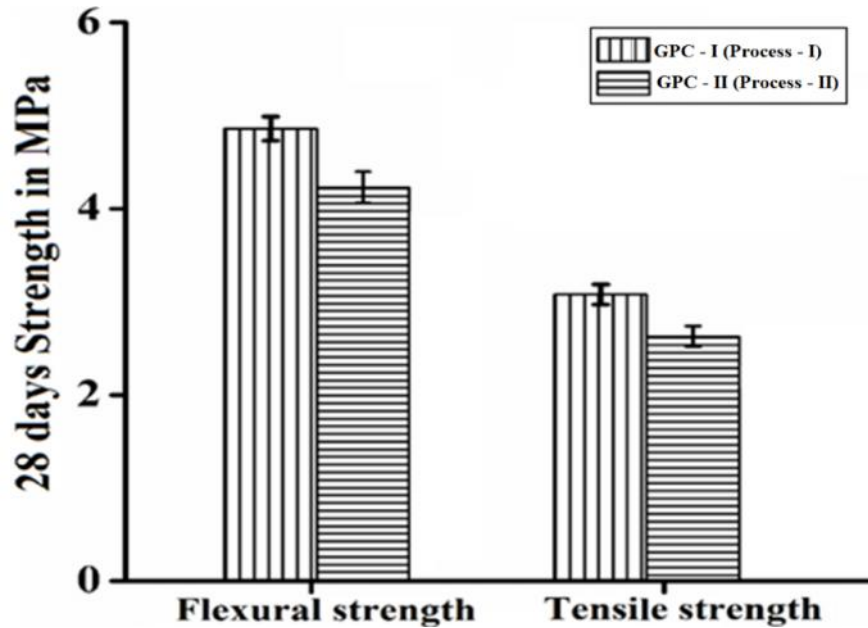


Figure – 5.45: Compressive strength of GPC – I and GPC – II geopolymer concrete at 3, 7 and 28days.



The flexural strength of Process – I geopolymer concrete (GPC – I) and Process – II geopolymer concrete (GPC – II) at 28 days are presented in Figure 5.46. It reveals that the processes modified geopolymer concrete GPC – I shows better flexural strength than conventional geopolymer concrete GPC – II. The similar result is observed for split tensile strength of GPC – I and GPC – II at the age of 28 days of curing (Refer Fig. 5.46).



**Figure – 5.46: Flexural and tensile strength of GPC – I and GPC – II geopolymer concrete at 28 days of curing.**

Therefore, the mechanical strength (compressive, flexural and tensile strength) of GPC – I is comparatively better than conventional GPC – II concrete at fluid to fly ash ratio 0.35. It reveals that the rate of polymerization in presence of alkali activator is much higher in case of GPC – I (Process – I) concrete at early age than GPC – II (Process – II) concrete. Due to higher rate of polymerization of alkali activator and fly ash before casting, the mechanical strength of GPC – I concrete shows better structural performance than GPC – II concrete.

Figure 5.47 demonstrates the bond stress vs. slip curves of 20mm diameter reinforcement bars (deformed; 0.2% of proof stress & mild steel; yield stress = 250 MPa) in both the geopolymer concrete (GPC – I and GPC – II) after 28 days of curing. The result shows that the Process – I (GPC – I) geopolymer concretes possesses better bond strength than conventional geopolymer concrete as per Process – II (GPC – II) for both deformed and mild steel bars. All the samples are failed by the pull-out load of the rebar. The slip for plain

bars seems to be more compared to deformed bar at equal pull-out load for both GPC – I and GPC – II geopolymer concrete.

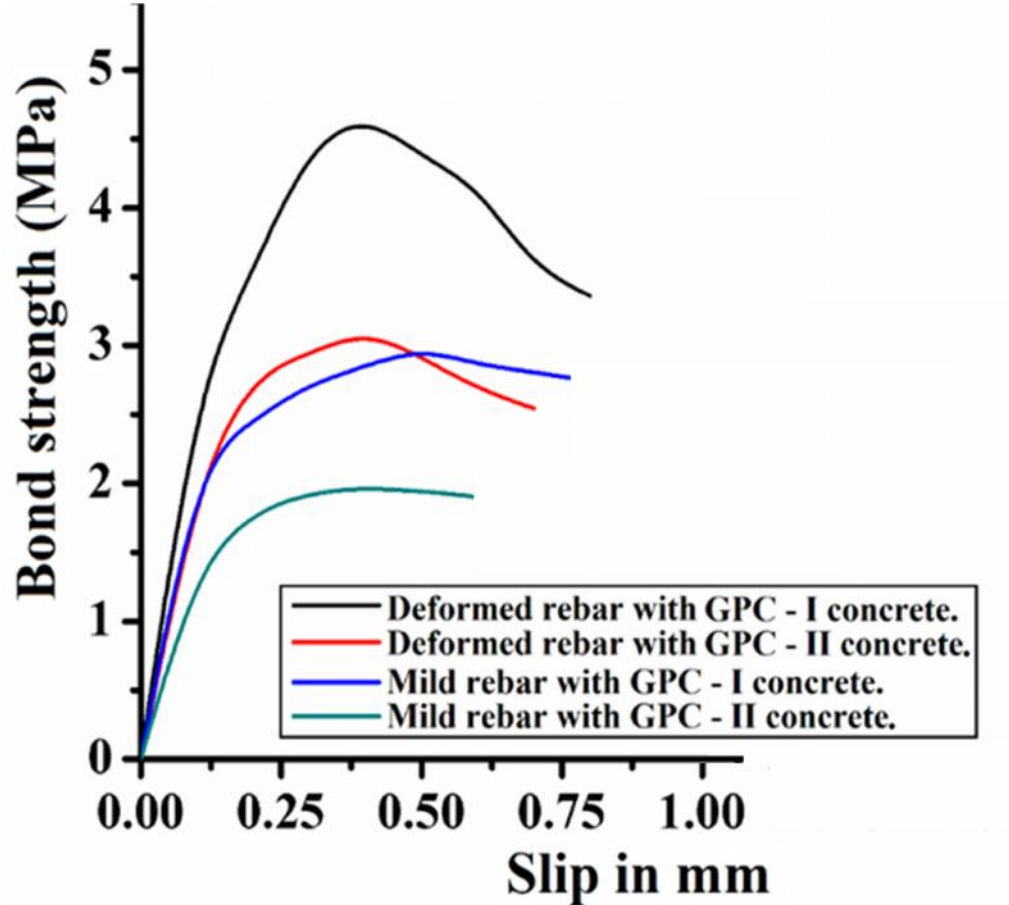


**Figure – 5.47: Bond stress vs. slip curve of GPC – I and GPC – II geopolymer concrete with deformed and mild rebar.**

The bond strength of GPC – I and GPC – II geopolymer concrete are increased with the increase of compressive strength as expected. As the compressive strength and split tensile of GPC – I geopolymer concrete is more than GPC – II geopolymer concrete, the better bond strength has been developed between GPC – I mix and reinforcement bar (deformed and mild steel rebar) compare to GPC – II mix. The higher rate polymerization in GPC – I geopolymer concrete produces a denser or stronger interfacial transition zone (ITZ) between aggregates and geopolymer matrices as compared to the conventional GPC – II geopolymer concrete. The modulus of elasticity of GPC – I geopolymer concrete is 30.0 GPa

at compressive strength of 36.85 MPa, whereas the for GPC – II geopolymer concrete is 26.65 GPa at compressive strength of 25 MPa.

The demoulding time of specimens after casting in Process – I geopolymer mortar/concrete is comparatively less (about 1/3 times) than that of Process – II geopolymer mortar/concrete. Also, in Process – I the mixture have been heated only for 45 minutes compared to that of Process – II where the specimens have been heated for 48 hours at 60°C. The calculated energy requirements for Process – I and Process – II are 1.5 kWh and 98 kWh respectively. Therefore, about 98 % less energy is required for Process – I than Process – II for heat activation only. Therefore, Process – I geopolymer mortar/concrete can be used in practical construction in terms of strength, Durability and energy savings.

After the mechanical strength assessment of process modified geopolymer concrete, the microstructural properties of GPC – I and GPC – II geopolymer concrete samples are analysed by using Field Emission Scanning Electron Microscopy with Energy-dispersive X-ray spectroscopy and X-Ray Diffraction analysis. The X-ray diffractograms of the GPC – I and GPC – II geopolymer concrete are represented in Figure 5.48. It is noted that the large number of amorphous and crystalline compounds are observed in GPC – I geopolymer concrete than that of GPC – II geopolymer concrete.

Figure 5.49 shows FESEM images of GPC – I concrete (Process – I) and GPC – II (Process – II) concrete respectively. It is observed from FESEM images that a large number of crystalline compound in rod shape are present in case of GPC – I concrete than GPC – II concrete. Also, the density of GPC – I matrix seems to be higher than GPC – II geopolymer matrix. The elemental analysis of GPC – I and GPC – II shows that Si/Al ratio of GPC – I concrete is much higher than GPC – II concrete as observed in Figure 5.50. Also, the EDS analysis confirms that the presence of Ca compound is very less, as our experimental programme is based on low calcium fly ash.

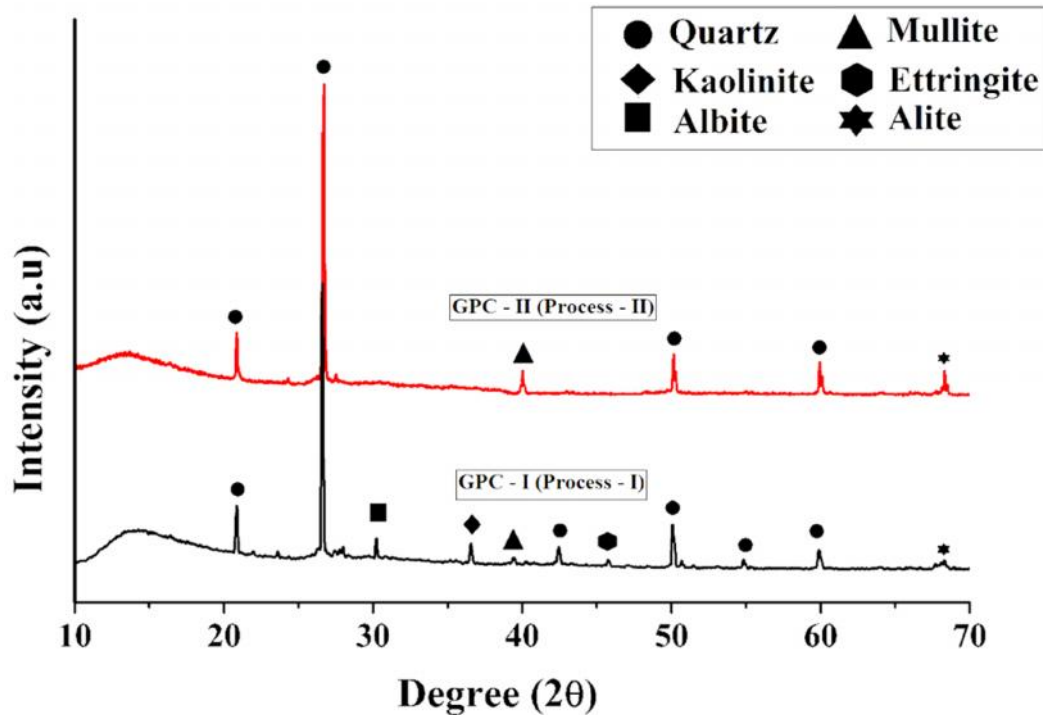


Figure – 5.48: XRD analysis of GPC – I and GPC – II concrete.

The microstructure analysis of GPC – I and GPC – II concrete reveals the main cause behind the strength enhancement of GPC – I geopolymer concrete (Process – I) than GPC – II geopolymer concrete (Process – II). In the XRD analysis, a broad hump has been registered between  $2\theta = 25^\circ - 30^\circ$  in both GPC – I and GPC - II, indicating the dissolution of the fly ash amorphous phase and the formation of a new amorphous phase in the matrix. Also, a more number of amorphous and crystalline phase are observed in GPC – I geopolymer concrete than GPC – II geopolymer concrete, due to higher rate of polymerisation processes. Similar result is observed in the FESEM analysis of GPC – I and GPC – II concrete. The large number of rod shaped crystalline compounds are observed in GPC – I concrete (Fig.5.49). The elemental analysis shows that Si/Al ratio of GPC – I is much higher than GPC – II concrete, which is the main reason behind the mechanical strength enhancement of GPC – I geopolymer concrete (Process – I) over GPC – II (Process – II) geopolymer concrete.

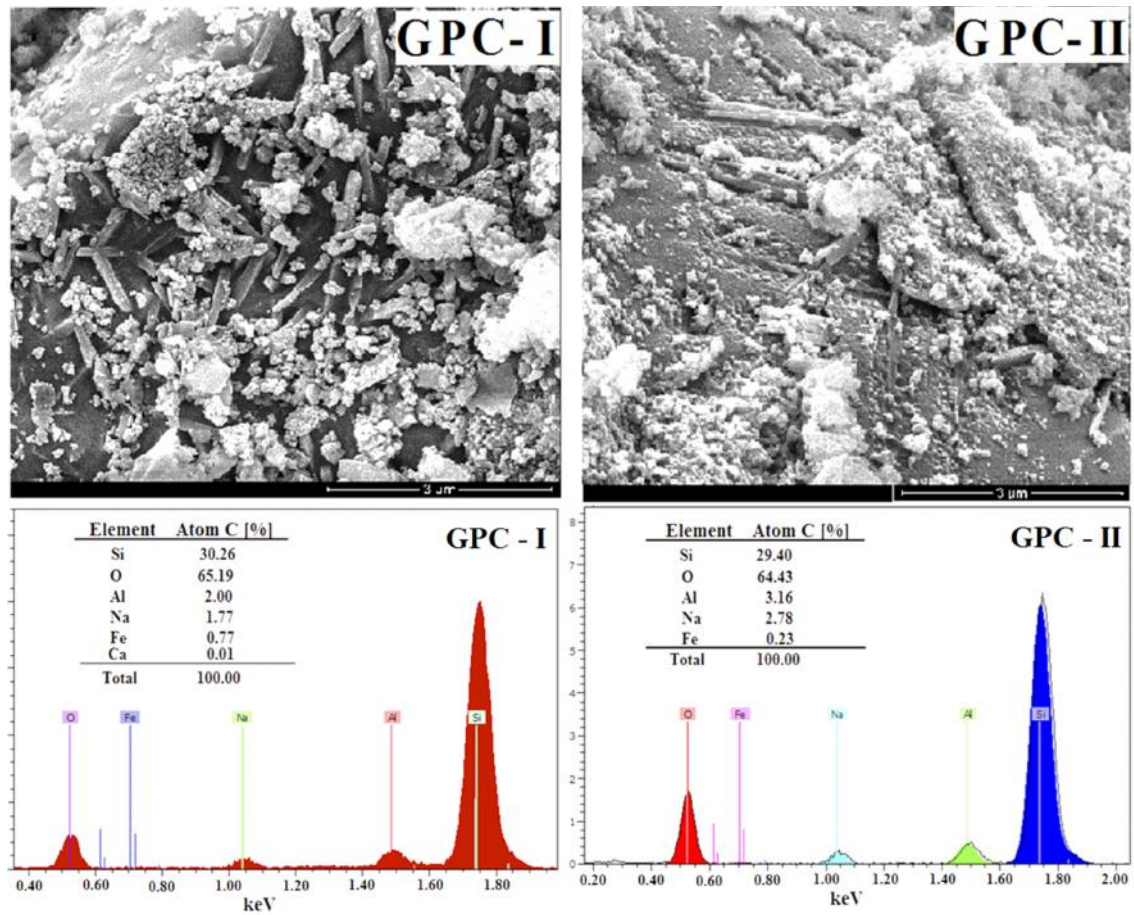


Figure – 5.49: FESEM images EDS analysis of GPC – I and GPC – II concrete.

## REFERENCES:

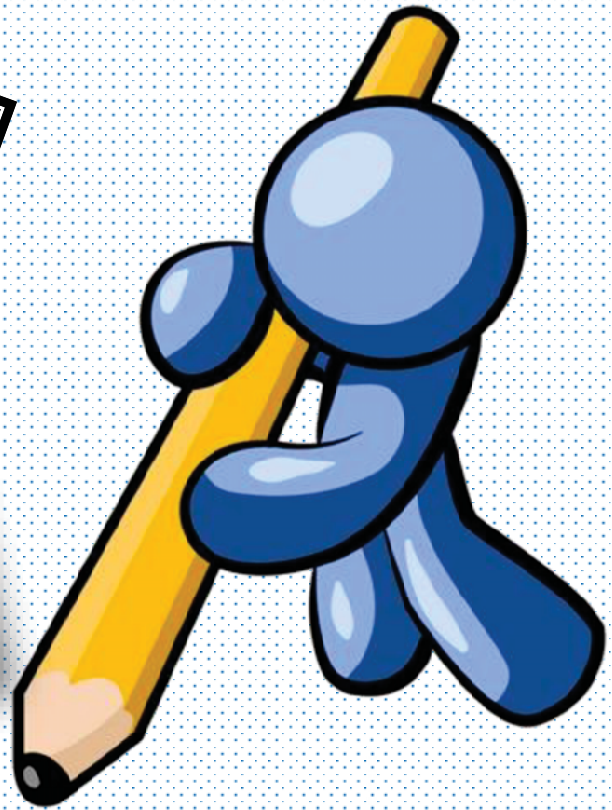
---

1. Bolhassani, Mohammad, and Mohammadreza Samani. "Effect of type, size, and dosage of nanosilica and microsilica on properties of cement paste and mortar." *ACI Materials Journal* 112.2 (2015).
2. Khaloo, A. R.; Vayghan, A. G.; and Bolhassani, M., "Mechanical and Microstructural Properties of Cement Paste Incorporating Nano Silica Particles with Various Specific Surface Areas," *Key Engineering Materials*, V. 478, 2011, pp. 19-24. doi: 10.4028/www.scientific.net/KEM.478.19
3. Kong, Deyu, et al. "Influence of nano-silica agglomeration on fresh properties of cement pastes." *Construction and Building Materials* 43 (2013): 557-562.
4. Senff, Luciano, et al. "Effect of nano-silica on rheology and fresh properties of cement pastes and mortars." *Construction and Building Materials* 23.7 (2009): 2487-2491.
5. García, N. M., et al. "Effect of fly ash and nanosilica on compressive strength of concrete at early age." *Advances in Applied Ceramics* 114.2 (2015): 99-106.
6. Riahi, Shadi, and Ali Nazari. "The effects of nanoparticles on early age compressive strength of ash-based geopolymers." *Ceramics International* 38.6 (2012): 4467-4476.
7. Khater, H. M., et al. "Effect of nano-clay on alkali activated water-cooled slag geopolymer." *British Journal of Applied Science & Technology* 3.4 (2013): 764.
8. Sofi, M., et al. "Engineering properties of inorganic polymer concretes (IPCs)." *Cement and Concrete Research* 37.2 (2007): 251-257.
9. D. Hardjito, B. V. Rangan, Development and properties of low calcium fly ash-based geopolymer concrete. Research report GC1. Faculty of Engineering, Curtin University of Technology, Western Australia, 2005.
10. Zain, Muhammad Fauzi Mohd, et al. "Prediction of splitting tensile strength of high-performance concrete." *Cement and Concrete Research* 32.8 (2002): 1251-1258.
11. Lee, W. K. W., and J. S. J. Van Deventer. "The interface between natural siliceous aggregates and geopolymers." *Cement and Concrete Research* 34.2 (2004): 195-206.
12. Barbosa, Valeria FF, Kenneth JD MacKenzie, and Clelio Thaumaturgo. "Synthesis and characterisation of materials based on inorganic polymers of alumina and silica: sodium polysialate polymers." *International Journal of Inorganic Materials* 2.4 (2000): 309-317.
13. IS 456 Plain Reinforced Concrete – Code of Practice; Bureau of Indian Standard, New Delhi, India, 2000.

14. Panias, Dimitrios, Ioanna P. Giannopoulou, and Theodora Perraki. "Effect of synthesis parameters on the mechanical properties of fly ash-based geopolymers." *Colloids and Surfaces A: Physicochemical and Engineering Aspects* 301.1 (2007): 246-254.
15. Salih, Moslih Amer, Abang Abdullah Abang Ali, and Nima Farzadnia. "Characterization of mechanical and microstructural properties of palm oil fuel ash geopolymer cement paste." *Construction and Building Materials* 65 (2014): 592-603.
16. Klabprasit, T., et al. "Influence of Si/Al ratio on compressive strength of rice husk-bark ashes and fly ash-based geopolymer paste." *The 3rd ACF International Conference-ACF/VCA*. 2008.
17. De Silva, Pre, K. Sagoe-Crenstil, and Vute Sirivivatnanon. "Kinetics of geopolymerization: role of Al<sub>2</sub>O<sub>3</sub> and SiO<sub>2</sub>." *Cement and Concrete Research* 37.4 (2007): 512-518.
18. Schabes-Retchkiman, P. S., et al. "Biosynthesis and characterization of Ti/Ni bimetallic nanoparticles." *Optical materials* 29.1 (2006): 95-99.
19. Gu, Hongwei, et al. "Presenting vancomycin on nanoparticles to enhance antimicrobial activities." *Nano letters* 3.9 (2003): 1261-1263.
20. Ahmad, Zahoor, et al. "Alginate nanoparticles as antituberculosis drug carriers: formulation development, pharmacokinetics and therapeutic potential." *Indian journal of chest diseases and allied sciences* 48.3 (2006): 171.
21. Gong, Ping, et al. "Preparation and antibacterial activity of Fe<sub>3</sub>O<sub>4</sub>@Ag nanoparticles." *Nanotechnology* 18.28 (2007): 285604.
22. Kim, Young Hwan, et al. "Synthesis and characterization of antibacterial Ag-SiO<sub>2</sub> nanocomposite." *The Journal of Physical Chemistry C* 111.9 (2007): 3629-3635.
23. Kobayashi, Yoshio, et al. "Silica coating of silver nanoparticles using a modified Stöber method." *Journal of colloid and interface science* 283.2 (2005): 392-396.
24. Kobayashi, Yoshio, Verónica Salgueiriño-Maceira, and Luis M. Liz-Marzán. "Deposition of silver nanoparticles on silica spheres by pretreatment steps in electroless plating." *Chemistry of Materials* 13.5 (2001): 1630-1633.
25. Kim, Jun Sung, et al. "Antimicrobial effects of silver nanoparticles." *Nanomedicine: Nanotechnology, Biology and Medicine* 3.1 (2007): 95-101.
26. Rispoli, Fred, et al. "Understanding the toxicity of aggregated zero valent copper nanoparticles against *Escherichia coli*." *Journal of hazardous materials* 180.1 (2010): 212-216.

27. Yeaman, Michael R., and Nannette Y. Yount. "Mechanisms of antimicrobial peptide action and resistance." *Pharmacological reviews* 55.1 (2003): 27-55.
28. Amro, Nabil A., et al. "High-resolution atomic force microscopy studies of the *Escherichia coli* outer membrane: structural basis for permeability." *Langmuir* 16.6 (2000): 2789-2796.
29. Nikaido, Hiroshi. "Molecular basis of bacterial outer membrane permeability revisited." *Microbiology and molecular biology reviews* 67.4 (2003): 593-656.
30. Vijai, K., R. Kumutha, and B. G. Vishnuram. "Effect of types of curing on strength of geopolymer concrete." *International Journal of Physical Sciences* 5.9 (2010): 1419-1423.
31. Guo, Xiaolu, Huisheng Shi, and Warren A. Dick. "Compressive strength and microstructural characteristics of class C fly ash geopolymer." *Cement and Concrete Composites* 32.2 (2010): 142-147.
32. Hussin, M. W., et al. "Performance of blended ash geopolymer concrete at elevated temperatures." *Materials and Structures* 48.3 (2015): 709-720.





Con**clu**sion



&

Future Scope





## CONCLUSION:

---

*Based on the experimental work reported in this study, the following conclusions are drawn:*

➤ *The colloidal nano silica addition can be used effectively in the fly ash based geopolymer mortar to achieve appreciable strength and durability cured at ambient temperature in air (without any heat activation) compared to conventional heat cured fly ash based geopolymer mortar. About 6% nano silica addition (replacement of fly ash) shows optimum for the present material type and mixture proportion.*

➤ *The compressive strength, flexural strength and split tensile strength of the developed nano silica modified geopolymer mortar under ambient temperature curing found to be 12%, 11% and 10% more than that of corresponding heat cured geopolymer mortar at 28 days respectively (Refer Fig. 5.1 – 5.7).*

➤ *The water absorption and the amount of charge passed in RCPT are also less in the nano silica modified fly ash based geopolymer mortar (under ambient temperature curing) compared to that of corresponding heat activated geopolymer mortar (Refer Fig. 5.8 & 5.9). Such improvements in the strength and durability of nano silica modified geopolymer mortar are mainly due to the transformation of amorphous to crystalline compound.*

➤ *The fly ash based geopolymer concrete with the addition of 6% of nano silica also shows better mechanical strength and durability cured at ambient temperature in air than the corresponding heat cured conventional fly ash based geopolymer concrete (Fig. 5.12 & Table - 5.1).*

➤ *This nano silica modified geopolymer concrete also possesses better bond strength than the control cement concrete and the corresponding conventional geopolymer concrete (without nano silica) of equivalent compressive strength against both HYSD (0.2% proof stress = 500 MPa) bar and mild steel (yield stress = 250 MPa) bar (Refer Fig. 5.14). This is mainly due to the presence of soluble silicates from nano silica in*

---

---

such geopolymer concrete that produces a denser or stronger interfacial transition zone (ITZ) between reinforcement bar and nano silica modified geopolymer matrices.

➤ In reinforced beam made with nano silica based geopolymer concrete under ambient temperature curing in air, the flexural strength seems to be comparatively higher than that of heat activated geopolymer concrete (without nano-silica) and conventional cement concrete (Fig. 5.15 – 5.19). The higher mechanical strength and improved bond behaviour of such nano silica modified geopolymer concrete with rebar seem to improve the flexural strength of nano silica modified geopolymer concrete.

➤ Based on the microstructural analysis of nano silica modified geopolymer mortar/concrete, it can be concluded that the nano silica increases the dissolution rate of Si and Si-Al phases, which strongly affect the rate of polymerization (Refer Fig. 5.21 & 5.23). The presence of nano-silica in geopolymer mixture seems to be the key factor to enhance the polymerisation process for its amorphous property and the high specific area which increase the Si / Al ratio and enhances the crystalline phases in geopolymer matrices at ambient temperature.

➤ Low calcium fly ash based silver-silica modified geopolymer mortar cured at room temperature shows almost similar strength and durability but better anti-bacterial property than nano silica modified geopolymer mortar. Due to positive charge, silver nano particles in the liquid growth medium are attracted electrostatically to the negatively charged cell wall of bacteria (Refer Fig. 5.29, 5.30 & 5.31). A few oxidized silver ions/Nano Particles also get attached electrostatically to the bacterial membrane and thus decreases the osmotic stability of the cell, trailed by consequent leakage of intracellular constituents. The anti-bacterial activity of silver-silica modified geopolymer mortar has been developed by introducing silver nano particles on the surface of silica nano particles which is the main ingredients for anti-bacterial activity of geopolymer mortar.

➤ The amount of heat activation required in conventional geopolymer mortar/concrete (termed as Process – II) can also be reduced substantially modifying the preparation process termed as Process – I. This Process – I method also help to make easily feasible practical construction. In Process – I, the geopolymer mortar (cured for only 45 minutes at 60°C) shows better mechanical strength (compressive, flexural and split tensile

---

---

strength) than the conventional heat cured geopolymer mortar, Process – II cured for 48 hours at 60°C (Refer Fig. 5.32 – 5.40). Further, the Process – I geopolymer mortar shows better durability performance in terms of RCPT, water absorption, sulphate test compared to Process – II geopolymer mortar (Refer Fig. 5.41, Table – 5.4 & 5.5). In this study nano silica has not been used.

➤ This improvement in strength and durability of process modified geopolymer mortar/concrete (Process – I) is mainly due to the uniform polymerisation of fly ash and formation of crystalline compound as per FESEM micrographs. The presence of more amount of silica compound in the Process – I geopolymer mortar/concrete matrix as per EDS analysis also confirms such improvements. The elemental analysis shows that the Si / Al ratio of Process – I geopolymer mortar/concrete is higher than conventional Process – II geopolymer mortar/concrete that causes in such improvement in properties (Refer Fig. 5.45, 5.46 & 5.51).

➤ The XRD analysis results confirm the formation of new phase crystalline compound in the form of  $\text{SiO}_2$ ,  $\text{Ca}_3\text{SiO}_5$ ,  $\text{Na}(\text{AlSi}_3\text{O}_8)$ ,  $\text{Na}_2\text{Si}_2\text{O}_7$ ,  $\text{CaCO}_3$ ,  $\text{Fe}_2\text{O}_3$  and mullite in geopolymer mortar/concrete. A broad hump registered between  $2\theta = 25^\circ - 30^\circ$  in both Process – I and Process – II geopolymer mortar/concrete, indicating the dissolution of the fly ash amorphous phase and the formation of a new semi amorphous and crystalline phase in the matrix (Refer Fig. 5.44 & 5.50). Also more number of amorphous and crystalline phase has been observed in Process – I geopolymer mortar/concrete than Process – II geopolymer mortar/concrete, due to higher rate of polymerisation processes.

➤ The demoulding time of specimens after casting in Process – I geopolymer mortar/concrete is comparatively less (about 1/3 times) than that of Process – II geopolymer mortar/concrete. Also, in Process – I the mixture have been heated only for 45 minutes compared to that of Process – II where the specimens have been heated for 48 hours at 60°C. The calculated energy requirements for Process – I and Process – II are 1.5 kWh and 98 kWh respectively. Therefore, about 98 % less energy is required for Process – I than Process – II for heat activation only. Therefore, Process – I geopolymer mortar/concrete can be used in practical construction in terms of strength, Durability and energy savings.

➤ *The compressive strength of Process – I geopolymer concrete is about 15 % higher than that of similar Process – II geopolymer concrete at all ages. The flexural strength of Process – I geopolymer concrete at 28 days is higher than and Process – II geopolymer concrete by about 35%. The similar results have been observed for split tensile strength of Process – I and Process – II geopolymer concrete after 28 days of curing.*

➤ *The bond strength of Process – I concrete is higher than Process – II concrete after 28 days curing for both mild steel and deformed reinforcement bar.*

➤ *The rate of polymerization in presence of alkali activator has been much higher in case of Process – I concrete at early age than Process – II concrete. Due to higher rate of polymerization of alkali activator and fly ash before casting at early age the mechanical strength of Process – I concrete has been showed better structural performance than Process – II geopolymer concrete.*

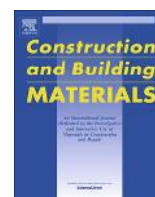
## ⊖ **FUTURE SCOPE OF THE STUDY:**

The following research areas may be suggested for future scope of study.

- ❖ Thermal expansion and shrinkage behavior (coefficient of thermal expansion) of nano silica modified geopolymer concrete and process modified geopolymer may be an important area of research.
- ❖ The long term properties of nano silica modified geopolymer concrete and process modified geopolymer concrete (Process – I) may be studied in detail.
- ❖ Detailed stress strain behaviour of modified geopolymer concrete may be an important area of study
- ❖ The study on the thermal behaviour of such geopolymer concrete (nano silica modified and process modified) at elevated temperature may be an interesting area of research.
- ❖ Similar studies can be executed on slag based geopolymer concrete instead of fly ash. Even a combination of fly ash and slag in the modified process may be an area of research.







# Effect of nano-silica on strength and durability of fly ash based geopolymer mortar



D. Adak<sup>a</sup>, M. Sarkar<sup>b</sup>, S. Mandal<sup>a,\*</sup>

<sup>a</sup> Department of Civil Engineering, Jadavpur University, Kolkata 700032, India

<sup>b</sup> Department of Physics, Jadavpur University, Kolkata 700032, India

## HIGHLIGHTS

- Addition of nano SiO<sub>2</sub> in geopolymer mortar improves strength and durability.
- Optimum strength at ambient temperature due to addition of 6% of nano SiO<sub>2</sub>.
- Water absorption and RCPT shows appreciable improvement with addition of nano SiO<sub>2</sub>.
- Presence of crystalline compound is more in nano SiO<sub>2</sub> modified geopolymer mortar.

## ARTICLE INFO

### Article history:

Received 25 March 2014

Received in revised form 7 July 2014

Accepted 23 July 2014

### Keywords:

Nano silica

Ambient temperature curing

Mechanical strength

Rapid Chloride Ion Penetration Test (RCPT)

Field Emission Scanning Electron

Microscope (FESEM)

X-ray Diffraction test (XRD)

## ABSTRACT

In general, the fly ash based geopolymer concrete/mortar needs heat activation for early strength developments depending on the molar concentration of activator. To overcome the above shortcomings, an experimental program has been taken up on low calcium fly ash geopolymer mortar having three molar concentrations (8 M, 10 M and 12 M) of activator liquids along with different percentage of nano silica addition (0%, 4%, 6%, 8% and 10% of fly ash). Geopolymer mortar with the addition of 6% nano silica shows appreciable improvement in compressive, flexural and tensile strength at 28 days under ambient temperature curing. The water absorption and charge passed in RCPT are also seemed to be comparatively less for 6% addition of nano silica modified geopolymer mortar. Such improvement of nano silica modified geopolymer mortar is due to transformation of amorphous compound to crystalline compound as noted in the XRD and FESEM analysis.

© 2014 Elsevier Ltd. All rights reserved.

## 1. Introduction

Worldwide production of coal combustion products in the form of fly ash was approximately 780 Mt tones in the year of 2011–2012. Although effective utilisation of fly ash was limited to 415 Mt or 53% of total production and widely varies within countries [1]. The power requirements throughout the world are rapidly increasing with the growth of the industrial sectors particularly in India and China. Recently, the application of alkali activated geopolymer concrete using fly ash (without cement) becomes an important area of research [2–6].

Most of the research works on fly ash based geopolymer are on the mix proportion and strength variation of geopolymer concrete cured at different temperature range of 45–80 °C for about 2–3 h [7–13]. It is noted that the strength of such geopolymer mortar is

more at 60 °C compared to 80 °C for a given molar concentration [14,15]. It also provides poor strength at ambient temperature of about 27 ± 2 °C curing due to slow polymerisation process. There are limited literatures on available on geopolymer to eliminate the shortcomings of ambient temperature curing [16–18]. However, incorporating nano silica in conventional cement concrete or high volume fly ash concrete had showed better results in terms of strength and durability [19–23]. Use of nano silica and nano aluminium oxide in geopolymer paste for high calcium based fly ash is also reported for a particular molar concentration [24]. The early strength is also achieved in geopolymer mortar (fly ash + rice husk ash) having different percentage of nano silica and nano aluminium oxide with heat activation for 2, 4 and 8 h at different temperatures [25]. The improvement of strength for addition of nano silica on slag based geopolymer is also reported at 38 °C [26].

This paper investigates the effect of different percentage of nano silica addition in low calcium based fly ash geopolymer mortar of different molar concentrations and cured at the ambient

\* Corresponding author. Tel.: +91 9432236510.

E-mail address: [mailtosarojmandal@rediffmail.com](mailto:mailtosarojmandal@rediffmail.com) (S. Mandal).

**Table 1**  
Chemical analysis report of fly ash.

Material	Chemical composition (in percentage)									
Fly Ash	SiO <sub>2</sub>	Al <sub>2</sub> O <sub>3</sub>	Fe <sub>2</sub> O <sub>3</sub>	CaO	MgO	Na <sub>2</sub> O	K <sub>2</sub> O	SO <sub>4</sub>	LOI	
	64.97	26.64	5.69	0.33	0.85	0.49	0.25	0.33	0.45	

temperature. The mechanical strength of such geopolymer mortar was analyzed by compressive strength, flexural strength and splitting tensile strength. Also, durability property based on rapid chloride ion permeability test and water absorption test was incorporated. The micro structural property of nano silica modified geopolymer mortar was assessed via Field Emission Scanning Electron Microscope (FESEM) and X-ray Diffraction test (XRD).

**Table 2**  
Physical analysis report of fly ash.

Material	Particle size distribution						
Fly ash	>500 $\mu$	300–500 $\mu$	150–300 $\mu$	150–90 $\mu$	90–45 $\mu$	<45 $\mu$	Specific gravity
	NIL	0.05	6.02	33.32	53.40	6.21	2.05

**Table 3**  
Basic properties of colloidal nano silica.

Colloidal nano silica type	Average particle size (nm)	Solid content (wt%)	Viscosity (Pa S)	pH	Solid density (g/cm <sup>3</sup> )
CemSynXLP	4–16 nm	30%	8.5	9.0–9.6	2.37

**Table 4**  
Mix proportion varying molar concentration, percentage of nano silica and curing condition.

Sample mark	Fly ash: sand	Molar concentration	% of Nano silica w.r.t fly ash	Curing conditions
Control	1:3	–	0.0	Water curing
8M0	1:3	8 (M)	0.0	Heat cured at 60 °C for 48 h
8M4	1:3	8 (M)	4.0	Ambient temperature(27 ± 2 °C) curing
8M6	1:3	8 (M)	6.0	Ambient temperature(27 ± 2 °C) curing
8M8	1:3	8 (M)	8.0	Ambient temperature(27 ± 2 °C) curing
8M10	1:3	8 (M)	10.0	Ambient temperature (27 ± 2 °C) curing
10M4	1:3	10 (M)	4.0	Ambient temperature(27 ± 2 °C) curing
10M6	1:3	10 (M)	6.0	Ambient temperature(27 ± 2 °C) curing
10M8	1:3	10 (M)	8.0	Ambient temperature(27 ± 2 °C) curing
10M10	1:3	10 (M)	10.0	Ambient temperature(27 ± 2 °C) curing
12M0	1:3	12 (M)	0.0	Heat cured at 60 °C for 48 h
12M4	1:3	12 (M)	4.0	Ambient temperature(27 ± 2 °C) curing
12M6	1:3	12 (M)	6.0	Ambient temperature(27 ± 2 °C) curing
12M8	1:3	12 (M)	8.0	Ambient temperature (27 ± 2 °C) curing
12M10	1:3	12 (M)	10.0	Ambient temperature (27 ± 2 °C) curing

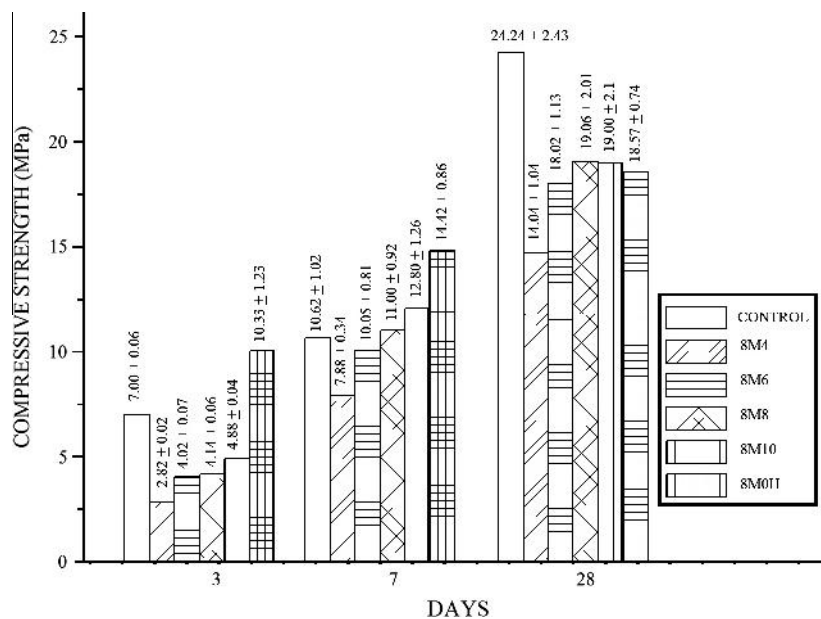


**Fig. 1A.** Compressive strength of fly ash based geopolymer mortar (with or without nano silica) having molar concentration of 8 (M) and cement mortar samples.

2. Material and methods

2.1. Materials

Low Calcium Class F (American Society for Testing and Materials 2001) dry fly ash obtained from National Thermal Power Corporation Ltd, Farakka plant in India has been used as the base material. The properties of fly ash and the grain size distribution (dry condition) were presented in Tables 1 and 2 respectively. The sodium hydroxide (NaOH) was the commercial grade in pellet forms with 99% purity and white in colour. Liquid sodium silicate (Na<sub>2</sub>SiO<sub>3</sub>) was also a commercial grade having 45% solid content and specific gravity of 1.53 gm/cc. It is light grey in colour and highly viscous. The basic properties of colloidal nano silica, as provided by the manufacturer, were listed in Table 3.

2.2. Mix proportion and curing

Three different molar concentration of NaOH such as 8 (M), 10 (M) and 12 (M) were mixed with Na<sub>2</sub>SiO<sub>3</sub> solution in the proportion of 1:1.75 (by weight) to make alkali activator fluid. Colloidal nano silica with 4%, 6%, 8% and 10% of fly ash by weight was also added to the fluid. Water present in the colloidal nano silica is adjusted from the activator solution during the preparation. Locally available sand (specific gravity 2.52, water absorption 0.50%, and fineness modulus of 2.38) was

used for the present study. The ratio of fly ash: sand and activator fluid (with/without nano silica) to fly ash were fixed at 1:3 (by weight) and 0.40 respectively. At first, sand and fly ash was dry mixed for two minutes and the appropriate amount of activator fluid (with/without) nano silica was added and mixed thoroughly. For the preparation of controlled mortar sample, Ordinary Portland Cement of 43 Grades (IS 8112) [19] was mixed with sand. The geopolymer mortar specimens without nano silica were cured at 60 °C temperature for 48 h within the hot air oven after 2 days of casting and were kept at ambient temperature until testing. However, the geopolymer mortar specimens with nano silica were removed from the mould after one day of casting and were placed at ambient temperature (27 ± 20 °C) until testing. Conventional water curing was made for the normal cement mortar specimens after one day of casting. The details of all the mixtures are shown in Table 4.

3. Sample preparation and testing

3.1. Sample preparation for mechanical strength test and water absorption test

The standard mortar cube specimens of size 70.6 mm × 70.6 mm × 70.6 mm were cast for different mixes to determine

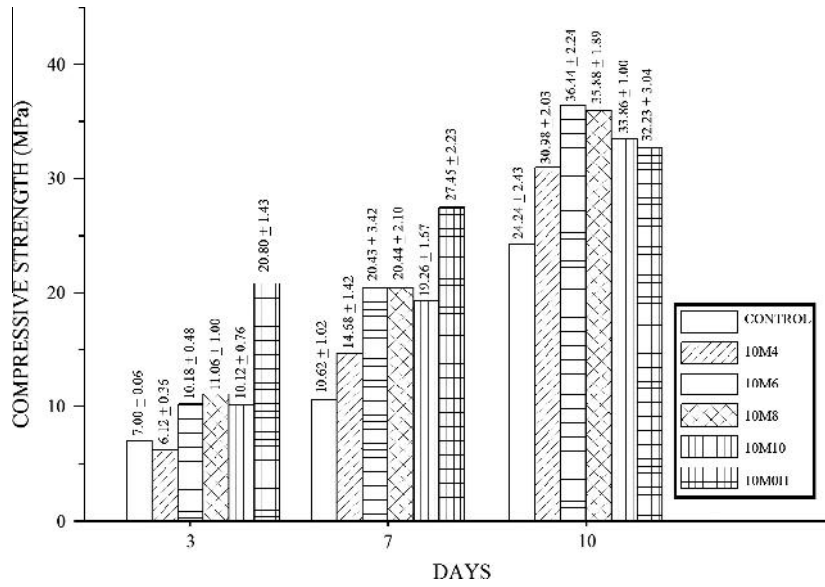


Fig. 1B. Compressive strength of fly ash based geopolymer mortar (with or without nano silica) having molar concentration of 10 (M) and cement mortar samples.

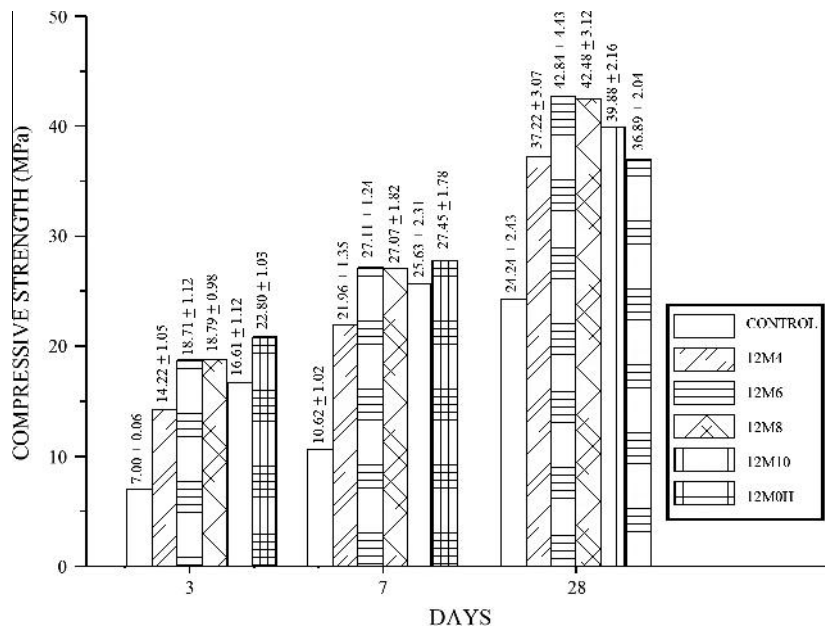


Fig. 1C. Compressive strength of fly ash based geopolymer mortar (with or without nano silica) having molar concentration of 12 (M) and cement mortar samples.

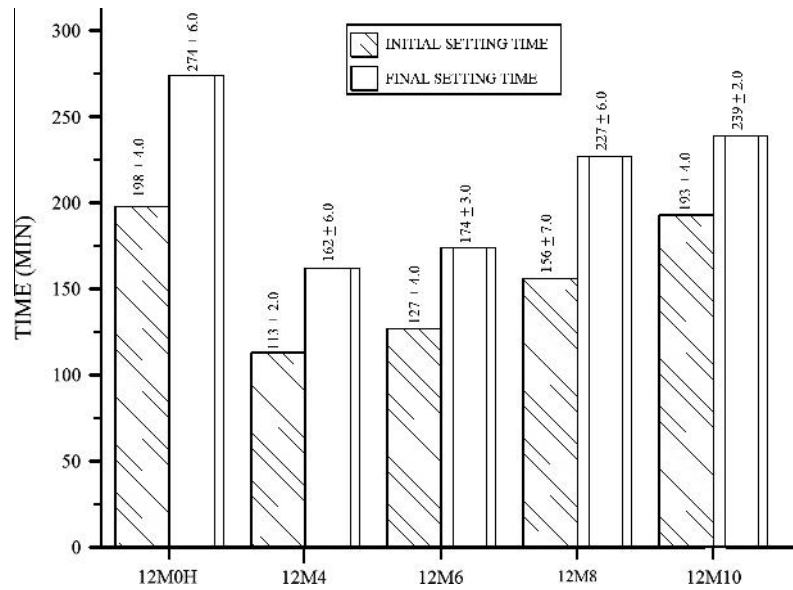


Fig. 1D. Initial and final setting time of fly ash based geopolymer mortar (with or without nano silica) having molar concentration of 12 (M).

the compressive strength of mortar [27]. All the specimens were tested at 3 days, 7 days, and 28 days after casting to determine the compressive strength at different ages. Flexural strength testing was carried out on 50 mm × 50 mm × 200 mm geopolymer mortar bar at different molar concentration and percentage of nano silica addition. These specimens were tested after 28 days from the date casting. The centre point loading method was adopted for determination of flexural strength (AASHTO T 67) [28]. Water absorption tests were done on standard cube samples of size 70.7 mm × 70.7 mm × 70.7 mm after 28 days of casting.

### 3.2. Sample preparation for rapid chloride ion penetration test

For chloride ion penetration, test cylinder specimen (100 mm diameter × 200 mm height) was sliced into core specimens of thickness 50 mm. The specimens were subjected to RCPT by

impressing 60 V. Two halves of the specimens are sealed with PVC container. One side of the container is filled with 3% sodium chloride solution (that side of the cell shall be connected to the cathode terminal of the power supply) and other side filled with 3 (M) sodium hydroxide solution. The current is passing through the specimen less than 60 V was recorded at 30 min interval over a period of 6 h and total charge in Coulombs was calculated.

### 3.3. Sample preparation for XRD analysis and FESEM analysis

After curing, the mortar samples possessing best result of compressive strength of different mixtures (12M0, 12M6, control) were dried and sieved to make the size less than 5 μm for X-ray diffraction analysis in powder X-ray diffractometer (Bruker AXS Inc, Model D8, WI, USA) with a scan speed 0.5 s/step at 40 kV. The XRD spectrum was analyzed in the range  $2\theta = 10^\circ$  to  $2\theta = 70^\circ$  and the peak positions were marked and compared from JCPDS file. For FESEM analysis, the fine powder was diluted with ethanol (99.9%) to make a film on carbon tape and then kept under vacuum desiccators for evaporation. Finally, the dried samples were gold

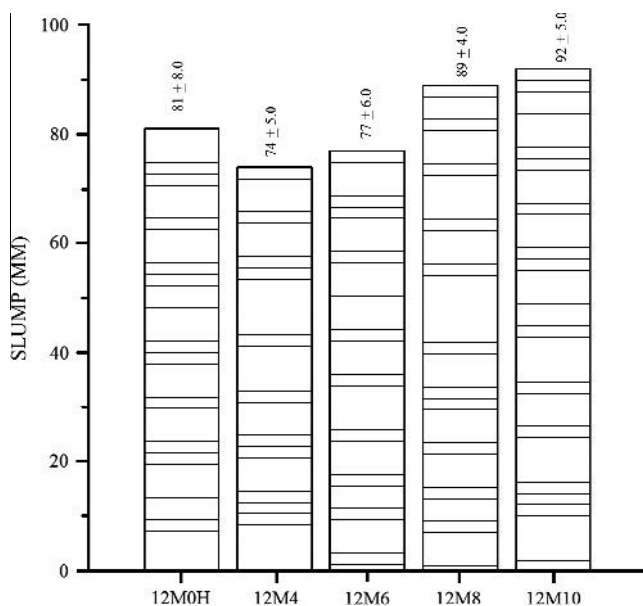


Fig. 1E. Slump test of fly ash based geopolymer mortar (with or without nano silica) having molar concentration of 12 (M).

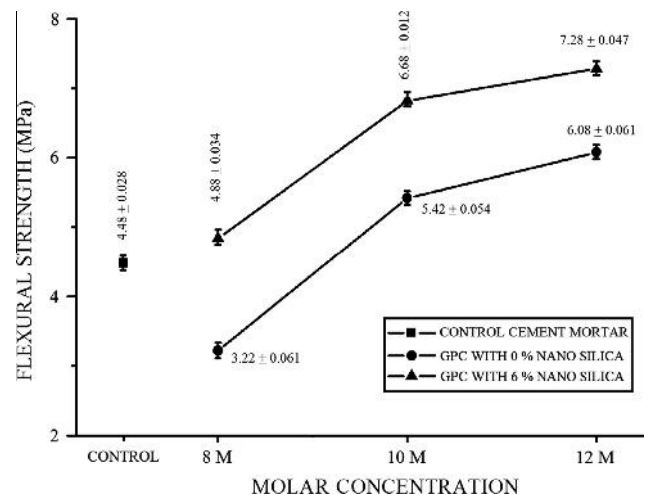


Fig. 2. Flexural strength of fly ash based geopolymer mortar (with (6%) or without nano silica) at molar different concentration and cement mortar samples.

coated for field emission scanning electron microscope FESEM (HITACHI S-4800, JAPAN) analysis.

## 4. Results and discussion

### 4.1. Compressive strength and setting time

Fig. 1A shows compressive strength of fly ash based geopolymer mortar samples having molar concentration of 8 (M) without nano silica (with heat curing) and 4%, 6%, 8% and 10% of nano silica (without heat curing). Figs. 1B and 1C show the results for molar concentration of 10 (M) and 12 (M). The strength of controlled sample (cement and sand) made with OPC cement is also compared. It is well accepted that the strength of geopolymer mortars without nano silica and cured at 60 °C for 48 h were more than conventional control cement mortar of (cement and sand ratio-1:3) at all ages. The compressive strength of geopolymer mortars with or without nano silica is more at higher molar concentration due to the higher rate of alkali activation.

However, addition of nano silica in the fly ash based geopolymer mortar up to 6% of fly ash seems to provide comparable strength at ambient temperature curing as shown in Figs. 1B and 1C at 28 days. Beyond 6% of nano silica addition, a reduction in compressive strength at all ages is noted. The initial and final setting time of 12 (M) geopolymer mortar with or without nano silica are also presented in Fig. 1D. Also Fig. 1E presents the slump test result of the different mixes (12M0H, 12M4, 12M6, 12M8 and 12M10). At the early ages, the compressive strength gain of 8 M and 10 M geopolymer mortar with nano silica and cured at ambient temperature is not so satisfactory. Similar results are reported for with fly ash (3%) and rice husk ash (93%) based geopolymer mortar with different percentage of nano SiO<sub>2</sub> and Al<sub>2</sub>O<sub>3</sub> (1%, 2%, 3% by weight) oven cured for 2, 4 and 8 h at temperature of 25 °C, 70 °C and 90 °C [25]. It may be concluded that at about 6% colloidal nano silica addition provides optimum 28 days strength without any heat curing for activation.

### 4.2. Flexural strength and tensile strength

Figs. 2 and 3 show that the both flexural strength and split tensile strength at 28 days of geopolymer mortar specimen increase with the increase in molar concentration of activator solution due to the availability of more alkali in the mix. In case of

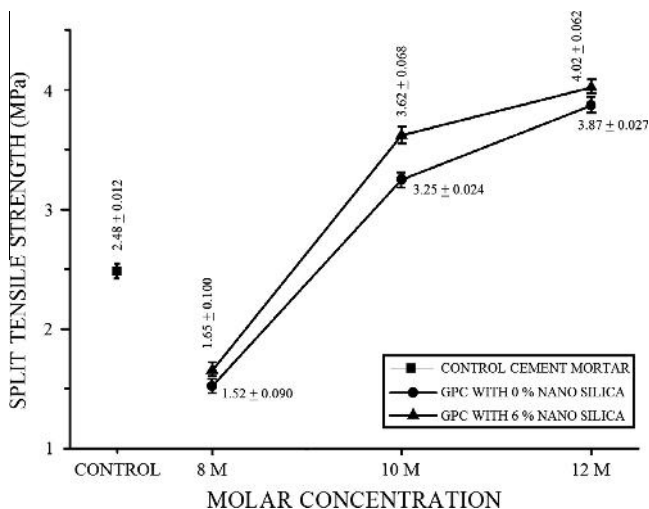


Fig. 3. Tensile strength of fly ash based geopolymer mortar samples (with (6%) or without nano silica) at molar different concentration and cement mortar samples.

geopolymer mortar with the addition of 6% nano silica and cured at ambient temperature shows better flexural and tensile strength than that of geopolymer mortar without nano silica (with heat curing) and the corresponding conventional concrete.

### 4.3. RCPT result analysis

A comparison of test results of RCPT value for both geopolymer mortar with (6%) and without nano silica at different molar concentration (8, 10 and 12 M) and conventional cement mortar samples are presented in Fig. 4. It may be mentioned here that for a particular molar concentration of geopolymer mortar with or without nano silica, the concentration of NaOH in the samples is remain same, thus the difference in RCPT values for such case may be compared. It is noted that less amount of charge passed through geopolymer mortar with nano silica (ambient temperature curing) than that of geopolymer mortar without nano silica (heat cured). This indicates that the diffusion coefficient will be less due to presence more amount of crystalline compound in nano silica modified geopolymer mortar thereby improving the durability.

### 4.4. Water absorption test

The results of saturated water absorption on mortar specimens (8M0, 10M0, 12M0, 8M6, 10M6, 12M6 and control) after 28 days curing are presented in Fig. 5. It indicates the lesser water absorption in geopolymer mortar having 6% nano silica (8M6, 10M6 and 12M6) compared to geopolymer mortar without nano silica (8M0, 10M0 and 12M0) and control mortar. It may be concluded that 6% nano silica addition is optimum for better pore structure modification [26]. The strength is also better at this optimal percentage of nano silica.

### 4.5. XRD result analysis

Fig. 6, shows the XRD analysis of conventional mortar (control), geopolymer concrete without nano silica (12M0) and with 6% nano silica (12M6). In geopolymer mortar with 6% nano silica, some specific extra peak positions are noted. It indicates the formation of new phase SiO<sub>2</sub>, Ca<sub>3</sub>SiO<sub>5</sub>, Na(AlSi<sub>3</sub>O<sub>8</sub>), Na<sub>2</sub>Si<sub>2</sub>O<sub>8</sub> and CaCO<sub>3</sub> compared to the geopolymer mixture 12M0 (without nano silica) samples. In case of controlled sample only few numbers of pick of SiO<sub>2</sub>, Ca<sub>3</sub>SiO<sub>5</sub> and Ca(OH)<sub>2</sub> are present. However, in XRD analysis crystalline quartz was easily detected in the region of 26–32° 2θ, which

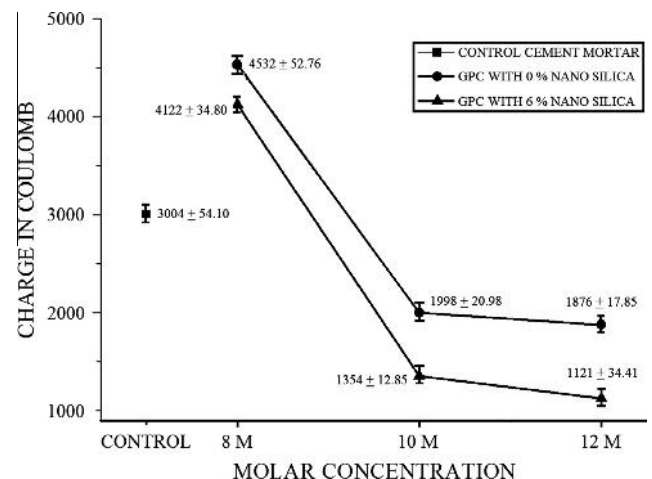


Fig. 4. Charge passed through fly ash based geopolymer mortar samples (with (6%) or without nano silica) at molar different concentration and cement mortar samples.

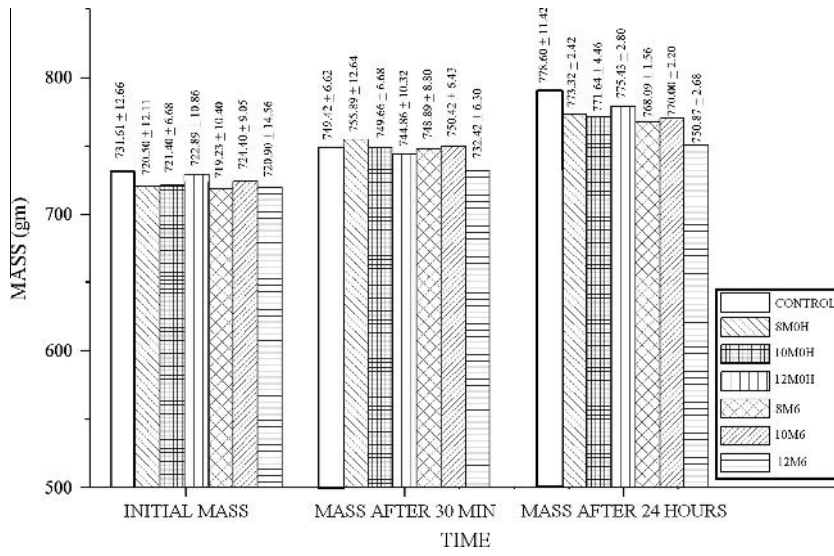


Fig. 5. Change of mass in water absorption test on fly ash based geopolymer mortar samples (with (6%) or without nano silica) of molar different concentration and cement mortar samples.

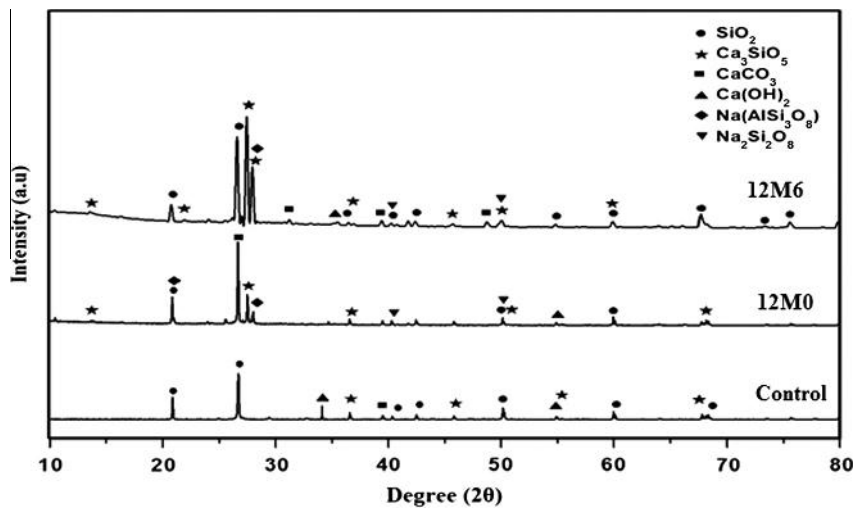


Fig. 6. XRD analysis report of fly ash based geopolymer mortar sample (12M0 and 12M6) and cement mortar samples (control).

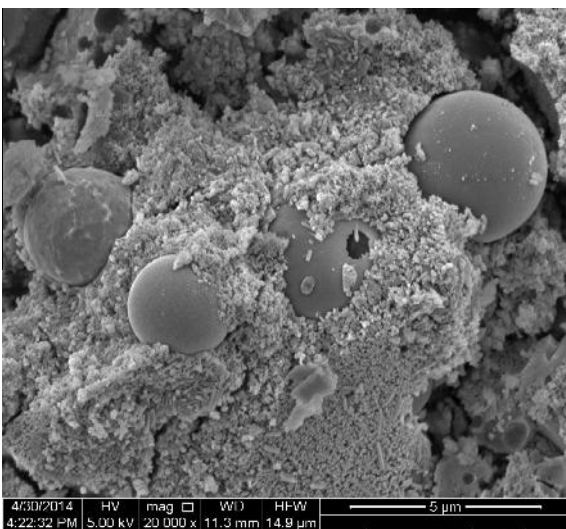


Fig. 7A. FESEM image of fly ash based geopolymer mortar sample (12M0) without nano silica.

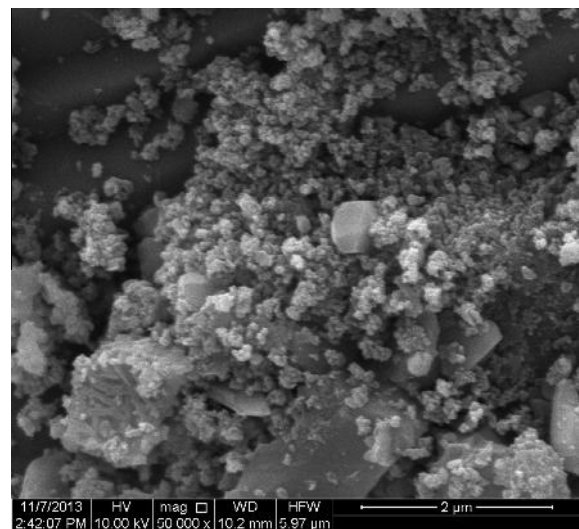


Fig. 7B. FESEM image of fly ash based geopolymer mortar sample (12M6) with 6% of nano silica.

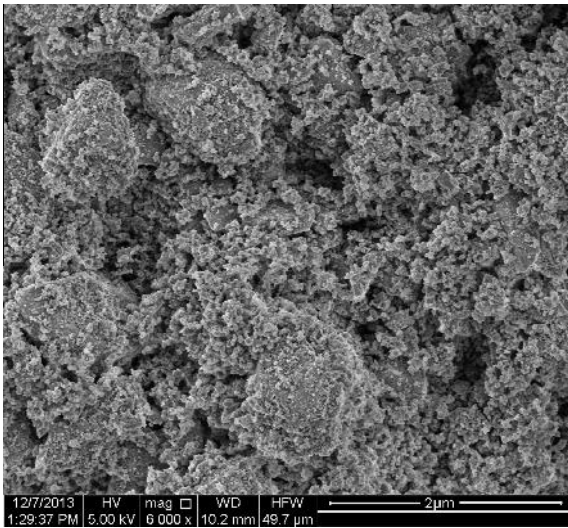


Fig. 7C. FESEM image of control cement mortar sample (control).

may be due to the formation of crystalline compound in geopolymer matrix. It may be concluded that the strength of 12M6 sample (with nano silica) is more than 12M0 (without nano silica) sample due to presence of more amount of crystalline compound in the geopolymer matrix [26].

#### 4.6. FESEM analysis

The morphology of the geopolymer samples with (0% and 6%) nano silica addition and conventional cement mortar was examined by using a Field Emission Scanning Electron Microscope (FESEM) and are shown in Figs. 7A, 7B and 7C respectively. The matrices of geopolymer with 6% nano silica seemed to consist of more amount of crystalline compound transformed from amorphous compound than of geopolymer mortar without nano silica. It may be note that in conventional cement mortar matrix and geopolymer mortar sample (12M0) without nano silica is less denser than geopolymer mortar with 6% nano silica (12M6). Also geopolymer mortar sample (12M0) without nano silica has more numbers of unreacted fly ash particles than 12M0 sample as shown in Figs. 7A and 7B. Due to the presence of nano silica in geopolymer mixes, the matrix possesses an extra enhancement of polymerisation process for its amorphous property and high specific area.

#### 5. Conclusion

Based on the present experimental study it is concluded that the colloidal nano silica addition can be used in the geopolymer mortar at an optimum percentage of 6% of fly ash to achieve appreciable compressive strength under ambient curing (without heat). Similar results were obtained for flexural and tensile strength. The water absorption and charge passed in RCPT is also less in the nano silica (with 6%) modified fly ash based geopolymer mortar (ambient temperature curing) compared to heat activated geopolymer mortar. The matrices of geopolymer with 6% nano silica execute

better results than geopolymer mortar or conventional mortar due to transformation of amorphous to crystalline compound.

#### References

- [1] Heidrich C, Joachim FH, Anne W. Coal combustion products: a global perspective. In: 2013 world of coal ash (WOCA) conference, April 22–25 in Lexington.
- [2] Davidovits J. Geopolymer, inorganic polymeric new materials. *J Therm Anal* 1991;37:1633–56.
- [3] Hardjito D, Wallah SE, Rangan V, et al. Fly ash-based geopolymer concrete. *Aust J Struct Eng* 2005;6(1).
- [4] Hardjito D, Wallah SE, Sumajouw DMJ, et al. Fly ash-based geopolymer concrete. *Aust J Struct Eng* 2005;6:1–9.
- [5] Fernandez Jimenez A, Monzo M, Vicent M, et al. Alkaline activation of metakaolin – fly ash mixtures: obtain of zeoceramics and zeocements. *Microporous Mesoporous Mater* 2008;108:41–9.
- [6] Xie Z, Xi Y. Hardening mechanism of an alkaline-activated class F fly ash. *Cem Concr Res* 2001;31:1245–9.
- [7] Pal S, Mandal S. Different thermal activation effect on fly ash based geopolymer concrete. *Indian Concr Inst J* 2011;12:23–5.
- [8] Daniel LYK, Jay GS. Effect of elevated temperatures on geopolymer paste, mortar and concrete. *Cem Concr Res* 2010;40:02.
- [9] Chindaprasirta P, Rattanasakb U, Taebuanhuadb S. Role of microwave radiation in curing the fly ash geopolymer. *Adv Powder Technol* 2013;24:03.
- [10] Peigang H, Dechang J, Meirong W, et al. Thermal evolution and crystallization kinetics of potassium-based geopolymer. *Ceram Int* 2011;37:01.
- [11] Hussin MW, Bhutta MAR, Azreen M, et al. Performance of blended ash geopolymer concrete at elevated temperatures. *Mater Struct* 2014. <http://dx.doi.org/10.1617/s11527-014-0251-5>.
- [12] Vijai K, Kumutha R, Vishnuram BG. Effect of types of curing on strength of geopolymer concrete. *Int J Phys Sci* 2010;5(9).
- [13] Guo X, Shi H, Dick WA. Compressive strength and microstructural characteristics of class C fly ash geopolymer. *Cement Concr Compos* 2010;32:2.
- [14] Gorhan G, Kurklu G. The influence of the NaOH solution on the properties of the fly ash based geopolymer mortar cured at different temperature. *Compos Part B* 2014;58:371–7.
- [15] Barbosa FFV, Mackenzie JDK, Thaumaturgo C. Synthesis and characterisation of materials based on inorganic polymers of alumina and silica: sodium polysialate polymers. *Int J Inorg Mater* 2000;309–17.
- [16] Temuujin J, Williams RP, Van Riessen A. Effect of mechanical activation of fly ash on the properties of geopolymer cured at ambient temperature. *J Mater Process Technol* 2009;209:5276–80.
- [17] Deb PS, Nath P, Sarkar PK. Strength and permeation properties of slag blended fly ash based geopolymer concrete. *Adv Mater Res* 2013;05:168–73.
- [18] Giasuddina HM, Sanjayan Jay G, Ranjithb PG. Strength of geopolymer cured in saline water in ambient conditions. *Fuel* 2013;07:34–9.
- [19] Zhang MH, Islam J. Use of nano-silica to reduce setting time and increase early strength of concretes with high volumes of fly ash or slag. *Constr Build Mater* 2012;29:573–80.
- [20] Shaikh FUA, Supit SWM, Sarker PK. A study on the effect of nano silica on compressive strength of high volume fly ash mortars and concretes. *Mater Des* 2014;60:433–42.
- [21] Li G. Properties of high-volume fly ash concrete incorporating nano-SiO<sub>2</sub>. *Cem Concr Res* 2004;34:1043–9.
- [22] Yu R, Spiesz P, Brouwers HJH. Effect of nano-silica on the hydration and microstructure development of Ultra-High Performance Concrete (UHPC) with a low binder amount. *Constr Build Mater* 2014;65:140–50.
- [23] Quercia G, Spiesz P, Husken G, et al. SCC modification by use of amorphous nano-silica. *Cement Concr Compos* 2014;45:69–81.
- [24] Phoo-ngernkham T, Chindaprasirt P, Sata V, et al. The effect of adding nano-SiO<sub>2</sub> and nano-Al<sub>2</sub>O<sub>3</sub> on properties of high calcium fly ash geopolymer cured at ambient temperature. *Mater Des* 2014;55:58–65.
- [25] Riahi S, Nazari A. The effects of nano particles on early age compressive strength of ash based geopolymer. *Ceram Int* 2012;38:4467–76.
- [26] Khater HM, El-Sabbagh BA, Fanny M. Effect of nano-silica on alkali activated water-cooled slag geopolymer. *ARPN J Sci Technol* 2012;02:02.
- [27] IS 10080 – 1982. Specification for vibration machine, Bureau of Indian Standards, New Delhi, India.
- [28] AASHTO T 67-05. Standard method of test for standard practices for force verification of testing machines, standard published by American Association of State and Highway Transportation Officials.







Cite this: *RSC Adv.*, 2015, 5, 64037

## Anti-microbial efficiency of nano silver–silica modified geopolymer mortar for eco-friendly green construction technology

Dibyendu Adak,<sup>a</sup> Manas Sarkar,<sup>b</sup> Moumita Maiti,<sup>b</sup> Abiral Tamang,<sup>b</sup> Saroj Mandal<sup>\*a</sup> and Brajadulal Chattopadhyay<sup>b</sup>

A silver–silica nano composite based geopolymer mortar has been developed by simple adsorption of silver in a suitable amount of a colloidal silica suspension for anti-bacterial property development. The silver nanoparticles (3–7 nm) were attached on the surface of 20–50 nm sized silica nanoparticles. The silver–silica nano-composite was characterized by Transmission Electron Microscopy (TEM), X-Ray Diffraction (XRD) and energy dispersive X-ray spectral analysis. Mechanical strength, durability and mechanistic anti-bacterial activity of the silver–silica nano composite modified geopolymer mortar (GM<sub>Ag-Si</sub>) were investigated and compared to nano silica modified geopolymer mortar (GM<sub>Si</sub>) and control cement mortar (CM). To access the anti-microbial efficacy of the samples, 99% mortality for Gram positive and Gram negative bacteria was calculated. Minimum Inhibitory Concentration (MIC) and Minimum Bactericidal Concentration (MBC) values were determined from batch cultures. The addition of 6% (w/w) of the silver–silica nano composite in the geopolymer mortar cured at ambient temperature shows substantial improvement in mechanical strength, durability and anti-bacterial property. Reactive Oxygen Species (ROS) generation and cell wall rupture as observed from fluorescence microscopy and Field Emission Scanning Electron Microscopy (FESEM) may be possible reasons behind the anti-bacterial efficacy of silver–silica nano composite modified geopolymer mortar.

Received 1st July 2015  
Accepted 21st July 2015

DOI: 10.1039/c5ra12776a

www.rsc.org/advances

### 1. Introduction

The sustainability of the cement and concrete industries is imperative to the wellbeing of our planet and human development. The production of Portland cement, an essential constituent of concrete, releases greenhouse gas emissions both directly and indirectly. It is well accepted that about one tone of carbon dioxide (CO<sub>2</sub>) is emitted into the atmosphere during the production of one tone of cement.<sup>1</sup> Coal based thermal power stations produce a huge amount of fly ash which is annually estimated to be around 780 million tons throughout the world.<sup>2</sup> The utilization of fly ash is about 35% in the construction of landfills, embankments, production blended cement *etc.* and remains as an industrial hazard. Alkali activated geopolymer concrete/mortar have been introduced to reduce the rapid utilization of Portland cement concrete throughout the world. In the last few decades the application of geopolymer concrete using mainly fly ash (without cement) has become an important area of research.<sup>3–6</sup>

Geo-polymeric reaction generally depends on the activation with alkali solutions and temperature curing at 40–75 °C to

obtain similar strength and durability to normal concrete.<sup>7–11</sup> Thus the use of geopolymer concrete is limited to the precast member due to requirement of heat activation after casting. Several researchers have proposed to improve the strength development of fly ash based geopolymer cured at ambient temperature.<sup>12–14</sup> Geopolymer mortar, with the addition of 6% nano silica shows appreciable improvement in mechanical strength and durability at 28 days under ambient temperature curing.<sup>15</sup> However, it is necessary to explore the role of geopolymer composite different aspects like structural behavior and in the application of antimicrobial field.

Usually fresh concrete/mortar has a pH of 10 to 12 depending upon the mixture. Consequently with this high alkalinity it does not allow the growth of any microbes. However, this high pH is slowly reduced over the time due to presence of carbon dioxide (CO<sub>2</sub>) and hydrogen sulfide (H<sub>2</sub>S) in the atmosphere producing weak acids (carbonic acid, thio-sulphuric acid *etc.*) in presence of water. When pH of the concrete/mortar is reduced to below 9.0, bacterial attack or deposition on concrete surface begins.<sup>16</sup> The microbial colonies on the concrete surface, capillaries and micro/macro fissures cause concrete damage through bio-deterioration.<sup>17</sup> Bio-deterioration of conventional concrete structure such as sewage pipes, maritime structures, bridges, tanks, pipelines and cooling towers occurs due to the presence of harmful bacteria.<sup>18,19</sup> Various studies suggest that

<sup>a</sup>Department of Civil Engineering, Jadavpur University, Kolkata-700032, India. E-mail: mailtosarojmandal@rediffmail.com; smandal@civil.jdvu.ac.in; Tel: +91-9432236510

<sup>b</sup>Department of Physics, Jadavpur University, Kolkata-700032, India

use of silver NPs in minimum concentration shows promising anti-bacterial property.<sup>20,21</sup> With this background, use of silver-silica nano composite modified low calcium based fly-ash geopolymer mortar cured at ambient temperature, may be a favorable contender to Portland cement concrete. In this study, mechanical strength, durability and mechanistic anti-bacterial activity of fly ash based silver-silica nano composite modified geopolymer mortar ( $GM_{Ag-Si}$ ) has been investigated and compared with silica modified geopolymer mortar ( $GM_{Si}$ ) and control cement mortar (CM).

## 2. Materials and method

### 2.1. Ingredients

Low calcium class F dry fly ash, locally available sand (specific gravity 2.52, water absorption 0.50%, and fineness modulus of 2.38), alkali activator fluid (mixture of sodium hydroxide, sodium silicate and deionized water) have been used as basic ingredients of geopolymer mortar.<sup>22,23</sup> For control cement mortar, Ordinary Portland Cement (OPC) and deionized water has been used.

Nutrient Broth (NB) media ingredients like peptone, beef extract, yeast extract, NaCl, agar (Hi-media Pvt. Ltd, India), silver nitrate (Merck Germany), deionized water, carbonic acid, *E. coli* (MTCC 1652 strain), *S. aureus* (MTCC 96 strain) bacteria have been used. All reagents were prepared with milli-Q ultra-pure water. The basic properties of colloidal nano silica, as provided by the manufacturer, are mentioned in Table 1.

### 2.2. Preparation of silver silica nano composite

For preparation of silver nanoparticles (Ag NPs) on the surface of colloidal silica nanoparticles ( $SiO_2$  NPs), 100 mM colloidal silica NPs water solution was taken and the 5 mM silver nitrate ( $AgNO_3$ ) were added drop-wise under vigorous stirring at ambient temperature for 6 h.<sup>24</sup>

### 2.3. Confirmative test for silver-silica nano composite

The silver-silica nano solution was lyophilized (EYELA FDU-1200, Japan) and crushed to make a uniform fine powder. The surface morphology of the synthesized nano structured samples were evaluated using High Resolution Transmission Electron Microscopy (HRTEM; JEOL, JEM 2100). The surface charges and size distribution of silica NPs and silver-silica nano composite were determined by using Zeta Potential Analyzer (Brookhaven Instruments Corp. Holtsville, USA). XRD analysis was performed (Bruker AXS, Inc., Model D8, WI, USA) with monochromatised Cu-K $\alpha$  radiation of wavelength 1.5406 Å at 55 kV and 40 mA. The sample was examined at  $2\theta$  from 10° to 80° and

identified by referring to data of Joint Committee on Powder Diffraction Standards (JCPDS) files.

### 2.4. Preparation of mortar mixtures ( $GM_{Si}$ , $GM_{Ag-Si}$ and CM)

Two different fly-ash based geopolymer mortars ( $GM_{Si}$ ,  $GM_{Ag-Si}$ ) and a conventional control mortar (CM) were prepared for the present study. The activator fluid to fly ash ratio was taken at 0.40. The activator fluid was made by mixing 12 M NaOH with  $Na_2SiO_3$  at weight ratio of 1 : 1.75. This solution was mixed with colloidal nano silica solution (activator 1) for the preparation of  $GM_{Si}$  geopolymer specimens. For preparation of  $GM_{Ag-Si}$  geopolymer mortar, activator 2 was prepared by 12 M NaOH and  $Na_2SiO_3$  at same weight ratio with nano silver-silica solution. The amount of nano silica and silver-silica nano composite in the respective activator 1 and activator 2 solutions was 6% (w/w) of fly ash used. For the preparation of control mortar sample (CM), OPC of 43 grade sand and distilled water were used.<sup>25</sup> Details of all mixes are shown in Table 2. For determination of mechanical strength (compressive strength, flexural and split tensile strength) and durability (RCPT), the samples of mix  $GM_{Si}$  and  $GM_{Ag-Si}$  were removed from the mould after 24 h and kept in ambient temperature and tested after 3, 7 and 28 days of air curing. Conventional water curing was made for the CM specimens until the test.

### 2.5. Sample preparation and testing of mechanical strength

The standard mortar cube specimens of dimension 70.6 mm  $\times$  70.6 mm  $\times$  70.6 mm were prepared for different mixes to determine the compressive strength of mortars. All the specimens were tested at 3 days, 7 days, and 28 days after casting to determine the compressive strength. Flexural strength testing was carried out on mortar bars (50 mm  $\times$  50 mm  $\times$  200 mm) for all ( $GM_{Si}$ ,  $GM_{Ag-Si}$ , CM) samples. The center point loading method was adopted for the determination of flexural strength (ASTM C293).<sup>26</sup> Cylinder specimens (100 mm diameter  $\times$  200 mm height) were tested for split tensile strength test for each category after 28 days from the date of casting.

### 2.6. Durability test

Rapid Chloride ion Penetration Test (RCPT) was adopted for the durability assessment of different mortar mixes. Test cylinder specimens (100 mm diameter  $\times$  200 mm height) were sliced into core specimens of thickness 50 mm and subjected to RCPT by impressing 60 V.<sup>27</sup> All the specimens were tested after 28 days of casting.

### 2.7. Anti-bacterial study

Mortar samples ( $GM_{Si}$  and  $GM_{Ag-Si}$  & CM) were immersed in 0.5 N carbonic acid solutions until the pH value of all samples

Table 1 Basic properties of colloidal nano silica

Colloidal nano silica type	Average particle size (nm)	Solid content (wt%)	Viscosity (Pa S)	pH	Solid density ( $g\ cm^{-3}$ )
CemSynXTX	20 to 50 nm	31%	8.5	9.0–9.6	2.16

Table 2 Nano silica modified geopolymer (GM<sub>Si</sub>), silver silica modified geopolymer mortar (GM<sub>Ag-Si</sub>) and control mortar (CM), mix proportions<sup>ab</sup>

Sample mark	Fly ash sand	Activator solutions	% of SiO <sub>2</sub> NPs	% of Ag-SiO <sub>2</sub> NPs	Curing condition
GM <sub>Si</sub>	1 : 3	Activator-1	6.0	Nil	Air curing at room temp.
GM <sub>Ag-Si</sub>	1 : 3	Activator-2	Nil	6.0	Air curing at room temp.
CM (cement : sand)	1 : 3	Water	Nil	Nil	Water curing

<sup>a</sup> Activator-1 – NaOH + Na<sub>2</sub>SiO<sub>3</sub> + nano silica. <sup>b</sup> Activator-2 – NaOH + Na<sub>2</sub>SiO<sub>3</sub> + nano silver-silica.

become less than 9.0. After getting the pH < 9.0, the samples were crushed by hand mortar and sieved in uniform sized powder for the anti-bacterial study purpose.

**2.7.1. Bacterial kinetics study.** Bacterial kinetics of mortar samples from GM<sub>Si</sub>, GM<sub>Ag-Si</sub> and CM were investigated against *S. aureus* (gm +ve) and *E. coli* (gm –ve) bacterial strains distinctly. From an overnight growing fresh culture of both bacteria, a volume of culture approximately representing ~10<sup>7</sup> CFU ml<sup>-1</sup> was washed and suspended in PBS buffer. The fresh culture was then diluted by 5 ml nutrient broth (0.5% peptone, 0.1% beef extract, 0.2% yeast extract, 0.5% NaCl, pH 7) at a final cell concentration of 10<sup>4</sup> CFU ml<sup>-1</sup> and incubated at 37 °C. For anti-bacterial assay, 2 mg ml<sup>-1</sup> (~2 × MIC) of each dry dust samples (pH < 9) (GM<sub>Si</sub>, GM<sub>Ag-Si</sub> and CM) were used to treat the inoculated broth separately. Time dependent killing was determined by plating the culture from the treated geopolymer mortar samples and control cement mortar sample in agar plate (15%) after different time of incubation (0, 2, 4, 6, 8, 12, 24 h). Plates were incubated at 37 °C and the numbers of colonies were counted after 24 h. The whole experiment was repeated thrice.

**2.7.2. Determination of MIC and MBC test.** Using batch culture process, the Minimum Inhibitory Concentration (MIC) was observed by the varying concentration of different geopolymer samples.<sup>28</sup> Growth medium containing initial cell concentration (10<sup>7</sup> CFU ml<sup>-1</sup>) of each strain was taken distinctly. The different mortar powders (GM<sub>Si</sub>, GM<sub>Ag-Si</sub> and CM) were added in the growth medium distinctly and inoculated at 37 °C on a rotary shaker. In 5 ml NB, the powder samples (0.1% to 5.0% w/v) of each category were added separately in several marked tubes. The growth inhibitions (GM<sub>Si</sub> and GM<sub>Ag-Si</sub> treated bacterial cells) were measured against control at 620 nm by a UV-visible spectrophotometer (ELICO, SL 196 Spectropharm).<sup>29,30</sup>

Minimum bactericidal concentration (MBC) is defined as the lowest concentration of silver nanoparticles present in GM<sub>Ag-Si</sub> samples that kills 99.9% of the bacteria. The presences of viable microorganisms were examined and lowest concentrations causing bactericidal effect were reported as MBC for the growth inhibitory concentrations.<sup>31</sup> The experiment was performed by plating (nutrient agar plate 15%) the bacterial cultures with upper amounts above the MIC. The agar plates were inoculated at 37 °C for 24 h. All the experiments were carried out in triplicate.

**2.7.3. Reactive oxygen species (ROS) detection and fluorescence microscopic analysis.** The generations of superoxide radical activity were measured according to method given by Su

*et al.*<sup>32</sup> freshly prepared pure log phased cultures of *E. coli* and *S. aureus* were taken separately for this purpose. 10<sup>4</sup> CFU ml<sup>-1</sup> containing fresh NB were inoculated and treated with GM<sub>Si</sub> and GM<sub>Ag-Si</sub> with their MIC values at 37 °C for 1 h distinctly. Bacterial pellets were washed with phosphate buffer (pH 7.0) several times and treated with 10 μM DCFHDA for 30 min. So that DCFDA diffuses through the cell membrane, enzymatically hydrolyzes by intracellular esterase and oxidizes to produce a fluorescent 2',7'-dichlorofluorescein (DCF) in the presence of ROS. From fluorescence spectrophotometer, the ROS level was measured at 490 nm (excitation) and emission at 520 nm using SYBR Green and PI for living and dead cells respectively. The intensity of fluorescence is proportional to the level of intracellular reactive oxygen species.<sup>33</sup> The working solution of 10 μl each of SYBR Green DMSO solution (1 : 100 v/v) and PI water solution (1 mg ml<sup>-1</sup>) were taken in to 1 ml of each treated GM<sub>Si</sub> & GM<sub>Ag-Si</sub> and CM samples. After incubation at 37 °C for 30 min, each sample was mounted immediately over slides and pictures were captured by the fluorescence microscope for this experiment.<sup>34</sup>

**2.7.4. Morphological investigation for bacterial strains.** Certain volume of NB medium and powder samples of the three different mortar specimens (GM<sub>Si</sub>, GM<sub>Ag-Si</sub> & CM) were added separately to 5 ml cultures of each bacteria resulting in final concentration of 1 mg ml<sup>-1</sup> samples and bacterial concentration of 10<sup>8</sup> CFU ml<sup>-1</sup>. This experiment was performed for both bacteria (*E. coli* & *B. subtilis*) and for three different test samples separately. For morphological analysis, bacterial growth medium in mid exponential phase and with the same cell density were treated with samples (GM<sub>Si</sub>, GM<sub>Ag-Si</sub> and CM) for 6 h at 37 °C. The bacterial samples were then washed with milli-Q water, fixed with 2% glutaraldehyde and placed on a silicon platelet (Plano, Wetzlar, Germany). A series of ethanol dehydration steps were carried out followed by staining with 3% uranyl acetate in 25% ethanol. Finally, the samples were washed with buffer solution (0.1 M sodium phosphate, pH 7.2) and investigated using FESEM (INSPECT F50 SEM, The Netherlands).

**2.7.5. DNA agarose gel electrophoresis.** The genomic DNA were isolated from the cells (*E. coli* & *S. aureus*) and purified by phenol chloroform method. 1 μl of GM<sub>Si</sub> and GM<sub>Ag-Si</sub> water solution (1 μg ml<sup>-1</sup>) were mixed to the extremely pure two types of naked DNA separately. After 15 min incubation at room temperature, the treated and pure DNA was run in 1% low melting agarose gel. The images of DNA were taken under trans-illuminator (Fotodyne 110 V UV Trans-illuminator).

**2.7.6. Statistical analysis.** Experiments were performed in triplicate. Error bars on graph represent the standard error. One way ANOVA was used to compare three or more groups defined by a single factor. Comparisons were made between two different geopolymer samples ( $GM_{Si}$  and  $GM_{Ag-Si}$ ) and control samples (CM) with the treatment of two types of different microbial strains. All data were expressed as mean  $\pm$  SD of six separate experiments. Where  $N \geq 10$  were taken for each category.

## 3. Results

### 3.1. Characterization of nano silver-silica composite

Transmission electron microscopy analysis of silica NPs and silver-silica nano composite shows their very regular spherical shape (Fig. 1A and B). Fig. 1B shows the silver NPs (mean  $\pm$  SD:  $4 \pm 1$  nm) are formed on the surface of silica NPs ( $30 \pm 10$  nm). Elemental analysis of newly synthesized silica NPs and silver-silica nano composites are shown in Fig. 1A and B (inset). The presence of the elements O and Si were observed at 0.562 keV (O), 1.75 keV (Si) respectively. The Si, O and Ag peaks are clearly shown in Fig. 1B (inset), which indicates that the presence of silver nano particles on to the silica surface. It was confirmed from TEM images that nano-particles are pure in colloidal form but the particles are of hybrid-type in silver-silica nano composites. Also the average size of the silica NPs 20–40 nm was analyzed by using zeta size distribution graph (Fig. 1C-I). The silver NPs ( $4 \pm 1$  nm) were attached on the surface of silica NPs which was showed in Fig. 1D-I. Also in Fig. 1D-I, comparatively broad peak is revealed that the greater size distribution of silver-silica nano composite, which is also much correlated

with TEM result (Fig. 1B). The overall surface charge of the pure silica NPs (Fig. 1C-II) was negative ( $-50$  mV) whereas silver silica nano-composite (Fig. 1D-II) showed some greater positive charges ( $>-50$  mV) which was confirmed by zeta potential analysis.

The X-ray diffraction profiles of newly synthesized silica NPs and silver-silica nano-composite were matched up with JCPDS data file (Fig. 2A). The XRD pattern of silver-silica NPs showed the presence of sharp peaks which are absent in silica NPs. The sharp peaks indicate that the newly synthesized nano particles are either very small crystallite size or semi-crystalline in nature. The average crystallite size of silver nano particles were estimated by Scherrer's equation for the (122), (220), and (222) diffraction peaks at  $2\theta = 38.118$ ,  $45.593$ ,  $57.937$  and  $71.101$  respectively. Therefore, it is clearly confirmed that silver-silica nano composite particles were successfully synthesized.

### 3.2. Presence of silver NPs in $GM_{Ag-Si}$ mortar

The XRD spectra of nano silica modified geopolymer mortar ( $GM_{Si}$ ) and nano silver-silica nano composite modified geopolymer ( $GM_{Ag-Si}$ ) mortar were represented in Fig. 2B. In case of geopolymer mortar with nano silver-silica composite, some additional peak positions were observed at same specific positions ( $2\theta$ ) that confirmed the presence of silver nano particles in  $GM_{Ag-Si}$  mortar.

### 3.3. Strength and durability of different mortars

Fig. 3A represents the compressive strength of fly ash based nano silica modified geopolymer ( $GM_{Si}$ ) mortar and nano silver-silica modified geopolymer mortar ( $GM_{Ag-Si}$ ) samples

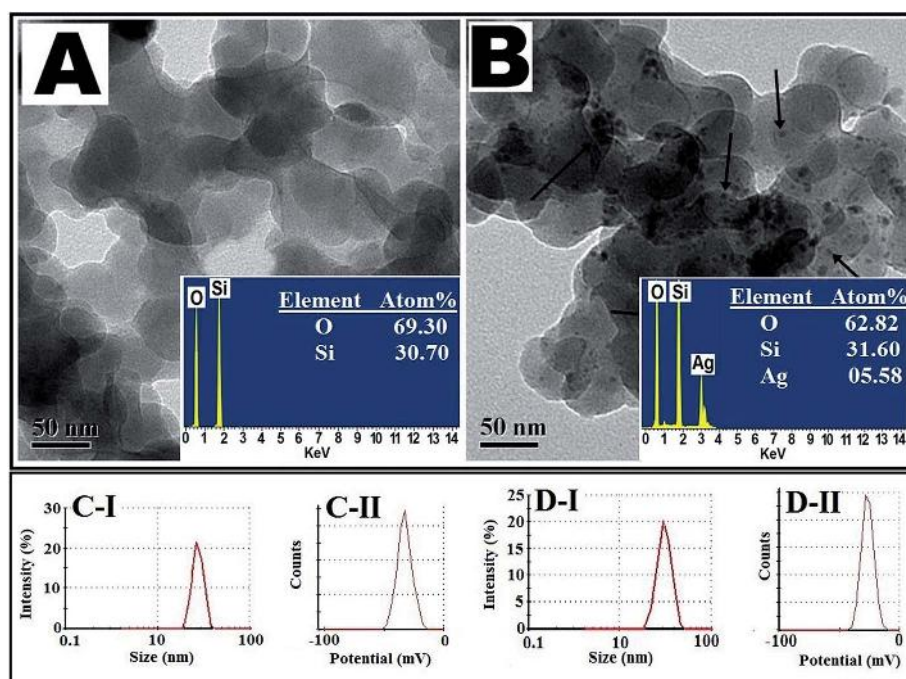


Fig. 1 TEM image of (A) silica NPs & (B) silver-silica NPs with inset representing elemental analysis by EDS. Zeta size (C-I & D-I) and zeta potential (C-II & D-II) distribution graph of silica NPs & silver-silica NPs respectively.

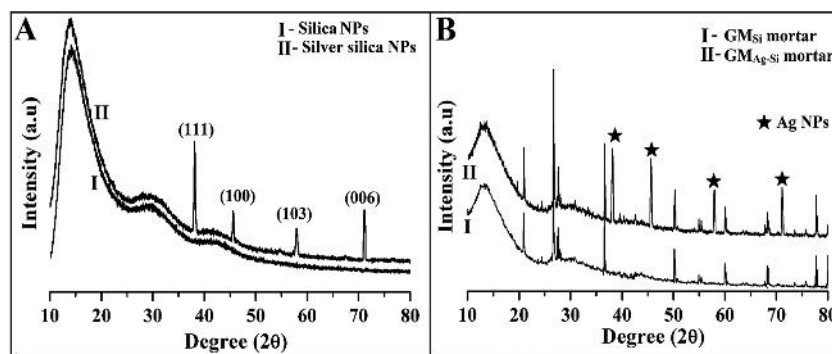


Fig. 2 (A) XRD spectra of (I) SiO<sub>2</sub> NPs & (II) Ag-SiO<sub>2</sub> NPs. (B) XRD spectra of (I) GM<sub>Si</sub> and (II) GM<sub>Ag-Si</sub>.

cured at ambient temperature. The strength of control sample made from OPC cement was also compared. It was observed that both the geopolymer mortar samples (GM<sub>Si</sub> and GM<sub>Ag-Si</sub>) show better compressive strength than CM samples at all ages. However, addition of silica NPs and silver-silica nano composite (6% of fly ash by weight) in geopolymer mortar seems to provide similar compressive strength cured at ambient temperature. It is noted that the presence of silver NPs attached on the surface of silica NPs do not affect the strength of modified geopolymer mortar.<sup>15</sup> Similar behavior was also observed on flexural strength and split tensile strength of geopolymer mortars and control mortar samples (Fig. 3B). A comparison of RCPT value for GM<sub>Si</sub>, GM<sub>Ag-Si</sub> and CM samples were presented in Fig. 3C. It is observed that less amount of ions passed through geopolymer (GM<sub>Ag-Si</sub> and GM<sub>Si</sub>) matrices than CM matrices. This indicates that the diffusion coefficient will be less due to presence of crystalline compound in GM<sub>Si</sub> and

GM<sub>Ag-Si</sub> modified geopolymer mortars thereby improving the durability.

### 3.4. Anti-bacterial study

The bactericidal kinetics of exponentially growing Gram negative *E. coli* and Gram positive *S. aureus* bacteria were observed against GM<sub>Si</sub>, GM<sub>Ag-Si</sub>, and CM samples by time killing assay. The result revealed that the populations of *E. coli* and *S. aureus* bacteria were reduced by 99% after 8 h and 6 h (Fig. 4C and D) for GM<sub>Ag-Si</sub> respectively. The anti-bacterial effect was shown by plate culture of bacteria after 8 h treatment (Fig. 4A and B). A large number of colonies were found in GM<sub>Si</sub> and control specimens whereas none was seen in case of GM<sub>Ag-Si</sub> sample.

The MIC and MBC values of GM<sub>Ag-Si</sub> sample against Gram +ve and Gram -ve microorganisms are represented in Tables 3 and 4. Table 3 indicates that considerably low amount of GM<sub>Ag-Si</sub> (0.15 mg ml<sup>-1</sup>) was able to eradicate the Gram (-ve) bacterial cells (>99%). Gram -ve organisms were more resistant to the growth inhibiting effect of the sample (0.10 mg ml<sup>-1</sup>) compared to Gram +ve bacterial cell. The anti-bacterial activities of GM<sub>Ag-Si</sub> geopolymer mortar samples are significantly higher than the other specimens (GM<sub>Si</sub> & control sample). The MBC for silver-silica nano composite treated cells are not more than 4 times their respective MIC values indicating that the nano composites are bactericidal rather than bacteriostatic. The MBC value (Table 4) indicates that considerably lower amount of silver (0.43 μg ml<sup>-1</sup>) was able to eradicate the Gram positive bacterial (*S. aureus*) cells. The Gram negative organisms (*E. coli*) were more resistant to the growth inhibiting effect of silver NPs (0.32 μg ml<sup>-1</sup>).

The ROS level of the cells (*E. coli* & *S. aureus*) treated with GM<sub>Si</sub> and GM<sub>Ag-Si</sub> were compared to CM treated cells. The level of ROS for the CM treated cells was considered as 100%. For GM<sub>Ag-Si</sub> treated cells the intensity was about 5 times higher with respect to the control for both *E. coli* and *S. aureus* (Fig. 5A). As observed, the oxidative stress in the GM<sub>Ag-Si</sub> treated cells was much higher as compared to the CM and GM<sub>Si</sub> treated microorganisms.

The purified bacterial genomic DNA of *E. coli* and *S. aureus* are shown (Fig. 5B) in gel electrophoresis (lane-1 and lane-4) whereas the GM<sub>Si</sub> treated DNA was observed in lane-2

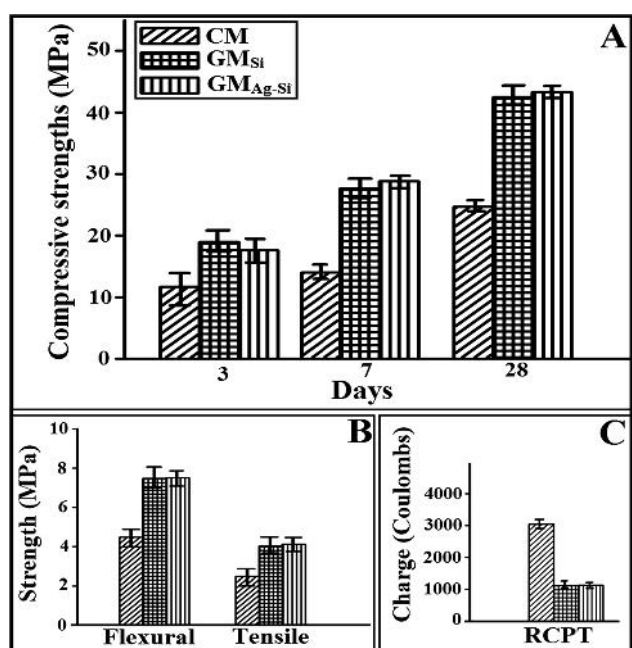


Fig. 3 (A) Compressive strengths, (B) flexural & tensile strengths, (C) RCPT of different mortar samples (CM, GM<sub>Si</sub> & GM<sub>Ag-Si</sub>).

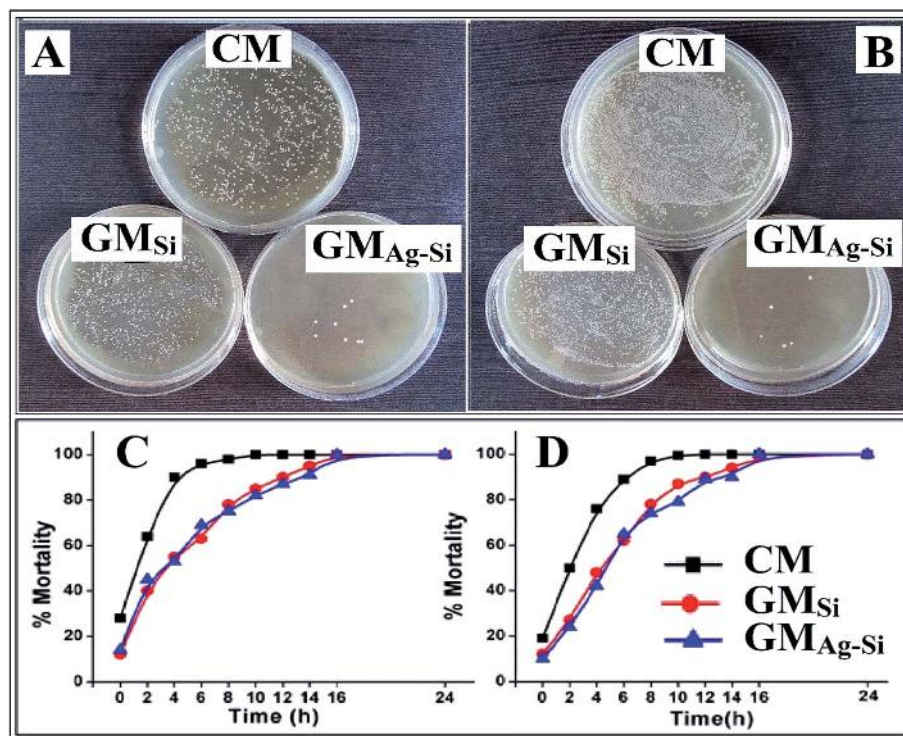


Fig. 4 Photographs of colonies of (A) *E. coli* & (B) *S. aureus* incubated on agar plates obtained from cultivated suspensions with (CM,  $GM_{Si}$  &  $GM_{Ag-Si}$ ). Mortality curve of (C) Gram -ve bacteria (D) Gram +ve bacteria in presence of CM,  $GM_{Si}$  &  $GM_{Ag-Si}$ .

Table 3 MIC assay

Bacteria	Control ( $mg\ ml^{-1}$ )	$GM_{Si}$ ( $mg\ ml^{-1}$ )	$GM_{Ag-Si}$ ( $mg\ ml^{-1}$ )
<i>E. coli</i>	—	—	0.10
<i>S. aureus</i>	—	—	0.15

Table 4 MBC assay

Bacteria	Control ( $mg\ ml^{-1}$ )	$GM_{Si}$ ( $mg\ ml^{-1}$ )	$GM_{Ag-Si}$ ( $mg\ ml^{-1}$ )
<i>E. coli</i>	—	—	0.32
<i>S. aureus</i>	—	—	0.43

and lane-5. The  $GM_{Ag-Si}$  treated DNA was fragmented in lane-3, lane-6.

The SYBR Green is a bacterial cell membrane permeant dye which stains both live and dead cells. The fluorescence microscopic images show that control cells and  $GM_{Si}$  treated cells (*E. coli* and *S. aureus*) are intensely stained with SYBR Green whereas  $GM_{Ag-Si}$  treated cells are found to be PI positive (Fig. 6). The PI is an impermeant dye that stains only dead and membrane compromised cells due to loss of the plasma membrane integrity. The result of morphological analysis of  $GM_{Ag-Si}$  treated cells represents extensive membrane destruction and disruption of cells after 8 h of incubation (Fig. 7C) in respect to control and  $GM_{Si}$  treated *E. coli* cells (Fig. 7A and B)

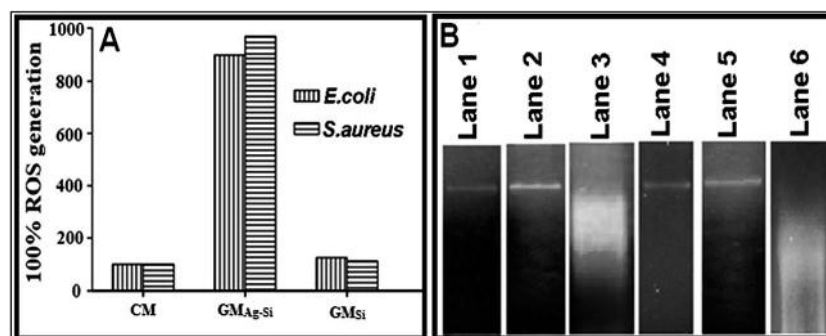


Fig. 5 ROS count of (A) different samples and (B) gel electrophoresis images (lane-1) CM treated DNA (*E. coli*), (lane-2)  $GM_{Si}$  treated DNA (*E. coli*), (lane-3)  $GM_{Ag-Si}$  treated (*E. coli*), (lane-4) CM treated DNA (*S. aureus*), (lane-5)  $GM_{Si}$  treated DNA (*S. aureus*), (lane-6)  $GM_{Ag-Si}$  treated DNA (*S. aureus*).

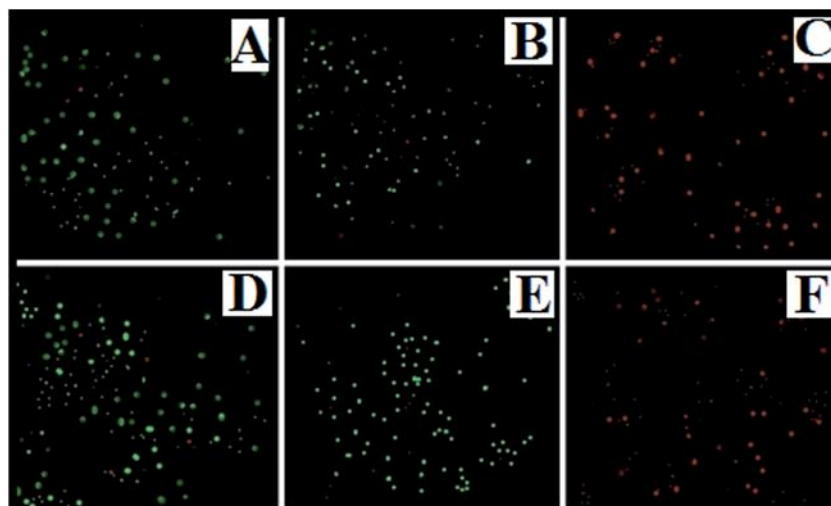


Fig. 6 Fluorescence microscopic images of (A) CM treated *E. coli*, (B)  $\text{GM}_{\text{Si}}$  treated *E. coli*, (C)  $\text{GM}_{\text{Ag-Si}}$  treated *E. coli*, (D) CM treated *S. aureus*, (E)  $\text{GM}_{\text{Si}}$  treated *S. aureus*, (F)  $\text{GM}_{\text{Ag-Si}}$  treated *S. aureus* bacterial cells.

respectively. Control and  $\text{GM}_{\text{Si}}$  treated cells shows distinct spherical morphology of coccus shaped *S. aureus* (Fig. 7D and E respectively), whereas membrane deformation and pore formation can be seen along with cell debris in case of  $\text{GM}_{\text{Ag-Si}}$  treated cells (Fig. 7F).

## 4. Discussion

In this present study, the silver NPs (2–5 nm) has been attached on the surface of silica NPs of 30–50 nm (Fig. 1B) to develop the antimicrobial activity of the geopolymer mortar. In presence of positively charged silver NPs on the surface of the negatively charged silica NPs, the overall charges of silver–silica nano-composite (Fig. 1C-II) is reduced. The incorporation of this newly formed silver NPs in the low calcium fly-ash based geopolymer mortar has improved its anti-bacterial property.

However, the strength and durability do not affected due to the presence of such silver NPs in geopolymer mortar cured at ambient temperature. The strength and durability of geopolymer mortar ( $\text{GM}_{\text{Ag-Si}}$ ) is not affected by the presence of silver NPs (Fig. 3). The silver has the potential to kill bacteria in minimum time period.<sup>29,35</sup> The different bacterial cell wall disruptions (Fig. 7) indicate that the anti-bacterial property has been developed in desired geopolymer mortar. Silver–silica nano composite having 6% by weight of fly ash in geopolymer mortar was sufficient to resist the bacterial growth. The growth for both types of bacteria (Gram –ve/Gram +ve) was stopped within 6–8 h only in presence of silver NPs modified  $\text{GM}_{\text{Ag-Si}}$  geopolymer mortar. Bacterial growth population in general depends on numerous external factors like pH, temperature, concentration of nano-particles.<sup>36,37</sup> In various studies, it is reported that due to the high alkali property of fresh concrete/

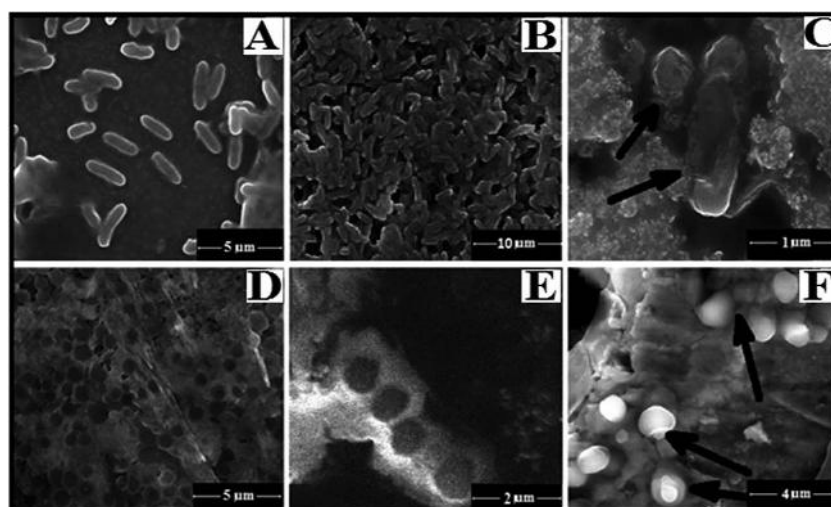


Fig. 7 FESEM images of (A) CM treated *E. coli*, (B)  $\text{GM}_{\text{Si}}$  treated *E. coli*, (C)  $\text{GM}_{\text{Ag-Si}}$  treated *E. coli*, (D) CM treated *S. aureus*, (E)  $\text{GM}_{\text{Si}}$  treated *S. aureus* and (F)  $\text{GM}_{\text{Ag-Si}}$  treated *S. aureus*.

mortar at early age, it will not allow any bacterial growth. However, the pH of concrete/mortar is slowly reduced over time by the effect of carbon dioxide and hydrogen sulfide gas and growth of bacteria starts.

Silver silica nano composite modified geopolymer mortar shows better resistance to bacterial attack than nano silica modified geopolymer and control samples. Silver nano particles incapacitate enzymes through binding of sulfhydryl (thiol) groups in amino acids of bacterial cell and promote the release of ions/NPs with subsequent hydroxyl radical formation.<sup>38,39</sup> Gram-negative bacteria possess an outer membrane outside the peptidoglycan layer which is absent in Gram-positive organisms.<sup>40</sup> The outer membrane protects bacteria from harmful agents, such as detergents, drugs, toxins and degradative enzymes by functioning as selective permeability barrier. The cell wall disruption by the lower amount of silver NPs in geopolymer particle (~MIC) may be the main reason of bactericidal kinetics. Farther, the unfavorable intracellular ROS generation also facilitates to destroy these bacteria by biological targeting of DNA, RNA, proteins and lipids. Initiation of lipid peroxidation *via* damage of membrane poly unsaturated fatty acids was caused by free radical generation.

The effect of silver NPs on bacteria is observed by the structural and morphological changes (Fig. 7). It is suggested that in undisturbed state, the replication of DNA can be effectively conducted and loses its replication ability in that form. The DNA molecule turns into condensed form and loses its replication ability when the presence of silver ions/NPs within the bacterial cell, leading to cell death.<sup>41</sup> The DNA damage images (Fig. 5B) are also correlated with the previously reported discussion.

The influence of lipid peroxidation process shrinks the membrane fluidity through alteration membrane properties and can disrupt membrane-bound proteins significantly.<sup>42</sup> In contact of silver NPs, DNA was completely destroyed and fragmented (Fig. 5B). The activity of the silver NPs was extremely detrimental for DNA molecules by breaking its double helical structure. DNA loses its replication ability and cellular proteins become inactivated on silver NPs treatment.<sup>41</sup>

## 5. Conclusion

It may be concluded that low calcium fly ash based silica modified geopolymer mortar cured at room temperature shows almost similar strength and durability but better anti-bacterial property. Silver-silica modified geopolymer mortar demonstrates better anti-bacterial property than conventional cement mortar and silica modified geopolymer mortar. Due to positive charge, silver NPs in the liquid growth medium are attracted electrostatically to the negatively charged cell wall of bacteria. A few oxidized silver ions/NPs also get attached electrostatically to the bacterial membrane and thus decreases the osmotic stability of the cell, trailed by consequent leakage of intracellular constituents. The anti-bacterial activity of GM<sub>Ag-Si</sub> was developed by introducing silver NPs on the surface of silica NPs which is the main ingredients for anti-bacterial activity of geopolymer mortar. It is an ecofriendly,

non-hazard, cost effective and more durable building materials which can show the new hope for better green construction technology.

## Reference

- 1 P. K. Mehta, *Concr. Int.*, 2001, **23**(10), 61–66.
- 2 C. Heidrich, F. H. Joachim and W. Anne, *World of Coal Ash (WOCA) Conference*, Lexington, 2013.
- 3 J. Davidovits, *J. Therm. Anal.*, 1991, **37**, 1633–1656.
- 4 D. Hardjito, S. E. Wallah, V. Rangan and B. V. Rangan, *Aust. J. Struct. Eng.*, 2005, **6**, 1–9.
- 5 J. A. Fernandez, M. Monzo, M. V. Cabedo, A. Barba and A. Palamo, *Microporous Mesoporous Mater.*, 2008, **108**, 41–49.
- 6 Z. Xie and Y. Xi, *Cem. Concr. Res.*, 2001, **31**, 1245–1249.
- 7 P. Chindaprasirt, T. Chareerat and V. Sirivivatnanon, *Cem. Concr. Compos.*, 2007, **29**, 224–229.
- 8 S. Pangdaeng, T. Phoo-ngernkham, V. Sata and P. Chindaprasirt, *Mater. Des.*, 2014, **53**, 269–274.
- 9 M. S. Villarreal, A. M. Ramírez, S. S. Bulbarelaa, J. R. Gasca-Tirado, J. L. Reyes-Araiza and J. C. Rubio-Avalos, *Mater. Lett.*, 2011, **65**, 995–998.
- 10 G. Gorhan and G. Kurklu, *Composites, Part B*, 2014, **58**, 371–377.
- 11 F. F. V. Barbosa, J. D. K. Mackenzie and C. Thaumaturgo, *Int. J. Inorg. Mater.*, 2000, 309–317.
- 12 J. Temuujin, R. P. Williams and A. van Riessen, *J. Mater. Process. Technol.*, 2009, **209**, 5276–5280.
- 13 P. S. Deb, P. Nath and P. K. Sarkar, *Adv. Mater. Res.*, 2013, **05**, 168–173.
- 14 H. M. Giasuddin, G. Sanjayan and P. G. Ranjith, *Fuel*, 2013, **07**, 34–39.
- 15 D. Adak, M. Sarkar and S. Mandal, *Construct. Build. Mater.*, 2014, **70**, 453–459.
- 16 Con Shield: Technical presentation, Florida, Orlando, 1998.
- 17 H. Viitanen, J. Vinha and K. Salminen, *J. Build. Phys.*, 2010, **33**, 201–224.
- 18 A. K. Parande, P. L. Ramsamy, S. Ethirajan, C. R. K. Rao and N. Palanisamy, *Proc. Inst. Civ. Eng. Municip. Eng.*, 2006, **159**, 11–20.
- 19 M. Sanchez-Silva and D. Rosowsky, *J. Mater. Civ. Eng.*, 2008, **20**, 352–365.
- 20 A. Panáček, L. Kvítek, R. Prucek, M. Kolář, R. Večeřová, N. Pizúrová, V. K. Sharma, T. Nevěčná and R. Zbořil, *J. Phys. Chem. B*, 2006, **110**, 16248–16253.
- 21 J. R. Morones, J. L. Elechiguerra, A. Camacho, K. Holt, J. B. Kouri, J. T. Ramirez and M. J. Yacaman, *Nanotechnology*, 2005, **16**, 2346–2353.
- 22 ASTM C618–12a, *Standard Specification for Coal Fly Ash and Raw or Calcined Natural Pozzolan for Use in Concrete*, ASTM International, West Conshohocken, PA, 2012.
- 23 D. Adak and S. Mandal, *Indian Concr. J.*, 2015, **89**, 31–40.
- 24 V. Pol, D. N. Srivastava, O. Palchik, V. Palchik, M. A. Slifkin and A. M. Weiss, *Langmuir*, 2002, **18**, 3352–3357.
- 25 M. Sarkar, T. Chowdhury, B. Chattopadhyay, R. Gachhui and S. Mandal, *J. Mater. Sci.*, 2014, **49**, 4461–4468.



- 26 ASTM C293–10, *Standard Test Method for Flexural Strength of Concrete (Using Simple Beam with Center-Point Loading)*, ASTM International, West Conshohocken, PA, 2010.
- 27 ASTM C1202–12, *Standard Test Method for Electrical Indication of Concrete's Ability to Resist Chloride Ion Penetration*, ASTM International, West Conshohocken, PA, 2012.
- 28 L. Qi, Z. Xu, X. Jiang, C. Hu and X. Zou, *Carbohydr. Res.*, 2004, **339**, 2693–2700.
- 29 J. Ruparelia, A. Chatterjee, S. P. Duttagupta and S. Mukherji, *Acta Biomater.*, 2008, **4**, 707–716.
- 30 G. Ren, D. Hu, C. Cheng, M. A. Vargas-Reus, P. Reip and R. P. Allaker, *Int. J. Antimicrob. Agents*, 2009, **33**, 587–590.
- 31 M. R. Avadia, A. M. M. Sadeghib, A. Tahzibic, Kh. Bayati, M. Pouladzadeh, Z. Mehr and M. R. Thehrani, *Eur. Polym. J.*, 2004, **40**, 1355–1361.
- 32 H. L. Su, C. C. Chou, D. J. Hung, S. H. Lin, I. C. Pao, J. H. Lin, F. L. Huang, R. X. Dong and J. J. Lin, *Biomaterials*, 2009, **30**, 5979–5987.
- 33 S. A. Shoichet, A. T. Bäumer, D. Stamenkovic, H. Sauer, A. F. Pfeiffer, C. R. Kahn, D. M. Wieland, C. Richter and M. Ristow, *Hum. Mol. Genet.*, 2002, **11**, 815–821.
- 34 S. Barbesti, S. Citterio, M. Labra, M. D. Baroni, M. G. Neri and S. Sgorbati, *Cytometry*, 2000, **40**, 214–218.
- 35 S. Agnihotri, S. Mukherji and S. Mukherji, *RSC Adv.*, 2014, **4**, 3974–3983.
- 36 J. S. Kim, E. Kuk and K. N. Yu, *Nanomedicine*, 2007, **3**, 95–101.
- 37 F. Rispoli, A. Angelov, D. Badia, A. Kumar, S. Seal and V. Shah, *J. Hazard. Mater.*, 2010, **180**, 212–216.
- 38 M. R. Yeaman and N. Y. Yount, *Pharmacol. Rev.*, 2003, **55**, 27–55.
- 39 N. A. Amro, L. P. Kotra, K. W. Mesthrige, A. Bulychev, S. Mobashery and G. Liu, *Langmuir*, 2000, **16**, 2789–2796.
- 40 H. Nikaido, *Microbiol. Mol. Biol. Rev.*, 2003, **67**, 593–656.
- 41 Q. L. Feng, J. Wu, G. Q. Chen, F. Z. Cui, T. N. Kim and J. O. Kim, *J. Biomed. Mater. Res.*, 2000, **52**, 662–668.
- 42 E. Cabisco, J. Tamarit and J. Ros, *Int. Microbiol.*, 2000, **3**(1), 3–8.



# ICJ



June 2015, Vol. 89, No. 6, Rs. 100. 72 pages.

THE INDIAN CONCRETE JOURNAL

PUBLISHED BY ACC LIMITED



# Study on the modified process for the development of fly ash based geopolymer mortar cured at ambient temperature

Dibyendu Adak and Saroj Mandal

Geopolymer, a novel class of inorganic polymer emerged as one of the most powerful alternative to make environmental friendly concrete. Most of the previous studies in literature are based on heat curing at elevated temperatures to demonstrate the properties of alkali activated geopolymer concrete/mortar. However, such heat curing at elevated temperature possesses a practical problem for the use of geopolymer concrete/mortar. This paper investigates a modified geopolymer process (Process -I) in which heat activation of fly ash and activator fluid mixture has been made before casting. The mechanical strength and durability behaviour of this modified geopolymer mortar have been compared to that of general heat activation process (Process -II) in which the heat activation has been made after casting. Geopolymer mortar made by Process -I shows better strength and durability than Processes -II geopolymer mortar at different fluid to fly ash ratio (0.35, 0.40, 0.45). In Process-I geopolymer mortar, fly ash is more uniformly polymerised within whole matrix than Process-II geopolymer mortar as per FESEM analysis. EDS and XRD analysis also confirms the presence more crystalline compound in Process-I geopolymer mortar than process-II geopolymer mortar. Finally, an economical benefit for the Process-I in terms of energy savings and practical application has been presented.

**Keywords:** *Geopolymer; heat activation, mechanical strength; FESEM (field emission scanning electron microscopy); EDS (energy dispersive spectroscopy).*

## 1. INTRODUCTION

Demand for concrete as a construction material is rapidly increasing due to the development of civilization, economic progress and stability of the quality of life. In order to address environmental effects associated with Portland cement, there is an urgent need to develop alternative binders to make concrete. Geopolymer technology is one of revolutionary development related to novel material as an alternative to Portland cement [1-3]. Development of geopolymer concrete is an important area of research because low-calcium fly ash-based geopolymer concrete has excellent physical and mechanical strength [4-9]. Also

it is reported that geopolymer is a cost effective and environment friendly material [10-13].

Geopolymer is an inorganic alumino-silicate polymer synthesized from alkaline activation of various alumino-silicate materials of geological origin or by product materials like fly ash, metakaolin, blast furnace slag etc. [14, 15]. To accelerate the polymerization process heat activation is in general needed for development of physical and mechanical properties of geopolymer concrete [16-20]. The scope of geopolymer concrete is limited to the precast member due to requirement of heat activation after casting. Most of the studies on fly ash

based geopolymer concrete are mainly associated with Process-II (Refer. Figure 1) where the samples are being activated for a specific period at a specific temperature after casting the structural members [21-23]. There are limited literatures available on geopolymer concrete/ mortar cured at ambient temperature [24-26].

A modified process (Process-I) has been developed for the practical use of fly ash based geopolymer concrete/ mortar. The effect of different fluid /fly ash ratios of 0.35, 0.4 and 0.45 has been considered. Mechanical strength (compressive strength, flexural strength and tensile strength) and durability (water absorption, sulphate attack and RCPT test) of mortar samples have been

compared between two processes. The microstructure study in terms of FESEM, EDS and XRD analysis has also been made for the samples of two such processes. It is concluded that that Process-I is more economical in terms of strength, durability and energy consumption than the conventional method (Process-II).

## 2. MATERIAL & METHODS

### 2.1 Materials

Low Calcium Class F (American Society for Testing and Materials 2001) dry fly ash obtained from National Thermal Power Corporation Ltd, Farakka plant in India has been used as the base material. The properties of

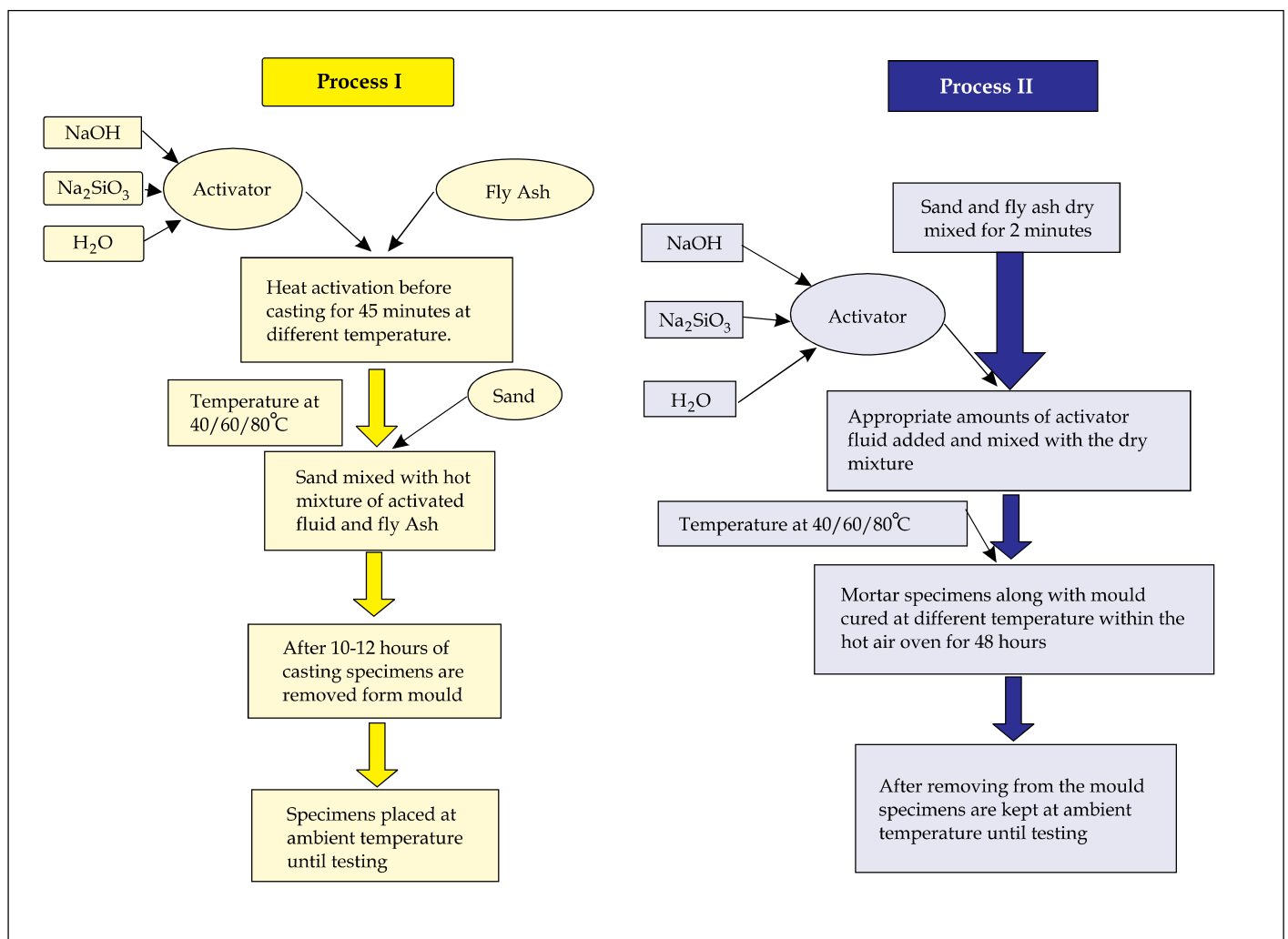


Figure 1. Details of process-I and process-II

**Table 1. Chemical analysis report of fly ash**

Material	Chemical composition (in percentage)								
	SiO <sub>2</sub>	Al <sub>2</sub> O <sub>3</sub>	Fe <sub>2</sub> O <sub>3</sub>	CaO	MgO	Na <sub>2</sub> O	K <sub>2</sub> O	SO <sub>4</sub>	LOI
Fly Ash	64.97	26.64	5.69	0.33	0.85	0.49	0.33	0.25	0.45

**Table 2. Physical analysis report of fly ash**

Material	Particle size distribution						
	>500μ	300-500μ	150-300μ	150-90μ	90-45μ	< 45μ	Specific gravity
Fly ash	NIL	1.42	11.67	48.06	31.98	6.87	2.05

fly ash and the grain size distribution are presented in Tables 1 and 2 respectively. The activator solution consists of sodium hydroxide (NaOH) and sodium silicate (Na<sub>2</sub>SiO<sub>3</sub>). The sodium hydroxide is the commercial grade in pellet forms with 99% purity and white in colour. Liquid sodium silicate is also a commercial grade having 45% solid content and specific gravity of 1.53 g/cc. It is light grey in colour and highly viscous.

**2.2 Mix proportion and different process of polymerisation**

8(M) NaOH was mixed with Na<sub>2</sub>SiO<sub>3</sub> solution in the proportion of 1:1.75 (by weight) to make alkali activated fluid. Locally available river sand (Specific gravity 2.52, water absorption 0.50%, and fineness modulus of 2.38) was used for the present study. The ratio of fly ash: sand was fixed at 1:3 (by weight). Three different activator fluids to fly ash ratio of 0.35, 0.40 and 0.45 were considered in two processes of geopolymer mortar.

In Process-I (Refer. Figure 1), fly ash was mixed with appropriate quantity of activated fluid and stirred in a hot air oven for 45 minutes at different temperatures of 40°C, 60°C and 80°C. River sand was immediately mixed with the hot mixture of activated fluid and fly ash thoroughly for two minutes. The different specimens were cast with the above geopolymer mortar mixture. Finally, the mortar specimens were removed from the mould after 10-12 hours of casting and were placed at ambient temperature (27± 20 °C) until testing.

In Process-II (Refer Figure 1), sand and fly ash was dry mixed for 2 minutes and the appropriate quantity of activator fluid was added and mixed thoroughly at

**Table 3. Mix proportion for different process (process-I and processes-II)**

Mix no.	Fluid : fly ash	Process type	Temperature, °C	Heat curing process
G1	0.35	Process-I	40	Heat curing of fly ash and activated fluid for 45 minutes before casting at different temperatures.
G2			60	
G3			80	
G4	0.35	Process-II	40	Heat curing of samples after casting for 48 hours at different temperatures.
G5			60	
G6			80	
G7	0.40	Process-I	40	Heat curing of fly ash and activated fluid for 45 minutes before casting at different temperatures.
G8			60	
G9			80	
G10	0.40	Process-II	40	Heat curing of samples after casting for 48 hours at different temperatures.
G11			60	
G12			80	
G13	0.45	Process-I	40	Heat curing of fly ash and activated fluid for 45 minutes before casting at different temperatures.
G14			60	
G15			80	
G16	0.45	Process-II	40	Heat curing of samples after casting for 48 hours at different temperatures.
G17			60	
G18			80	

ambient laboratory temperature. The different specimens were cast with the geopolymer mortar. After one hour, the mortar specimens along with the mould were cured at three different temperatures of 40°C, 60°C and 80°C within the hot air oven for 48 hours. Finally, the specimens were kept at ambient temperature after removing from the mould until testing. The details of all the mixtures are shown in Table 3.

### 2.3 Sample preparation

For each processes, 99 numbers of mortar cubes (70.7 mm x 70.7 mm x 70.7 mm), 27 numbers of bar (50 mm x 50 mm x 200 mm) and 27 numbers of cylinders (100 mm diameter x 200 mm height) were cast for different mixes. Compressive strength of the mortar cubes was determined at 3 days, 7 days and 28 days. Flexural strength on mortar bar and tensile strength on cylinders were determined at 28 days for the different mixes. All strength values are based on the average of three specimens. For chloride ion penetration test, cylinder specimen was sliced into core specimen of thickness 50 mm at the age of 28 days for all the mixes. The sliced specimens were then subjected to RCPT by impressing 60V. Cube specimen having fluid to fly ash ratio of 0.35 were immersed in water for 30 minutes and 24 hours for water absorption test. Also cube specimens were immersed in sulphate solution for one month for sulphate test. For FESEM (Field Emission

Scanning Electron Microscopy) analysis, EDS (Energy dispersive spectroscopy) and XRD (X-ray Diffraction test) analysis, the broken samples of maximum compressive strength at 28-day for both process (Process-I and Process-II) were dried and sieved to make the size less than 5 µm. Fine powder was diluted with ethanol (99.9%) to make a film on carbon tape and then kept under vacuum desiccators for evaporation. Finally, the dried samples were gold coated for FESEM and EDS analysis. For X-ray diffraction analysis in powder X-ray diffractometer with a scan speed 0.5 s/step at 40 KV. The XRD spectrum was analysed in the range  $2\theta = 10^\circ$  to  $2\theta = 70^\circ$  and the peak positions were marked and compared from JCPDS file.

## 3. RESULTS AND DISCUSSION

### 3.1 Compressive Strength, FESEM, EDS and XRD analysis

Figure 2 shows the compressive strength of fly ash based geopolymer mortar for both Process-I and II having fluid to fly ash ratio 0.35 at 3 days, 7 days and 28 days. Similar test results are presented in Figures 3 and 4 for fluid to fly ash ratio of 0.40 and 0.45 respectively. It is noted that at all fluid to fly ash ratio, the geopolymer mortars under Process-I show substantially higher compressive strength than similar mortar under Process-II at all ages up to 28 days.

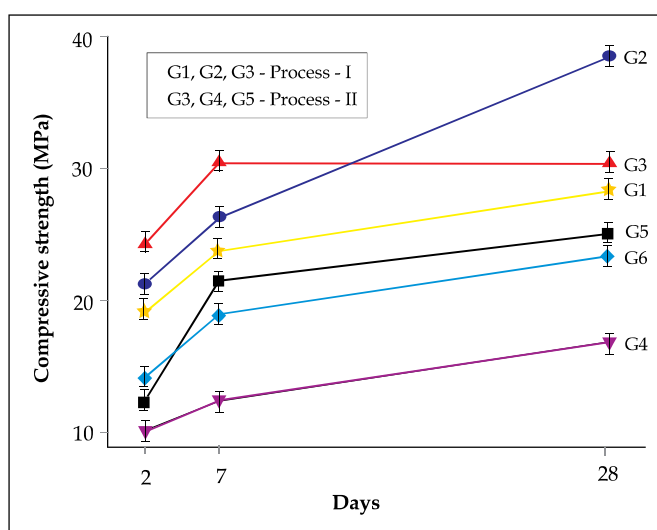


Figure 2. Compressive strength of geopolymer mortar at fluid/ Fly ash ratio 0.35 in process-I and process-II.

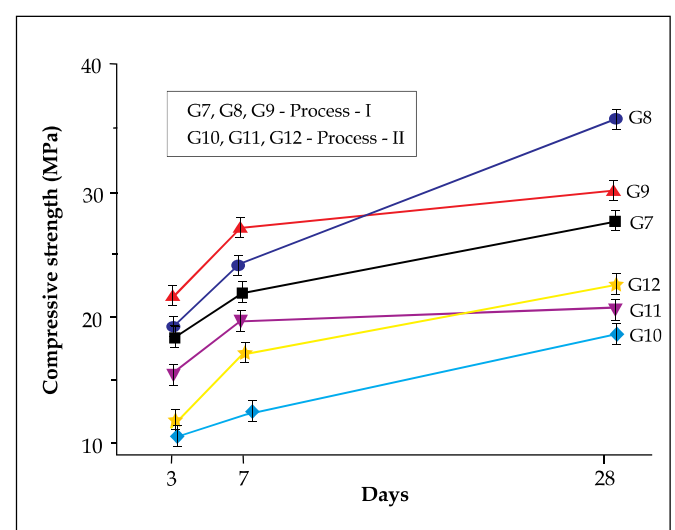


Figure 3. Compressive strength of geopolymer mortar at fluid/ fly ash ratio 0.40 in process-I and process-II.

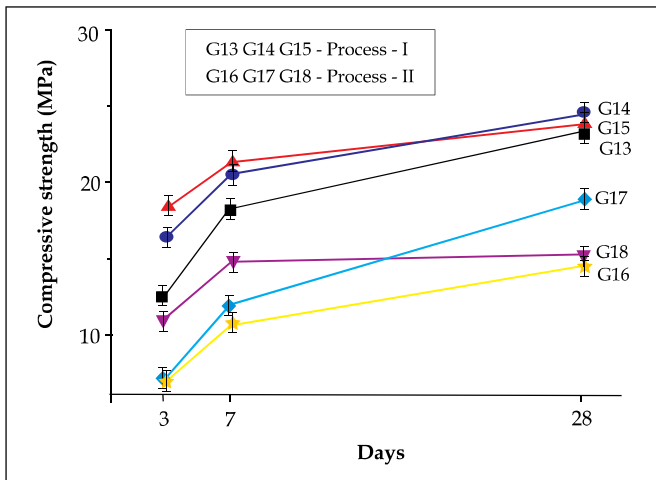


Figure 4. Compressive strength of geopolymer mortar at fluid/ fly ash ratio 0.45 in process-I and process-II.

In Process-I, the maximum compressive strength of geopolymer mortar developed at an optimum temperature of 60°C at 28 days and it is higher than that of Process-II. It may be concluded that the mix G2 provides maximum compressive strength at 28 days at ambient temperature curing after casting.

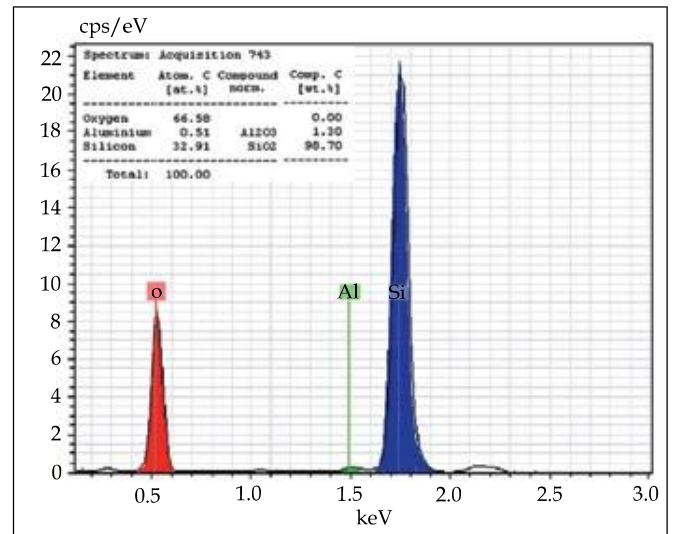


Figure 6. EDS analysis of process I geopolymer mortar

It is observed from FESEM images that in Process-I, polymerisation of fly ash is more uniform within whole matrix than Process-II as shown in Figure 5. From EDS analysis the presence silica compound in Process-I and Process-II is 98.87% and 81.12% respectively (Figures 6 and 7). In Process-I geopolymer mortar, some specific extra peak positions are noted in XRD analysis due to transformation of amorphous to crystalline compound.

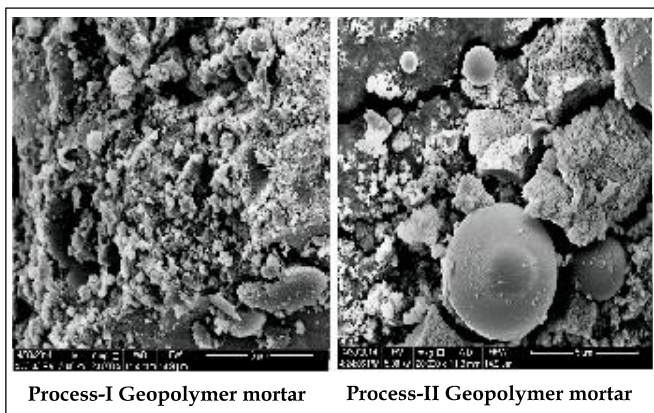


Figure 5. FESEM image of process I and process II geopolymer mortar

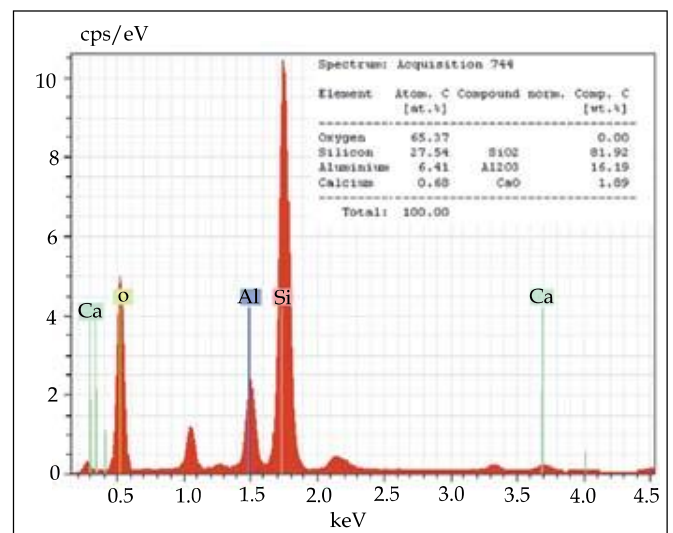


Figure 7. EDS analysis of process II geopolymer mortar



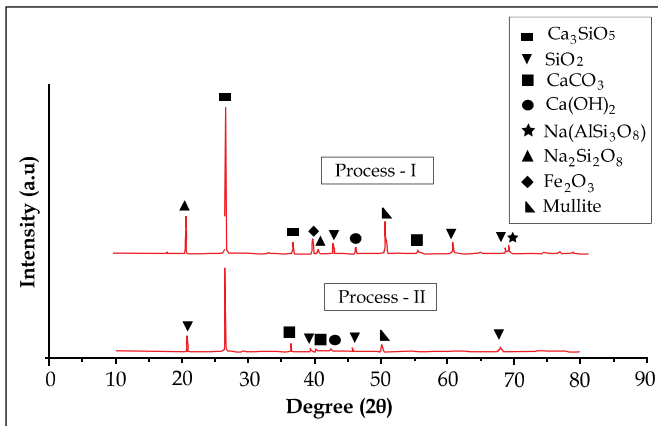


Figure 8. XRD analysis report of fly ash based geopolymer mortar samples of process-I and process-II at fluid/fly ash ratio 0.35

It also confirms the formation of new phase crystalline compounds in Process I in the form of SiO<sub>2</sub>, Ca<sub>3</sub>SiO<sub>5</sub>, Na(AlSi<sub>3</sub>O<sub>8</sub>), Na<sub>2</sub>Si<sub>2</sub>O<sub>8</sub>, CaCO<sub>3</sub>, Fe<sub>2</sub>O<sub>3</sub> and mullite is more (in terms of peak) than Process-II geopolymer mortar as shown in Figure 8.

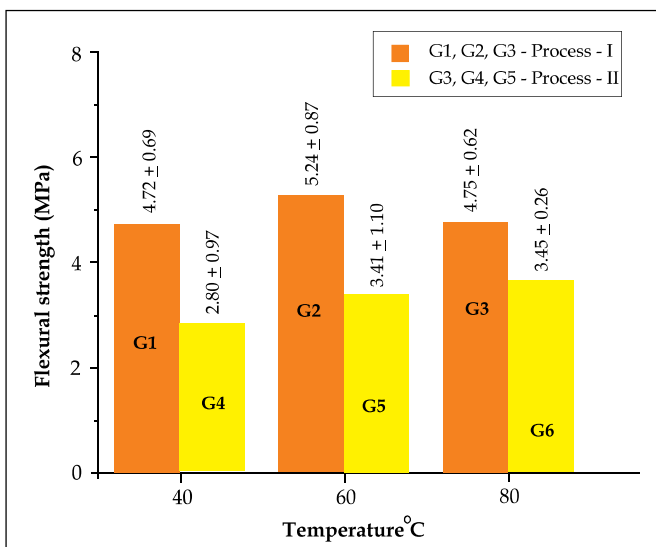


Figure 9. Flexural strength of geopolymer mortar at fluid/ fly ash ratio 0.35 in process-I and process-II.

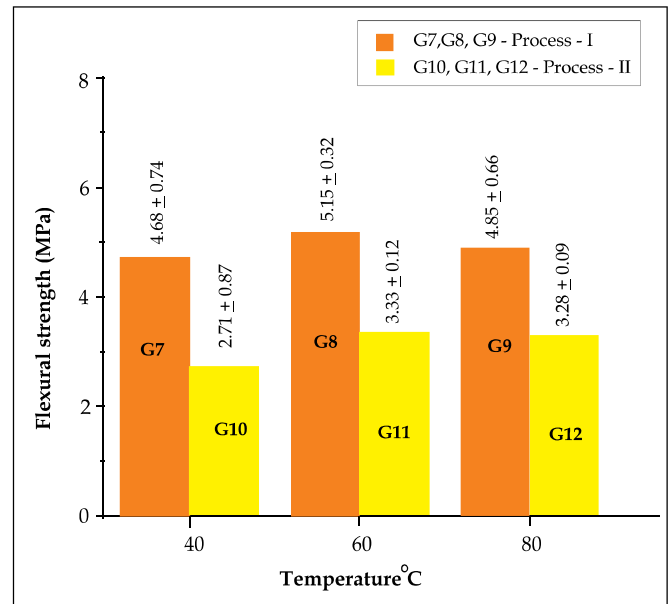


Figure 10. Flexural strength of geopolymer mortar at fluid/ fly ash ratio 0.40 in process I and process II.

### 3.2 Flexural strength and split tensile strength

Figures 9, 10 and 11 show the flexural strength of Process-I geopolymer and Process-II geopolymer mortar specimens of fluid to fly ash ratio 0.35, 0.40 and 0.45 at

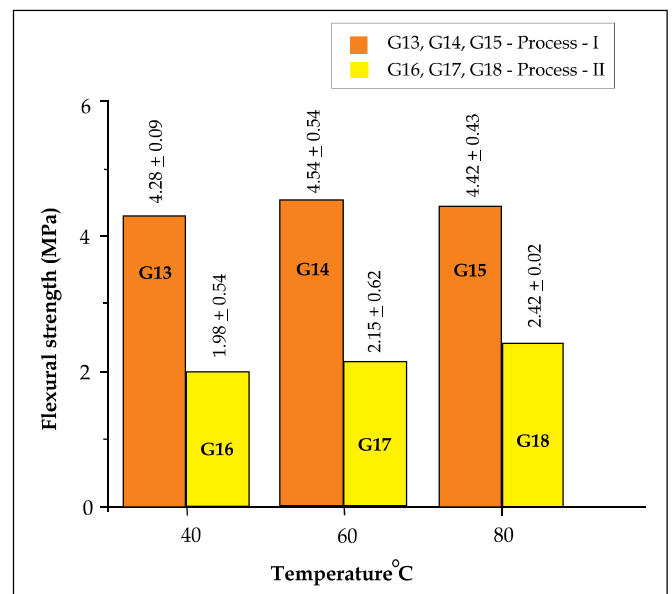


Figure 11. Flexural strength of geopolymer mortar at fluid/ fly ash ratio 0.45 in process I and process II.

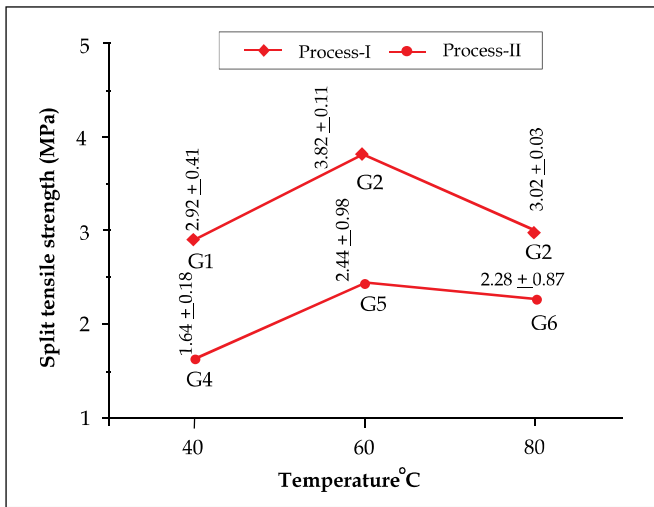


Figure 12. Split tensile strength of geopolymer mortar at fluid/ fly ash ratio 0.35 in process I and process II

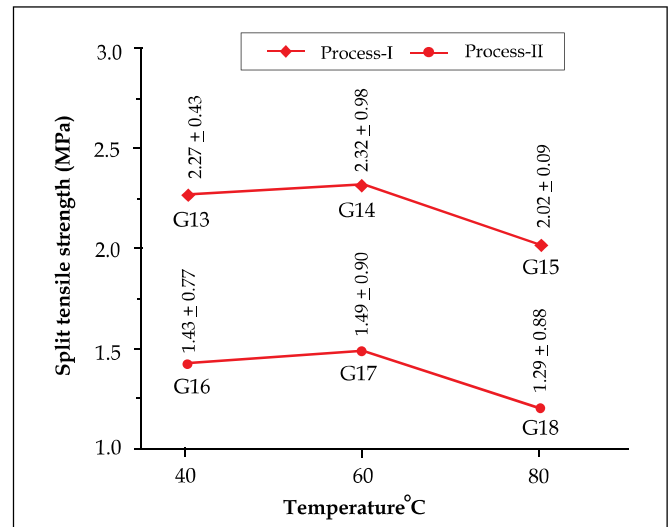


Figure 14. Split tensile strength of geopolymer mortar at fluid/ fly ash ratio 0.45 in process I and process II.

28 days. Similarly Figure 12, 13 and 14 show the split tensile strength of Process-I geopolymer and Process-II geopolymer mortar specimens at 28 days. It is observed that Process-I geopolymer mortar shows better flexural and split tensile strength than that of Process-II mainly due formation of more crystalline compound and uniform polymerisation of fly ash.

### 3.3 RCPT result analysis

The results of RCPT value for both Process-I and Process-II geopolymer mortar samples (28 days) are shown in Figure 15, 16 and 17 for different fluid to fly ash ratio. It may be mentioned here that as the concentration of NaOH in the samples remain same, the difference in RCPT values for two processes may be compared. The amount

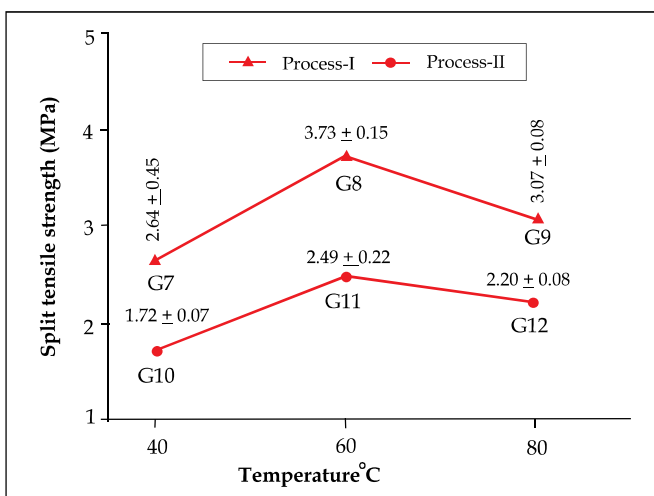


Figure 13. Split tensile strength of geopolymer mortar at fluid/ fly ash ratio 0.40 in process I and process II.

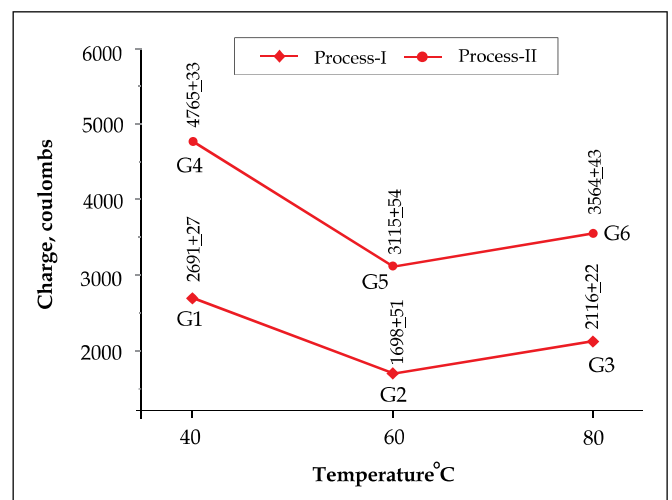


Figure 15. Charge passed through geopolymer mortar at fluid/ fly ash ratio 0.35 in process I and process II.

of charge passing through Process-I geopolymer mortar is comparatively less than that of Process-II geopolymer mortar. This indicates that the diffusion coefficient will be less due to presence of more amount of crystalline compound in modified Process-I geopolymer mortar thereby improving the durability.

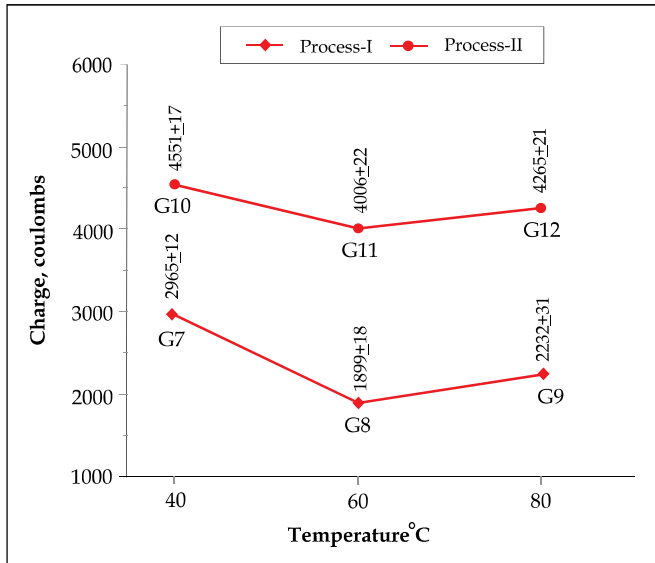


Figure 16. Charge passed through geopolymer mortar at fluid/ fly ash ratio 0.40 in process I and process II.

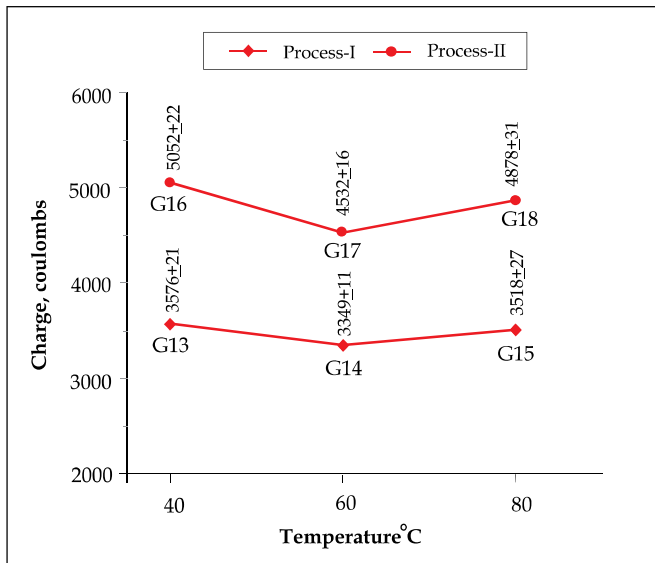


Figure 17. Charge passed through geopolymer mortar at fluid/ fly ash ratio 0.45 in process I and process II.

### 3.4 Water absorption and sulphate test

Table 4 shows saturated water absorption of geopolymer cube specimens after immersion in water for 30 minutes and 24 hours. Similarly sulphate test results of geopolymer mortar are shown in Table 5 after immersion of specimen in sulphate solution for one month. It indicates lesser water absorption and sulphate attack (in terms of weight gain) in Process-I geopolymer mortar compared to Process-II geopolymer mortar due to better pore structure modification.

### 4. ECONOMICAL BENEFIT

A comparison of electrical energy required for heat curing of geopolymer mortar in two different processes are made assuming other requirements are almost same. In Process -I the mixture is heated only for 45 minutes compared to that of Process II where the specimens are heated for 48 hours. The calculated energy requirement for Process-I and Process-II are 1.5 kWh and 98 kWh respectively.

Table 4. Water absorption test results of geopolymer mortar samples in process I & II (fluid/fly ash = 0.35)

Mix no.	Initial average mass (gm.)	Average mass after 30 min (gm.)	% increment	Average mass after 24 hours (gm.)	% increment
G1	731.6	749.5	2.39	785.6	4.60
G2	720.9	735.8	2.02	751.6	2.10
G3	728.6	739.3	1.44	762.9	3.10
G4	729.7	754.6	3.30	793.2	4.87
G5	733.7	756.3	3.00	781.6	3.26
G6	720.3	739.3	2.56	767.3	3.65

Table 5. Sulphate test results of geopolymer mortar samples in process I & II (fluid/fly ash = 0.35)

Mix no.	Initial average mass (gm.)	Average mass after sulphate attack (gm.)	% increment
G1	731.6	766.3	4.53
G2	720.9	745.3	3.28
G3	728.6	774.0	5.86
G4	729.7	766.3	4.78
G5	733.7	764.0	3.97
G6	720.3	758.7	5.05

Therefore, about 98% of less energy is required for Process-I than Process-II for heat activation only.

## 5. CONCLUSION

Based on the experimental study, it is concluded that the strength and the durability of geopolymer mortar in Process-I is higher than that of Process-II. This improvement is mainly due to the uniform polymerisation of fly ash and formation of crystalline compound as per FESEM micrographs. The presence of more amount of silica compound in the Process-I geopolymer matrix as per EDS analysis also confirms such improvements. XRD analysis results confirmed the formation of new phase crystalline compound in the form of  $\text{SiO}_2$ ,  $\text{Ca}_3\text{SiO}_5$ ,  $\text{Na}(\text{AlSi}_3\text{O}_8)$ ,  $\text{Na}_2\text{Si}_2\text{O}_7$ ,  $\text{CaCO}_3$ ,  $\text{Fe}_2\text{O}_3$  and mullite. The demoulding time of specimens after casting in Process-I is comparatively less (about 1/3 times) than that of Process-II. Therefore, Process-I geopolymer mortar can be used in practical construction in terms of strength, durability and energy savings.

## References

1. A. Kirschne, H. Harmuth (2004), "Investigation of geopolymer binders with respect to their application for building materials", *Ceramic-Silikaty*, 48, 3.
2. H.C. Wu, P. Sun (2007), "New building materials from fly ash-based lightweight inorganic polymer", *Construction and Building Materials*, 21, 1.
3. M. C. G. Juenger, F. Winnefeld, J. L. Provis, and J. H. Idekerd (2011), "Advances in alternative cementations binders", *Cement and Concrete Research*, 41, 12.
4. D. Khale, R. Chaudhary (2007), "A review: Mechanism of geopolymerization and factors influencing its development", *Journal of Materials Science*, 42 (3), 729-746.
5. F. P. Torgal, J. C. Gomes, and S. Jalali (2008), "Alkali-activated binders: A review. Part 2. About materials and binders manufacture", *Construction and Building Materials*, 22 (7), 1315-1322.
6. T. S. Ng, Y. L. Voo, and S. J. Foster (2012), "Sustainability with ultra-high performance and geopolymer concrete construction", *Innovative Materials and Techniques in Concrete Construction*, doi: 10.1007/978-94-007-1997-2\_5.
7. G. S. Ryua, Y. B. Leeb, K. T. Koh, and Y. S. Chung (2013), "The mechanical properties of fly ash-based geopolymer concrete with alkaline activators", *Construction and Building Materials*, 47, 409-418.
8. A. Islam, U. J. Alengaram, M. Z. Jumaat, and I. I. Bashar (2014), "The development of compressive strength of ground granulated blast furnace slag-palm oil fuel ash-fly ash based geopolymer mortar", *Materials & Design*, 56, 833-841.
9. D. W. Law, A. A. Adam, T. K. Molyneaux, I. Patnaikuni, and A. Wardhono (2014), "Long term durability properties of class F fly ash geopolymer concrete", *Materials and Structures*, doi: 10.1617/s11527-014-0268-9.
10. J. Temuujin, R. P. Williams, and A. Riessen (2009), "Effect of mechanical activation of fly ash on the properties of geopolymer cured at ambient temperature", *Journal of Materials Processing Technology*, 209; 5276-5280.
11. B. C. McLellan, R. P. Williams, J. Lay, A. Riessen, G. D. Corder (2010), "Costs and carbon emissions for geopolymer pastes in comparison to ordinary Portland Cement", *Journal of Cleaner Production*, 19, 1080-1090.
12. J. S. J. Deventer, P. J. L. Van, and P. Duxson (2012), "Technical and commercial progress in the adoption of geopolymer cement", *Minerals Engineering*, 29, 89-104.
13. A. Hasanbeigi, L. Pricea, and E. Linb (2012), "Emerging energy-efficiency and CO2 emission-reduction technologies for cement and concrete production: A technical review", *Renewable and Sustainable Energy Reviews*, 16,8.
14. J. Davidovits (1991), "Geopolymer, inorganic polymeric new materials", *Journal of Thermal Analysis*, 37, 1633-56.
15. M. F. M. Zain, M. Jamil, M. R. Karim, and F. C. Lai (2013), "Fabrication of a non-cement binder using slag, palm oil fuel ash and rice husk ash with sodium hydroxide", *Construction and Building Materials*, Volume 49, pp. 894-902.
16. D. Hardjito, S. Wallah, M. Sumajouw, and V. Rangan (2005), "Fly ash-based geopolymer concrete", *Australian Journal of Structural Engineering*, 6, 1.
17. L. Y. K. Daniel, G. S. Jay (2010), "Effect of elevated temperatures on geopolymer paste, mortar and concrete", *Cement and Concrete Research*, 40, 2.
18. S. Pal, S. Mandal (2011), "Different thermal activation effect on fly ash based geopolymer concrete", *Indian Concrete Institute Journal*, 12-23-25.
19. H. Peigang, J. Dechang, W. Meirong, and Y. Zhou (2011), "Thermal evolution and crystallization kinetics of potassium-based geopolymer", *Ceramics International*, 37, 1.
20. P. Chindaprasirta, U. Rattanasakb, and S. Taebuanhuadb (2013), "Role of microwave radiation in curing the fly ash geopolymer", *Advanced Powder Technology*, 24, 3.
21. K. Vijai, R. Kumutha, and B. G. Vishnuram (2010), "Effect of types of curing on strength of geopolymer concrete", *International Journal of the Physical Sciences*, 5(9).
22. X. Guo, H. Shi, and W. A. Dick (2010), "Compressive strength and microstructural characteristics of class C fly ash geopolymer", *Cement and Concrete Composites*, 32, 2.

23. M. W. Hussin, M. A. R. Bhutta, M. Azreen, P. J. Ramadhansyah, and J. Mirza (2014), "Performance of blended ash geopolymer concrete at elevated temperatures", *Materials and Structures*, doi: 10.1617/s11527-014-0251-5.
24. D. Adak, M. Sarkar, and S. Mandal (2014), "Effect of nano-silica on strength and durability of fly ash based geopolymer mortar", *Construction and Building Materials*, 70, 453-459.



**Dibyendu Adak** holds an M.E (structures) from Jadavpur University. He is presently pursuing his PhD in the Department of Civil Engineering at Jadavpur University, Kolkata. His area of interest is fly ash based geopolymer concrete.

**Dr. Saroj Mandal** is Professor and Former Head of the Department of Civil Engineering, Jadavpur University, Kolkata, India. He has experience in teaching and research over 23 years in various capacities. His main research interests are concrete material and structures - high performance concrete, recycled aggregate concrete, self-compacting concrete, geopolymer concrete and bacterial concrete. He has two patents in the area of Bacterial concrete. Professor Mandal is also associated with national and international journals as a reviewer. Various scientific papers and communications are credited to him in reputed National and International journals.



## What is your opinion ?

Do you wish to share your thoughts/views regarding the prevalent construction practices in the construction industry with our readers? If yes, the Indian concrete Journal gives a change to the engineering fraternity to express their views in its columns.

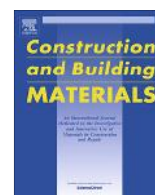
These shall be reviewed by a panel of experts. Your views could be supplemented with good photographs and neat line drawings. Send them across by e-mail to [editor@icjonline.com](mailto:editor@icjonline.com)

The logo for The Indian Concrete Journal (ICJ), featuring the letters 'ICJ' in a bold, red, sans-serif font.

### Write to :

The Editor, The Indian Concrete Journal,  
ACC Limited, L.B. Shastri Marg, Thane - 400 604.  
[editor@icjonline.com](mailto:editor@icjonline.com) [www.icjonline.com](http://www.icjonline.com)





# Structural performance of nano-silica modified fly-ash based geopolymer concrete



Dibyendu Adak<sup>a</sup>, Manas Sarkar<sup>b</sup>, Saroj Mandal<sup>a,\*</sup>

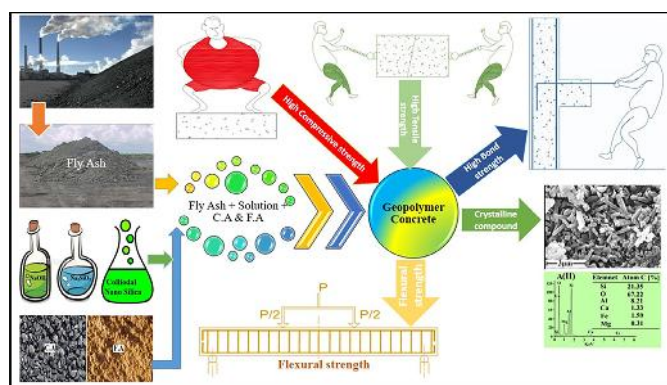
<sup>a</sup> Department of Civil Engineering, Jadavpur University, Kolkata 700032, India

<sup>b</sup> Department of Physics, Jadavpur University, Kolkata 700032, India

## HIGHLIGHTS

- Nano silica based geopolymer concrete shows excellent strength at room temperature.
- Flexural strength of 12GC6 reinforced concrete beam is higher than 12GCOH and CC.
- Bond performance of rebar with 12GC6 concrete is better than that of 12GCOH and CC.
- Nano silica enhances the geopolymerization process at ambient temperature.

## GRAPHICAL ABSTRACT



## ARTICLE INFO

### Article history:

Received 20 April 2016

Received in revised form 2 November 2016

Accepted 21 December 2016

### Keywords:

Fly ash  
Nano silica  
Geopolymer concrete  
Structural performance  
Micro structure

## ABSTRACT

The fly ash based geopolymer concrete generally requires heat activation of different temperatures, which has been considered as an important limitation for its practical application. Such limitation can be overcome by the addition of appropriate amount of nano-silica in the mixture. Therefore, a fly ash based geopolymer concrete can be developed using 6% nano silica replacing fly ash. The structural performance of such geopolymer concrete in terms of bond strength, flexural strength and micro structural behaviour has been explored. Such nano silica modified fly ash based geopolymer concrete shows appreciable improvement in structural behaviour at different ages without any heat activation. The bond strength between reinforcement bars (deformed or mild steel) and surrounding geopolymer concrete materials (with/without nano silica) has been also compared to the conventional cement concrete. The nano silica modified geopolymer concrete exhibits better structural performance than heat cured geopolymer concrete (without nano silica) and conventional cement concrete samples. The microstructural properties of such geopolymer concrete (with/without nano silica) and cement concrete have been analyzed through Field Emission Scanning Electron Microscope (FESEM) with Energy Dispersive X-ray Spectroscopy (EDS), Fourier Transform Infrared Spectroscopy (FTIR) analysis and X-ray Diffraction (XRD) techniques. The enhancement of structural performance is mainly due to the transformation of amorphous phase to crystalline phase in the geopolymer concrete matrices in the presence of nano-silica.

© 2016 Elsevier Ltd. All rights reserved.

\* Corresponding author.

E-mail address: [mailtosarojmandal@rediffmail.com](mailto:mailtosarojmandal@rediffmail.com) (S. Mandal).

## 1. Introduction

Geopolymer is a novel inorganic polymer binding material produced from the reaction of fly ash with the alkaline activator fluid; to ensure strength, durability and environmental sustainability. It is emerging as a greener alternative to Ordinary Portland Cement (OPC) in the construction field over the last two decades as the cement industry is the second largest producer of the greenhouse gas. The production of 1.0 ton Ordinary Portland Cement produces about 1.0 ton of carbon dioxide into the atmosphere [1]. Total CO<sub>2</sub> production attributed to cement production contributes around 8% of global CO<sub>2</sub> emission to the atmosphere [2].

The larger uses of the cement are becoming the global threats to the living organism day by day. The scientists and the researchers are trying to reduce the uses of cement as well as CO<sub>2</sub> production. The alternative products like nanomaterial, admixtures, chemicals, microorganisms are used in cementitious materials to enhance the strengths and to reduce the cement consumption [3–6]. However, their uses have some drawbacks and finally fail to reach the desired result. On the other hand, total coal combustion products in the form of fly ash were approximately 780 Mt in the year of 2011–2012 all over the world. Although effective utilization of fly ash was limited to only 415 Mt or 53% of total production and excess remains as an industrial hazard [7]. Thus, low calcium contain fly ash based geopolymer concrete are emerging as an alternative low emission binding material compared to OPC [8].

Fly ash are normally amorphous spherical particles, in addition to unburnt carbon, crystalline mullite, quartz and hematite. The mineralogical and chemical composition of fly ash, in general, depends on the source of coal and types of power plants [9]. The higher molarity of NaOH in fly-ash based geopolymer appeared to provide higher compressive strength together with a considerable effect on the early strength cured at 60 °C for 48 h [10,11].

It was already established that to accelerate the polymerization process, heat activation is generally needed for the development of physical and mechanical properties of geopolymer concrete [12–14]. The structural behaviour of heat cured fly ash based geopolymer concrete shows better performance than the conventional cement concrete [15–18]. The scope of such concrete is limited to the precast members due to the requirement of the heat activation after casting unlike conventional concrete. Thus, the exploration/investigation is required to develop the fly ash based geopolymer concrete cured at an ambient temperature [19,20]. The geopolymer paste made of the mechanically activated fly ash (vibration mill with milling media to powder ratio of 10:1) leads to an 80% increase in compressive strength when compared with the geopolymer made from raw fly ash [21]. The compressive strength of high volume fly ash mortars with the addition of nano-silica has significantly improved at room temperature curing [22]. The early strength is also achieved in geopolymer mortar (fly-ash + rice husk ash) having a different percentage of nano-silica and nano aluminum oxide with heat activation for 2, 4 and 8 h at different temperatures [23]. Also, the addition of nanoparticles in fly ash geopolymer mortar shows the appreciable strength at ambient temperatures curing [24–27]. The addition of colloidal nano-silica (6% w/w) in low calcium fly ash based geopolymer mortar at room temperature exhibited the maximum improvement of strength and durability [28].

The aim of this present exertion is to elucidate the effect of the addition of nano-silica on the structural behaviour (compressive strength & split tensile strength) of fly ash based geopolymer concrete cured at ambient temperature and to compare with heat cured fly ash based geopolymer concrete as well as conventional cement concrete. The flexural behaviour of reinforced concrete beams (with/without nano silica modified geopolymer concrete and control cement concrete) has been studied at different percentages of reinforcement (tension, compression and shear). Also, this study includes the bond strength between reinforcement bars and surrounding concrete matrices (both geopolymer concrete and control cement concrete). Microstructural properties of nano silica modified geopolymer concrete, and other type of concretes has been assessed through Field Emission Scanning Electron Microscope (FESEM) with Energy Dispersive X-ray Spectroscopy (EDS), Fourier Transform Infrared Spectroscopy (FTIR) analysis and X-ray Diffraction (XRD) test.

## 2. Materials & methods

### 2.1. Ingredients

Fly ash from National Thermal Power Corporation Ltd, Farakka plant in India has been used as the base material [29,30]. The basic properties of the fly ash and the grain size distribution are presented in Tables 1A and 2 respectively. Locally available sand (Specific gravity 2.52, water absorption 0.50%, and fineness modulus of 2.38) and 12 mm down coarse aggregates (Specific gravity 2.78, water absorption 0.42%, and fineness modulus of 4.89) have been used for the present study. The sodium hydroxide (NaOH) pellet of 99% purity and liquid sodium silicate (Na<sub>2</sub>SiO<sub>3</sub>) (specific gravity 1.53 gm./cc) having 45% solid content are used as an activator fluid [31]. The basic properties of nano silica used are represented in Table 3. The Ordinary Portland Cement (OPC) of 43 grade (Refer Table 1B) has been used for the conventional cement concrete mixture. The mild steel (yield stress = 250 MPa) and the deformed steel bar (0.2% proof stress = 500 MPa) of 20 mm diameter are used for bond strength test. The deformed steel bar of 6 mm and 8 mm diameter have been used as longitudinal (tension and compression) and shear reinforcement for reinforced concrete flexural members.

**Table 1B**  
Chemical analysis report of OPC 43 grade cement.

Material	Chemical composition (in percentage)
<i>OPC (43 grade):</i>	
Los in ignition	1.55
Insoluble residue	2.00
Magnesium Oxide	1.40
Lime saturation factor	0.87
Alumina Iron ratio	1.00
Sulphuric Anhydride	1.90
Alkalis	0.60
Chlorides	0.01

**Table 1A**  
Chemical analysis report of fly ash.

Material	Chemical composition (in percentage)									
Fly Ash	SiO <sub>2</sub>	Al <sub>2</sub> O <sub>3</sub>	Fe <sub>2</sub> O <sub>3</sub>	CaO	MgO	Na <sub>2</sub> O	K <sub>2</sub> O	SO <sub>4</sub>	LOI	
	64.97	26.64	5.69	0.33	0.85	0.49	0.25	0.33		0.45



**Table 2**  
Physical analysis report of fly ash.

Material	Particle Size Distribution						Specific Gravity
Fly Ash	>500 $\mu$	300–500 $\mu$	150–300 $\mu$	150–90 $\mu$	90–45 $\mu$	<45 $\mu$	2.05
NIL	0.00	1.42	11.67	48.06	31.98	6.87	

**Table 3**  
Basic properties of colloidal nano silica.

Colloidal Nano Silica type	Average particle size (nm)	Solid content (% Wt.)	Viscosity (Pa·S)	pH	Solid density (g/cm <sup>3</sup> )
CemSynXLP	4 to 16 nm	31	8.5	9.0–9.6	2.37

**Table 4**  
Details of nano-silica modified geopolymer (12GC6), conventional heat cured geopolymer (12GCOH) concrete and control cement concrete mix.

Mix Type	Cement (kg/m <sup>3</sup> )	Fly-ash (kg/m <sup>3</sup> )	F.A* (kg/m <sup>3</sup> )	C.A <sup>s</sup> (kg/m <sup>3</sup> )	Fluid/fly-ash	Percentage of nano silica	Curing conditions
12GC6	Nil	440	723	1085	0.40	6.0%	Ambient curing, 25 °C
12GCOH	Nil	440	723	1085	0.40	0.0%	Heat curing 60 °C, 48 h.
CC	400	0.00	690	1205	0.40 (W/C)	0.0%	Water curing.

\*\* (xGCy, Where “GC – Geopolymer concrete”, “x – Molar concentration”, “y – percentages of nano-silica”, “OH – Heat cured without nano silica”, “CC – Conventional concrete” and “W/C – Water/Cement”).

F.A\* – Fine aggregate, C.A<sup>s</sup> – Coarse aggregate. (W/C = Water/Cement).

## 2.2. Mix proportion and curing environments

The NaOH solution (12 M) has been mixed with Na<sub>2</sub>SiO<sub>3</sub> in the proportion of 1:1.75 (by weight) to prepare the alkali activator fluid for each category of geopolymer concretes (with or without nano-silica) [24]. Colloidal nano-silica with 6% of fly-ash (by weight) has been also added to the activator fluid. The amount of water present in the colloidal nano-silica has been adjusted from the activator solution during the preparation. The details of the various mixes are shown in Table 4. The nano-silica modified geopolymer concrete (12GC6) specimens are removed from the mould after 24 h of casting and are cured at ambient temperature (27 ± 2 °C) until the testing. However, the specimens with geopolymer concrete without nano-silica (12GCOH) are cured at a 60 °C temperature for 48 h only within the hot air oven [15,18,32,33]. Further, these samples are kept at ambient temperature until the test. The conventional water cured cement concrete (CC) specimens having similar compressive strength of heat cured geopolymer concrete (12GCOH) have been prepared by the addition of 0.1% ViscoCrete-10R admixture and are marked as control specimens. The compacting factor and slump values of the mixes 12GC6, 12GCOH and CC have been determined as per IS: 1199 (1959) and IS: 7320 (1974) [34,35].

## 2.3. Sample preparation and testing procedures

### 2.3.1. Mechanical strength

The standard cube specimens (150 mm × 150 mm × 150 mm) were prepared for all three mixes (12GC6, 12GCOH & CC) to determine the compressive strength of concrete samples at different ages [36]. The split tensile strength was determined on 100 mm (diameter) × 200 mm (height) concrete cylinder specimens (CC, 12GCOH, 12GC6) at 28 days [37]. The cylinder concrete specimens (150 mm diameter and 300 mm height) were also prepared for the determination of modulus of elasticity in a strain controlled machine.

### 2.3.2. Bond behaviour between concrete and reinforcement bars

The bond behaviour was studied by pull out test on the deformed rebar or mild steel rebar embedded concentrically on cubical specimens of 150 mm × 150 mm × 150 mm (Fig. 1). Dur-

ing casting and subsequent compaction, the steel bars were held in position using a steel mould arrangement. The specimens for each category of mixes (12GC6, 12GCOH and CC) were tested after 28 days of curing. The slip of the embedded bar from the concrete specimens corresponding to the load was noted and the corresponding bond behaviour between steel bar and concrete was calculated as per IS 2770 (Part – 1): 2007 [38].

### 2.3.3. Flexural strength analysis of reinforced concrete beams

The size of the reinforced concrete beam specimens for three mixes was 100 × 150 mm (B × D) in cross section and 1200 mm in length. The specimens were tested as simply supported over an effective span (l) of 900 mm as shown in Fig. 2. The details of three different percentages of tensile, compression and shear reinforcement are shown in Table 5. The load has been applied on two point, each 150 mm away from the centre of the beam. The maximum experimental bending moment for each beam was calculated at mid span is  $M_{exp} = P \times (l/3)$ , where P is each point load (maximum) and ‘l’ is the effective span of the beam (Refer Fig. 2). The maximum theoretical bending moment ( $M_{th}$ ) of each beam was calculated as per IS 456-2000 [39] depending on the grade of concrete and percentage of reinforcement and compared to  $M_{exp}$ .

### 2.3.4. Microstructural analysis

After the strength determination of each concrete specimen, fragments were collected for the micro structural properties. The fragment samples were grinded and sieved to make the size less than 5  $\mu$ m for X-ray Diffraction analysis using the powder X-ray diffractometer (Bruker AXS Inc, Model D8, WI, USA) with a scan speed 0.5/s/step at 40 kV. The XRD spectra were analysed in the range  $2\theta = 20^\circ$  to  $80^\circ$  and the peak positions were marked and compared from JCPDS files.

Fourier Transform Infrared Spectroscopy (FT-IR410 JASCO, U.S. A.) was used for structural information of 12GC6 and 12GCOH geopolymer concretes. Samples were prepared by the KBr pellet (97% KBr) technique for the FTIR analysis.

The fine powder was diluted with ethanol (99.9%) to make a film on carbon tape and then kept under vacuum desiccators for evaporation and the dried samples were gold coated for Field Emission Scanning Electron Microscope FESEM (INSPECT F50 SEM, The Netherlands) analysis. The elemental analysis was performed by

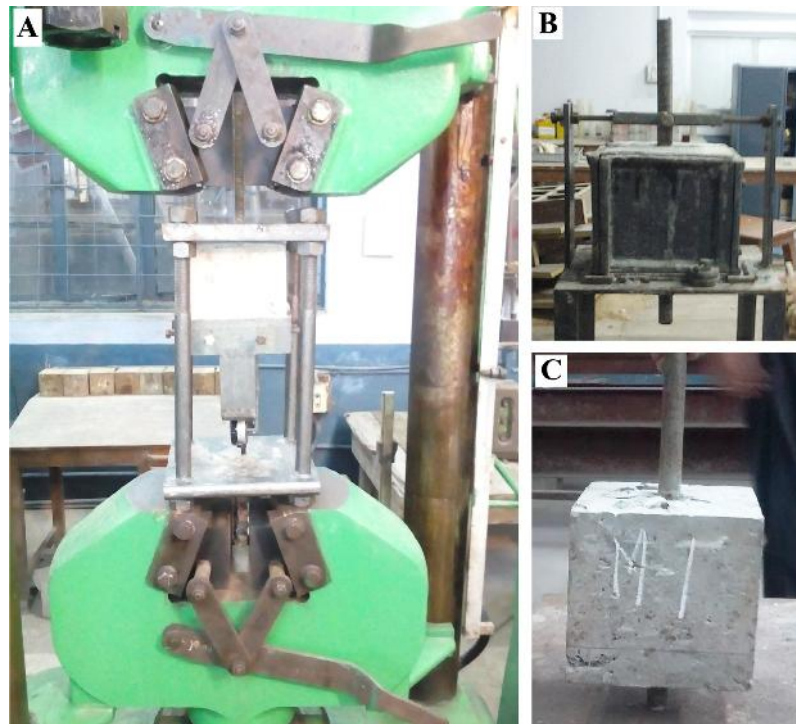


Fig. 1. Test setup for bond behaviour: (A) testing machine; (B) specimen mould; (C) failure sample.

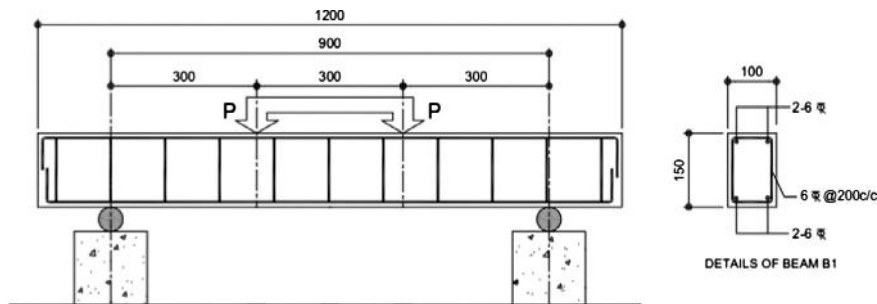


Fig. 2. Typical reinforced concrete beam (B1) details and loading arrangement.

Table 5

Reinforcement details of nano-silica modified geopolymer (A1–A7), conventional heat cured geopolymer (B1–B7) concrete and control cement concrete (C1–C7) beam.

Beam Mark	Length (mm)	Reinforcement		Percentage of reinforcement		Shear Spacing (6 Φ)
		Tensile (bottom)	Compressive (Top)	(Top)	(Bottom)	
A1	1200	2-6Φ	2-6Φ	0.45	0.45	200
A2	1200	3-6Φ	2-6Φ	0.67	0.45	200
A3	1200	2-8Φ	2-6Φ	0.81	0.45	200
A4	1200	2-8Φ	3-6Φ	0.81	0.67	200
A5	1200	2-8Φ	2-8Φ	0.81	0.81	200
A6	1200	2-8Φ	2-6Φ	0.81	0.45	150
A7	1200	2-8Φ	2-6Φ	0.81	0.45	100
B1	1200	2-6Φ	2-6Φ	0.45	0.45	200
B2	1200	3-6Φ	2-6Φ	0.67	0.45	200
B3	1200	2-8Φ	2-6Φ	0.81	0.45	200
B4	1200	2-8Φ	3-6Φ	0.81	0.67	200
B5	1200	2-8Φ	2-8Φ	0.81	0.81	200
B6	1200	2-8Φ	2-6Φ	0.81	0.45	150
B7	1200	2-8Φ	2-6Φ	0.81	0.45	100
C1	1200	2-6Φ	2-6Φ	0.45	0.45	200
C2	1200	3-6Φ	2-6Φ	0.67	0.45	200
C3	1200	2-8Φ	2-6Φ	0.81	0.45	200
C4	1200	2-8Φ	3-6Φ	0.81	0.67	200
C5	1200	2-8Φ	2-8Φ	0.81	0.81	200
C6	1200	2-8Φ	2-6Φ	0.81	0.45	150
C7	1200	2-8Φ	2-6Φ	0.81	0.45	100

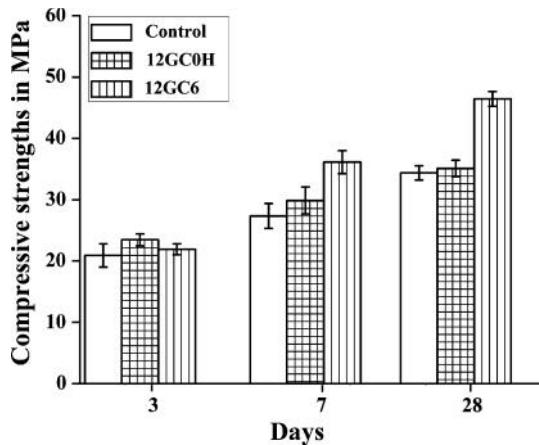


Fig. 3. Compressive strength of nano-silica modified geopolymer (12GC6), conventional heat cured geopolymer concrete (12GC0H) and control cement concrete (CC) at 3 d, 7 d and 28 d.

the energy dispersive spectra (EDS) using QUANTAX ESPRIT 1.9 software.

#### 2.4. Statistical analysis

For each category of testing, five samples were tested. Each experiment was repeated for three times. Data were presented as average (over 15 samples) and  $\pm$  SD (Standard deviation).

### 3. Results

#### 3.1. Mechanical strength

The compressive strength of geopolymer concrete (12GC6 & 12GC0H) and control concrete (CC) samples at different ages (3, 7 and 28) are presented in Fig. 3. The strength of heat cured geopolymer (12GC0H) and control concrete (CC) samples are almost same as designed. However, the compressive strength of 12GC6 samples is higher than that of 12GC0H concrete samples at all ages. The Split tensile strength of 12GC0H is more than that of CC concrete though both the mixes have similar compressive strength. The nano silica modified geopolymer concrete (12GC6) shows higher split tensile strength than the others (Table 6). It is noted that the modulus of elasticity of 12GC0H geopolymer concrete is less than CC at their equivalent compressive strength [40,41]. The modulus of elasticity of 12GC6 samples is higher than that of the others. Fresh concrete properties (slump test and compacting factor test) of nano-silica modified geopolymer concrete (12GC6) are almost similar to that of 12GC0H and CC samples (Table 6).

#### 3.2. Bond behaviour between reinforcement bars and concretes

Fig. 4 and Table 7 demonstrate the bond behaviour of 20 mm diameter reinforcement bars (deformed; 0.2% proof stress = 500 MPa & mild steel; yield stress = 250 MPa) for both

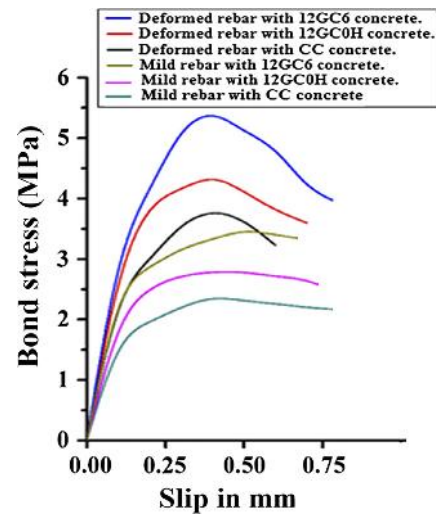


Fig. 4. Bond stress vs. slip curve of geopolymer concrete (12GC6 & 12GC0H) and control cement concrete (CC) with deformed and mild steel bar.

types of geopolymer concrete (12GC6 & 12GC0H) and control cement concrete (CC) after 28 days of curing. A comparison of bond stress has been made at failure and at load corresponding to the slip of 0.25 mm. With the mild steel rebar, the maximum stress is not very different from the stress at the first visible slip but in case of deformed bar the maximum stress may correspond to a large slip which may not in fact be obtained in practice before other types of failure occurs. Thus, the comparison of bond stress has been made at 0.25 mm slip also [38]. The result shows that the geopolymer concretes (12GC6 & 12GC0H) possess higher bond stress than that of control concrete for both deformed and mild steel bars. Also the nano silica modified geopolymer concrete (12GC6) exhibits the better bond behaviour than 12GC0H geopolymer concrete for both type of reinforcement bars. All the samples are generally failed by the pull out load of the rebar. The slip for mild steel rebar is more compare to deformed rebar at an equal pull-out load (Fig. 4). Similar results have been reported by other researchers [42–44].

#### 3.3. Flexural strength of the reinforced concrete beam

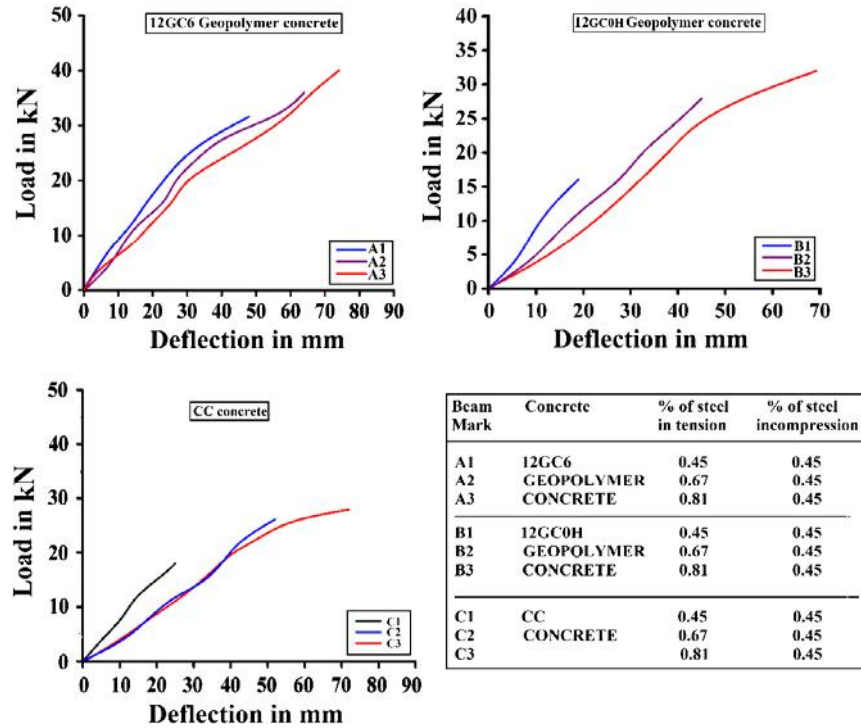
The load deflection behaviour of steel reinforced beams with nano-silica modified geopolymer concrete (12GC6), conventional heat cured geopolymer concrete (12GC0H) beams and control cement concrete (CC) is shown distinctly in Figs. 5–7. As the applied load is increased, the beam starts to deflect and flexural cracks are developed near the centre of the beams. As all the beams are designed as under-reinforced, they are generally failed by the yielding of the reinforcement bar followed by the overwhelming of concrete. As expected, the flexural capacity of the beams increases significantly with the enhancement of the tensile reinforcement for all types of concrete mixes (12GC6, 12GC0H and CC). It is noted that the flexural capacity of 12GC6 concrete beams is increased by 12%, 7% and 18% compared to that of 12GC0H con-

Table 6  
Mechanical strength and fresh concrete property of different mixes.

Mix	Compressive strength (28 day) (MPa)	Split tensile strength (28 day) (MPa)	Modulus of elasticity (28 day) (GPa)	Slump (mm)	Compacting factor
12GC6	46.43	4.33	37.28	120	0.90
12GC0H	35.11	3.39	30.81	110	0.89
Control	34.77	2.78	32.58	105	0.87

**Table 7**  
Comparison of bond stress (MPa) for different mixes.

Rebar	Mix-12GC6		Mix-12GC0H		Mix-CC	
	At failure	At 0.25 mm slip	At failure	At 0.25 mm slip	At failure	At 0.25 mm slip
Mild Steel	3.49	3.12	2.71	2.67	2.37	2.26
Deformed Steel	5.47	5.16	4.44	4.11	3.82	3.56



**Fig. 5.** Load vs. deflection curve and bending moment capacity of 12GC6, 12GC0H and CC concrete beams with different percentages of tensile reinforcement.

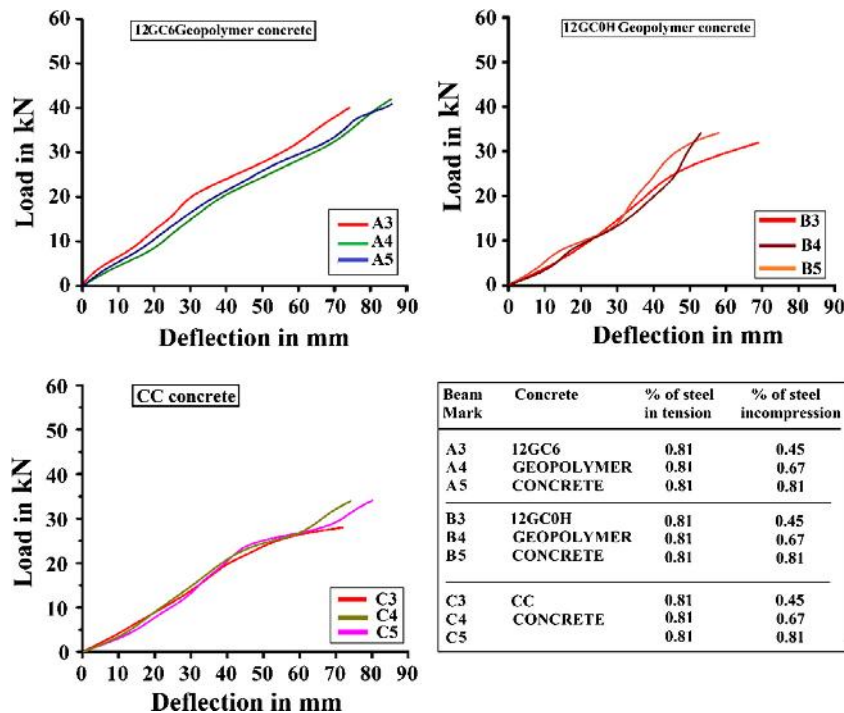


**Fig. 6.** Load vs. deflection curve and bending moment capacity of 12GC6, 12GC0H and CC concrete beams with different percentages of compressive reinforcement.

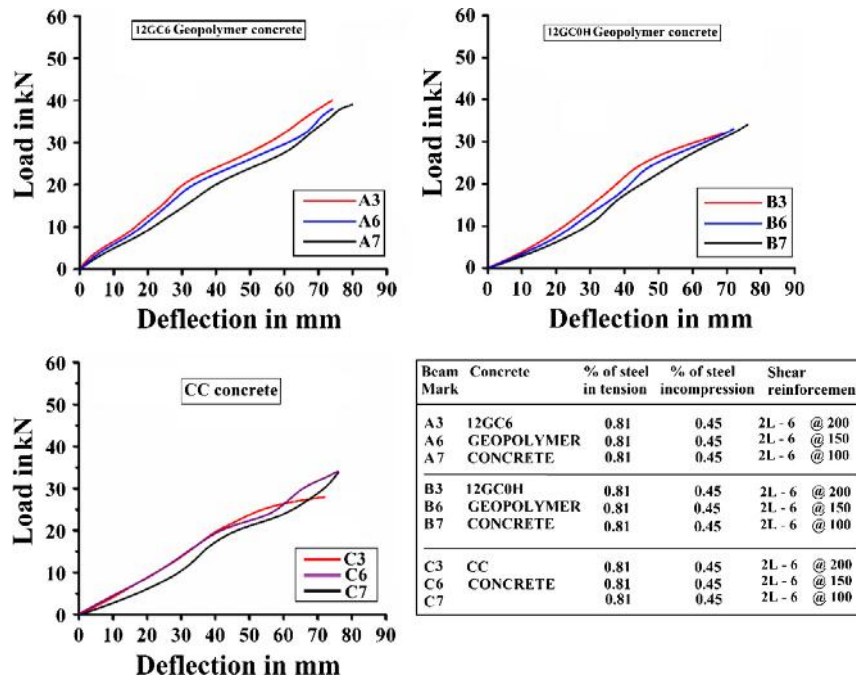


Fig. 7. Load vs. deflection curve and bending moment capacity of 12GC6, 12GC0H and CC concrete beams with different percentages of shear reinforcement.

Table 8

Theoretical ( $M_{th}$ ) and experimentally ( $M_{exp}$ ) calculated bending moment (kN-m) of reinforced concrete beams for mixes 12GC6, 12GC0H and CC.

Percentage of reinforcement		$M_{th}$ (as per Code)	CC	12GC0H	12GC6
$p_t$	$p_c$		$M_{exp}$	$M_{exp}$	$M_{exp}$
0.45	0.45	2.65	2.80	2.50	4.98
0.67	0.45	3.82	4.07	4.30	5.57
0.81	0.45	4.34	4.37	5.02	5.98
0.81	0.67	4.34	4.68	5.18	6.16
0.81	0.81	4.34	4.76	5.23	6.21

$p_t$  = percentage of steel in tension (Top),  $p_c$  = percentage of steel in compression (Bottom).

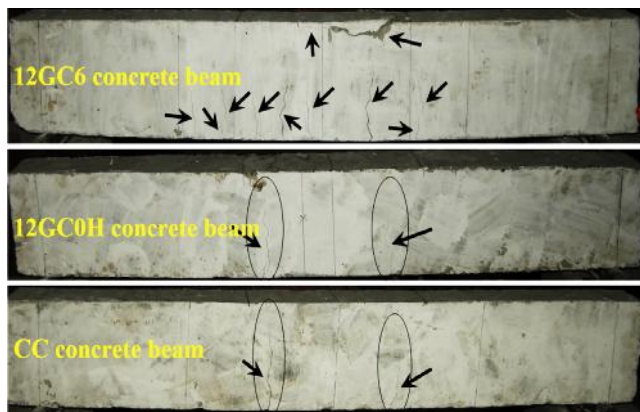


Fig. 8. Crack pattern of 12M6 & 12M0H geopolymer concrete and CC concrete beams.

crete beams for 0.45%, 0.67% and 0.81% of tensile reinforcement respectively (Fig. 5). The flexural capacity of 12GC6 concrete beams at different percentages of compression (Fig. 6) and shear reinforcement (Fig. 7) are also more than that of the 12GC0H and CC beam samples. Table 8 shows the experimental bending moment capacity (calculated from experimental load values) of the reinforced beams (12GC6, 12GC0H and CC) and corresponding theoretical bending moment calculated as per IS 456 – 2000 [39]

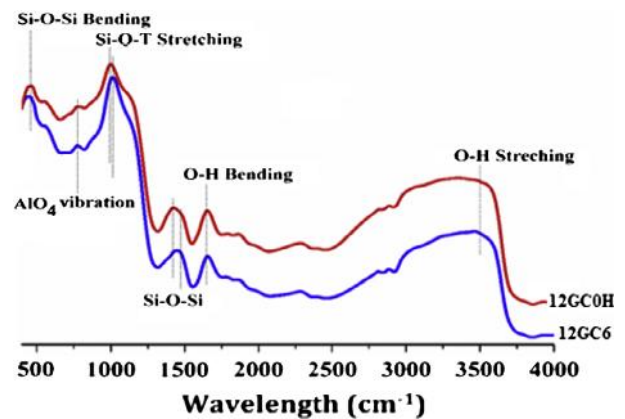


Fig. 9. FTIR analysis of geopolymer concrete (12GC6 & 12GC0H).

for all mixes. It is noted that the experimental moment capacity of beams with 12GC6 concrete is significantly higher than that of beams with 12GC0H and CC concrete. Therefore, the design of geopolymer beams will be safer compared to that of normal concrete beam.

The crack patterns of concrete beams with 12GC6, 12GC0H and CC are observed and the flexure cracks are initiated in the bending zone as expected. These cracks in samples were further propagated

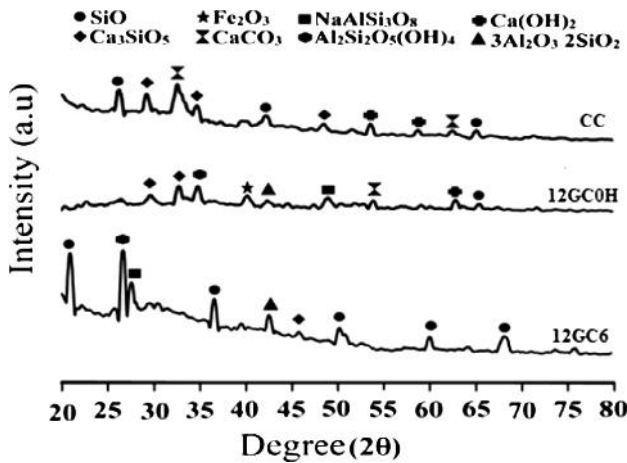


Fig. 10. XRD analysis of geopolymer concrete (12GC6 & 12GC0H) and control cement (CC) concrete.

with the load increment and the other new cracks were also developed along the span (Fig. 8). The first cracking load of 12GC6 concrete beams is more than 12GC0H and CC concrete beams.

3.4. Microstructure analysis

The infra-red spectroscopic results of 12GC6 and 12GC0H samples were shown in Fig. 9. The distinct intensity band near  $460\text{ cm}^{-1}$  is recognised for the Si-O-Si bending vibration [45]. The band between  $750\text{ cm}^{-1}$  and  $800\text{ cm}^{-1}$  is observed due to the  $\text{AlO}_4$  vibration. Another peak for the asymmetric stretching and vibration band of Si-O-T (T = Al, Si) which is described as the strongest band, was registered in the region of  $950\text{ cm}^{-1}$ – $1050\text{ cm}^{-1}$  [46]. The position ( $1420\text{ cm}^{-1}$ ) of Si-O-Si in 12GC0H is shifted to the right position ( $1485\text{ cm}^{-1}$ ) in 12GC6. A significant band is also located at approximately  $3450\text{ cm}^{-1}$  for OH stretching bonding.

XRD patterns of 12GC6 and 12GC0H geopolymer and CC concrete are represented in Fig. 10. The intensity of quartz, mullite and hematite are more in 12GC6 due to the presence of additional nano-silica in the matrix. Some extra peaks are shown in nano-silica modified geopolymer concrete (12GC6) which indicate the formation of the new phases of quartz ( $\text{SiO}_2$ ), albite ( $\text{NaAlSi}_3\text{O}_8$ ), kaolinite ( $\text{Al}_2\text{Si}_2\text{O}_5(\text{OH})_4$ ), alite ( $\text{Ca}_3\text{SiO}_5$ ), mullite ( $3\text{Al}_2\text{O}_3 \cdot 2\text{SiO}_2$ ) and  $\text{Ca}(\text{OH})_2$  crystalline compound compared to the others (12GC0H and CC concretes). The wide diffraction hump is detected around  $2\theta = 25\text{--}30^\circ$  which confirms the presence of crystalline phases in 12GC6 geopolymer matrices [28].

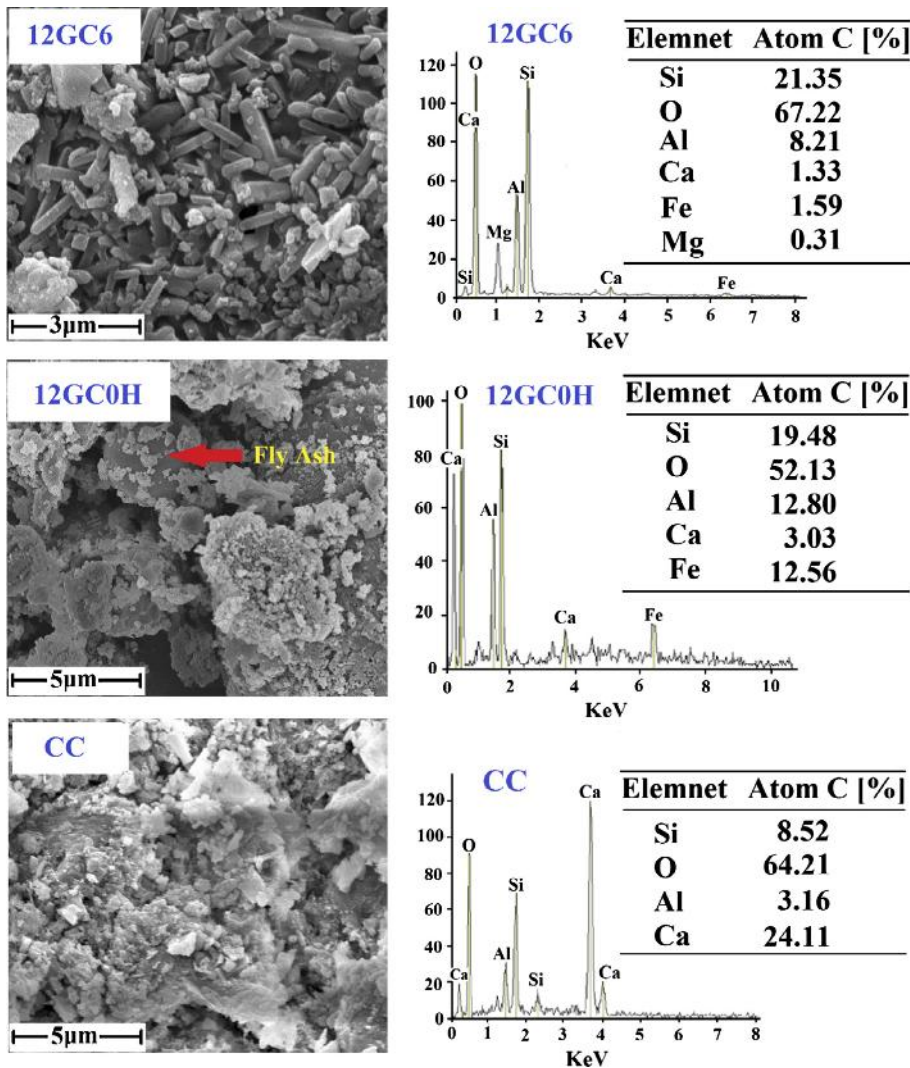


Fig. 11. SEM micrographs and EDX analysis of nano-silica modified geopolymer concrete (12GC6), heat cure geopolymer concrete (12GC0H) and control cement (CC) concrete.

Fig. 11 exhibits FESEM micrographs of 12GC6 and 12GC0H and CC concrete matrices. The elemental analysis of 12GC6, 12GC0H and CC specimens are shown in Fig. 11. The major elements like Si, Al, Ca with some amount of Fe are also present in geopolimer concrete samples (12GC6 & 12GC0H) and control cement (CC) concrete in different ratios. As the experimental work has been made on low calcium fly-ash geopolimer concrete, the presence of Ca in geopolimer concrete (12GC6 & 12GC0H) is less than control cement concrete. However, the ratios of Si/Al for the 12GC6 and 12GC0H geopolimer concretes are 2.60 and 1.52 respectively. Also, Fig. 11 shows that the amount of crystalline compound in 12GC6 is more than that of 12GC0H concrete.

#### 4. Discussion

The nano-silica modified geopolimer concrete (12GC6) exhibits better mechanical strength than the heat cured geopolimer concrete (12GC0H) due to the presence of nano-silica in the mixture (Figs. 3 and 4 & Table 6). Geopolimer concrete with nano-silica increases the dissolution rate of Si and Si–Al phases, which strongly affects the rate of polymerization. The presence of nano-silica in geopolimer mixture is the key factor to enhance the polymerisation process for its amorphous property and the high specific area [25]. The asymmetric stretching vibration band of Si–O–T (T = Al, Si) of 12GC6 geopolimer matrix shifted to right with respect to 12GC0H geopolimer matrix. This may be due to less polymerised structure of 12GC0H matrix at  $990\text{ cm}^{-1}$  and non-dissolved high polymerised structures at  $1025\text{ cm}^{-1}$  (Fig. 9). The Si–O–Si position in 12GC0H ( $1420\text{ cm}^{-1}$ ) is shifted to the right in 12GC6 ( $1485\text{ cm}^{-1}$ ) matrices due to the chemical changes in the geopolimer matrix with the addition of colloidal nano-silica [46,47]. The broad hump registered between  $2\theta = 25^\circ\text{--}30^\circ$  in the XRD diagram (Fig. 10) of 12GC6 geopolimer concrete, indicating the dissolution of the amorphous phase of fly ash and the formation of a new amorphous and crystalline phase in the matrix [47]. The large amount of crystalline compounds is transformed from the amorphous phase in nano-silica modified cementitious matrix (Fig. 11). The unreacted heterogeneous fly-ash remains in 12GC0H matrices due to the lower polymerization rate that leads lower mechanical strength.

The augmentation of the mechanical strengths of 12GC6 geopolimer concrete is due to the large number of crystalline geopolimer plates spread all over the surface. The alumina leaching in nano-silica modified geopolimer concrete is higher than heat cured geopolimer concrete (Fig. 11). The ratio of Si/Al ratio of 12GC6 geopolimer matrices is higher than 12GC0H concrete that causes the higher mechanical strength of nano silica modified geopolimer concrete [48,49]. The higher amount of the Si/Al ratio and homogeneous texture of crystalline plates in the matrix exhibit higher mechanical strength of nano-silica modified geopolimer concrete.

The bond strength of 12GC6 concrete is also more than 12GC0H and CC concrete, as the split tensile strength nano-silica modified geopolimer concrete (12GC6) is higher than the other concretes [41,50]. The presence of soluble silicates in geopolimer concrete produces a denser or stronger interfacial transition zone (ITZ) between aggregates and geopolimer matrices as compared to the cement matrices [50–53].

The elastic property and the flexural behaviour of reinforced nano silica modified geopolimer concrete (12GC6) cured at ambient condition are almost similar to the control cement (CC) concrete whereas the bending moment capacity is significantly higher than the CC concrete beam. The higher mechanical strength of 12GC6 concrete and better bond behaviour of geopolimer concrete with rebar help to provide the improvement of flexural

strength of 12GC6 concrete. Therefore, the design provisions contained in the current standards and codes (for conventional concrete) can be used to design the reinforced low-calcium fly-ash-based nano-silica geopolimer concrete structural members as per the present test results.

#### 5. Conclusion

The fly-ash based nano-silica modified geopolimer concrete (cured at ambient temperature) shows excellent mechanical strength compared to conventional heat cured geopolimer concrete and OPC concrete. The flexural strength of reinforced beam and bond strength of reinforcement bars using such geopolimer concrete with nano-silica cured at ambient temperature is comparatively higher than the heat activated geopolimer concrete (without nano-silica) and conventional cement concrete. Polymerization reaction has been accelerated by the application of nano-silica, which increases the Si/Al ratio, enhances the crystalline phases in geopolimer matrices at ambient temperature. Therefore, the design method applicable for conventional concrete can be also applied safely for geopolimer concrete with nano silica (at ambient temperature curing)/without nano silica (under heat curing).

#### Conflict of interest

None.

#### Acknowledgements

The authors would like to thank to concrete technology laboratory in Civil Engineering department, Jadavpur University for the technical support and University Grants Commission (India) for the financial support.

#### Appendix A. Supplementary data

Supplementary data associated with this article can be found, in the online version, at <http://dx.doi.org/10.1016/j.conbuildmat.2016.12.111>.

#### References

- [1] V. M. Malhotra, P. K. Mehta, High-performance, high-volume fly ash concrete: materials, mixture, proportioning, properties, construction practice, and case histories. Ottawa: Supplementary Cementing Materials for Sustainable Development Incorporated, second ed., 1–124, 2005.
- [2] J. Olivier, G. Janssens, J. Peters, Trends in Global CO<sub>2</sub> Emissions; 2012 Report, PBL Netherlands Environmental Assessment Agency, The Hague, Netherlands, 2012.
- [3] M. Sarkar, T. Chowdhury, B. Chattopadhyay, R. Gachhui, S. Mandal, Autonomous bioremediation of a microbial protein (bioremediase) in Pozzolana cementitious composite, *J. Mater. Sci.* 49 (2014) 4461–4468.
- [4] M. Sarkar, N. Alam, B. Chaudhuri, B. Chattopadhyay, S. Mandal, Development of an improved *E. coli* bacterial strain for green and sustainable concrete technology, *RSC Adv.* 5 (2015) 32175–32182.
- [5] L. Sorellia, G. Constantinides, F.J. Ulm, F. Toutlemonde, The nano-mechanical signature of ultra high performance concrete by statistical nano-indentation techniques, *Cem. Concr. Res.* 38 (2008) 1447–1456.
- [6] G.Y. Li, P.M. Wang, X. Zhao, Mechanical behavior and microstructure of cement composites incorporating surface-treated multi-walled carbon nanotubes, *Carbon* 43 (2005) 1239–1245.
- [7] C. Heidrich, F.H. Joachim, W. Anne, Coal Combustion Products: A Global Perspective 2013, World of Coal Ash (WOCA) Conference, Lexington, 2013.
- [8] J. Davidovits, Geopolymers: inorganic polymeric new materials, *J. Mater. Educ.* 16 (1994) 91–139.
- [9] V.K. Jha, M. Matsuda, M. Miyake, Resource recovery from coal fly ash waste: an overview study, *J. Ceram. Soc.* 116 (2008) 167–175.
- [10] A. Palomo, M.W. Grutzeck, M.T. Blanco, Alkali-activated fly ashes a cement for the future, *Cem. Concr Res.* 29 (1999) 1323–1329.
- [11] G. Gorhan, G. Kurklu, The influence of the NaOH solution on the properties of the fly ash based geopolimer mortar cured at different temperature, *Comp. Part B: Eng.* 58 (2014) 371–377.

- [12] L.Y.K. Daniel, G.S. Jay, Effect of elevated temperatures on geopolymer paste, mortar and concrete, *Cem. Concr. Res.* 40 (2010) 334–339.
- [13] P. Chindaprasirt, U. Rattanasak, S. Taebuanhuad, Role of microwave radiation in curing the fly ash geopolymer, *Adv. Powder Technol.* 24 (2013) 703–707.
- [14] M.W. Hussin, M.A.R. Bhutta, M. Azreen, Performance of blended ash geopolymer concrete at elevated temperatures, *Mater. Struct.* 48 (2015) 709–720.
- [15] V. B. Rangan, D. Sumajouw, S. Wallah, Reinforced low-calcium fly ash-based geopolymer concrete beams and columns. Proceedings of 31st Conference on Our World in Concrete & Structures, Singapore, 2006.
- [16] A. Castel, S. Foste, Bond strength between blended slag and Class F fly ash geopolymer concrete with steel reinforcement, *Cem. Concr. Res.* 72 (2015) 48–53.
- [17] N. Ganesan, R. Abraham, S.D. Raj, D. Sasi, Stress–strain behaviour of confined Geopolymer concrete, *Constr. Build. Mater.* 7 (2014) 326–331.
- [18] P. Sarker, R. Haque, K.V. Ramgolam, Fracture behaviour of heat cured fly ash based geopolymer concrete, *Mater. Des.* 44 (2013) 580–586.
- [19] K. Somna, C. Jaturapitakkul, P. Kajitvichyanukul, NaOH-activated ground fly ash geopolymer cured at ambient temperature, *Fuel* 90 (2011) 2118–2124.
- [20] T. Xie, T. Ozbakkaloglu, Behavior of low-calcium fly and bottom ash-based geopolymer concrete cured at ambient temperature, *Ceram. Int.* 41 (2015) 5945–5958.
- [21] J. Temuujin, R.P. Williams, A.V. Riessen, Effect of mechanical activation of fly ash on the properties of geopolymer cured at ambient temperature, *J. Mater. Process. Tech.* 209 (2009) 5276–5280.
- [22] P.S. Deb, P. Nath, P.K. Sarker, Strength and permeation properties of slag blended fly ash based geopolymer concrete, *Adv. Mater. Res.* 05 (2013) 168–173.
- [23] S. Riahi, A. Nazari, The effects of nanoparticles on early age compressive strength of ash based geopolymer, *Ceram. Int.* 38 (2012) 4467–4476.
- [24] T. Phoo-ngernkham, P. Chindaprasirt, V. Sata, The effect of adding nano-SiO<sub>2</sub> and nano-Al<sub>2</sub>O<sub>3</sub> on properties of high calcium fly ash geopolymer cured at ambient temperature, *Mater. Des.* 55 (2014) 58–65.
- [25] H.M. Khater, B.A. El-Sabbagh, M. Fanny, Effect of nano-silica on alkali activated water cooled slag geopolymer, *ARPN J. Sci. Technol.* 02 (2012) 2.
- [26] X. Gao, Q.L. Yu, H.J.H. Brouwers, Characterization of alkali activated slag–fly ash blends containing nano-silica, *Constr. Build. Mater.* 98 (2015) 397–406.
- [27] P.S. Deb, P.K. Sarker, S. Barbhuiya, Effects of nano-silica on the strength development of geopolymer cured at room temperature, *Constr. Build. Mater.* 101 (2015) 675–683.
- [28] D. Adak, M. Sarker, S. Mandal, Effect of nano-silica on strength and durability of fly ash based geopolymer mortar, *Constr. Build. Mater.* 70 (2014) 453–459.
- [29] ASTM C618, Standard Specification for Coal Fly Ash and Raw or Calcined Natural Pozzolan for Use in Concrete, ASTM International, West Conshohocken, PA, 2002.
- [30] D. Adak, S. Mandal, Study on the modified process for the development of fly ash based geopolymer mortar cured at ambient temperature, *Indian Concr. J.* 89 (2015) 31–40.
- [31] D. Adak, M. Sarker, M. Maiti, A. Tamang, S. Mandal, B. Chattopadhyay, Anti-microbial efficiency of nano silver-silica modified geopolymer mortar for eco-friendly green construction technology, *RSC Adv.* 5 (2015) 64037–64045.
- [32] J.C. Swanepoel, C.A. Strydom, Utilisation of fly ash in a geopolymeric material, *Appl. Geochem.* 17 (2002) 1143–1148.
- [33] D.M.J. Sumajouw, D. Hardjito, S.E. Wallah, B.V. Rangan, Fly ash-based geopolymer concrete: study of slender reinforced columns, *J. Mater. Sci.* 42 (2007) 3124–3130.
- [34] IS: 1199 Methods of Sampling and Analysis of Concrete, Bureau of Indian Standard, New Delhi, India, 2004.
- [35] IS: 7320 Specification for Concrete Slump test Apparatus, Bureau of Indian Standard, New Delhi, India, 2008.
- [36] IS: 516 Methods of Tests for Strength of Concrete, Bureau of Indian Standard, New Delhi, India, 1999.
- [37] IS 5816 Splitting Tensile Strength of Concrete Method of Test, Bureau of Indian Standard, New Delhi, India, 1999.
- [38] IS 2770 (Part-1) Method of Testing Bond in Reinforced Concrete, Bureau of Indian Standard, New Delhi, India, 1997.
- [39] IS 456 Plain Reinforced Concrete – Code of Practice, Bureau of Indian Standard, New Delhi, India, 2000.
- [40] M. Sofi, J.S.J. van Deventer, P.A. Mendis, Engineering properties of inorganic polymer concretes (IPCs), *Cem. Concr. Res.* 37 (2007) 251–257.
- [41] D. Hardjito, B. V. Rangan, Development and properties of low calcium fly ash-based geopolymer concrete. Research report GC1. Faculty of Engineering, Curtin University of Technology, Western Australia, 2005.
- [42] M.J. Prince, B. Singh, Bond behaviour of deformed steel bars embedded in recycled aggregate concrete, *Constr. Build. Mater.* 49 (2013) 852–862.
- [43] Ee Hui Chang, Prabir Sarker, Natalie Lloyd, B. Vijaya Rangan, Bond behaviour of reinforced fly ash-based geopolymer concrete beams, in: R.I. Gilbert (Ed.), *Concrete Solutions 09*, The 24th Biennial Conference of the Concrete Institute of Australia, Sep 17 2009, Concrete Institute of Australia, Luna Park, Sydney, 2009.
- [44] S. Pul, Loss of concrete-steel bond strength under monotonic and cyclic loading of lightweight and ordinary concretes, *Iran. J. Sci. Technol. Trans. B: Eng.* 34 (2010) 397–406.
- [45] H. Günzler, H. Gremlich, *IR Spectroscopy: An Introduction*, Wiley-VCH Verlag GmbH, Germany, 2002.
- [46] M.A. Salih, A. Ali, N. Farzadnia, Characterization of mechanical and microstructural properties of palm oil fuel ash geopolymer cement paste, *Constr. Build. Mater.* 65 (2014) 592–603.
- [47] D. Papias, I.P. Giannopoulou, T. Perraki, Effect of synthesis parameters on the mechanical properties of fly ash-based geopolymers, *Col. Surf. A: Phys. Eng. Aspects* 301 (2007) 246–254.
- [48] T. Klabprasit, C. Jaturapitakkul, W. Chalee, P. Chindaprasirt, S. Songpiriyakij, Influence of Si/Al ratio on compressive strength of rice husk–bark ashes and fly ash-based geopolymer paste, *The 3rd ACF International Conference–ACF/VCA*, 2008.
- [49] P. De Silva, K. Sagoe-Crenstil, V. Sirivivatnanon, Kinetics of geopolymerization: Role of Al<sub>2</sub>O<sub>3</sub> and SiO<sub>2</sub>, *Cem. Concr. Res.* 37 (2007) 512–518.
- [50] M.F.M. Zaïn, H.B. Mahmud, A. Ilham, Prediction of splitting tensile strength of high performance concrete, *Cem. Concr. Res.* 32 (2002) 1251–1258.
- [51] W.K.W. Lee, J.S.J. Van Deventer, The interface between natural silicious aggregates and geopolymers, *Cem. Concr. Res.* 34 (2004) 195–206.
- [52] Y.S. Zhang, W. Sun, Z. Li, Hydration process of interfacial transition in potassium polysialate (K-PSDS) geopolymer concrete, *Mag. Concr. Res.* 57 (2004) 33–38.
- [53] V. Barbosa, K. MacKenzie, C. Thaumaturgo, Synthesis and characterisation of materials based on inorganic polymers of alumina and silica: sodium polysialate polymer, *Int. J. Inorg. Mater.* 2 (2000) 309–317.





Cite this: *RSC Adv.*, 2015, 5, 105363

# Genetically-enriched microbe-facilitated self-healing concrete – a sustainable material for a new generation of construction technology

Manas Sarkar,<sup>a</sup> Dibyendu Adak,<sup>b</sup> Abiral Tamang,<sup>a</sup> Brajadulal Chattopadhyay<sup>\*a</sup> and Saroj Mandal<sup>b</sup>

The fundamentals of engineering and structural properties such as mechanical strength, durability, bond strength, and self-healing behaviour of a genetically-enriched microbe-incorporated construction material have been explored in the present study. The alkaliphilic *Bacillus subtilis* bacterium is able to survive inside the concrete/mortar matrices for an extended period due to its spore forming ability. The bioremediase-like gene of a thermophilic anaerobic bacterium BKH2 (GenBank accession no. KP231522) was thus transferred to the bacillus strain to develop a true self-healing biological agent. Incorporation of the transformed bacterial cells at different concentrations in the bio-concrete/mortar exhibited higher mechanical strengths and improved durability of the samples in comparison to the normal cement–sand mortar/concretes. Microstructural analyses confirmed the formation of a novel gehlenite ( $\text{Ca}_2\text{Al}_2\text{SiO}_7$ ) phase besides calcite deposition inside the matrices of the transformed *Bacillus subtilis*-amended cementitious materials. The gradual development of nano rod-shaped gehlenite composite within the bio-mortar matrices was due to the biochemical activity of the bioremediase-like protein expressed within the incorporated bacterial cells. This development significantly increased the true self-healing property as well as enhanced the mechanical strength of the bio-concrete/mortar material which was sustained for a prolonged period. This study demonstrates a new approach towards the enhancement of structural properties and true self-healing activity by genetically-enriched spore-forming *Bacillus* sp. with advancement towards sustainable and green construction technology.

Received 8th October 2015  
Accepted 7th December 2015

DOI: 10.1039/c5ra20858k

[www.rsc.org/advances](http://www.rsc.org/advances)

## 1. Introduction

Growing trends in the development of self-healing properties of cementitious materials in construction technology has given rise to several smart materials with versatile properties and high sustainability.<sup>1–3</sup> The self-healing phenomenon is an important aspect for construction technology which prolongs the service life of infrastructures. The key notion of this concept is that minor damage in concrete structures is not an issue as long as it is counteracted by a subsequent autonomous process of removing or ‘healing’ the structural damage. Several types of micro cracks are of common occurrence which arise due to the relatively low tensile strength as well as due to the lack of a suitable instant treatment for the concrete. The potential of mineral precipitating bacteria for crack remediation and durability improvement have been thoroughly investigated in different studies.<sup>1,2,6</sup> Recently, attempts are being made to establish autonomous-healing activity by incorporating mineral producing microbes in the concrete mix.<sup>1,2</sup> But the efficient self-

healing phenomenon through the process of bacteria assisted bio-mineralization occurs at the initial stage of concretization.<sup>1–6</sup> Self-healing on the cracks within the concrete that appear over a prolonged period will be the most desirable and challenging task that yet to be established. Furthermore, the application of the genetically-modified bacteria for eco-friendly engineering and true self-healing process over a prolonged period will create a new hope for sustainable concrete technology.<sup>7</sup>

Earlier reports demonstrate the applications of anaerobic hot spring bacteria in cementitious material executing higher mechanical strength and enhancing the durability due to the formation of a new phase (gehlenite) inside the cementitious matrices.<sup>7</sup> However, the application of anaerobic bacterium as a self-healing agent depends on its survival inside the concrete matrices for a prolonged period. The short lifetime of the bacterium inside the concrete matrices restricts it from behaving as a true self-healing activator over sustained duration.<sup>9</sup> Genetically improved *E. coli* bacterium by incorporation of the bioremediase-like gene, was seen to increase the mechanical strength and durability of the mortar samples.<sup>7</sup> However, the transformed bacterium could not survive inside the high alkaline cement matrices for an extended period. In

<sup>a</sup>Department of Physics, Jadavpur University, Kolkata-700032, India. E-mail: [bdc\\_physics@yahoo.co.in](mailto:bdc_physics@yahoo.co.in); Tel: +91-9433343917

<sup>b</sup>Department of Civil Engineering, Jadavpur University, Kolkata-700032, India

contrast, alkaliphilic spore forming bacterium, *Bacillus* sp. can persist in viable form within the concrete for an extended period and is also capable of forming crack plugging minerals (calcium carbonate) in concrete structure for autonomous healing.<sup>2–6</sup>

In this work, biosilicification gene (bioremediase-like protein gene) of BKH2 has been transformed in a spore forming bacterium *Bacillus subtilis* (*B. subtilis*) and then the genetically-enriched bacterium has been used in Ordinary Portland Cement (OPC; 43 grade) based concrete material for healing of cracks over long periods to develop a new self-healing material. A comparative investigation has been studied based on structural behaviour (compressive, split tensile, flexural and bond strength) and self-healing attributes of bio-concrete/mortar materials prepared by incorporating both transformed and non-transformed *Escherichia coli* (*E. coli*) and *B. subtilis* bacteria respectively to cementitious material. The promising outcomes of this study reveal the true self-healing capability of the transformed *B. subtilis* (T-*B. subtilis*) for future concrete industries.

## 2. Experimental details

### 2.1. Materials

All analytical grade chemicals were purchased from the Sigma-Aldrich, USA; Merck-Germany; and the Spectrochem Pvt. Ltd. of India. Locally available sand (Specific gravity 2.52, water absorption 0.50%, and fineness modulus of 2.38) and 12 mm down aggregates (specific gravity 2.78, water absorption 0.42%, and fineness modulus of 4.89) were used as fine and coarse aggregates respectively. Ordinary Portland Cement (OPC) grade 43 and 20 mm diameter high yield strength deformed rebar and mild steel rebar of grade Fe500 were also used in the study. *E. coli* strain (JM107; MTCC 1669) and *B. subtilis* (MTCC 441) strain were procured from IMTECH, Chandigarh, India. The transformed JM107 (T-JM107) strain, a genetically-modified *E. coli* strain was obtained from the stock culture of Biophysics Laboratory, Department of Physics of Jadavpur University.<sup>7</sup>

### 2.2. The bacteria and growth conditions

The T-JM107 and JM107 strains were cultured in Luria Bertani (LB) medium (0.5% peptone, 1% yeast extract, 0.5% NaCl, pH 7.0) at 37 °C. Similarly the alkaliphilic spore forming *B. subtilis* bacterium was cultured in Luria-broth (LB) medium. To enhance the sporulation (spore formation) of the *B. subtilis* bacterial culture, a specific mineral media (pH 10.0) containing 0.2 g NH<sub>4</sub>Cl, 0.02 g KH<sub>2</sub>PO<sub>4</sub>, 0.225 g CaCl<sub>2</sub>, 0.2 g KCl, 0.2 g MgCl<sub>2</sub>·6H<sub>2</sub>O, 0.01 g MnSO<sub>4</sub>·2H<sub>2</sub>O, 1 ml trace element solution (SL12B), 0.1 g yeast extract, 5.16 g citric acid tri sodium salt, 4.2 g NaHCO<sub>3</sub> and 5.3 g Na<sub>2</sub>CO<sub>3</sub> per litre distilled water was used.<sup>10</sup> The cultures containing large number of spores were washed by repeated centrifugation and re-suspension of the cell pellet in sterile ultrapure Milli-Q water to harvest the spores. Suspensions were subsequently heated for 30 min at 80 °C to inactivate the present vegetative cells and numbers of viable spores in water suspension were quantified by using haemocytometer.

### 2.3. Genetic transformation to develop improved *Bacillus subtilis* strain

The bioremediase-like protein (molecular weight about 28 kDa) secreted by BKH2 is capable of leaching silica from silicate substrates.<sup>7</sup> The corresponding gene (~800 bp.) of the bioremediase-like protein was fished out from the whole genome of BKH2 as described earlier.<sup>7</sup> The isolated gene was amplified by Polymerase Chain Reaction (PCR) and cloned into T-vector. The transformation of bioremediase gene through T-vector to *B. subtilis* was carried out by calcium chloride treatment of the bacterial cells as described by Lederberg and Cohen.<sup>11</sup> The transformed *Bacillus subtilis* (T-*B. subtilis*) was grown in ampicillin (0.5 mg ml<sup>-1</sup>) containing agar plate and pure culture of T-*B. subtilis* strain was obtained from a single colony grown on the agar plate.

The expression of the transformed gene in *B. subtilis* was confirmed by observing the protein profile of transformed bacterial cells. The expressed protein (bioremediase-like) was purified by using Sephadex G-100 gel filtration chromatographic technique and detected through sodium dodecyl sulphate polyacrylamide gel electrophoresis (SDS-PAGE) along with marker proteins (Sigma-Aldrich, USA). The biosilicification activity of purified proteins was confirmed by the standard biosilicification assay.<sup>7,12</sup>

### 2.4. Application of transformed *B. subtilis* (T-*B. subtilis*) in concrete and mortar

**2.4.1. Compressive strength and ultrasonic-pulse velocity (UPV) test.** Mortar specimens (50 mm × 50 mm × 50 mm dimension) were prepared in which the cement vs. sand ratio was taken as 1 : 3 and water vs. cement ratio was 0.4 for this study. The concentrations of the T-*B. subtilis* bacterial cells in the mortar specimens were varied from 10<sup>2</sup>–10<sup>6</sup> cells per ml water and the compressive strength of the bacterial cells amended samples was investigated at different periods of water curing.

Concrete specimens (150 mm × 150 mm × 150 mm dimension) were prepared by using the 43 grades OPC, normal river sand and 16 mm down coarse aggregates. The cement, sand and coarse aggregates ratio was maintained as 1 : 1.45 : 3.25 and the water-cement ratio were fixed at 0.48. To achieve the maximum compressive strength, a bacterial cells concentration of 10<sup>5</sup> cells per ml of water for T-*B. subtilis* strain and 10<sup>8</sup> cells per ml of water for T-JM107 strain were used in all further experiments.<sup>7</sup> The compressive strength of concrete and mortar specimens were tested after 3, 7, 28 and 90 days of water curing.<sup>13</sup> The ultrasonic-pulse velocity of the samples was measured by Pundit plus PC1007 UPV meter as per ASTM C597-02 20.<sup>14</sup>

**2.4.2. Flexural strengths & split tensile strengths measurement.** Concrete beam specimens (100 mm × 100 mm × 500 mm dimension) were prepared for the determination of flexural strength as per ASTM C293.<sup>15,16</sup> The specimens were cured under water for 28 days. Split tensile strength of all the concrete mixtures were carried out by using the cylindrical

concrete specimens (100 mm diameter  $\times$  200 mm height) after 90 days of water curing.

**2.4.3. Rapid chloride ion permeability test (RCPT).** Rapid chloride ion permeability test is a measure for durability character of concrete in which cylindrical concretes (100 mm diameter  $\times$  200 mm height) were prepared by using cement-sand-aggregate mixture along with different bacterial strains (JM107, T-JM107, *B. subtilis*, T-*B. subtilis* and BKH2). After 90 days of water curing, the RCPT of the samples were tested as per ASTM C1202.<sup>17,18</sup>

**2.4.4. Bond strengths measurement.** The bond test specimens consisted of concrete cubes of similar size (150 mm  $\times$  150 mm  $\times$  150 mm dimension), with a single reinforcing bar (deformed and mild) embedded vertically (projected down for a distance  $\sim$ 10–15 mm from the bottom face of the cube) along a central axis in each specimen. In this experiment, deformed (Fe-500) and plane (Fe-250) bar were used for each category of concrete specimens. The test was performed as per IS2770 after 28 days of water curing.<sup>19</sup>

## 2.5. Self-healing study

Different bacterial cells incorporated mortar cubes (50 mm  $\times$  50 mm  $\times$  50 mm dimension;  $N = 20$ ) were prepared for self-healing study in which the cement-sand ratio was taken as 1 : 3 and water-cement ratio was fixed at 0.4. Bacterial cell concentrations were also chosen as  $10^8$  cells per ml of water used for JM107 and T-JM107 whereas for BKH2 amended samples it was taken as  $10^5$  cells per ml of water. Mortar samples of similar dimension were also prepared by incorporating the endospore of *B. subtilis* and T-*B. subtilis* at a concentration of  $10^5$  spores per ml water used. After 120 days of air curing, the average UPV and breaking load of each category mortars ( $n = 10$ ) were measured. After measuring the breaking load, 50% of the corresponding breaking load was applied to the rest bio-mortars ( $n = 10$ ) of each category of samples. The artificial cracks with various widths and depths were generated on every specimen as viewed by Crack detection microscope (VJT6330, VJ Tech, England). The samples were then immersed in a closed bucket containing 10% LB-medium (v/v) in water for next 28 days at ambient temperature. Closed environment was set up to avoid free diffusion of oxygen and carbon dioxide over the water-air interface through the entire curing period. After curing, the UPV and breaking load of the remaining samples ( $n = 10$ ) were measured. Specimens were air dried for stereomicroscopic inspection by crack detection microscope to investigate the crack-healing attributes.

The development of gehlenite phases inside the T-*B. subtilis* incorporated mortars under 10% LB curing was examined by using Field Emission Scanning Electron Microscope (FESEM; INSPECT F50 SEM, FEI Europe BV, The Netherlands).

## 2.6. Microstructure analysis of self-healed bio-material

The crack-healing materials developed inside the cracks of the *B. subtilis* and T-*B. subtilis* incorporated mortar samples was collected and crushed into fine powder by using pestle-mortar. The powder samples were examined under the FESEM and

analysed by energy dispersive spectra (EDS) for elemental quantification studies. The morphology of the self-healing material (from the crack of T-*B. subtilis* incorporated mortar samples) was evaluated by using Transmission Electron Microscopy (TEM; JEOL, JEM 2100). XRD analysis was also performed (Bruker AXS, Inc., Model D8, WI, USA) with monochromatic Cu-K $\alpha$  radiation of wavelength 1.5406 Å at 40 kV and 40 mA. The samples were examined at  $2\theta$  from  $10^\circ$  to  $70^\circ$  and identified by referring to data of Joint Committee on Powder Diffraction Standards (JCPDS) files.

**2.6.1. Statistical analysis.** There were 10 concrete samples prepared for each category of testing and each experiment was repeated thrice. Data are represented as mean over 30 samples  $\pm$  SD in the bar diagram.

## 3. Results

### 3.1. Gene transformation & protein isolation

The corresponding gene of the bioremediase-like protein was fished out from the whole genome of BKH2 by using the primers constructed from the sequence of carbonic anhydrase II of *Bos taurus*.<sup>7,12</sup> The DNA fragment was amplified by PCR technique and the product was then transformed into *B. subtilis* bacterium through a suitable T-vector. The transformation was confirmed by growing the bacterial cells (colonies) in an ampicillin-containing LB-agar plate, as shown in Fig. 1A and B. Fig. 1C shows the whole-cell protein profiles of *B. subtilis* and genetically improved *B. subtilis* (T-*B. subtilis*) when analysed by SDS-PAGE. A new protein band appeared in the protein profile of T-*B. subtilis* bacterium, molecular weight was  $\sim$ 28 kDa. This newly expressed protein was purified from the crude mixture of whole cell protein through the column chromatographic technique. The silica leaching activity of the purified protein (28 kDa) was confirmed by biosilicification assay (Table 1).

### 3.2. Compressive strength and ultrasonic-pulse velocity analysis

T-*B. subtilis* cells showed compressive strengths increasing attributes for the mortars when incorporated at different cell

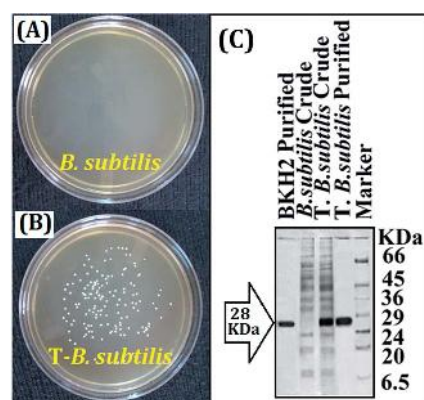


Fig. 1 (A) Host cell *B. subtilis* (B) T-*B. subtilis* in agar plate containing ampicillin; (C) SDS-PAGE images of protein profiles.

Table 1 Biosilicification activity of protein(s)<sup>a</sup>

Samples	Total protein (mg)	Activity (units)	Sp. activity (units per mg)
Crude bioremediase like protein (BKH2)	5	144	28.8
Purified bioremediase like protein (BKH2)	2	410	205
Crude whole cell protein ( <i>B. subtilis</i> )	5	—	—
Crude whole cell protein (transformed <i>B. subtilis</i> )	5	186	37.2
Purified bioremediase like protein (transformed <i>B. subtilis</i> )	2	570	285

<sup>a</sup> One unit activity of bioremediase protein is expressed as  $\mu\text{g}$  of silica released per mg of protein.

concentrations for different days of incubation (Fig. 2A). The maximum strength increment of the bacteria amended bio-mortars was achieved at a concentration of  $10^5$  cells per ml of water used. The T-*B. subtilis* incorporated mortar (TBM) samples also exhibited better compressive strengths and UPV in comparison to the other bacteria incorporated samples at all ages (Fig. 2B and C).

### 3.3. Mechanical strength and durability analysis

Fig. 3A exhibits the improvement of compressive strength of different bacterial amended bio-concrete samples. All the bacteria incorporated bio-concrete samples except *E. coli* (JM107) amended samples, exhibited higher compressive

strength with respect to control samples. The maximum increment of compressive strength of the transformed *Bacillus* bacterial cells incorporated bio-concrete (TBC) cubes was observed with the addition of  $10^5$  cells per ml of water used at all curing ages. From the split-tensile strength and the flexural strength analysis, it was observed that the T-*B. subtilis* bacterium increased the mechanical strengths significantly (Fig. 3B). The experimental bond strength (under tension) of bio-concretes and control concrete with rebar (deformed and mild steel) are shown in Fig. 3C and D. The ultimate bond strength and characteristic bond strength of deformed rebar and mild steel rebar were calculated from bond strength vs. slip curve. The bond strength of the TBC with deformed and mild steel rebar were significantly greater compared to other samples. The rapid chloride permeability test revealed that the least amount of charge penetration was realized inside the TBC matrices (Fig. 3E). Fig. 3F demonstrated the better workability of TBC in the slump test.

### 3.4. Self-healing study of biotechnologically modified building material

Fig. 4A and B show the variation of compressive strength and UPV respectively of the different bio-mortars after 120 days of air curing. After applying the 50% of their corresponding breaking load, the simultaneously measured compressive strength of each sample were decreased. After 28 days of water (with 10% LB v/v) curing, the compressive strength as well as the UPV of all the samples were increased. The rate of increment was highest in case of the TBM samples.

Images of the cracks and their progressive healings were examined by Crackscope. Partial and complete crack healing abilities were observed in the case of *B. subtilis* and T-*B. subtilis* incorporated mortar samples respectively after 28 days water (with 10% LB v/v) curing period (Fig. 5). Gradual formation of

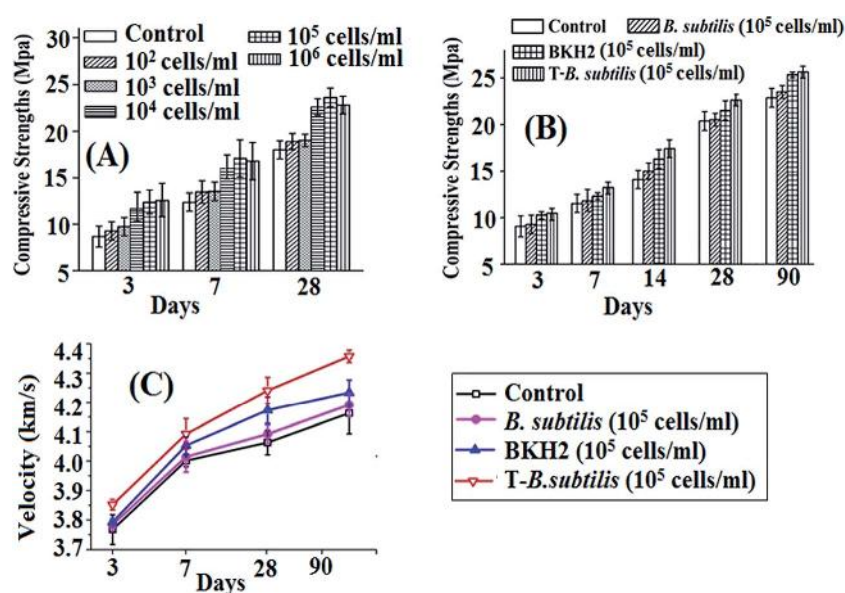


Fig. 2 (A) Compressive strengths of T-*B. subtilis* amended mortars; (B) comparison of compressive strengths for different bio-mortars; (C) ultrasonic pulse velocity for different bio-mortars.

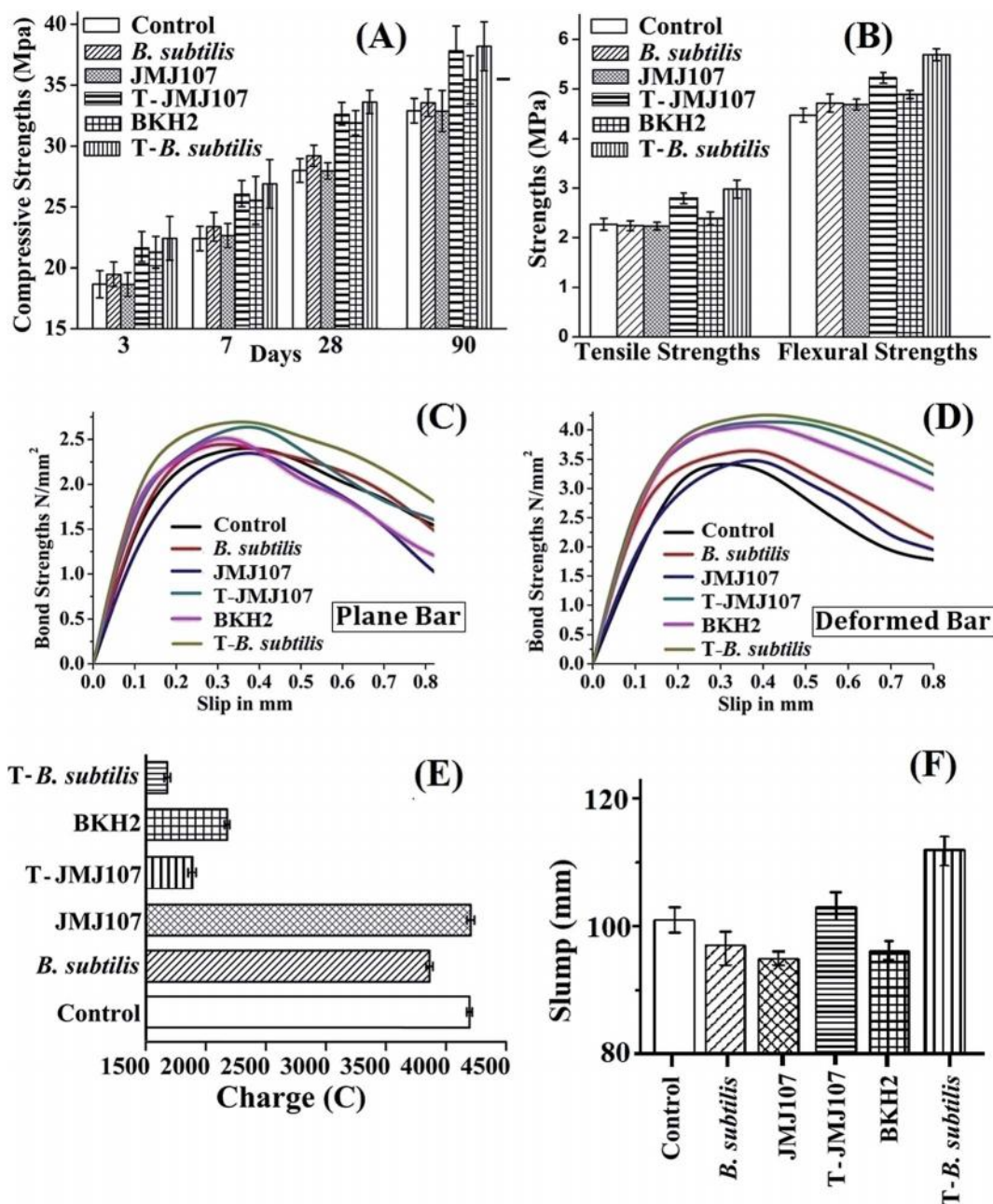


Fig. 3 (A) Compressive strengths; (B) tensile strengths and flexural strengths; (C) bond strength of different bio-concretes (plane bar); (D) bond strength of different bio-concretes (deformed bar); (E) rapid chloride permeability test; (F) slump test of concretes.

nano rod-shaped gehlenite along with calcite crystals were observed in T-*B. subtilis* incorporated mortar samples as investigated by FESEM (Fig. 6).

### 3.5. Microstructural analysis

FESEM analysis of the powder samples obtained from the cracked portions of the *B. subtilis* showed irregular crystalline materials (Fig. 7A). The self-healing materials collected from the cracks of the TBM samples showed regular nano needle-like structures (Fig. 7B). The EDS analysis determined that the self-healing materials consisted of calcium, aluminium, oxygen

and silicon atoms. The TEM analysis (Fig. 7C(i) and (ii)) of the gehlenite shows rod shaped morphology (diameter ~ 85 nm) which is in agreement with the FESEM image (Fig. 7B). The XRD analysis of self-healing materials exhibit that additional peaks appear in the TBM matrices (Fig. 7D(ii)) which confirms the formation of gehlenite (calcium aluminium silicate) phase absent in *B. subtilis* (Fig. 7D(i)) incorporated mortar samples.

## 4. Discussion

Cementitious matrices may seem unhealthy for life, as it is very dehydrated and extremely alkaline compared to natural

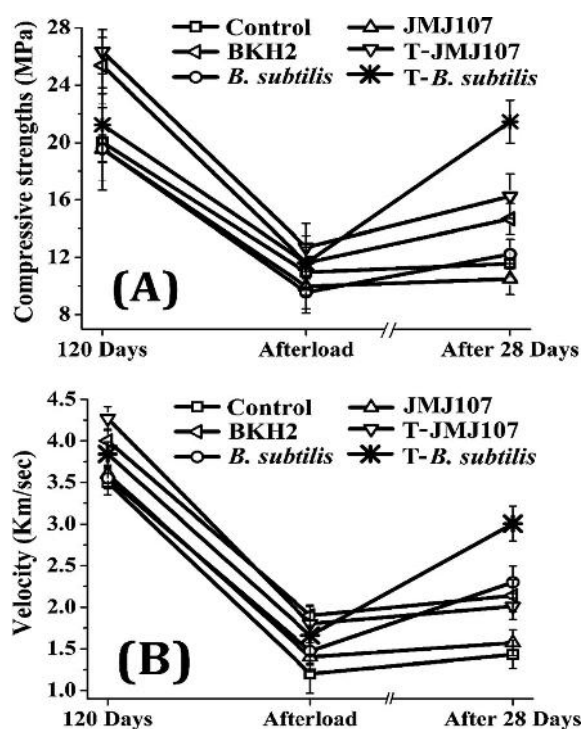


Fig. 4 Self-healing study of different bio-mortars by (A) compressive strengths (B) ultrasonic pulse velocity measurement.

environment of bacterial existence. Nevertheless, some bacteria are found within the earth shell inside rocks in deserts as well as in ultra-basic environments at great depths.<sup>20–22</sup> Under favourable conditions some common aerobic and active alkaliphilic soil bacteria like *Bacillus* sp., *Pseudomonas* sp. can continuously precipitate/mineralize impermeable calcite layer over the surface of existing concrete layer which may act as self-healing agent within the concrete structures.<sup>3,5,6</sup> A low metabolic activity and extremely long lifetime characterize spores and some sp. are known to produce spores which are viable for up to 200 years.<sup>23</sup> Such *Bacillus* sp. spores when immobilized within cementitious materials, produced copious amounts of mineral crystals on exposed surface of the media, therefore able to seal cracks by bio-mineral formation after being revived by water and growth nutrients entering the freshly formed cracks.<sup>2,10</sup> Self-healing processes of bio-concrete need additional nutritious environmental stimuli as triggers, such as calcium lactate and urea along with suitable environment.<sup>6,10,24–27</sup> Though some anaerobic hot spring bacteria (BKH1 & BKH2) and its secretory protein(s) both are able to increase the compressive strength and durability of the mortar/concrete samples, they fail to survive for a long period in the harsh environment of the concrete.<sup>7,8,12</sup> The biosilicification activity is prolonged inside the concrete through the gene transformation into the spore

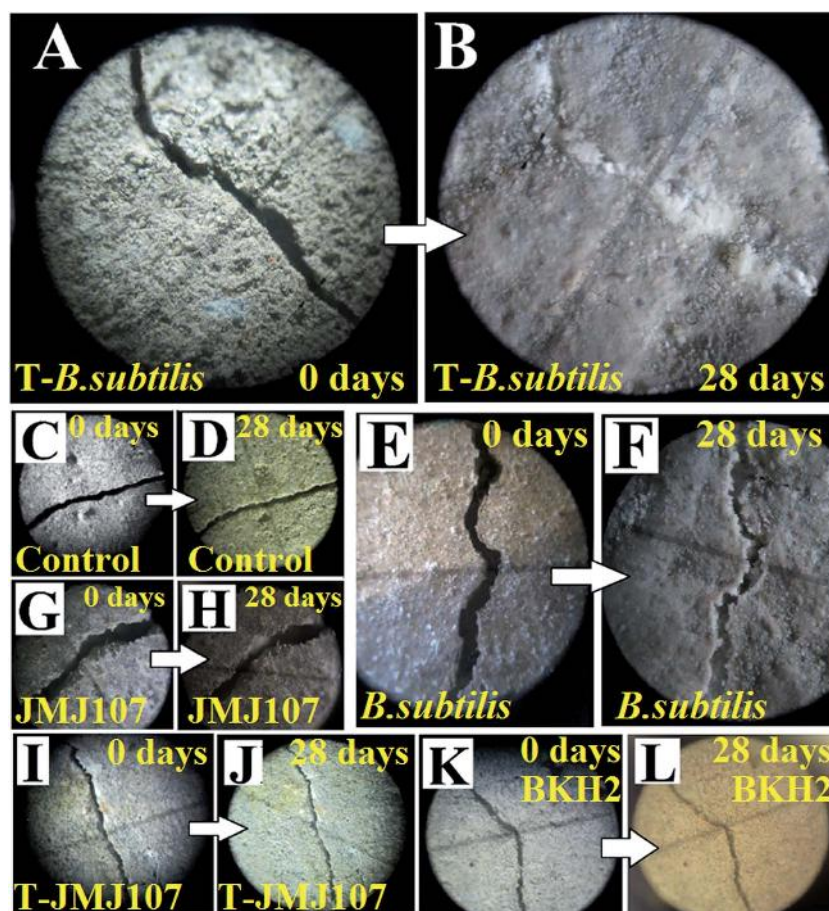


Fig. 5 Images of the cracked and healed surfaces of mortars.

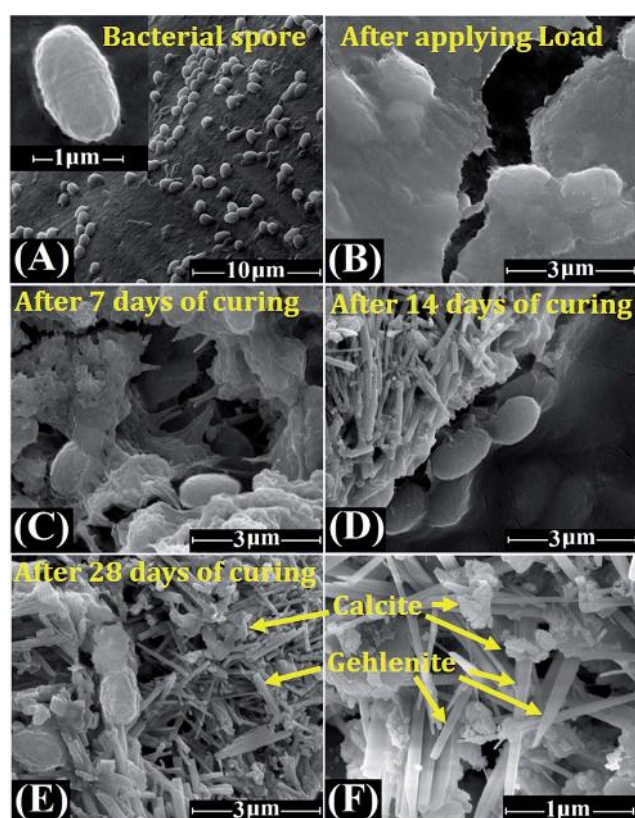


Fig. 6 FESEM images of the progress of gehlenite formation inside the mortar in presence of *T-B. subtilis* in different days.

forming *B. subtilis* stain for realization of sustainability and true self-healing phenomenon (Fig. 1 & Table 1).

This study demonstrates that the transformed *Bacillus subtilis* bacterial strain possesses better efficacy for the strength and durability of the incorporated mortar specimens (Fig. 2A and B) due to the formation of gehlenite along with calcite precipitation inside the mortar matrices. The increased compactness of the mortar sample is reflected by the results of ultrasonic-pulse velocity tests of the samples (Fig. 2C). The compressive strength, split tensile strength and flexural strength are the important factors of concrete which support the stability and longevity of the concrete based structures. Our experimental results confirm that TBC possess the property for overall increasing mechanical strength (Fig. 3). It is already reported that the bacteria *Bacillus* sp. is able to deposit calcite phase inside the concrete matrices when incorporated to the mortar samples.<sup>2,6,10,24–26</sup> The biochemical activity of the bioremediase-like protein has been found to synthesize gehlenite phase inside the concrete/mortar matrices.<sup>7</sup> These two phases are synergistically developed inside the TBC matrices and exhibited better mechanical strength by filling the micro pores inside the samples (Fig. 3A and B). Bond strength of the TBC shows better performance than others, as greater split tensile strength of TBC (Fig. 3C and D). The presence of adequate amount of gehlenite beside calcite in the TBC matrices makes the concrete denser and produce stronger interfacial transition zone (ITZ) between aggregates and the matrix, which increases the bond strength between the reinforcement bar and surrounding concrete. The RCPT result suggests that small amounts of free chloride ions are permitted

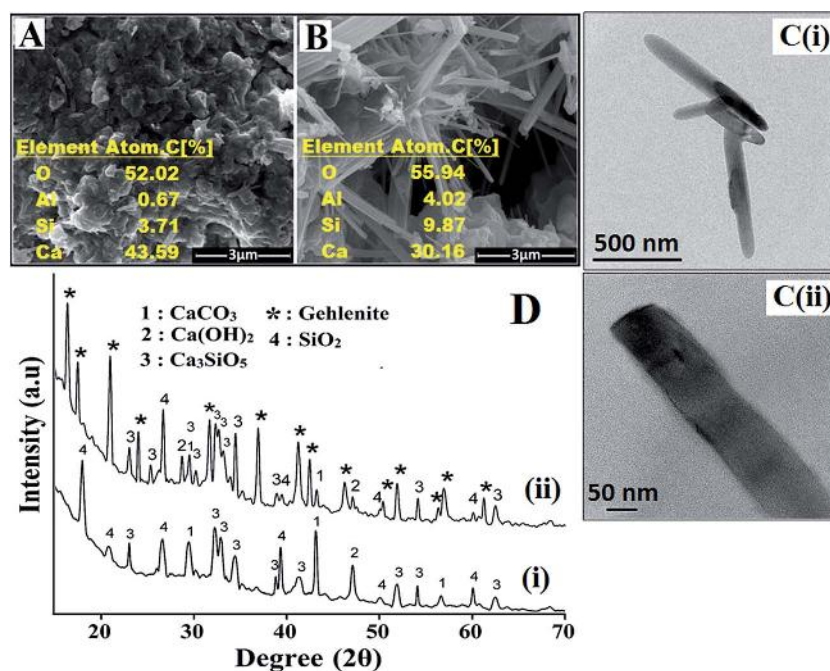


Fig. 7 FESEM images of self-healing materials obtained from (A) *B. subtilis* (B) *T-B. subtilis* incorporated cementitious matrices (C) TEM images of *T-B. subtilis* incorporated cementitious matrices (D) XRD spectra of self-healing materials obtained from (i) *B. subtilis* and (ii) *T-B. subtilis* incorporated cementitious matrices.

through the less porous TBC matrices implying better durability of the samples (Fig. 3E).

The self-healing study of cementitious material incorporated with the bacterial cells of BKH2, T-JMJ107 and *B. subtilis*, it is clear that these bacterial strains are able to fulfil the self-healing behaviour to some extent. It is observed that both the bacterial strains BKH1 and BKH2 can survive inside the concrete matrices only for 7–8 days.<sup>7,12</sup> The genetically modified *Bacillus* sp. has been investigated for green and sustainable (self-healing) concrete as it can survive inside the concrete in dormant phase over an extensive period which is not possible for other bacterial strains like *E. coli* bacterium (T-JMJ107).

The T-*B. subtilis* bacterial cells are found to act as a proper self-healing agent to catalyse the process of autonomous repair of micro and macro cracks inside the concrete and thereby increasing the strength and durability of the structures. Endospores remain in dormant phase as they are capable of surviving without nutrients and are resistant to ultraviolet radiation, desiccation, high temperature, extreme freezing and chemical disinfectants.<sup>28</sup> In presence of the favourable environment, the endospore becomes active *i.e.*, it transforms from the dormant phase to the vegetative phase. In this experiment, it is observed that the genetically enriched *B. subtilis* (T-*B. subtilis*) bacterial spore became active after a prolonged time of dormancy under favourable environment (introduction of LB in air cured cracked mortar sample), initiating the biosilicification and biomineralization processes (Fig. 6). This subsequently leads to the self-healing of the mortar as the cracks are filled with the newly formed needle-shaped nano-calcium aluminium silicate (gehlenite) phase beside calcite inside the cementitious matrices (Fig. 7).

The non-transformed *Bacillus subtilis* bacterial cells (host cells) produce a protein which can synthesis calcite phase only inside the mortar samples. No such self-healing phenomenon was observed in the other bacterial cells like (wild type and transformed *E. coli*) incorporated mortar samples as they do not have the spore forming ability and perish. Microstructures analysis of the self-healing material obtained from *B. subtilis* and T-*B. subtilis* bacteria treated mortar samples show contrasting textures of their matrices (Fig. 7). The matrix of the *B. subtilis* amended mortar samples is appeared to be amorphous, showing no signature of conspicuous crystal growth. On the other hand, the TBM samples show crystalline matrix where the individual crystals can be recognized. The formation of crystalline calcium carbonate phase inside the matrices of *Bacillus* sp. bacteria incorporated mortars is elaborately described in several studies earlier.<sup>3,22–27</sup> The development of calcite and gehlenite phases within the TBM matrices are shown in the Fig. 7 which clearly demonstrates the true self-healing behaviour of the T-*B. subtilis* bacterial strain in cementitious composite.

## 5. Conclusion

Genetically improved endospore forming *B. subtilis* strain enhances the autonomous healing property of cementitious composites. The formation of gehlenite phase by the enriched

microbes with high longevity inside the mortar/concrete is the main reason behind the increment of its strength and durability. Development of a newly transformed strain and exploration of its overall property for sustainable green concrete would be a promising area for future construction technology. This study will provide an eco-friendly, pollution free, non-hazardous biotechnologically improved way for fulfilling the mostly desired “green” self-healing concrete for modern.

## Conflict of interest

None.

## Acknowledgements

The financial assistance to this investigation received from Department of Biotechnology, New Delhi, Government of India, and their R&D Grant is gratefully acknowledged.

## References

- 1 M. Sarkar, T. Chowdhury, B. D. Chattopadhyay, R. Gachhui and S. Mandal, *J. Mater. Sci.*, 2014, **49**, 4461–4468.
- 2 H. M. Jonkers, Self-Healing Concrete: A Biological Approach, in *Self-Healing Materials: An Alternative Approach to 20 Centuries of Material Science*, ed. S. van der Zwaag, Springer, The Netherlands, 2007, pp. 195–204.
- 3 V. Wiktorski and H. M. Jonkers, *Cem. Concr. Compos.*, 2011, **33**, 763–770.
- 4 S. K. Ramachandran, V. Ramakrishnan and S. S. Bang, *ACI Mater. J.*, 2001, **98**, 3–9.
- 5 S. S. Bang, J. K. Galinat and V. Ramakrishnan, *Enzyme Microb. Technol.*, 2001, **28**, 404–409.
- 6 W. de Muynck, D. Debrouwer, N. de Belie and W. Verstraete, *Cem. Concr. Res.*, 2008, **38**, 1005–1014.
- 7 M. Sarkar, N. Alam, B. Chaudhuri, B. D. Chattopadhyay and S. Mandal, *RSC Adv.*, 2015, **5**, 32175.
- 8 S. Majumdar, M. Sarkar, T. Chowdhury, B. D. Chattopadhyay and S. Mandal, *Open J. Civ. Eng.*, 2012, **2**, 218–228.
- 9 S. Ghosh, M. Biswas, B. D. Chattopadhyay and S. Mandal, *Cem. Concr. Compos.*, 2009, **31**, 93–98.
- 10 H. M. Jonkers, A. Thijssen, G. Muyzer, O. Copuroglu and E. Schlangen, *Ecol. Eng.*, 2010, **36**, 230–235.
- 11 E. M. Lederberg and S. N. Cohen, *J. Bacteriol.*, 1974, **119**, 1072–1074.
- 12 M. Biswas, S. Majumdar, T. Chowdhury, B. D. Chattopadhyay, S. Mandal, U. Halder and S. Yamasaki, *Enzyme Microb. Technol.*, 2010, **46**, 581–587.
- 13 IS 10080, *Specification for vibration machine*, Bureau of Indian Standards, New Delhi, India, 1982.
- 14 ASTM C597–02, *Standard test method for pulse velocity through concrete*, ASTM International, West Conshohocken.
- 15 ASTM C293–08, *Standard Test Method for Flexural Strength of Concrete (Using Simple Beam with Centre-Point Loading)*.
- 16 D. Adak, M. Sarkar and S. Mandal, *Construct. Build. Mater.*, 2014, **70**, 453–459.



## Paper

- 17 ASTM C1202, *Standard test method for electrical indication of concretes ability to resist chloride ion penetration*, West Conshohocken, 2000.
- 18 D. Adak, M. Sarkar, M. Maiti, A. Tamang, S. Mandal and B. D. Chattopadhyay, *RSC Adv.*, 2015, **5**, 64037–64045.
- 19 IS 2770-1, *Methods of testing bond in reinforced concrete*, Part 1: Pull-out test, 1967.
- 20 R. Jose and B. M. Goebel, *Appl. Environ. Microbiol.*, 2003, **69**(7), 3858–3867.
- 21 P. Fajardo-Cavazos and W. Nicholson, *Appl. Environ. Microbiol.*, 2006, **72**(4), 2856–2863.
- 22 B. B. Jorgensen and S. D'Hondt, *Science*, 2003, **314**, 932–934.
- 23 H. G. Schlegel, *General microbiology*, Cambridge University Press, 7th edn, 1993.
- 24 K. V. Tittelboom, N. de Belie, W. de Muynck and W. Verstraete, *Cem. Concr. Res.*, 2010, **40**, 157–166.
- 25 V. Achal, A. Mukherjee, P. C. Basu and M. S. Reddy, *J. Ind. Microbiol. Biotechnol.*, 2009, **36**(3), 433–438.
- 26 W. de Muynck, N. de Belie and W. Verstraete, *Proceedings of the first international conference on self-healing materials*, Noordwijk aan Zee, The Netherlands, 2007.
- 27 F. Hammes, N. Boon, J. de Villiers, W. Verstraete and S. D. Siciliano, *Appl. Environ. Microbiol.*, 2003, **69**(8), 4901–4909.
- 28 P. Setlow, *J. Appl. Microbiol.*, 2006, **101**, 514–525.